The spatio-temporal dynamics of cell membranes deformations and cell migration

Angélique Stéphanou

UNIVERSITE JOSEPH FOURIER-GRENOBLE 1
SCIENCES ET GEOGRAPHIE
and
UNIVERSITY OF DUNDEE

A Thesis submitted for the degree of
DOCTEUR DE L'UNIVERSITE JOSEPH FOURIER
Spécialité Modèles et Instruments en Médecine et Biologie
&
DOCTOR OF PHILOSOPHY OF THE UNIVERSITY OF DUNDEE

Angélique STEPHANOU

4^{th} of February 2002

The Spatio-temporal Dynamics of Cell Membrane Deformations and Cell Migration

A Characterization from Image Sequences and Theoretical Modelling

THESIS SUPERVISORS

Dr P. Tracqui Pr M.A.J. Chaplain

THESIS JURY:

Pr P. Maini (University of Oxford, UK)
Pr J.P. Mazat (University of Bordeaux, France)
Pr V. Norris (University of Rouen, France)
Dr B. Vasiev (University of Dundee, UK)

Acknowledgements

I would like to acknowledge my supervisors Dr. P. Tracqui, who offered me the opportunity to pursue in this thesis the work initiated during the master degree on "Modelling in Medicine and Biology", and Pr. M.A.J. Chaplain for accepting to take part in that project and for his help and advice during all my stays in the Mathematical Department of Dundee.
I would like to thank X. Ronot of the E.P.H.E. (Institut Albert Bonniot, La Tronche) and his team A. Doisy and C. Alcouffe, for preparing the cells and the videomicroscopy sequences and for helpful discussions concerning all experimental aspects of this work.
Thanks also to D. Brau representing Photonic Sciences society who provided the video camera for the images acquisition.
Last, very special thanks to Anotida Madzvamuse of Oxford University for his constant support and encouragement during all the thesis and for his help and valuable advice for the writing and much more.
The thesis was financially supported by the Région Rhône-Alpes and was part of the project "Métrologie du vivant" also funded by the Région.

Abstract

Résumé

Cette thèse concerne l'étude des déformations cellulaires et s'intéresse à deux approches complémentaires, l'une expérimentale et l'autre théorique. L'approche expérimentale est motivée par la mise en évidence lors de travaux antérieurs, de l'existence d'une certaine auto-organisation des schémas des déformations membranaires. Cette auto-organisation se traduit par la récurrence de schémas protrusifs dans l'espace et dans le temps. Ceci a été démontré en particulier pour des cellules arrondies (de types leukocyte ou keratinocyte), qui présentent une organisation relativement simple du cytosquelette d'actine. Nous avons choisi de nous intéresser ici au cas de fibroblastes murins (lignée L929). Les fibroblastes présentent en effet, de longues extensions membranaires de type filopode. Ce type de protrusion implique cette fois une organisation plus complexe du cytosquelette d'actine, où les filaments s'assemblent en paquets. Notre but a été de déterminer s'il existait également une composante auto-organisée pour les déformations membranaires de ces fibroblastes.

La caracterisation expérimentale a été réalisée à partir de séquences d'images où les cellules sont observées par vidéomicroscopie en contraste de phase. Les données morphodynamiques des cellules ont été extraites des séquences d'images par deux methodes: (i) une segmentation classique des contours pour l'étude individuelle des zones protrusives de la cellule et (ii) une méthode de flot optique pour une caractérisation globale du mouvement sur toute la cellule. Les résultats obtenus montrent que les cellules présentent le plus souvent des morphologies symétriques ayant de 2 à 4 protrusions. Les morphologies à 4 protrusions (morphologies en croix) observées pour les cellules les plus isolées se caractérisent dynamiquement par un mouvement pulsant synchronisé entre les 2 directions protrusives perpendiculaires où l'extension dans une direction s'accompagne de la rétraction simultanée dans l'autre direction. Dans ce cas une periodicité de l'ordre de 30 minutes a pu être identifiée pour la pulsation.

Sur le plan théorique, nous nous sommes interéssés à un modèle cytomécanique des déformations basé sur une description de la dynamique de polymérisation/depolymérisation de l'actine en relation avec les interactions mécaniques entre la membrane et le cytosquelette. Les simulations effectuées ont montré la capacité de ce modèle à générer qualitativement des états pulsants tels que ceux observés sur les fibroblastes, en particulier le comportement spontané à 4 protrusions.

Deux extensions du modèle ont alors été proposées afin de prendre en compte deux situations d'interaction de la cellule avec son environnement. La première considère l'interaction cellule-cellule et la modélisation du phénomène d'inhibition de contact de l'activité protrusive.

Ce processus a été modélisé en considérant une altération locale des paramètres d'élasticité du cortex cellulaire. La seconde extension du modèle concerne la modélisation de la migration cellulaire par chimiotaxie. Dans ce cas, la cellule interagit avec un gradient de facteur extracellulaire à travers une dépendance des propriétés d'élasticité de la membrane et du cortex cellulaire avec la concentration locale du facteur. Des comportements migratoires réalistes de la cellule vers la source ont ainsi pu être simulés. Finalement, une nouvelle formulation du modèle initial a été proposée pour modéliser de façon plus réaliste (modélisation quantitative) les longs prolongements membranaires (filopodes) développés par les fibroblastes.

En conclusion, nous définissons comment le travail realisé sur le plan experimental permet de proposer la possibilité d'utiliser les paramètres morphodynamiques issus de la caractérisation comme critères d'indentification des phénotypes cellulaires. Nous discutons également comment la modélisation théorique peut orienter le choix de protocoles expérimentaux nouveaux.

This thesis concerns the study of cell deformations and is interested in two complementary approaches, an experimental one and another theoretical one. The experimental approach is motivated by the demonstration from previous works of the existence of a certain auto-organization of the deformation patterns. This auto-organization consists of the appearance of recurring protrusive patterns in space and time. This has been shown, in particular, for round-shaped cells (leukocytes or keratinocytes) which present a relatively simple organization of the actin cytoskeleton. We have chosen to study murin fibroblasts (L929 line). The fibroblasts exhibit long membrane extensions such as filopods. This time, this type of protrusion is related to a more complex organization of the actin cytoskeleton, where the filaments tend to form bundles. Our aim has been to determine if there exists a similar self-organized component of these fibroblasts membrane deformations.

Experimental characterization has been performed from image sequences where the cells were observed by phase contrast videomicroscopy. The morphodynamical data of the cells have been extracted from the images with two different methods: (i) a classical segmentation of the cell boundaries for the individual study of each protrusive zone of the cell and (ii) an optical flow method for a global characterization of the movement of the whole cell. The results obtained show that the cells exhibit mainly symmetrical morphologies with 2 to 4 protrusions. The 4-protrusion state (cross morphology), observed for the most isolated cells, is dynamically characterized by a synchronized pulsating movement between the two perpendicular protrusive directions, where the extension in one direction is accompanied by the simultaneous retraction in the other direction. In that case a periodicity of about 30 minutes could be identified for the pulsation.

Theoretically, we have been interested in a cytomechanical model of deformations based on the description of the polymerization/depolymerization dynamic of actin in relation to the mechanical interactions between the membrane and the cytoskeleton. The simulations carried out have demonstrated the ability of the model to generate qualitatively pulsating states such as those observed in the fibroblasts, in particular the 4-protrusion pulsating

behaviour.

Two extensions of the model were proposed in order to take into account of two cases of interaction of the cell with its environment. The first one considers cell-cell interactions and the modelling of the phenomenon of contact inhibition of cell protrusive activity. This process was modelled on the basis of a local alteration of the elasticity parameters of the cell cortex. The second extension of the model concerns the modelling of cell migration by chemotaxis. In that case, the cell interacts with a factor of extracellular gradient through a dependency of the elastic properties of the membrane and the cell cortex with the local concentration of the factor. Realistic migratory behaviour of the cell towards the source could be simulated. Finally, a new formulation of the initial model has been proposed to model more realistically (quantitative modelling) the long membrane extensions (filopods) observed on the fibroblasts.

In conclusion, we defined how the work realized experimentally allows us to propose the possibility to use the morphodynamical parameters obtained from the characterization as criteria to identify the cell phenotypes. We also discuss how theoretical modelling can orientate the choice of new experimental protocols.

Contents

General Introduction

Introduction Générale

L'étude de la dynamique des déformations membranaires et de la migration cellulaire s'inscrit dans le cadre plus général de l'étude du comportement cellulaire. Cette étude a pour but de comprendre quels sont les phénomènes internes qui animent la cellule, qui la conduisent à se déformer et à migrer mais aussi comment elle perçoit son environnement, intègre les informations externes et fournit une réponse adaptée. Comprendre ces phénomènes requiert une approche pluridisciplinaire qui intègre à la fois des aspects moléculaires, biochimiques, physiques et mécaniques.

L'intérêt manifesté pour l'étude du comportement cellulaire a été initié par les travaux d'Abercrombie (Abercrombie and Heaysman, 1953) dans les années 50. De nombreuses hypothèses ont alors été formulées à partir de l'observation de cultures cellulaires par microscopie optique (Abercrombie *et al.*, 1970a, 1970b; Abercrombie, 1980) pour expliquer la motilité des cellules, c'est à dire leur capacité à se mouvoir dans leur environnement. Depuis cette époque, beaucoup de ces hypothèses ont eu l'occasion d'être testées grâce aux progrès considérables effectués dans ce domaine. Les dix dernières années ont été particulièrement riches de découvertes avec notament l'avènement de la biologie moléculaire (Pollard *et al.*, 2000), de la génétique (Peckham *et al.*, 1999) mais aussi plus récement, grâce aux dévelopements conjugués des approches biophysiques et biomécaniques (Zhu *et al.*, 2000). Ces différents travaux ont ainsi permis de mieux comprendre les principes d'organisation structurelle et dynamique mis en jeu à l'intérieur de la cellule.

L'observation au microscope de la migration de la cellule sur un substrat bidimensionnel ne permet pas d'imaginer l'extraordinaire complexité des processus conduisant à ce phénomène d'apparence si simple. Malgré les progrès énormes effectués, de nombreuses questions n'ont toujours pas trouvé de réponses définitives. Comprendre et contrôler la motilité des cellules reste l'un des grands challenge de la biologie cellulaire en raison des implications considérables physiologiques et pathologiques de ce processus multifactoriel. En effet, la motilité de la cellule intervient dans de nombreux contextes *in vivo*. Par exemple, la défense de l'organisme à une infection microbienne implique la migration des macrophages. La cicatrisation des plaies implique une migration des cellules du tissu épithelial et du derme. Au cours de l'embryogénèse, la migration des cellules de la crête neurale est essentielle. La migration cellulaire est également un processus clé dans de nombreuses pathologies telles que l'inflammation, qui induit la migration des leukocytes, ou encore la formation de métastases par la migration de cellules cancéreuses qui se détachent du foyer tumoral originel.

Considérant tous ces exemples, il est évident que la capacité de la cellule à se déplacer dépend du bon ou mauvais (selon les cas) fonctionnement de la machinerie interne de la cellule. Cette machinerie implique à la fois la gestion et la distribution de l'énergie pour la génération et l'application des forces nécessaires aux mouvements. Cela est réalisé en coordination étroite avec les mécanismes de perception du milieu extracellulaire et d'intégration des signaux en provenance de l'environnement. Le challenge de la compréhension de la motilité cellulaire réside dans cette très grande complexité. Comprendre les mécanismes les plus fins autoriserait un contrôle sur la migration en particulier l'inhibition sélective de la migration selon le type de cellule dont l'importance en cancérologie est de première évidence.

L'une des découvertes majeures sur le comportement des cellules sur laquelle se fonde notre étude, est la mise en evidence au début des années 1990, d'une certaine auto-organisation de la dynamique spontanée des déformations cellulaires jusque là courament considérée comme aléatoire. Il a été démontré pour plusieurs types cellulaires kératinocytes (Alt *et al.*, 1995) , leukocytes (Alt, 1990) et pour l'amibe *Dictyostelium* (Killich *et al.*, 1993, 1994) l'existence de schémas de déformations membranaires récurrents, telle que l'apparition d'ondes en rotation autour du corps cellulaire. Ces observations ont entrainé le dévelopement de plusieurs modèles théoriques (Alt and Tranquillo, 1995; Killich *et al.*, 1994; Le Guyader and Hyver 1997) tentant d'intégrer à la fois des éléments moléculaires, chimiques et mécaniques dans le but de déterminer et de tester l'importance relative des divers éléments et structures cellulaires responsables de cette auto-organisation.

L'existence d'une dynamique spontanée de la cellule, c'est à dire en l'absence de stimulations de la part de son environnement, est un élément fondamental à considérer puisqu'il prédispose la capacité de la cellule à réagir lorsqu'elle se trouvera stimulée. Malgré l'intérêt évident que présente la dynamique cellulaire spontanée, relativement peu d'études s'y sont intéressées, et restent dans la plupart des cas focalisées sur le comportement migratoire.

C'est pourquoi dans notre étude, nous avons choisi de nous intéresser plus spécifiquement au cas de la dynamique spontanée des déformations, que nous avons choisi d'aborder par deux approches complémentaires: (i) une première approche expérimentale, qui porte sur la caractérisation de la dynamique des déformations observées sur des cultures cellulaires par vidéomicroscopie et (ii) une seconde approche théorique, avec la présentation de modèles mathématiques fondés sur des hypothèses mécano-chimiques et destinée à rendre compte de certains aspects de nos observations expérimentales. Les deux approches font respectivement l'objet de deux des trois grandes parties de la thèse.

La première partie présente l'état de l'art de la dynamique des mouvements cellulaires (motilité cellulaire). Le but de cette première partie est de rappeler quelques aspects essentiels de la structure et de la dynamique de la cellule, de façon à ensuite pouvoir aborder les éléments de notre problématique et enfin de développer les choix de notre approche pour tenter de répondre aux diverses questions soulevées. Cette partie se subdivise en quatre chapitres. Le chapitre 1 donne une description de la cellule et de son architecture et fait une présentation des divers états dynamiques et de leurs motivations. Le chapitre 2 présente une revue des différents mécanismes proposés pour rendre compte de la protrusion cellulaire. Le chapitre 3 présente un revue des techniques utilisées pour la caractérisation mécanique de la cellule et plus spécialement du cytosquelette et de la membrane. Enfin le chapitre 4 présente les choix

et les motivations de notre approche qui couple une analyse expérimentale à la modélisation théorique.

La seconde partie, consacrée à notre approche expérimentale, concerne la caractérisation quantitative de la dynamique des déformations membranaires de fibroblastes en culture, realisée à partir de l'analyse de séquences d'images acquises par vidéomicroscopie. Le chapitre 5 décrit les matériels et méthodes utilisés et en particulier les méthodes qui permettent d'extraire des séquences d'images les données morphodynamiques pertinentes. Le chapitre 6 présente les résultats de la caractérisation de la dynamique spontanée et le chapitre 7 les résultats de la caractérisation dans le cas d'interaction de type contact entre cellules.

La troisième partie est consacrée à la modélisation théorique des divers aspects de la dynamique cellulaire. Le chapitre 8 présente les hypothèses mécano-chimiques d'un modèle des déformations spontanées précédement utilisé et explore sa capacité à décrire de nouveaux comportements dynamiques de nature de ceux observés dans notre étude expérimentale. Deux extensions de ce modèle de base sont proposées pour rendre compte de deux situations typiques d'interactions de la cellule avec son environnement, c'est à dire d'une part les interactions cellule-cellule que nous avons abordé expérimentalement, et d'autre part la migration cellulaire induite par un gradient de facteur extracellulaire. Ces deux cas sont traités respectivement dans les chapitres 9 et 10. Enfin le chapitre 11 présente une extension du modèle initial dans le but d'une approche plus réaliste de la dynamique membranaire dans le cas de fortes déformations. Diverses perspectives d'extensions de ce nouveau modèle sont abordées.

En conclusion générale, nous présentons une synthèse de nos résultats dans le contexte des découvertes les plus récentes de façon à proposer les perspectives qui découlent de ce présent travail.

The study of cell membrane deformations and cell migration is part of the more general study of cell behaviour. The aim of this study is to understand what are the internal phenomena which animate the cell and make it deform and migrate, but also how the cell perceives its environment, integrates the external informations and reacts in an adapted way. Understanding these phenomena requires a multi-disciplinary approach which considers at the same time molecular and biochemical aspects as well as physical and mechanical aspects.

The interest for cell behaviour has been initiated by the work of Abercrombie (Abercrombie and Heaysman, 1953) in the fifties. Many hypotheses have since been formulated from cell culture observations by optical microscopy (Abercrombie *et al.*, 1970a, 1970b; Abercrombie, 1980), to explain the motility of the cells, namely their ability to move in their environment. Since that period many of these hypotheses could be tested thanks to the considerable progress made in this field. The last ten years have been especially rich,

not only with discoveries in the advent of molecular biology (Pollard *et al.*, 2000) and genetics (Peckham *et al.*, 1999) but also more recently, thanks to the combined developments in biophysics and biomechanics (Zhu *et al.*, 2000). These various works have thus allowed a better understanding of the structural and dynamical organization principles involved inside the cell.

Observation with the microscope of the cell migration on a bidimensional substrate does not allow to imagine the extraordinary complexity of the processes leading to this apparently so simple phenomenon. Despite the huge progress made, lots of questions concerning cell motility still remain unanswered. Understanding and controlling cell motility remains one of the biggest challenge of cell biology because of the considerable physiological and pathological implications of this multifactorial process. Actually there are many cases in which cell motility takes place *in vivo*. For example, the defense of the organism to a microbial infection involves the migration of macrophage cells. Wound healing requires the migration of epithelial tissue cells and dermal cells. During embryogenesis, migration of neural crest cells is essential. Cell migration is also a key process in numerous pathologies such as inflammation which leads to leukocytes migration or the formation of metastasis with the migration of cancer cells which detach from the original tumour.

Considering all these examples it is obvious that the ability of the cell to move depends on the good or bad (depending on the case) functioning of the internal cell machinery. This machinery implies both the management and distribution of energy for the generation and application of the forces required for the movements. This is realized in close relationship with the mechanisms of perception of the extracellular medium and the integration of the signals from the environment. The challenge of understanding cell motility lies in this big complexity. Understanding accurately the mechanisms involved would allow a control on migration, in particular the selective inhibition of migration for a given cell type whose importance to cancerology is more than obvious.

One of the major discovery on cell behaviour on which our study is based is the demonstration at the beginning of the nineties of a certain self-organization of cell spontaneous deformation dynamics which was until then widely considered as random. It was demonstrated for various cell types such as keratinocytes (Alt *et al.*, 1995) , leukocytes (Alt 1990) and the dictyostelium amoebae (Killich *et al.*, 1993, 1994) the existence of recurring patterns of deformation such as the appearance of rotating waves of deformation around the cell body. These observations have driven the development of several theoretical models (Alt and Tranquillo, 1995; Killich *et al.*, 1994; Le Guyader and Hyver, 1997) which tried to integrate molecular, chemical and mechanical elements in order to determine and test the relative importance of the various elements and structure of the cell responsible for this self-organization.

The existence of cell spontaneous dynamic, namely outside any stimulations from its environment is a fundamental element to consider as it predisposes the ability of the cell to react once stimulated. Despite the relevance of the spontaneous cell dynamic, relatively very few studies have been interested in it and remain for most of the cases focused on the migratory behaviour.

That is why in our study we have chosen to focus more specifically on the spontaneous deformation dynamic case. We chose to tackle this case from two complementary

approaches, a first experimental approach deals with the characterization of deformation dynamic observed on cultured cell by mean of videomicroscopy and a second theoretical approach focuses on the presentation of mathematical models based on mechano-chemical assumptions in order to explain some aspects of the experimental observations. Both approaches are respectively the subject of two out of the three parts of the thesis.

The first part presents the state of the art of cell motility. The aim of this first part is to give the necessary requirements on the cell in order to further tackle the elements of our problem and to be able to develop the choices of our approach to try to answer the various questions evoked. This part is divided in four chapters. Chapter 1 describes the cell and its architecture and presents the various dynamical states and their aims. Chapter 2 presents a review on the various mechanisms proposed to account for cell protrusion. Chapter 3 presents a review on the techniques used to characterized mechanically the cell and especially the cytoskeleton and the membrane. Finally chapter 4 presents the choices and motivations of our own approach which couples experimental analysis and theoretical modelling.

The second part, devoted to our experimental approach concerns the quantitative characterization of dynamics of membrane deformations of cultured fibroblasts from the analysis of image sequences acquired by video-microscopy. Chapter 5 describes the materials and methods used and in particular the methods which allow us to extract from the image sequences relevant morphodynamical data. Chapter 6 presents the characterization results of the spontaneous dynamics and chapter 7 the characterization results in case of cell-cell interactions.

The third part is devoted to the theoretical modelling of various aspects of the cell dynamic. Chapter 8 presents the mechano-chemical hypotheses of a model for spontaneous cell membrane deformations previously used and explores its ability to describe new dynamical behaviours such as those observed in our experimental study. Two extensions of this model are proposed in order to take into account two typical interaction situations of the cell with its environment, namely the case of cell-cell interactions which we have considered experimentally and the case of cell migration induced by an extracellular gradient. Both these cases are respectively considered in the chapters 9 and 10. Finally chapter 11 presents an extension of the initial model for a more realistic approach of the membrane dynamic in the case of large deformations. Various perspectives of extension of this new model are suggested.

As a general conclusion, we present a synthesis of our results in the context of the most recent discoveries in order to propose the perspectives which result from this work.

Part I

Cell Motility

Chapter 1

Biological background

Cadre biologique

Il existe environ 200 types de cellules dans le corps humain qui s'organisent essentiellement en deux types de tissus: le tissu épithélial, qui isole les organes où les cellules sont organisées dans des structures en feuillets, et le tissu conjonctif (ou tissu de maintien) où les cellules (fibroblastes) sont disposées à travers un réseau de filaments de collagène composant de la matrice extracellulaire. *In vivo* la plupart des cellules sont amenées à migrer lors de cas pathologiques ou de stress (cicatrisation, inflammation, formation de tumeur). La migration cellulaire est déclenchée la plupart du temps par une stimulation externe à l'exception de la migration des cellules tumorales qui acquièrent cette capacité indépendement de cause externe directe.
La cellule eukaryote possède un noyau baignant dans le cytoplasme retenu par la membrane plasmique. Le milieu cytoplasmique est composé entre autre, du cytosquelette dont il est aujourd'hui admis qu'il constitue la structure responsable des mouvements. Le cytosquelette est constitué de 3 types de filaments interconnectés: les microtubules et les filaments intermédiaires dont les buts essentiels sont de maintenir la polarité et l'intégrité de la cellule respectivement, et les microfilaments d'actine aux propriétés hautement dynamiques. Les filaments d'actine s'organisent en différents types de structures associées à différents comportements dynamiques de la cellule. Lamellipodes et filopodes sont des structures dont la dynamique est liée à la polymérisation/dépolymérisation de l'actine et où les filaments présentent tous la même polarité. Les fibres de stress sont des structures de filaments aux polarités alternées qui autorisent une dynamique contractile en présence de myosine II. La dynamique de l'actine et la formation des structures spécifiques évoquées, est régulée par diverses protéines: (i) les protéines ARP (Actin Related Proteins) dont le complexe protéique Arp2/3 régule en particulier l'assemblage de nouveaux filaments au voisinage de la membrane; (ii) les protéines WASP (Wiskott-Aldrich Syndrom Proteins) qui se lient directement au complexe Arp2/3 pour stimuler sa capacité à nucléer de nouveaux filaments; (iii) les protéines Rho-GTPases (Guanosines Triphosphates) qui sont impliquées en amont, dans la réception et la transmission des signaux externes jusqu'aux complexes WASP-Arp2/3; (iv) enfin les protéines de régulation de la polymérisation qui contrôlent le taux de croissance des filaments en en bloquant l'extrémité

positive (barbed end).

1.1 Introduction

The individual cell is the most basic element of life. Ultimately all spatial organization that living systems undertake is the consequence of the way that individual cells interact with their local environment. There are around 200 types of cells in the human body and these are essentially organized in 2 types of tissue - epithelial tissue, whose role is to permit the separation of the various organs and structures, which is organized into superimposed sheets; and conjunctive tissue, whose role is to maintain the structures, which is made of various types of elastic fibers such as collagen around which another type of cell is organized, namely fibroblasts. Epithelial cells and fibroblasts have different roles and consequently exhibit different morphologies and dynamical states *in vitro* (Figure 1.6). However it is commonly acknowledged that the mechanisms at the origin of the cell movement share the same basic properties.

In vivo, cell motility plays an important role in development phases of embryogenesis during which the cells differentiate. However, once the cells have achieved their specificity and are organized in tissues, motility occurs for most cells in pathological cases such as wound healing, inflammation and tumor growth, as was described in the "General Introduction". In all of these cases, the cell is constrained to change its motile behaviour which necessitates it to break the connections with its environment (either cell-cell or cell-matrix), in order to free itself and migrate. This phenomenon can be triggered by the cell sensing an external stimulus which is either mechanical (such as a change in the topology of the medium through distortions or tensions) or chemical (such as a response to a chemoattractant signal) in nature. Other internal causes might exist which can, for example, be linked to the cell cycle, such as mitosis (cell division) or apoptosis (programmed cell death). Other, less explicit causes, such as genetic mutations of the DNA, may also play a role, and this might be one explanation for the appearance of cancer cells whose origin is still unclear.

Although the reasons which initiate the cells to move may not always be clear, on the other hand, it is now accepted that it is the actin cytoskeleton which is responsible for cell movements. Understanding cell movement therefore means understanding the actin dynamics, the way this dynamic is organized in an autonomous way, and how this is coordinated with internal and external events leading to new motile behaviour of the cell.

Before we go further with the complexity of the phenomena related to cell motility and the associated actin dynamics, we are going to present a basic description of an individual cell which is required for us to tackle our problems. First we will describe the cell structure and secondly, we will describe the various elements involved in cell dynamics.

1.2 Cell structure

1.2.1 Overview

The eukaryotic cell is composed of three essential elements which are:

- the nucleus,
- the membrane, and
- the cytoplasm

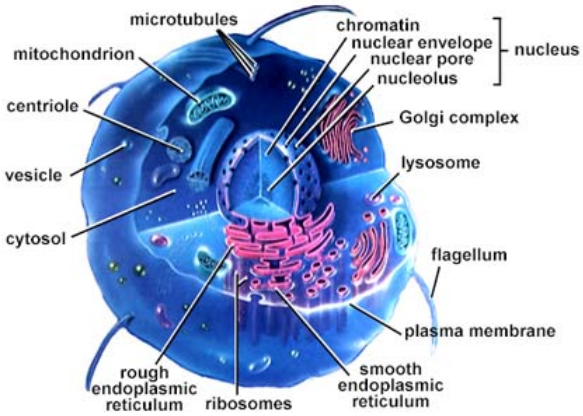

Figure 1.1: Schematic representation of the cell showing all the main structures

The nucleus

The nucleus confines the DNA of the cell in a double membrane (the nuclear envelope) (Figure 1.1). The role of the nucleus is to protect the genome against mechanical forces exerted by the cytoplasmic filaments of the cytoskeleton. The nuclear envelope allows to separate the mechanisms of transcription and translation of the DNA and ensure the selectivity of the exchange with the cytoplasm, thus increasing the number of regulation steps of the protein synthesis (Thiery and Grassi, 1999)

The membrane

The cell membrane is the boundary between the interior of the cell and the external medium (Figure 1.2). Its importance is fundamental for the interaction of the cell with its external environment. The membrane is made of a bilayer of phospholipids which contains numerous protein structures which are necessary for regulating and maintaining chemical differences between the cytoplasm and the external medium. Among these structures, are ionic channels (for Ca^{2+}, K^{+}, Na^{+}, ...) and membrane receptors. Membrane

receptors, once activated, trigger a chain of molecular events whose aim is to transmit the information to the nucleus which will then determine the adapted protein response (signal transduction). Cadherins and integrins are two examples of membrane specific receptors for cell-cell interactions and cell-extracellular matrix interactions respectively.

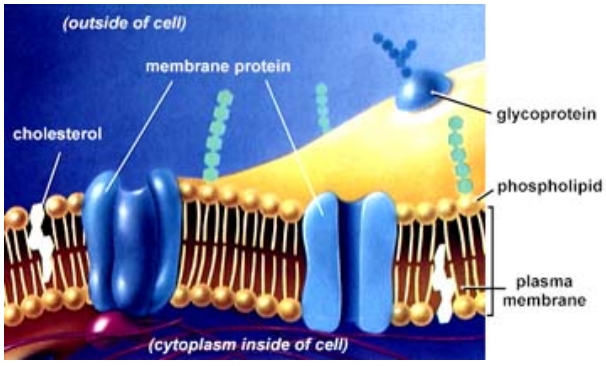

Figure 1.2: Schematic representation of the cell membrane

The cytoplasmic medium

The cytoplasmic medium which occupies the space between the nucleus and the cell membrane is a substance which contains the cytoskeleton and the cell organelles: mitochondria, endoplasmic reticulum, and Golgi apparatus, involved respectively in energy synthesis, protein synthesis and packing and transport of the proteins (Figure 1.1). The organelles are essentially located around the cell nucleus in a zone usually called the cell body. In this thesis, we assume that the dynamics of the cell body does not influence significantly cell membrane deformations. Although the global shape of the cell body may be altered during cell movements, we further assume that its shape remains constant in order to confine our analysis of the movement to the most peripheral part of the cytoplasm, namely the cell cortex.

1.2.2 The cytoskeleton

The cytoskeleton of the cell is the structure mainly responsible for maintaining the cell shape and is composed of three types of filaments:

- microtubules,
- microfilaments, and
- intermediate filaments

Microfilaments form a continuous network connected both to the (discontinuous) network of microtubules and to the endoplasmic reticulum (Figures 1.3 and 1.4).

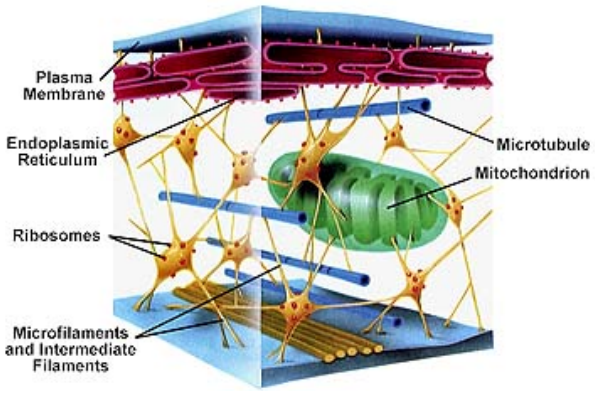

Figure 1.3: Schematic representation of the cell's filamentous network. The upper membrane is the nucleus membrane and the lower one is the cell membrane. On the inner surface of the cell membrane, microfilaments are organized to form stress fibers.

The microtubules

Microtubules appear (in longitudinal section) as thin rods of tubulin (protofilaments) which radiate from a centrosome located near the cell nucleus. In their cross section they appear as hollow tubes ringed by 13 subunits. The outer and inner diameters of the tubes are 30 nm and 14 nm respectively. The lengths of the microtubules vary from 2.5 to 10 μm in endothelial and muscle cells. Microtubules are polarized: they polymerize at one end (from dimers of tubulin α and β) and depolymerize at the other end. The most prominent role of microtubules in the cell is the transport of vesicles and organelles. Disruption of the microtubules with nocodazole, for example, leads to a significant increase in actomyosin-driven contractility (Bornens *et al.*, 1989). This suggests the involvement of microtubules in the stabilization of the cell polarity through the control of forces produced by the cell against the points at which the cell contacts the substrate or the extracellular matrix. Microtubules are also found in cilia and flagella where they participate actively to the propulsion of the cell.

The microfilaments

Microfilaments are 1 or 2 μm long with a diameter of about 5 to 7 nm. They are composed of actin which is one of the most abundant cellular protein, accounting for up to 25 % of the total amount of protein in non-muscle cells. Actin is a polymer (F-actin) of individual globular monomers (G-actin). Actin microfilaments form a double helix of F-actin. The polymerization of the filaments requires both Ca^{2+} and ATP which provides the energy by hydrolysis into ADP. Like microtubules, microfilaments are polarized as they polymerize at one end and depolymerize at the other end. Throughout this process, their length remains more or less constant. Regulation of polymerization and network organization occur via specialized actin binding proteins some of which are outlined in

Protein name	Role of the protein
α-actinin	Bundles actin filaments; binds them to the membrane
Capping protein	Inhibits polymerization at barbed end
Filamin	Cross-links actin filaments into gel
Fimbrin	Bundles actin filaments
Gelsolin	Breaks actin filaments
Profilin	Binds to actin monomers to prevent polymerization
Spectrin	Cross-links actin filaments
Villin	Cross-links and bundles actin filaments
Vinculin	Anchors actin filaments to membranes

Table 1.1: Some actin binding proteins involved in the regulation of F-actin polymerization and network organization

Table 1.1.

The intermediate filaments

Intermediate filaments have a diameter of about 7-11 nm i.e. their size is between the microtubules and microfilaments. Unlike the other two types, which have a rather homogeneous structure and composition, intermediate filaments show wide variations in composition and solubility because of the existence of several classes of these filaments. Moreover, whereas microtubules and microfilaments are rapidly polymerizing and depolymerizing, intermediate filaments appear to be considerably more stable. These filaments are in particular found around the nucleus where they form a dense network which seems to maintain a stable protective structure. Because of their high stability, microfilaments are essentially involved in the maintenance of the overall integrity of the cytoplasm.

From a dynamical point of view, the fact that filaments are polymers allows the cell some measure of reversible control over its shape. In the mathematical models we will formulate, we will not consider intermediate filaments since they are dynamically irrelevant in the cell dynamic. Microtubules, which are found to be mainly involved during cytokinesis and propulsion systems (such as flagella and cilia), are also not considered, even if we agree that their role in stabilization might be important in many dynamical events. In this thesis, we will therefore focus only on the dynamics of the actin microfilaments.

1.3 Cell dynamics

1.3.1 The cell cortex and the actin cytogel

The most dynamical part of cells cultured on a bidimensional substrate (e.g. a petri dish) is the cell cortex. This zone free of organelles is extremely flat (approximately 200 nm thick) and is found at the periphery of the cells. This zone essentially contains actin

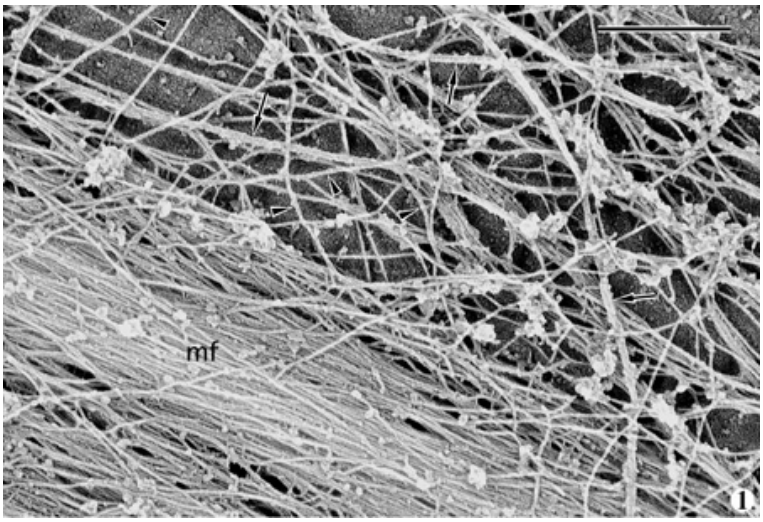

Figure 1.4: Cytoskeletal components in a fibroblast cell: microfilament bundles (mf), microtubules (arrows), intermediate filaments (arrowheads). Scale bar-0.5μm. From Svitkina *et al.* (1995)

under its two forms: filaments (F-actin) and free monomers (G-actin). Actin in the cortex is often described as a gel (the actin cytogel) whose mechanical properties (viscosity, elasticity and contractility) evolve depending on the local amount of F-actin and on the structural organization of the filaments, where the cytogel can either expand or contract (Oster, 1984). The dynamics of the cytogel thus leads to the movements of extension and retraction of the membrane and to the cell shape oscillations.

1.3.2 Actin organization and cell shapes

Cell shape and the nature of the cell movements strongly depend on the F-actin cytoskeleton organization. The F-actin cytoskeleton can be considered as an integrated array of interconnected filament-assemblies, each with a defined architectural organization (see Figures 1.4 and 1.8). The most important actin structures which develop in the cell cortex are lamellipodia and filopodia:

- A lamellipodium is a thin highly dynamic actin-rich band typically less than 0.5 μm thick which is situated at the periphery of many motile cell types. Actin filaments in the lamellipodia form a planar meshwork of unipolar actin filaments whose barbed end (plus end) are oriented outwards (towards the membrane) (Figure 1.5.A). Lamellipodia extend or retract through a combination of actin polymerization at the plasma membrane, depolymerization within the cytoplasm and myosin-mediated rearward movement of the actin fibers.

- Filopodia are long and thin cylindrical extensions of the lamellipodium. Microspikes have a similar structure as filopodia except that they are much smaller. Actin

filaments form bundles in these structures and are all oriented in the same direction (single polarity) (Figure 1.5.B)

An other type of organization of the actin filaments is found in stress fibers which develop in the thickest part of the cytoplasm:

- Stress fibers are formed from bundles of actin but this time with bipolar actin filaments and myosin II which provide them the ability to contract and to exert tension (Figure 1.5.C).

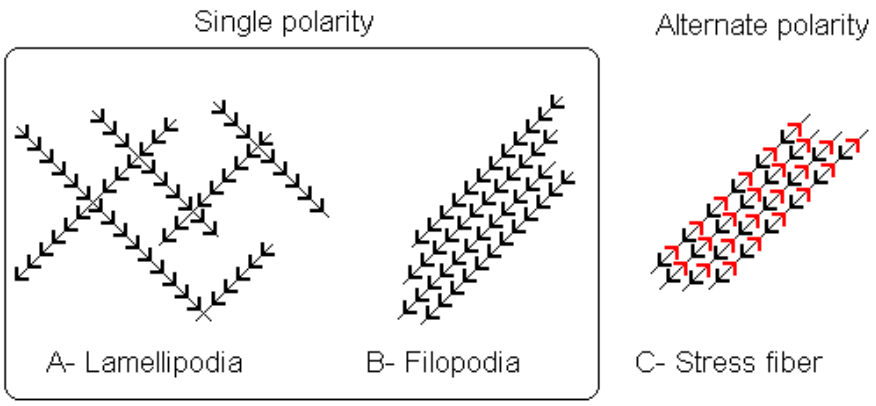

Figure 1.5: Diagram showing the polarity of filaments in the various F-actin structures.

Whereas lamellipodia and filopodia do not require the anchoring of the cell to the substrate in order that they appear, stress fibers do require cell anchoring (via focal adhesion points) to form and develop. The structures described are found with various degrees of importance depending on the cell type and on the dynamical state of the cell, namely the resting state or the migrating state. For example, stress fibers and lamellipodia are the two most prominent actin filaments structures found in fibroblasts (Cramer 1997). We illustrate the morphological differences between the two most widely studied type of cell *vis-à-vis* migration, fibroblasts and keratocytes (Figure 1.6).

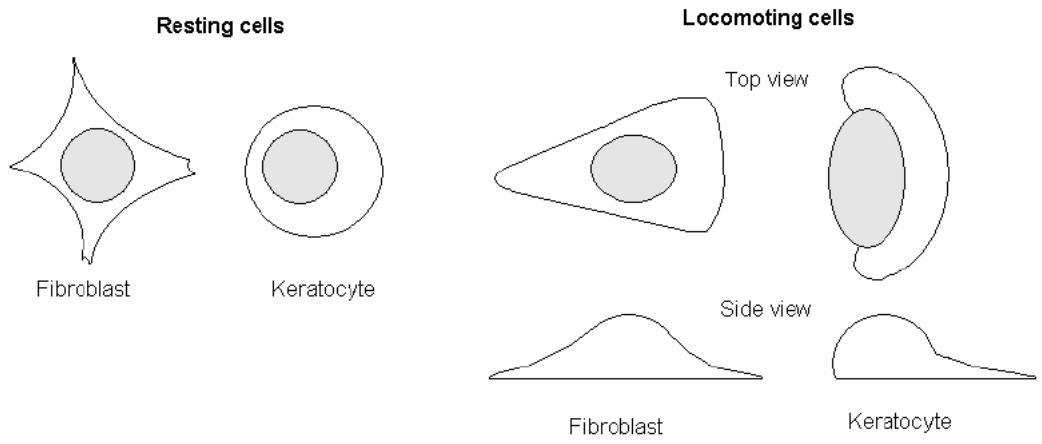

Figure 1.6: Various cell morphologies. In each case the grey area represents the cell nucleus. Resting cells usually display symmetrical shapes whereas locomoting cells are strongly polarized in the direction of migration.

1.3.3 The regulation of actin dynamics

The major molecular players in the control of actin dynamics are:

- actin related proteins (ARP) and more particularly the Arp2/3 complex, which regulates the assembly of new actin filaments at the leading edge of the cells.
- WASP proteins (Wiskott-Aldrich syndrome proteins), which bind directly to the Arp2/3 complex to stimulate its ability to promote the nucleation of new actin filaments (Svitkina and Borisy, 1999).
- Rho-GTPases proteins (Guanosines triphosphatases), which are involved upstream in the reception and transmission of external signals to the WASP-Arp2/3 complex (Hall 1998).
- Capping and severing proteins which are two regulators of actin polymerization which control the growth of the filaments by terminating elongation. They also mediate associations between actin and the plasma membrane and may promote or permit filament elongation under the control of membrane phospholipds (Machesky and Insall, 1999).

The Arp2/3 complex and WASP family

The interest for actin related proteins (ARP) family started in the early 1990s with the discovery of several novel proteins of this family which showed strong similarities with

conventional actin, sharing between 17 and 60 % of the same amino-acids. Since then, understanding the biological function of these proteins has been a major goal (See Schafer and Schroer, 1999 for a review). It appears that Arp proteins usually assemble and form stable complexes. One such protein which has been identified as playing a major role in actin filament assembly is the Arp2/3 complex. This complex is formed of Arp2 and Arp3 proteins together with 5 other proteins (Machesky *et al.*, 1994). The Arp2/3 complex exhibits 3 types of interaction with actin:

- it binds the sides of the filaments (Figure 1.7.A),
- it caps the slow growing pointed end of actin filaments (Figure 1.7.B) and
- it promotes nucleation of actin monomers (Figure 1.7.C).

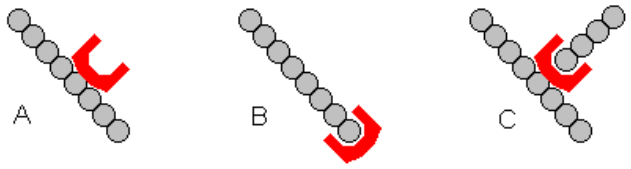

Figure 1.7: Interaction of the Arp2/3 complex with actin filaments

These properties are essential in the regulation of actin assembly as well as in the organization of the actin filaments that contribute to cell motility. The fact that the Arp2/3 complex can bind to the side of actin filaments suggests that this complex is a key element in the organization of the actin filaments into networks (Svitkina and Borisy, 1999).

Arp2/3-induced actin nucleation is activated by some members of the WASP family proteins such as Scar1 protein. In particular, this protein has been shown to enhance the spontaneous assembly of actin monomers *in vitro* in the presence of the Arp2/3 complex (Machesky and Insall, 1999). WASP-related proteins are moreover supposed to help link signal transduction pathways to stimulated actin assembly via small GTP-binding proteins.

In fibroblasts and amoebae, the Arp2/3 complex has been found to be localized by immunofluorescence in the actin-rich cortex at the leading edge of lamellipodia (Machesky *et al.*, 1997; Mullins *et al.*, 1997; Welch *et al.*, 1997). Imaging studies carried out on living cells (Schafer *et al.*, 1998) have moreover shown that the distribution of the Arp2/3 complex is dynamic and is modulated by Rho-family GTPases.

The Rho-family GTPases

The Rho-family of GTPases comprises four major members which are Rho, Rac, Cdc42 and Ras. They have been shown to be key regulators of the actin cytoskeleton in response

to external stimulations (Hall, 1998; Nobes and Hall, 1999). Each of these proteins appear to have a specific role:

- Rho was shown to induce the assembly of contractile actin-based filaments such as stress fibers and of associated adhesion complexes. It seems that Rho may act as a molecular switch to control a signal transduction pathway that links membrane receptors to the cytoskeleton.
- Rac is more specifically involved in the regulation of lamellipodia formation and ruffles, which are membrane folds that appear on the dorsal surface of the cell and travels rearwards (accompanying withdrawal of the lamellipodium).
- Cdc42 has been found to be responsible for filopodium extension. This protein also appears to be required for gradient sensing and cell polarization.
- Ras regulates focal adhesion and stress fibers turnover.

The effects of the proteins reported here on cells concern mainly fibroblasts. Distinct effects of the Rho, Rac, Cdc42 and Ras on the actin cytoskeleton organization have been observed in different type of cells including epithelial and endothelial cells. Although it is clear that the Rho-like GTPases play a pivotal role in the orchestration of changes in the actin cytoskeleton (namely in the elaboration of the signal transduction pathways) in response to receptor stimulation, the specific response of the different cell types depends on the way the stimulation is perceived. Variations of GTPases effects may thus depend on the cell's ability to form integrin-based cell-matrix or cadherin-based cell-cell adhesion complexes (Hall, 1998). A huge amount of literature is specially dedicated to the study of the transduction mechanisms involving Rho-GTPases proteins (Clark *et al.*, 1998; Hall, 1998; Chung *et al.*, 2000; Cox *et al.*, 2001).

Capping and severing proteins

These proteins bind to the barbed end of actin filaments to block their elongation. As most barbed ends in living cells appear to be capped, the removal of the caps in response to signals could trigger rapid and extensive actin polymerization (Machesky and Insall, 1999). Gelsolin is responsible for the severing activity where established filaments are severed and depolymerized by cofilin to maintain a pool of actin monomers required in the polymerization process (Machesky and Insall, 1999).

1.3.4 Parameter values

To complete this section on "Cell dynamics", we present in Table 1.2 the parameters related to actin dynamics.

Parameter	Mean ($\pm SD$)
Rate of the rearward transport of actin meshwork in fibroblasts lamellipodia [1]	13.8 $\mu m/min$
Length increment per monomer for F-actin [2]	2.72 mm/monomer
Mean acute angle subtended by actin filaments and lamellipodium margin	64.7±16.5 deg
Rate of assembly of F-actin at the leading edge	97±16 monomers/filament/s
Rate of actin monomer assembly per μm of margin	23500±8940 monomers/s
Polymerization rate [2]	11 $/s/\mu M$
Depolymerization rate [2]	1 /s
G-actin concentration at the leading edge [2]	8.5±1.4 μM
F-actin density at lamellipodial margin	1580±613μM of F-actin/μm^3
Area density of F-actin at lamellipodial margin	278±106 μM of F-actin/μm^2
Thickness of living lamellipodium	176±14 nm
Number of barbed ends supporting actin assembly per μm of margin	241±100
Density of barbed end associated with front	1370±578/μm^2
Estimated stall force for the barbed end of a rigid, anchored actin filament [3][4]	7.7±1.3 pN
Stall force for a 10μm-wide lamellipodium	18.6±8.3 nN
Stall force of keratocyte [5]	45 nN
Stall pressure for a lamellipodium	10.5±4.8 kPa

Table 1.2: Parameters taken from Abraham *et al.* (1999) where: [1] Fisher *et al.* (1988), [2] Pollard (1986), [3] Hill (1981), [4] Peskin *et al.* (1993), [5] Oliver *et al.* (1995)

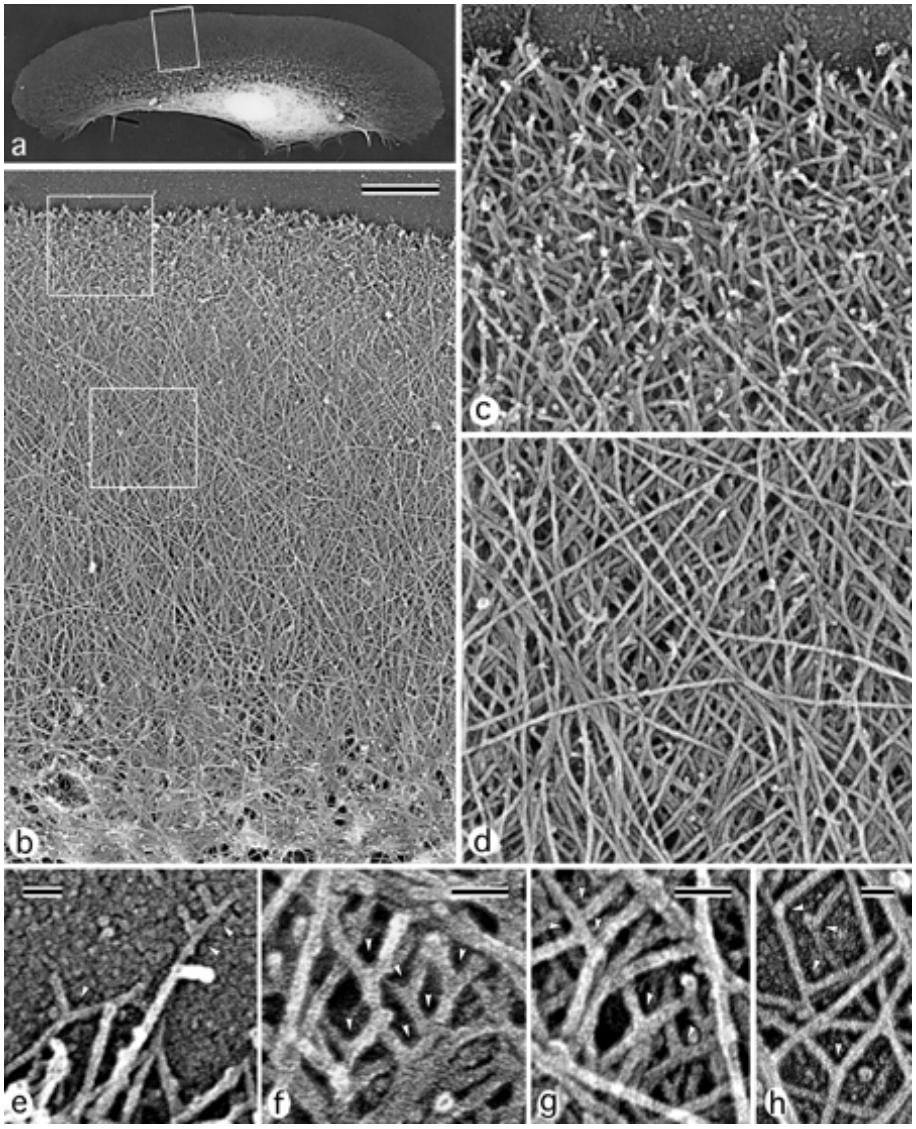

Figure 1.8: Visualization of the dense array of actin microfilaments in the lamellipodia of a keratocyte (a-d), and visualization of the filaments branching (e-h). Scale bar-0.1μm (b) and (d) same magnification as (c). From Svitkina and Borisy (1999b)

Chapter 2

Review of the hypotheses for cell protrusion and shape oscillations

Revue des hypothèses pour la protrusion et les oscillations de la forme cellulaire

Dans ce chapitre sont regroupées les principales hypothèses formulées dans le but d'expliquer soit le mécanisme de protrusion cellulaire (mécanisme local), soit les oscillations de la forme des cellules (mécanisme global). Les modèles locaux sont souvent associés au cas de la protrusion comme étape dans la migration, tandis que les modèles globaux tentent de rendre compte de la dynamique spontanée de la cellule. Bien que ces deux situations soient différentes, en particulier en ce qui concerne les causes du mouvement, il est admis que les mécanismes impliqués dans les deux cas ont les mêmes propriétés de base. Les modulations de ces propriétés sont supposées rendre compte des différences de comportement. Il existe quatre théories principales pour expliquer la protrusion membranaire; la théorie de la transition sol/gel proposée par Oster (1984) propose qu'une fuite locale d'ions à travers la membrane induit une augmentation locale du taux de calcium dans la cellule qui entraine la solation (expansion) du gel d'actine. L'expansion du gel est ainsi responsable de la protrusion de la membrane sur laquelle il exerce une force de pression croissante. Lorsque le taux de calcium re-décroit, l'actine se re-gélifie par re-formation des chaînes de filament et entraine la rétraction du réseau et par continuité, de la membrane. Une seconde théorie propose que la polymérisation de l'actine au voisinage de la membrane est la cause de la protrusion (Borisy and Svitkina, 2000; Abraham *et al.*, 1999; Carlier and Pantaloni, 1997; Theriot and Mitchison, 1991). Dans ce cas là, un mécanisme d'incrément Brownien a été proposé pour expliquer l'intercalation des monomères d'actine entre l'extrémité des filaments et la membrane (Peskin *et al.*, 1993; Mogilner and Oster, 1996). Dans ce mécanisme, l'espace nécessaire est créé par les fluctuations thermiques de la membrane et/ou les ondulations des filaments d'actine. La présence de monomères d'actine en quantité suffisante est assurée par la dépolymérisation de l'extrémité négative des filaments et par la diffusion rapide des monomères le long de ces filaments jusqu'à leur extrémité positive (Carlier and Pantaloni, 1997). L'hypothèse des moteurs moléculaires propose un rôle actif à la

myosine I qui couplée aux filaments d'actine, les propulsent par divers mécanismes en direction de la membrane, générant ainsi la protrusion (Small *et al.*, 1993; Lee and al., 1993).
L'hypothèse de la pression intracellulaire (Bereiter-Hahn and Luers, 1998) comme cause protrusive est suggérée par la contractilité du réseau d'actine en présence de myosine II. Dans cette théorie, les contractions du complexe d'actomyosine sont supposées générer des flux cytoplasmiques à travers la cellule qui augmentent la pression sur la membrane et entrainent sa protrusion là où celle-ci se trouve moins fortement liée au cytosquelette.
En ce qui concerne la modélisation des oscillations de la forme des cellules, 3 théories ont été retenues. La première montre que les oscillations observées sur des cellules dont le réseau microtubulaire a été détruit, peuvent être reproduites à partir d'un modèle de réaction-diffusion (Le Guyader and Hyver, 1997). Le modèle se base sur un ensemble de réactions autocatalytiques prenant en compte l'actine-F sous deux formes, liée à la membrane et libre, ainsi que les protéines de nucléation. Un second type de modèle considère les propriétés mécaniques du cytogel en relation avec la cinétique moléculaire du processus de polymérisation/dépolymérisation de l'actine (Lewis and Murray, 1992; Alt and Tranquillo, 1995). Le cytogel est caractérisé mécaniquement par ses propriétés viscoélastiques et contractiles. La force protrusive est supposée provenir de la pression intracellulaire. La prise en compte des propriétés mécaniques de la membrane, en plus de celles du cytogel, permet de générer des déformations très réalistes de la membrane telles que celles observées sur des keratinocytes (Alt *et al.*, 1995).

2.1 Introduction

In this chapter we present a review of the main hypotheses concerning actin dynamics which are proposed to explain either the mechanism of cell membrane protrusion (a local mechanism) or cell shape oscillations (a coordinated mechanism throughout the cell cortex).

Local models for cell protrusions usually concern the extension of the lamellipodium in connection to cell locomotion. In contrast, global models aim to describe the oscillatory and coordinated movements of the cell membrane, even in the case of a resting cell. Even if these 2 cases are quite different, especially concerning the cause of the movement and the morphologies displayed, it is assumed that the mechanisms involved share the same basic properties to a certain extent. Modulation of these properties would account for the different behaviours.

2.2 Local membrane protrusion

2.2.1 The solation/gelation model of Oster

The above model was proposed by Oster (1984), to explain the alternating rhythmic extension and contraction of a lamellipod. The motion of the cell is assumed to be driven by cycles of solation (expansion) and gelation (contraction) of the cortical actin gel, controlled by the level of calcium. An ionic leak triggers a release of the calcium assumed to be contained in internal membrane compartments distributed throughout the cytogel. The

elevated level of calcium activates solating factors such as gelsolin or severin. These factors break the gel network either by breaking the network chains or breaking the cross-links joining the network chains, or by inducing depolymerization of the chains. The number of chains capable of supporting the tensile stress of the gel network thus decreases. The gel is thus allowed to swell until a new equilibrium is reached between the swelling pressure and the elastic pressure. When the calcium is re-sequestered, the chains start to reform and re-gelation of the network occurs, increasing the gel elasticity which becomes able to contract again. Elevated calcium levels activate the actomyosin contractile machinery. When calcium falls, the actin contraction cycle commences. Calcium increase both triggers solation of the gel and activation of the actomyosin machinery, since there exists a micromolar window for contraction. Moreover, calcium is autocatalytically released when a threshold level is reached (Jaffe, 1980) in order to restart solation of the gel and commence a new cycle (Figure 2.1).

In this model activation of solation/gelation cycles thus requires an initial ionic leak at the leading edge of the membrane to trigger the first local increase in calcium concentration. Several hypotheses are proposed for the origin of this ionic leak. For example, it can be triggered either by the binding of ligands to membrane receptors or by electrical depolarization of the membrane or by mechanical stress at adhesion sites. Because of the necessity of an initiating process, this model is only valid when dealing with *cell locomotion*. In the case of *spontaneous membrane movements* there is nothing to trigger the cycle, and therefore the origin of the oscillations should be explained by a different process.

2.2.2 Actin polymerization

An alternative view for local cell membrane protrusion is that the process of actin polymerization at the leading edge of the cell can be responsible for the cell membrane extension (Borisy and Svitkina, 2000; Abraham *et al.*, 1999; Small *et al.*, 1993; Carlier and Pantaloni, 1997; Theriot and Mitchison, 1991). Indeed, it is commonly accepted that actin polymerization is a key event to power locomotion which occurs in response to external stimuli (Condeelis, 1993a). The two major questions raised by this theory are:

1. How does actin push ?
   Or, how can a subunit elongate a filament abutting a surface ?

2. What are the mechanisms which control the F-actin/G-actin ratio ?

The hypotheses formulated to answer these two fundamental questions are considered in the two following sections.

The Brownian ratchet mechanism

This mechanism has been proposed by Peskin *et al.*, (1993) to provide an explanation for the intercalation of actin monomers between the growing end of the actin filaments and the cell membrane. According to this mechanism, random fluctuations of the membrane create gaps so that the actin monomers can bind to the actin filaments, thus rectifying the

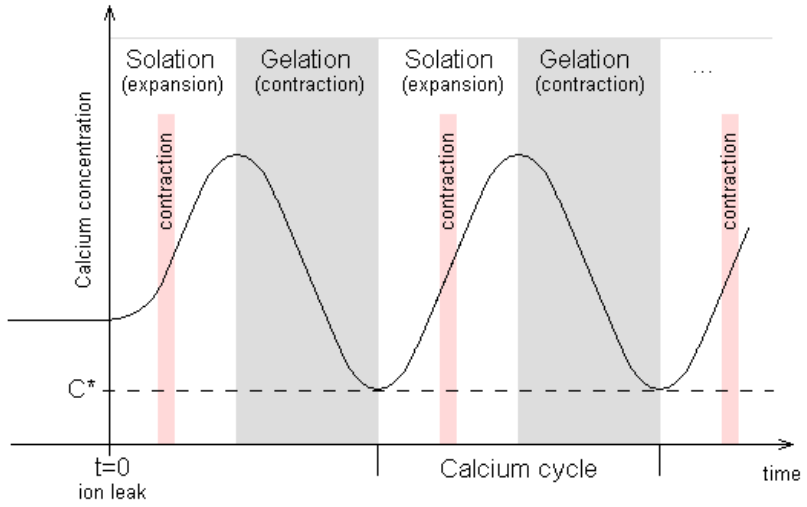

Figure 2.1: The solation/gelation cycle triggered by an ionic leak. Solation stops when calcium starts to be re-sequestered. C^* represents the threshold concentration of calcium from which calcium is autocatalytically released in order to start a new cycle. When calcium starts to increase it activates the actomyosin machinery in a micro-molar window. Contraction occurs during a short period in the solation process, until the number of chains becomes insufficient.

thermal motion of the membrane (Figure 2.2.A). The binding free energy of polymerization (13.6 k_BT per monomer) is assumed to supply the free energy required to implement the ratchet mechanism.

This hypothesis explains filopod-type protrusions, since the filaments are parallel to the load of the membrane. However it is not clear how this process acts for lamellipodial protrusion where the filaments present various other orientations relative to the membrane. In this case, it is difficult to see how the thermal motion can be efficiently rectified.

Molginer and Oster (1996) proposed an extension of the Brownian ratchet mechanism to solve this question. They assumed that the thermal fluctuations concern not only the membrane but also the actin fibers. In the latter case, thermal motion comes from the bending undulations of the fibers as they bend much more easily than they compress. They showed that if the membrane fluctuations are not sufficient to permit intercalation of monomers (this occurs, for example, when the membrane is loaded with proteins) then the filament tips undulations can accommodate intercalation to drive protrusion (Figure 2.2.B). In this case, the optimal filament angle for polymerization (angle relative to the perpendicular direction with the membrane) calculated theoretically is 48 degrees (Mogilner and Oster, 1996). This result was shown to be consistent with the measurements of Small (1995) for lamellipodia of fish epidermal keratocytes whereas the value reported in Table 1.2 gives 65 degrees (Abraham *et al.*, 1999). However if the membrane fluctuations are sufficient for monomer intercalation, then the optimal filament angle calculated is 0,

i.e. the filaments are parallel to the axis of the load of the membrane. This leads to the filopod-type protrusion considered by the initial model. Therefore, the new assumption of filament thermal fluctuations as an alternative to membrane fluctuations allows one to reconcile in a single theory an explanation valid for both filopodial and lamellipodial type protrusions.

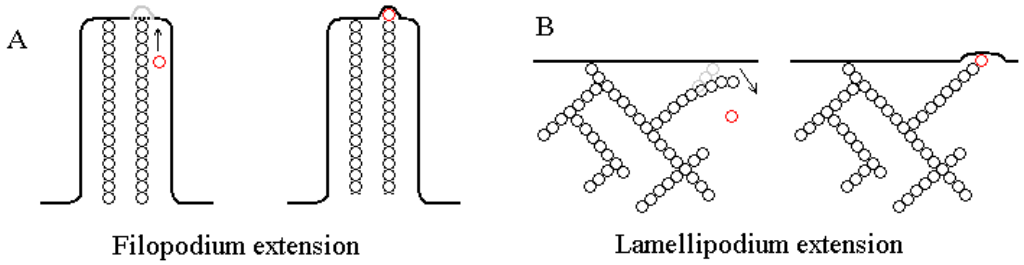

Figure 2.2: (A) membrane fluctuations can account for filopodium extension (in that case, the load of the membrane is parallel to the filaments) whereas in lamellipodium extension (B) undulations of the filament tip is required.

Treadmilling and nucleation release processes

In this section we present two mechanisms which were proposed to explain how the polymerization and depolymerization processes are connected in order to maintain a pool of available actin monomers which are necessary to sustain the forward protrusion mechanism.

The treadmilling process suggests that the actin subunits coming from the depolymerization of the rear of the lamella are recycled into new filaments assembled at the front (Carlier and Pantaloni, 1997) by diffusion along the filaments. This process is reported to be observed on locomoting keratocytes by Small (1995). The whole process is known to be mediated by capping proteins at both the pointed (depolymerization) and the barbed end (polymerization) of the filaments. However the full array of molecular mechanisms involved is still unclear.

The nucleation-release process is globally similar to the treadmilling process except that in this case, filaments are nucleated individually and later become connected to each other (Borisy and Svitkina, 2000). Moreover, in this model, filaments are uncapped and consequently depolymerization can occur at both ends of the filaments. This latter requirement was proposed by Theriot and Mitchison (1991) as a necessary condition to explain the uniform steady-state filament distribution observed in their moving keratocytes. The second argument proposed in favour of the nucleation-release process is that the rate of the treadmilling process is too slow to account for the movements of the keratocytes.

2.2.3 Molecular motors

The involvement of myosin-I has been proposed in many papers in different mechanisms (Small *et al.*, 1993; Condeelis, 1993b; Abraham *et al.*, 1999; Lee *et al.*, 1993). Small *et al.*, (1993) proposed a mechanism for cell protrusion which explains the observations of Theriot and Mitchison (1991) where moving keratocytes appear stationary relatively to the substratum. In this model (Figure 2.3.A) actin polymerization is coupled with myosin-I molecules. Membrane bound myosin-I molecules move along actin filaments (rendered stationary to the substrate via transmembrane linkages) at the same rate as actin depolymerizes. In this model myosin-I is also supposed to create the gap between actin filament ends and the membrane to allow insertion of the monomers. The monomers are transported anteriorly by myosin-I in order to feed the polymerization process.

An alternative view, described in the paper of Lee *et al.*, (1993) , proposes that myosin-I moves towards the barbed ends of actin filaments which are bounded to the substrate via transmembrane linkages (Figure 2.3.B). Actin filaments that are bound to myosin-I but not fixed to the substrate are pushed forward by myosin-I through a sliding movement, thus generating the protrusive force.

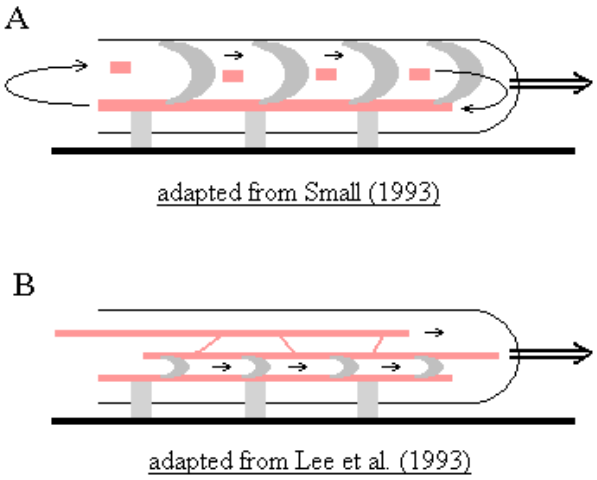

Figure 2.3: A- Myosin molecules (arc-shaped) are bound to the membrane and move along actin filaments at the same rate as actin depolymerizes (actin monomers and filaments appear in red). Myosin I is assumed to create the gap between the tip of the filament and the membrane to allow monomer intercalation. B- Actin filaments (in red) bound to myosin I molecules (arc-shaped) are pushed when myosin I moves towards the barbed end of the filaments oriented towards the membrane.

2.2.4 Intra-cellular pressure

The presence of myosin-II in the cell cortex suggests another possible mechanism often proposed to account for cell protrusion (Bereiter-Hahn and Luers, 1998; Alt *et al.*, 1995; Alt and Dembo, 1999; Abraham *et al.*, 1999). In this mechanism, contractions generated by the actomyosin complex are assumed to create cytoplasmic flux through the cortex. This flux increases the internal hydrostatic pressure which then pushes on the membrane and leads to protrusions where the links membrane/cortex become too weak to prevent extension. As we will see this phenomenon can account for protrusion in global cell shape oscillations (Alt and Tranquillo, 1995).

2.3 Shape oscillations

Cell shape oscillations are widely considered to occur through random movements. However some studies have shown that for different cell types there exists a certain auto-organization in the spontaneous dynamics of the cell movements. In particular, Killich *et al.*, (1993, 1994) have reported the appearance of various organized patterns of deformation for the amoebae *Dictyostelium discoideum*. They were able to simulate mathematically all the patterns observed on the basis of interacting sinusoidal waves. They suggested that these waves could be generated by the actin polymer dynamics. This hypothesis has been tested successfully in various models either based on chemical or mechanical assumptions. We present in this section examples of each model.

2.3.1 A chemical model (Le Guyader and Hyver, 1996)

A reaction-diffusion model is proposed to account for the periodic oscillatory dynamic of an actomyosin ring of human lymphoblasts, released by the disruption of the microtubules cytoskeleton with nocodazole. Experiments of Bornens *et al.*, (1989) using immunocytochemical labeling show that actin undergoes an overall oscillatory behaviour correlated with the movements of the ring. F-actin, either linked to the membrane or free in the cortex, appears to participate with myosin in the construction of the ring. Bornens *et al.*, (1989) proposed that nucleation proteins are involved and their concentrations oscillate from one pole of the cell to the other. This allows polymerization of new actin filaments which can be recruited for the formation of the ring and released after its passage.

The model thus considers 3 variables representing respectively, the nucleation proteins, F-actin bound to the membrane and free F-actin. The system of reaction-diffusion equations is built on the following hypotheses:

1. an autocatalytic synthesis of membrane-bound F-actin from nucleation proteins
2. an autocatalytic reaction controlling the transformation of membrane-bound F-actin into free F-actin
3. the depolymerization of F-actin

The results obtained by Le Guyader and Hyver with this model are in good agreement with the experimental observations of Bornens *et al.*, (1989) and they conclude that the oscillatory behaviour observed can be considered as a component of the F-actin system.

2.3.2 Mechanochemical models

The actomyosin cytogel model (Lewis and Murray, 1992)

The model proposed by Lewis and Murray (1992) is based on the hypothesis that the forces involved in the cell movements are generated by the contractile actomyosin gel. Following the idea of sol/gel transition proposed by Oster (1984), as a mechanism for cell protrusion, the model incorporates similar coupling between the molecular structure of the cytoplasm and its mechanical properties. Such mechanochemical models are usually represented by a system of partial differential equations describing quantitatively the sol/gel chemical kinetics and the associated stress-strain mechanical relationship within an element of cytogel. The model thus consists of two coupled equations. One represents the chemical dynamics of the gel whose kinetics is regulated by two strain-dependent rates converting gel into sol and sol into gel respectively (Figure 2.4.A). The second equation reflects the mechanical balance at any given time of the stress components acting upon the cytogel. These stress components whose qualitative behaviour is given in Figure 2.4.B are:

- a viscous stress σ_v,
- an elastic stress σ_e,
- an active traction σ_a and
- an osmotic pressure σ_{os}

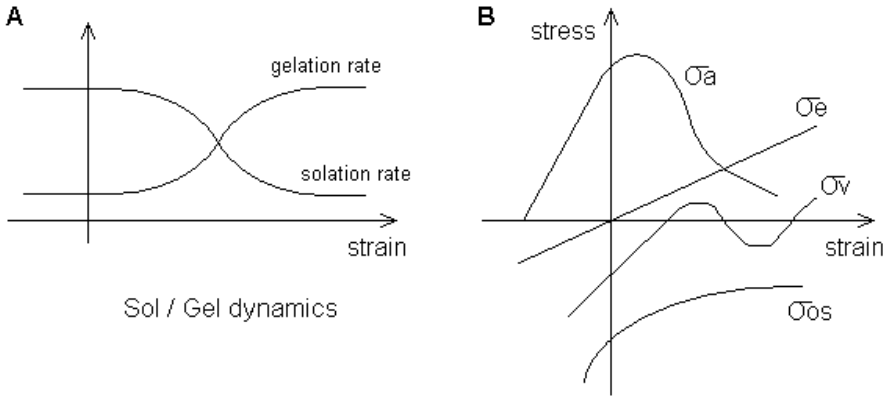

Figure 2.4: A- Sol/gel dynamics as a function of the strain. B- Stress-strain relationship for an actin gel (shown here for a constant gel concentration)

The ability of the actomyosin complex to generate intra-cellular force for movements and pattern formation is investigated through the model. In particular, patterns of actin density generated from simulations of the model appear to be able to explain the appearance of microvilli at the surface of cells.

The cytomechanical model (Alt and Tranquillo, 1995)

Keratinocytes when cultured on a bidimensional substrate exhibit strong and dynamic deformations. The outer cell periphery undergoes protrusion and retraction of pseudopods at different locations around the cell periphery. It is assumed that the cortical actin network and its polymerization/depolymerization dynamic is the motor for cell deformations. The model of Alt and Tranquillo (1995) concerned with cell movements is thus based on three hypotheses concerning the polymer dynamic. The polymer network is able to:

1. contract via myosin interaction like in muscle cells,
2. disassemble into monomeric actin at locations where it becomes condensed or where it is not needed any more,
3. to reassemble at locations where it is required as in protruding lamellipods.

The model moreover assumes that minor changes in hydrostatic pressure inside the cell are responsible for cell protrusion. Actin polymerization is thus considered as a secondary event which occurs spontaneously when enough space is available for the intercalation of monomers near the membrane. The movements of the membrane in the radial direction then result from a force balance between:

- the internal hydrostatic pressure,
- the retraction exerted by the filaments connected to the membrane and whose intensity depends linearly on the local amount of actin,
- a curvature-dependent stress due to the surface tension of the cortical actin-membrane complex, and
- a friction force due to the movements of the lamella.

Similarly the force balance in the tangential direction involves:

- a friction term,
- a shear stress due to the movement of actin in the cell cortex,
- a contraction/swelling stress depending in a non-linear way on the local actin density and
- a curvature-dependent compression/relaxation of the network.

The model thus consists of a system of partial differential equations which couples chemical events (actin polymerization/depolymerization dynamics) with mechanical forces. The model consists of 3 variables which are the actin density, the actin displacement velocity in the cortex and the length of the membrane extension from the cell body.

Simulations show that this model is able to capture the main features of keratinocyte deformations, namely the alternated and coordinated movement of extension/retraction of the protrusions around the cell body.

2.4 Discussion

This review chapter shows the huge complexity of the problem of cell motility and the difficulty in reconciling the various hypotheses formulated. For example, the theory of actin polymerization as the leading event for protrusion is often presented in opposition to the theory of pressure-driven extension. At first sight these two theories appear to contradict each other, since in the first case protrusion occurs due to a high level of actin being produced near the membrane, whereas in the second case the actin density should be low so that the bond between the network and the membrane is sufficiently weak to allow the pressure to push on the membrane.

However, both hypotheses are strongly supported experimentally, so there is no reason to favour one more than the other. Therefore it appears necessary to find how to make these apparently opposite and conflicting theories coexist.

One solution already suggested by Alt and Tranquillo (1995) (and confirmed by their simulations) is that the pressure replaces or reinforces the Brownian ratchet mechanism to provide the free space required for monomer intercalation between the tip of the filaments and the membrane. With this theory, the amount of actin is initially low and increases through the treadmilling process once the polymerization is initiated.

Another solution is to identify the dynamical state of the cells in which these mechanisms are more likely to occur. Indeed, polymerization-driven protrusion is always reported in the case of migrating cells. As was seen in the section concerning actin dynamics regulation, polymerization is activated through a cascade of molecular events initiated by the Rho-GTPases which are the proteins involved in signal detection. Consequently it appears that polymerization-driven protrusion has to be related and restricted to the case of cell migration.

On the other hand, the effect of the internal pressure pushing on the membrane exists permanently in the cell, but the effective membrane protrusion only occurs when the pressure is able to overtake the resistive force of the network bound to the membrane. It is assumed that the contraction of the actomyosin network may be responsible for increasing this pressure. Therefore pressure-driven protrusion is visible in the case of resting cells. This mechanism is in particular often used to model spontaneous and coordinated deformations as the pressure should be balanced throughout the whole cell cortex. It can be assumed that once the locomotion process is initiated, the mechanism of polymerization-driven membrane extension dominates the effects of pressure. This solution is perhaps the best reconciliation of the two competing theories as it can account for most of the

experimental observations.

It is obvious that the mechanisms involved in governing a particular behaviour of a cell are not exclusive and are often the result of the coordination of many simultaneous processes. Therefore it is important to be aware of the limits in which a particular mechanism occurs. The determination of its context and limitations is as important as the mechanism itself.

Chapter 3

Mechanical characterization of the cell

Caractérisation mécanique de la cellule

Ce chapitre présente un panel des méthodes principalement utilisées pour la caractérisation de la mécanique cellulaire. Cette caractérisation consiste essentiellement en la détermination des propriétés visco-élastiques du cytoplasme (et du réseau de filaments) et en la détermination des propriétés élastiques de la membrane.
Ces méthodes sont classées en 2 catégories. La première catégorie concerne les méthodes actives, c'est à dire les méthodes où les paramètres viscoélastiques sont déterminés à partir d'une interaction mécanique directe avec la cellule. Les méthodes présentées sont: la méthode d'aspiration par micropipette, la manipulation par microplaques, les pinces optiques, les pinces magnétiques et la microscopie par force atomique.
La seconde catégorie concerne les méthodes passives qui sont au contraire non-invasives pour la cellule. Les méthodes présentées sont: la méthode de microrhéologie par détection laser de microparticules naturelles dans la cellule, la méthode spectroscopique de diffusion d'onde, la méthode de microscopie acoustique et les méthodes utilisant des substrats déformables.
Les paramètres obtenus par l'ensemble des méthodes présentées sont complétés par les résultats issus d'autres méthodes de façon à proposer une caractérisation globale de l'ensemble des propriétés mécaniques de la cellule qui seront par la suite nécessaires à l'élaboration et à la validation des modèles théoriques.

3.1 Introduction

The aim of this chapter is to present the main methods used to characterize the cell from a mechanical viewpoint. The mechanical characterization of the cell essentially consists in the determination of the viscoelastic properties of the cytoplasm (and the network of filaments) and the determination of the membrane elastic properties. This review concerns essentially the methods for the cytoplasm and/or the cytoskeleton characterization. The methods have been divided into two categories and are presented in the following

two sections. The first category presents "active methods" i.e. methods where the determination of the viscoelastic parameters requires a mechanical interaction with the cell. The second category concerns "passive methods" which are non-invasive for the cell. The results of characterization of cells obtained using the various methods are summarized in the last section.

3.2 Methods for cell mechanical characterization

Active methods

3.2.1 Micropipette aspiration

We first consider the micropipette aspiration experiments of Merkel *et al.*, (2000). The experiments were made on adherent cells in order to determine how the viscoelastic properties of the cell envelope, that are regulated by the coupling of the actomyosin cortex to the membrane, control cellular shape changes.

Aspiration of the cell into the pipette is achieved above a threshold pressure. This initial step of aspiration is assumed to be associated with a mechanical instability. The high velocity of aspiration (about 10 $\mu m/s$) as well as the high suction pressure of several hundred Pascal (corresponding to a force of several nN) suggest that the deformation is mainly due to a fracture between the membrane and the cortex. This fracture therefore corresponds to the breaking of the bonds which link the cortex with the membrane. The deformation of the membrane depends both on the membrane's bending modulus and on its surface tension.

The results of this experiment show that the coupling of the actin cortex to the membrane is weaker at the front of the pseudopods.

3.2.2 Microplate manipulation

The micromanipulation system proposed by Thoumine and Ott (1997) allows one to impose uniaxial deformations on individual cells at varying frequencies which allow global measurements of cell structural properties. The cell is placed between two microplates. The lower rigid one on which the cell adheres is connected to a piezoelectric translator to control its displacements. The upper flexible microplate can be either non-adhesive (for compression) or adhesive (for traction and sinusoidal perturbation). Step and sinusoidal signals are input to the piezoelectric element to perform compression, traction or oscillatory deformations around the initial shape of the cell. The force applied on the cell is calculated from the measure of the flexible microplate deflection. The aim of the experiments performed was to discriminate between the active and passive responses of cells to mechanical perturbations. One advantage of this set-up is that repeated experiments can be performed on the same cell which makes it possible to address the question of whether cells retain a biochemical or rheological memory of previous perturbations.

The method applied to chick fibroblasts has made it possible to identify three time-scale dependent regimes:

- elastic behaviour for short time scales (order of seconds),
- viscous response at intermediate time scales (several minutes),
- contractile behaviour for observations on longer time scales

3.2.3 Optical tweezers

The laser optical trap (or optical tweezers) method is usually used to measure both the dynamic forces on, and the displacement of individual intra-cellular granules in living cells. From these data, the elastic moduli and viscosity of the network can be evaluated in a specific region of the cell. The intra-cellular granules are trapped by a laser beam and are oscillated by this optical trap at various frequencies.

The method has been applied on locomoting neutrophils by Yanai *et al.*, (1999) to exhibit regional differences in stiffness and viscosity for the body, leading and trailing regions of the cell. No significantly different stiffness and viscosity was found between the main body and the trailing region. Moreover, the measures revealed a lower stiffness and viscosity in the leading region namely the protruding pseudopod, which presents a fluid-like behaviour. This observation, as pointed out by the authors, favours the circulation of cytoplasmic flows driven by an increased intra-cellular pressure due to cortical network contraction rather than the hypothesis of actin polymerization. In this latter hypothesis the growing filaments are under compression from the membrane, therefore a larger stiffness than the one measured is expected.

The optical tweezers method has also been applied to study the mechanical behaviour of the cell membrane (Bar-Ziv *et al.*, 1998).

3.2.4 Magnetic tweezers

Magnetic tweezers allow one to apply mechanical stress on living cells through the control of magnetic beads either bound to the cell membrane or phagocytosed by the cell. In the first case, it thus gives one a means to apply mechanical stresses specifically to transmembrane integrin receptors and their associated cytoskeletal proteins (Bausch *et al.*, 1998; Alenghat *et al.*, 2000). In the second case, it is possible to measure the viscoelastic properties of the cytoplasm (Bausch *et al.*, 1999).

3.2.5 Atomic force microscopy

Atomic force microscopy is used as a tool for the quantitative determination of local elastic properties and combines in a unique way high spatial resolution with very high force sensitivity. The method provides a two-dimensional mapping of the sample elasticity which is achieved by recording force curves while the tip of the device is scanned across the sample. This mode of operation is called force mapping. From the forces curves, the cell topography at different loading forces can be calculated as well as the local elastic modulus.

The method has been applied by Rotsch *et al.*, (2000) to prove the crucial importance of the actin network for the mechanical stability of living cells. Various drugs that disrupt or stabilize the actin or microtubules networks respectively have been investigated. It was thus shown that the disaggregation of F-actin resulted in a loss of cell rigidity by a factor of approximately 3 whereas treatment with drugs like colchicine, colcemide or taxol that affect microtubules yielded no effect on elasticity. The authors concluded that the actin network is the structure that mainly determines the elastic properties of living cells.

Another example of the application of the atomic force microscopy method is proposed in another paper by Rotsch *et al.*, (1999), this time to investigate the extension and retraction dynamics of protruding and stable edges of motile 3T3 fibroblasts. The results show that there is no substantial decrease of the cell rigidity in the cell protruding edges relative to the stable ones. This is consistent with the idea of an actin polymerization-driven mechanism for cell protrusion, or one that combines obligatory actin polymerization with the action of myosin I-type motors to extend the leading edge. The hypothesis of a blebbing mechanism, or osmotic gel swelling mechanism (Oster 1984) are excluded as in that case a decrease in rigidity at the leading edge would be expected.

Passive methods

Passive methods are proposed as alternative methods to the traditional invasive (active) ones. Passive methods present the advantage to give results which are less method-dependent than the active ones.

3.2.6 Laser tracking microrheology

This non-invasive method proposes to estimate the mechanical properties of the cell by tracking the Brownian motion of individual particles naturally present in the cytoplasm of the cell. This idea is based on the demonstration by Xu *et al.*, (1998) that the Brownian motion of a particle embedded within a filamentous network is directly related to the network mechanical properties. More precisely, the amplitude of the particle motion is inversely related to the network mechanical modulus. Increases in both rigidity and viscosity will restrict particle motions.

In particular, this method has been applied to the cell line COS7 (Yamada *et al.*, 2000) whose flat and large lamella is rich with spherical granules identified as lipid droplets. The choice for these droplets as probes is essentially due to their high refractility. However the methods can be applied to track any other organelle properly stained. The method shows that the cytoplasmic viscoelasticity of COS7 cells varies with the sub-cellular region considered and is dynamic. In particular in a duration as short as 15 seconds, changes in local moduli as large as fourfold in magnitude were measured. The method also reveals a dense viscoelastic subregion near the nucleus where granules appear strongly embedded in a relatively rigid viscoelastic material rich in intermediate filaments such as vimentin. Intermediate filaments are thus strongly suspected to be responsible for this local viscoelasticity.

The main interest of this laser tracking microrheology method is that it is able to reveal the full viscoelastic complexity of the cytoplasm.

3.2.7 Diffusing wave spectroscopy

This technique is a close relative to the laser tracking microrheology method. Rather than monitoring a single particle, this method monitors the relative motion of many thousands of particles simultaneously. Diffusing wave spectroscopy is based on the measurements of the autocorrelation function of light multiply scattered from microspheres embedded in the network. As in the laser tracking method, the viscoelastic moduli are evaluated from the motions of the microspheres.

This method does not allow *in vivo* measurements. It has been applied on latex microspheres embedded in a highly purified uncrosslinked F-actin (Palmer *et al.*, 1999). In this experiment, the method revealed that the F-actin network modulus is not high enough to generate the rigidity required for cell activity such as cell locomotion, cell protrusion and prevention of cell collapse. Therefore it appears that F-actin needs the support of the other system of filaments to maintain the cell functions cited.

3.2.8 Scanning Acoustic microscopy

Images obtained from the scanning acoustic microscopy method (Zoller *et al.*, 1997; Bereiter-Hahn and Luers, 1998) show interference fringes which mark the topography of the cell surface. Large distances between the interference lines are found in regions that are almost flat whereas in zones with changing thickness of the cytoplasm, the lines are close together.

The fringes result from the interference of sound waves reflected from the plastic surface of the culture dish and the medium facing the surface of the cells respectively. The velocity of sound in the various regions of the cell can be derived from the intensities measured for adjacent constructive and destructive interferences. The velocity of longitudinal sound waves is proportional to the elasticity and density of the structure under observations and a high sound velocity represents tension in fibrillar elements.

3.2.9 Deformable substrates

Traction stresses exerted by locomoting cells can be investigated from the deformations they create on a flexible substrate. This approach can yield direct quantitative information about the detailed magnitude, direction and location of interfacial stresses.

The first successful attempt in detecting mechanical forces was made by Harris (1980) using a thin film of silicone rubber as the culturing substrate. Wrinkles created by the cell tractions at the surface of the film were interpreted as the result of compressive forces exerted by the locomoting fibroblasts. Although the method was subsequently further improved it still suffers from a limited spatial resolution and complex relationship between wrinkles and forces.

Another method is described in Oliver *et al.*, (1999). This new method proposes to evaluate the tractional force of the cells from the two-dimensional deformations of a non-

wrinkling silicon rubber film, by measuring the displacement of polystyrene latex beads embedded in the film. Computational techniques are then used to convert the displacement information into an image of the traction stress distribution (Dembo *et al.*, 1996). However this new method remains limited by the viscous component of the material which could lead to irreversible deformations when exerted with forces over a prolonged period of time.

With this limitation in mind, the flexible polyacrylamide substrate proposed by Pelham *et al.*, (1999) appears to be more adapted than the traditional silicon rubbers. This new substrate provides a controllable and nearly ideal elastic property. Moreover, it can easily be coated with extracellular matrix proteins to provide a more physiological environment for cell adhesion.

Galbraith and Sheetz (1997) proposed a micromachined substrate to measure the actual traction forces generated by the ventral surface of the cell during migration. The device is based upon a system of several thousand cantilever beams buried beneath the surface of the substrate. Each cantilever beam is connected to a miniature pad. Each pad is surrounded by a small square hole allowing the cell to displace the pad. The force that the region of the cell in contact with the pad exerts is calculated from the displacement of the pad and the stiffness of the beam.

3.3 The cytomechanical parameters

The results obtained from the various methods of characterization are summarized and completed by other measurements in order to provide a "global" table of the cell mechanical parameters.
Table 3.1 presents measurements of the elasticty of F-actin solutions under various experimental conditions.
Table 3.2 presents viscoelastic parameters of the cell determined from extracellular measurements or measurements performed on the whole cell (i.e methods such as micropipettes, microplates or deformable substrates).
Table 3.3 presents viscoelastic parameters determined from intra-cellular measurements (essentially performed with magnetic and optical tweezers).
Table 3.4 summarizes the results of the measurements of the traction forces exerted by the cell. These measurements are essentially obtained through the use of deformable substrates.
Table 3.5 presents some of the few measurements of the cell membrane mechanical properties.

Sol. type	Elasticity (N/m^2)	Viscosity (Ns/m^2)	Reference
F-actin	0.78-0.82	n.a.	Zaner and Valberg (1989)
F-actin + ABP	11.2-14.7	n.a.	Zaner and Valberg (1989)
uncross linked actin	0.6	n.a.	Palmer *et al.* (1999)
uncross linked actin	1-4	n.a.	Pollard (1986), Wachstock *et al.* (1993)
uncross linked actin	100-500	n.a.	Hvidt and Keller (1990), Janmey *et al.* (1994)
from *Physarum*	10^4	n.a.	Adams (1992)
F-actin	0.3	n.a.	Goldmann (2000)
F-actin + tropomyosine	0.9	n.a.	Goldmann (2000)
F-actin gel	2229-2254.10^6	1.3-9.4.10^{-3}	Wagner *et al.* (1999)
microtubules gel	2228-2547.10^6	1.5-124.10^{-3}	Wagner *et al.* (1999)

Table 3.1: Viscoelastic parameters from measurements on F-actin solutions

Technique	Cell type	Elasticity (N/m^2)	Viscosity (Ns/m^2)	Reference
magnetic twist	macrophage	n.a.	2500	Zaner and Valberg (1989)
magnetic twist	endothelial	2	n.a.	Wang *et al.* (1993)
magnetic twist	endothelial	10-12.5	n.a.	Pourati *et al.* (1998)
micropipette	leucocyte	0.75 23.8	33	Sung *et al.* (1988)
mech. rheometer	*Dictyostelium*	G'=55	G"=25	Eichinger *et al.* (1996)
micropipette	*Dictyostelium*	200 ± 10 (front)		Merkel *et al.* (2000)
		330 ± 20 (rear)		Merkel *et al.* (2000)
cell poker	neutrophil	118	n.a.	Zahalak *et al.* (1990)
atomic force m.	platelet	100-5000	n.a.	Radmacher *et al.* (1996)
microplates	fibroblast	1000	10^2-10^4	Thoumine and Ott (1997)
spont. retraction	fibroblast	1700	4.10^5	Ragsdale *et al.* (1997)
magnetic tweezers	fibroblast	30000	2.10^3	Bausch *et al.* (1998)
deformable substrat	fibroblast	2000	n.a.	Dembo and Wang (1999)
		6000 (front)	n.a.	Dembo and Wang (1999)

Table 3.2: Viscoelastic parameters from extracellular measurements or whole cell measurements

Technique	Cell type	Elasticity (N/m^2)	Viscosity (Ns/m^2)	Reference
magnetic twist	macrophage	15	2000	Valberg and Albertini (1985)
magnetic tweezers	macrophage	20-735	210	Bausch *et al.* (1999)
optical tweezers	neutrophil	1.1 (body)	0.35	Yanai *et al.* (1999)
		0.01 (front)	0.1	Yanai *et al.* (1999)
		0.75 (rear)	0.35	Yanai *et al.* (1999)
laser tracking	epithelial	G'=72.1	G"=38.2	Yamada *et al.* (2000)

Table 3.3: Viscoelastic parameters from intracellular measurements

Technique	Cell type	Traction force (nN)	Reference
deformable substrate	keratocyte	45 (ventral)	Oliver *et al.* (1995)
deformable substrate	keratocyte	10	Oliver *et al.* (1999)
micromachined	keratocyte	13 (max.)	Galbraith and Sheetz (1999)
		4.5 (ventral)	Galbraith and Sheetz (1999)
		0.158 (dorsal)	Galbraith and Sheetz (1999)
deformable substrate	keratocyte	100-200 (rear)	Burton *et al.* (1999)
		600-700 (body)	Burton *et al.* (1999)
		120-150 (flank)	Burton *et al.* (1999)
deformable substrate	fibroblast	300-800	Burton *et al.* (1999)
deformable substrate	fibroblast	2000	Dembo and Wang (1999)
microplate	fibroblast	40	Thoumine and Ott (1997)
magnetic tweezers	macrophage	0.05-0.9	Bausch *et al.* (1999)
	macrophage	2-10	Guilford *et al.*(1995)
micropipette aspiration	*Dictyostelium*	13 (retraction)	Merkel *et al.* (2000)

Table 3.4: Traction force measurements

Parameter	Value	Reference
membrane tension	$3.1 \pm 1.4\ \mu N/m$	Simson *et al.* (1998)
	0.035 pn/nm	Cevc and Marsh (1987)
	7.0 ± 0.5 pN	Raucher and Sheetz (2000)
bending modulus	$391 \pm 156\ k_BT$	Simson *et al.* (1998)
	$5 - 50\ k_BT$	Cevc and Marsh (1987)
adhesion energy	$22.0 \pm 12.2x10^6\ J/m^2$	Simson *et al.* (1998)

Table 3.5: Membrane tension

Chapter 4

Coupling the experimental and theoretical approaches

Coupler les approches expérimentales et théoriques

Nous avons choisi dans cette thèse d'aborder la dynamique spatio-temporelle des déformations membranaires à l'aide de deux approches complémentaires; une première approche expérimentale et une seconde approche théorique. Expérimentalement, le caractère auto-organisé des mouvements cellulaires a essentiellement été reporté pour des cellules de formes arrondies telles que les keratinocytes ou les leukocytes. Notre but a donc été d'étudier un type cellulaire totalement différent, c'est à dire des fibroblastes. Dans leur état de repos, ces cellules montrent de longs prolongements membranaires qui impliquent une organisation différente du cytosquelette d'actine avec la formation de paquets de filaments. Cette organisation particulière de l'actine conditionnée par le caractère adhérent de ce type cellulaire, tend à stabiliser la structure. Ces cellules apparaissent ainsi moins motiles que les cellules de forme arrondie, ce qui peut expliquer le peu d'interêt accordé à leur dynamique spontanée. Cependant, les pseudopodes des fibroblastes bougent. Ils s'étirent et se rétractent avec différentes amplitudes, mais jusqu'à présent ces mouvements ont été assimilé à des fluctuations aléatoires. Il est largement admis dans la litérature que les mécanismes de la motilité cellulaire doivent partager les mêmes propriétés de base. S'il en est ainsi, alors la composante auto-organisée doit exister dans les schémas de déformation des fibroblastes comme elle existe pour les keratinocytes, les leukocytes et l'amibe *Dictyostelium*. Afin de limiter les perturbations qui pourraient altérer la dynamique des fibroblastes, les déformations sont observées par microscopie à contraste de phase. Les séquences d'images sont ensuite analysées pour en extraire les données morpho-dynamiques pertinentes qui caractérisent le comportement des cellules. Les résultats expérimentaux ont confimé ce qui était attendu, c'est à dire l'existence de schémas de déformation organisés, coordonnés dans l'espace et dans le temps avec une périodicité définie. L'étape suivante a donc été de déterminer si cette dynamique observée pouvait être simulée sur la base des mêmes hypothèses que celles formulées pour décrire les oscillations organisées des cellules arrondies.

Le but est cette fois de tester la validité des hypothèses sur la dynamique de l'actine et sur les propriétés mécaniques de la cellule proposées par le modèle de Alt et Tranquillo (1995) pour rendre compte d'une variété plus étendue de comportements. Comme nous le verrons, le modèle est limité à la description de petites extensions membranaires. Par conséquent, nous avons été contraints dès le début à limiter la modélisation des mouvements des fibroblastes à leur comportement dynamique qualitatif dans la mesure où une description quantitative est évidement hors de portée du modèle. Malgré cette limitation, un comportement pulsant qualitatif comparable à celui observé sur les fibroblastes L929 a pu être simulé. Un pas supplémentaire vers la validation du modèle est proposé à partir d'une tentative d'identification des paramètres biomécaniques utilisés. Le but est ici de renforcer le lien entre les approches expérimentales et théoriques. Ceci est réalisé selon le diagramme présenté Figure 4.1. La caractérisation expérimentale fournie les données morpho-dynamiques (nombre de protrusions, nature des déformations, périodicité, ...) sur lesquelles le modèle peut-être calibré à travers la détermination des paramètres biomécaniques requis pour simuler un comportement donné. Le modèle est ainsi validé si les paramètres biomécaniques utilisés se trouvent dans la gamme des valeurs issues de la litérature consacrée à la caractérisation de la mécanique cellulaire. Réciproquement, l'influence des paramètres biomécaniques sur le comportement de la cellule peut être testée afin de prédire et d'orienter des expérimentations futures.

In this thesis we have chosen to tackle the spatio-temporal dynamics of cell membrane deformations using two complementary approaches; firstly an experimental approach and secondly a theoretical one. Experimentally, the self-organizing character of the cell movements has been reported essentially for rounded cell shapes such as keratinocytes or leukocytes. Our aim has thus been to investigate a totally different cell type, namely fibroblasts. In their resting state these cells exhibit long membrane extensions involving a different organization of the actin cytoskeleton with the formation of bundles of filaments. This particular actin organization due to the adherent character of this cell type tends to stabilize the structure. These cells thus appear less motile than rounded cells which might explain why so little interest has, up until now, been given to their spontaneous dynamics. However, the pseudopods of the fibroblasts move. They extend and retract with various amplitudes, but up to now these movements were supposed to be random fluctuations. It is widely assumed in the literature that the mechanisms for cell motility should share the same basic properties. If this is so, then a self-organized component might exist in the patterns of fibroblast deformations, as has already been shown to exist for leukocytes, keratinocytes and the amoebae *Dictyostelium*. In order to limit the perturbations which might alter fibroblast dynamics, the deformations are observed from standard phase contrast microscopy. Image sequences are thus analyzed to extract the relevant morpho-dynamical data characterizing the cell behaviour. Experimental results confirmed what was suspected, namely the existence of organized patterns of deformations coordinated in space and time with a defined periodicity. The next step has thus been to determine

whether these observed dynamics could be taken into account on the basis of the same hypotheses as those formulated to describe the organized oscillations of rounded cells. Namely the aim was to test the validity of the hypotheses concerning actin dynamics and cell mechanical properties of the model of Alt and Tranquillo (1995) in order to account for a wide variety of behaviour. As we will see, this model is limited to the description of small membrane extensions. Therefore, we were constrained from the beginning to limit our modelling of fibroblast movements to their qualitative dynamical behaviour, as obviously the quantitative description of large membrane extensions remains out of reach of the present model restriction. Despite this limitation, a qualitative pulsating behaviour such as that observed on L929 fibroblasts could be simulated. One more step towards the validation of the model is proposed through an attempt to identify the biomechanical parameters used. The aim here is to strengthen the links between the experimental and theoretical approaches. This is realized in our study according to the diagram presented in Figure 4.1.

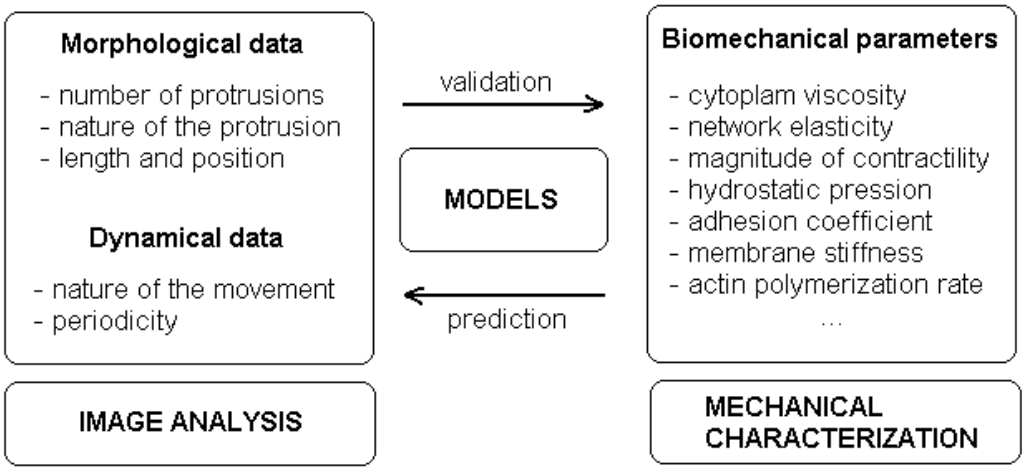

Figure 4.1: Diagram exhibiting the interactions and the complementarity between the experimental and theoretical approaches. Image analysis provides the morpho-dynamical information which characterizes the cell behaviour, whereas the mechanical characterization (whose methods were presented in chapter 3) provides the range for the values of the model parameters.

The experimental characterization provides the morpho-dynamical data (e.g. the number of protrusions, nature of the deformations, periodicity, ...) on which the mathematical model can be calibrated through the determination of the biomechanical parameters required to simulate an observed behaviour. The model is thus validated if the biomechanical parameters used are within a realistic range provided by the literature on cell biomechanical characterization. Conversely, the influence of the biochemical parameters on the cell behaviour can be tested to make predictions and suggest new future experiments.

Part II

Characterization of the Dynamics of Cell Deformations from Image Sequences

Chapter 5

Materials and methods

Matériels et Méthodes

Culture cellulaire et vidéomicroscopie

Les cellules étudiées sont des fibroblastes murins de la lignée L929 (ATCC, CCL 1) cultivés en milieu minimum essentiel sans antibiotiques (MEM, Gibco-BRL) supplémenté de 5% de sérum de veau foetal et de 2 mM de glutamine L, nécessaire au maintien de la viabilité et de la reproductivité des cellules. Les cellules croissent ainsi sur un support de verre durant 48 heures avant le début de l'acquisition des séquences. Les séquences d'images sont alors acquises avec une station d'imagerie (Figure 5.1) composée d'un microscope inversé (Axiovert 135M, Carl Zeiss) équipé d'une chambre d'incubation thermostatée à 37 degrés et maintenant un taux constant de CO_2 à $5\ \%$ (M-Incubator, Carl Zeiss), d'opturateurs automatisés et d'une caméra SIT (C2400-08 Hammamatsu Photonics) pour les séquences courtes de 60 minutes remplacée par la caméra Photonic Coolview 2 (Photonic Science) pour les séquences longues allant jusqu'à 15 heures. L'ensemble est couplé à un analyseur d'image SAMBA 2640 TM Unilog pour Hammamatsu et Image Pro Plus (version 4) pour la caméra Photonic Science. Le grossissement utilisé pour enregistrer la dynamique des déformations cellulaires est de $\times 400$ avec un intervalle de temps entre deux images successives de 3 minutes approprié au suivi des mouvements membranaires. Les champs d'interêts d'une dimension de 225 μm^2 sont choisis de façon à séléctionner des cellules relativement isolées soit environ une vingtaine de cellules par champ au maximum.

Techniques d'analyse des images

Les paramètres morphodynamiques des cellules sont extraits des images à partir de deux méthodes complémentaires qui sont le flot optique et la segmentation des contours cellulaires. Le flot optique consiste à déterminer le champ de déplacement des objets dans une image en se basant sur une loi de conservation de l'intensité lumineuse entre deux images successives. Les paramètres du champ de déplacement entre deux images sont calculés à partir d'un modèle affine du mouvement défini *a priori* et qui associe à chaque pixel de l'image son vecteur

vitesse de déplacement (Germain *et al.*, 1999). Le flot optique permet ainsi de caractériser de façon globale la nature des mouvements observés au cours de la séquence d'images. La seconde approche par segmentation des contours cellulaires, courament utilisée pour l'analyse des mouvements, consiste en l'extraction des coordonnées des contours du ou des objets d'intérêt dans l'image. Le mouvement est ainsi analysé en suivant l'évolution dans le temps de la position des points du contour.

Méthodes pour l'analyse de la dynamique des déformations cellulaires

Les contours cellulaires extraits par segmentation sont reconstruits en coordonnées polaires à partir de la définition d'un point de référence pour ce système de coordonnées (Figure 5.4). Ce point correspond au centre du noyau, à partir duquel la distance des points du contour membranaire est calculée ainsi que leur position angulaire par rapport à l'axe de référence horizontal. Cette représentation définit la carte de polarité de la cellule (Figure 5.5). La superposition temporelle des cartes de polarité donne une image spatio-temporelle de la déformation cellulaire. Le choix d'une valeur seuil de l'amplitude de déformation correspondant le plus souvent à l'amplitude moyenne permet de convertir la représentation spatio-temporelle à trois dimensions en une représention à deux dimensions en ne faisant apparaître selon un code couleur que les points de la membrane dont la distance avec le centre du noyau est supérieure au seuil défini.

Les fibroblastes en culture sur du verre ont la particularité de présenter des extensions membranaires qui restent généralement orientées dans une direction fixe au cours du temps. Une analyse individuelle pour chaque direction protrusive de la dynamique d'extension/rétraction est donc possible en isolant chaque zones protrusives par la définition d'un fenêtre angulaire. A chaque instant, le point du contour membranaire le plus éloigné du centre de la cellule et appartenant à la fenêtre angulaire précédement définie est ainsi suivi (Figure 5.6).

Afin de quantifier les interactions entre cellules, un domaine d'influence est représenté pour chaque cellule sous la forme d'un disque centré sur la position moyenne du noyau cellulaire et dont le rayon correspond à la plus grande extension membranaire enregistrée au cours de la séquence. L'intersection entre deux domaines d'influence correspond ainsi à un zone d'interaction qu'il est possible de visualiser sur les représentation spatio-temporelle 2D de façon à fournir une description globale de la morphologie de la cellule en connection avec son environnement (Figure 5.6).

Enfin deux analyses standards par transformée de Fourier et calcul des fonctions de corrélations sont utilisées de façon à mettre en évidence d'éventuelles périodicité du mouvement et auto-organisation des déformations.

5.1 Cell culture

The cell line studied is the L929 murine fibroblast line (ATTC, CCL 1) cultured in antibiotic-free minimum essential medium (MEM, Gibco-BRL), supplemented with 5% of fetal calf serum (FCS, Gibco BRL) and with 2 mM L-glutamine in order to maintain the

Sequence number	number of cells studied	duration of the sequence (min)	sampling time (min)	number of images
S1	5	60 (1h)	2	31
S2	6	135 (2h15)	3	45
S3	3	477 (≈8h)	3	159
S4	6	765 (12h45)	3	256
S5	3	459 (≈7h40)	3	154

Table 5.1: Information on the image sequences

viability and reproducibility of the cells. The cells are seeded on glass during 48 hours before the beginning of the acquisition. Only the cells which have spread sufficiently and are sufficiently isolated are then analyzed. The degrees of isolation and spreading of the cells are subjectively evaluated. The cells which disappear from the observation area or which divide during the observation duration are eliminated from the study.

5.2 Videomicroscopy

In order to minimize any perturbations on the cells which could affect their spontaneous deformation dynamics and in order to preserve their viability on an acquisition period of up to 13 hours in duration, no stainings were used except for a short sequence of 60 minutes where staining of the nucleus was made. The photonic microscopy technique which is best adapted to the study of living cells, without any coloration and spread on glass support, is the phase contrast microscopy. This technique allows one to amplify the mass volume variations where the areas of highest density appear in dark. Image sequences were acquired using an imaging workstation composed of an inverted microscope (Axiovert 135 M, Carl Zeiss) and automated shutters, a SIT camera (C2400-08 Hammamatsu Photonics) for the shortest sequences up to 135 minutes and a Coolview 2 camera (Photonic Science) for the longest sequences up to 765 minutes. Finally the whole system was coupled with an image analyzer (SAMBA 2640TM, Unilog) for Hammamatsu and Image Pro (version 4) for the Photonic Science camera. The magnification used to record the dynamics of the spontaneous deformations of the cells was $\times 400$ with a delay between two consecutive images of 3 minutes. Sampling times are short enough to be compatible with cell movements frequency. The zones of interest with a surface of 225 μm^2 are chosen in order to select an area of relatively isolated cells, that is to say approximately 20 cells per zone. Morphodynamical data have been extracted from 5 different sequences of images and the recorded characteristics are displayed in table 5.1.

In the subsequent sections and chapters, the notation S_i is used to denote the sequence number i and the notation c_j to denote the cell number j. Therefore the notation $S_i c_j$ denotes the cell j which belongs to the sequence i.

Figure 5.1: Imaging workstation: an inverted microscope coupled to the camera (on the top) with automated shutters and an incubation chamber connected to the controlled system on the right.

5.3 Image analysis techniques

The extraction of the morphodynamical parameters of the cells contained in the sequences of images was carried out using two complementary approaches: an optical flow analysis and a segmentation analysis. The first optical flow approach is a global approach which allows one to identify the nature of the movement for a given cell (oscillations, migration, etc. ...). In contrast, the second approach, segmentation, is a local approach which allows a selective analysis of the various dynamically relevant zones in the cell.

5.3.1 Optical flow analysis

Optical flow is the distribution of apparent velocities of movement of brightness patterns in an image and can thus arise from the relative motion of objects (Horn and Schunck, 1980). From the point of view of image analysis, the optical flow method is thus a direct approach in the sense that this method uses directly information on light intensity contained in each pixel $p(x, y)$ of the image. Consequently this method does not consider at all the nature of the objects in the image such as a cell on its substrate where no distinctions are made to differentiate the two objects, cell and substrate. The information on the movement is inferred locally from the spatial and temporal variations of light intensity $I(p, t)$. The displacement velocity of each pixel $w(p, t)$ is calculated from the hypothesis of the conservation of the light intensity with time, i.e the displaced frame difference (DFD)

Eigenvalue	**associated motion**
λ_1 and λ_2 real; $\lambda_1\lambda_2 > 0$	pure expansion
λ_1 and λ_2 real; $\lambda_1\lambda_2 < 0$	combined expansion and retraction (in an orthogonal direction)
λ_1 and λ_2 pure imaginary	pure rotation
λ_1 and λ_2 complex	combined rotation and expansion

Table 5.2: Determination of the nature of the motion field from the eigenvalues of the matrix

must be equal to zero:

$$DFD(w,p,t) = I(p + w(p,t), t + \Delta t) - I(p,t) = 0.$$

A first order Taylor expansion of $I(p+w(p,t), t+\Delta t)$ gives a relation which linearly relates the velocity of each pixel with their respective spatial and temporal intensities,

$$\nabla I^T(p,t)w(p,t) + \frac{\partial I}{\partial t}(p,t) = 0.$$

This is valid as long as the displacements $w(p,t)$ remain sufficiently small.

The method used is based on the existence of an *a priori* model of motion which assumes that every pixel of the image obeys the same law of movement. This law is here expressed by the following parametric model:

$$\omega(p) = \begin{pmatrix} a_0 \\ a_3 \end{pmatrix} + \begin{pmatrix} a_1 & a_2 \\ a_4 & a_5 \end{pmatrix} \begin{pmatrix} x \\ y \end{pmatrix}.$$

This affine relation thus allows one to calculate the apparent velocity of each pixel $p(x,y)$. The parameters a_0 and a_3 account for translation whereas the parameters a_1, a_2, a_4 and a_5 of the matrix determine the motion field behaviour (rotation, extension or retraction) according to the complex or real nature of the matrix eigenvalues (Table 5.2).
These parameters form the components of the vector $\phi(a_0, a_1, a_2, a_3, a_4, a_5)$ and are estimated by minimization of the following expression based on a least mean square:

$$E(\phi) = \sum_{p \in R} [\nabla I^T(p,t) w_\phi(p,t) + \frac{\partial I}{\partial t}(p,t)]^2,$$

where R represents the area of the image where the affine model is assumed applicable.

Application

For each pair of consecutive images of a sequence, the parameters $a_0, a_1, a_2, a_3, a_4, a_5$ are evaluated and thus define the motion field passing from one image to the following one (Figures 5.2 and 5.3). The eigenvalues of the motion matrix defined by the coefficients a_1, a_2, a_4, a_5 are calculated to give the nature of the movement according to the table 5.2. By plotting the evolution of the eigenvectors and eigenvalues with time we obtain a picture of the dynamical behaviour of the cell.

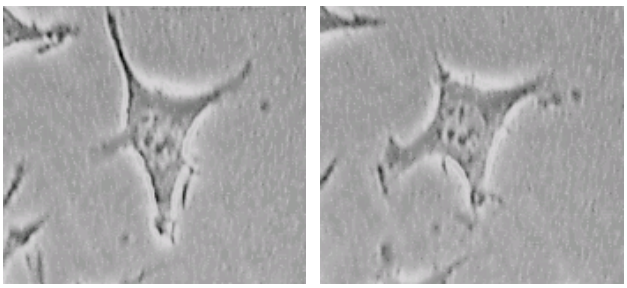

Figure 5.2: Snapshots of an isolated fibroblast (S_1c_5) taken at two different times with a time interval of about 10 minutes.

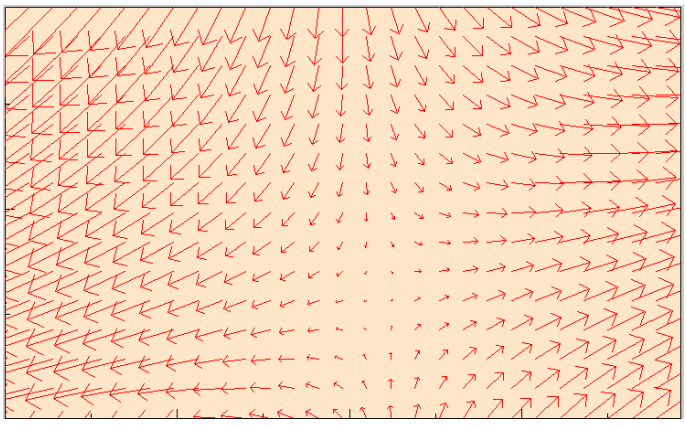

Figure 5.3: Motion field evaluated from the 2 snapshots above with the optical flow method. The motion field exhibits here an extension of the cell in the horizontal direction accompanied by a simultaneous retraction in the vertical one.

5.3.2 Cell outline segmentation

The alternative and complementary technique to the optical flow is the segmentation technique which is most commonly used to analyze the movements from a sequence of images. This method consists in the extraction of the coordinates of the boundary of the

objects of interest. Movement dynamics are thus analyzed by following the evolution in time of the position of the boundary which, in our case, is the membrane of adherent cells on a homogeneous substrate. The main limitation of this method is that it strongly depends on the quality of the images and in particular on their contrast. Detection of the boundary may be extremely difficult for poorly contrasted images which is often the case for our type of images. Automated methods of boundary detection are usually unstable with time (i.e. the boundary is lost), and that is the reason why we have chosen to detect the boundaries manually. Undefined boundaries have thus been extrapolated linearly, namely the medium position of each point of the contour is evaluated from its positions in the previous and subsequent images.

5.4 Methods for the analysis of cell deformation dynamics

Determination of the morphodynamical parameters of the cell is performed from the spatio-temporal reconstruction of the cell membrane dynamics which is detailed below. Further specific methods and representations have been proposed to analyze more precisely the local extension/retraction dynamics and to quantify cell-cell interactions.

5.4.1 Spatio-temporal representation of cell deformations

Polarity map

Cell outline segmentation provides for each cell a set of cartesian coordinates for the position of the points defining the cell edge. The cell outline can thus be reconstructed in polar coordinates from the definition of a referential point for this system of coordinates, inside the cell. This point approximates the position of the centre of the nucleus from which the distance of each point of the boundary is calculated as well as its angular position relative to the horizontal axis (Figure 5.4). The circular contour maps thus obtained exhibit the protrusive areas of the cell and are therefore also called polarity maps (Figure 5.5). Superposition of the polarity maps obtained for each instant in time gives the spatio-temporal image of the cell deformation. This spatio-temporal representation was initially proposed by Killich *et al.*, (1993) to demonstrate the deterministic oscillating component in the deformation patterns of the amoeba *Dictyostelium*. The spatio-temporal map of cell deformations is often represented as a topographic plot to convert the three-dimensional (3D) map into a more convenient two-dimensional (2D) one. A range of various dynamical behaviour, from standing wave patterns of deformation to rotating waves can be visualized for keratinocytes (Alt *et al.*, 1995). In a similar way, our own 3D spatio-temporal maps have been converted to 2D maps by plotting the points of the boundary whose distance from the cell center is above a given threshold (Figure 5.6). This threshold has been chosen, for most of the time, as the mean distance from the cell center to the cell edge.

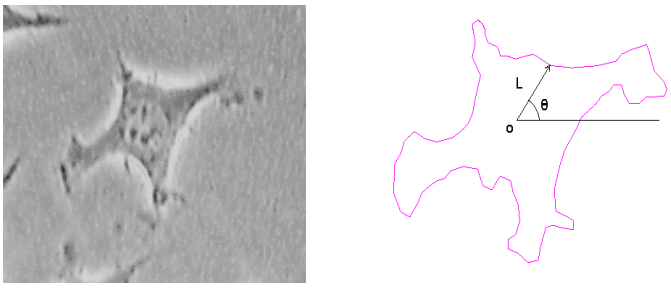

Figure 5.4: Segmentation of the cell boundary and definition of a polar reference point centered on the cell nucleus. The membrane position $L(\theta)$ for any given direction θ is measured from that point of reference.

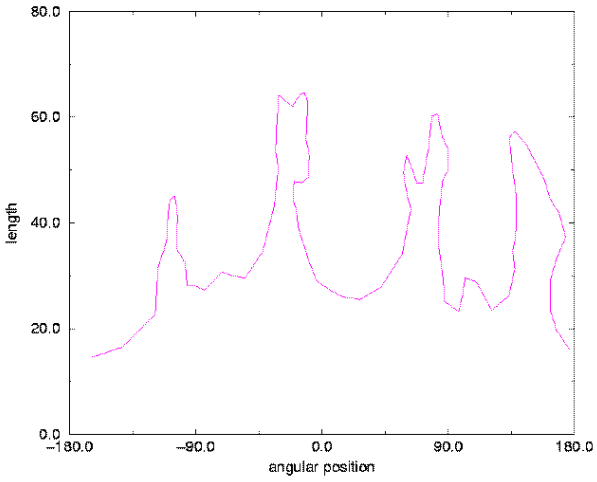

Figure 5.5: Polarity map, or polar reconstruction of the cell boundary. The membrane positions $L(\theta)$ are plotted for the directions θ.

5.4.2 Local analysis of membrane extension/retraction dynamics

As we will see in the next chapter, L929 fibroblasts cultivated on a glass substrate exhibit membrane deformations with constant protrusive directions over time. Consequently it is possible to analyze the extension/retraction dynamics of each protrusive direction individually. Each protrusive zone which is clearly identifiable from the 2D spatio-temporal representation is isolated from the selection of an angular window (Figure 5.6). In each window thus defined, the distance from the cell nucleus to the outermost point of the membrane is monitored. The temporal extension/retraction signal obtained thus neglects any angular displacement of the protrusion within its associated angular window. Moreover any folding of the membrane which sometimes occurs at the tip of the protrusion is eliminated by such a representation.

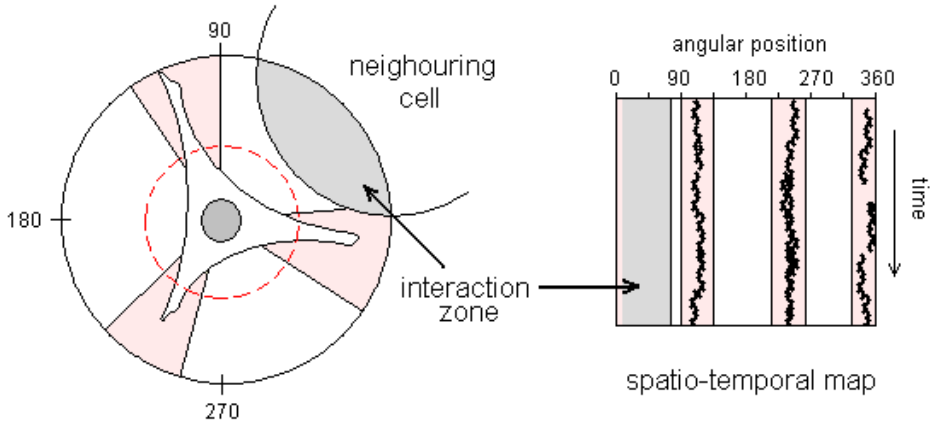

Figure 5.6: Each protrusive direction of the cell is isolated from the definition of an angular window. The dotted red line represents the threshold which is used to eliminate all the points of the boundary which do not belong to a protrusive zone (this in order to built the 2D spatio-temporal maps which appears on the left). Domains of influence are represented by a circular area (see text for details) and interaction zones correspond to the intersections between the domains. These zones when represented on the 2D spatio-temporal map allow us to have a global view of the evolution of the cell morphology in connection to the influence of neighbouring cells.

5.4.3 Cell-cell interaction analysis

Cell-cell interactions are analyzed from the definition of domains of influence for each cells. The domain of influence is represented by a circular area centered on the mean position of the cell nucleus (Figure 5.6). The radius of this area is the largest membrane extension recorded during the sequence. It thus confines the area in which the cell can potentially act on and influence its environment mechanically or/and chemically in terms

of short range effects. Intersections of domains of influence then correspond to interaction zones. They can be represented on the cell spatio-temporal map to provide a global picture of the cell deformations in connection to the cell environment.

5.4.4 Fourier analysis

The temporal signal corresponding to the evolution of the deformation amplitude in a specific angular window is analyzed by Fourier transform in order to detect the existence of any periodicity in the signal.

The discrete Fourier transform of the temporal signal x_n is given by:

$$TF(x_n) = X_k = \sum_{n=0}^{N-1} x_n e^{-\frac{2i\pi nk}{N}} \qquad \text{for} \quad k = -N/2, ..., 0, ..., N/2$$

with N, number of samples of the signal and X_k, amplitude for the sample k.
The Fourier transform is calculated as follow:

$$\begin{aligned} X_k &= \sum_{n=0}^{N-1} x_n \left[\cos\left(\frac{2\pi nk}{N}\right) - i \sin\left(\frac{2\pi nk}{N}\right)\right] \\ &= \sum_{n=0}^{N-1} x_n \cos\left(\frac{2\pi nk}{N}\right) - i \sum_{n=0}^{N-1} x_n \sin\left(\frac{2\pi nk}{N}\right) \end{aligned}$$

$$|X_k| = \sqrt{Re(X_k)^2 + Im(X_k)^2}$$

$$\begin{aligned} Re(X_k) &= \sum_{n=0}^{N-1} x_n \cos\left(\frac{2\pi nk}{N}\right) \\ Im(X_k) &= \sum_{n=0}^{N-1} x_n \sin\left(\frac{2\pi nk}{N}\right) \end{aligned}$$

The modulus of the signal calculated for each k from $-N/2$ to $N/2$ corresponds to the intensity of the signal for the associated frequency $\nu_k = k/N\Delta t$ where Δt is the sampling time of the signal.

Chapter 6

Characterization of the spontaneous dynamics of L929 fibroblasts

Caractérisation de la dynamique spontanée de fibroblastes L929

La plupart des études menées sur la morphologie cellulaire s'intéressent aux changements morphologiques induits par un stimulus externe pouvant être de nature très variée, chimique ou mécanique. Les mécanismes de changement de forme dans ces conditions impliquent donc nécessairement des processus complexes menant à la réponse cellulaire. Or ces processus ne peuvent être parfaitement compris si l'état spontané de la cellule, c'est à dire son état en dehors de contraintes externes imposées, n'a pas été caracterisé au préalable. Les cellules en culture sur des substrats de verre bidimensionnels montrent une activité spontanée de la membrane due à la dynamique de l'actine. Les mouvements observés ont longtemps été considérés comme aléatoires jusqu'à ce que des techniques d'analyse appropriées soient utilisées pour montrer l'existence d'une certaine auto-organisation de la dynamique cellulaire. Ainsi l'utilisation de cartes de polarité décrivant l'évolution des extensions membranaires au cours du temps ont permis de démontrer l'existence d'ondes en rotation autour du corps cellulaire pour l'amibe dictyostelium (Killich *et al.*, 1993, 1994) , les kératinocytes (Alt *et al.*, 1995) et les leukocytes (Alt 1990). Dans la présente étude, nous nous sommes proposés de caractériser la dynamique de fibroblastes L929 dont les morphologies sont très différentes des types cellulaires précédement étudiés et essentiellement caracterisées par de longs prolongements membranaires (protrusions). Les deux approches décrites dans le chapitre précédent, ont été utilisées pour analyser la dynamique de déformation des fibroblastes. Les résultats obtenus montrent que les fibroblastes présentent des morphologies globalement symmétriques pouvant impliquer de 2 à 4 protrusions. L'état à 4 protrusions semble correspondre à l'état spontané privilégié puisque c'est l'état adopté par les cellules les plus isolées. L'analyse temporelle des signaux protrusifs montre que les cellules ont une dynamique périodique avec une période moyenne mesurée sur

notre échantillon de cellules de 32 minutes. On remarque que cette période semble dépendre du nombre de protrusions de la cellule puisqu'elle augmente lorsque le nombre de protrusions diminue. La recherche d'une synchronisation des mouvement protrusifs est effectuée d'une part à partir des signaux temporels d'extension/rétraction et d'autre part à partir de la méthode du flot optique. Dans les deux cas les résultats coincident et montrent que l'état à 4 protrusions de la cellule est un état pulsant synchronisé entre les 2 axes protrusifs perpendiculaires de la cellule ou l'extension dans une direction est accompagnée de la rétraction simultanée dans l'autre direction.

6.1 Introduction

The morphology of a cell in a tissue depends on its interactions with neighbouring cells and the extracellular matrix. Thus, changes in cell shape can obviously result in the alteration of these cell interactions (Parnigotto *et al.*, 1993). Most of the studies conducted on cell shape changes have been interested in changes induced by external stimuli of different nature (chemical, mechanical ...). However, these already complex interactions and cellular responses cannot be completely understood if the spontaneous cell activity is not characterized. In this sense, the *in vitro* study of stationary isolated cells plated onto an inert substratum in the absence of additional external stimuli can shed light on the self-organized character of cell deformations. This concept has already been proposed in the early works of Goldacre (1961) and Weiss (1961), the latter suggesting that a cell expends energy to put its surface layer ... *"in a travelling dynamic oscillation between higher and lower contractile states synchronized over a large fraction of the cell surface and sweeping over in the manner of a pulse"*. It is now well documented that shape changes are mainly due to the dynamic rearrangements of the cell actin cytoskeleton (Schafer *et al.*, 1998; Small *et al.*, 1999), coupled to the dynamic polymerization process governing associated microtubule organization (Waterman-Storer and Salmon, 1999). However, the mechanisms driving the formation of cellular protrusions are still controversial. Alternative views consider that cell protrusions can be generated by the formation of F-actin bundles which push forward the cytoplasmic membrane in specific places, or consider that the initiating process is the local polymerization of an actin gel in a free volume located between the plasma membrane and the cell actin cortex (Condeelis, 1993a). Besides the formulation of theoretical models which take into account such hypotheses (Oster 1984; Peskin *et al.*, 1993; Alt *et al.*, 1995; Mogilner and Oster 1996), it is of particular interest to study cell shape dynamics from the analysis of relevant spatio-temporal signals obtained from time lapse videomicroscopy. Determination of the modification with time of cell contour perimeters provides a first basis for analyzing dynamic changes of cell morphology. This has been done for different type of cells, like keratinocytes (Alt *et al.*, 1995) or leukocytes (Alt 1990) as well as for amoeba (Killich *et al.*, 1993, 1994). However, it is known that cell contour segmentation remains quite an involved process, which can rarely be conducted in a fully automated manner. An alternative approach, based on optical flow methods, has been recently proposed for analyzing globally the dynamic changes of cell morphology (Germain *et al.*, 1999). This approach relies on the formulation of a simple *a priori*

motion model which takes into account most of the cell shape changes observed in isolated cells. In this chapter, we consider both approaches to study the self-organized character of murine fibroblast shape changes without any cell translocation. Indeed, cell morphology changes are commonly described as random processes, in which cell protrusion orientation and amplitude appear as stochastic processes temporally independent. We show here, in the case of L929 fibroblasts, that cell shape changes involve a periodic component and that cell membrane protrusions are correlated and synchronized. Using Fourier analysis of time signals obtained from both approaches, namely cell contour time-amplitude maps and time variations of the motion field eigenvalues, we characterize preferential cell morphology and cyclic aspects of pseudopod extension and retraction. Since both approaches are quite different in nature, we also compare their relevance to the analysis of cell deformation and quantification of protrusion dynamics, as well as their relevance for the extended analysis of cell locomotion.

6.2 Preliminary observations

Observations of L929 fibroblasts cultured in the conditions described in the previous chapter, show that cells spread on a two-dimensional glass substrate and exhibit starry configurations involving several membrane protrusions which are more or less evenly distributed around the cell body. The number of protrusions of a cell varies from 2 to 4 main stable protrusions. The appearance of additional protrusions sometimes occurs in the form of small spikes which are unstable and vanish within a few minutes. The cells thus cultured do not migrate, namely the displacement of the cell nucleus center remains small in front of the radius of the cell body during the duration of the sequence with only slight fluctuations around a medium position. Therefore no translocation of the cell occurs. Cells in such conditions can be considered as resting cells. However this does not mean they are static cells. Indeed, the membrane protrusions are continuously protruding or retracting. Our aim here is to investigate these movements in order to determine if they are a random dynamics or if they appear to be deterministic movements coordinated in space and periodic in time.

6.3 Spatial organization of membrane protrusions

The most convenient representation to exhibit the evolution in time of the spatial organization of cell membrane protrusions are the 2D spatio-temporal maps (see Materials and Methods). From this map we observe that each protrusive direction of the cells has the particularity to remain located along a given axis for up to 12 hours. A few examples of these maps corresponding to various cell morphologies with between 2 and 4 protrusions are displayed in Figure 6.1.

From the spatio-temporal maps, the mean directions of the cell protrusion axes can be evaluated graphically. We have been interested in the disposition of the membrane protrusions relative to each other in order to see if this distribution obeys a certain symmetry or

not. For each cell, the angular distance between 2 consecutive protrusions is plotted along the same axis. Two graphs are displayed (Figure 6.2), the first one for the cells exhibiting 3 protrusions (upper graph) and the second graph for the cells exhibiting 4 protrusions (lower graph).

Theoretical axes of symmetry are 120 degrees apart for cells with 3 protrusions and 90 degree apart for cells with 4 protrusions. In the first case (cells with 3 protrusions) we observe that 62 % of the angular distances measured between two consecutive protrusions are within 20 degrees from the distance of symmetry (darkest area). The proportion of angular distances between consecutive protrusions located from 20 to 40 degrees away from the distance of symmetry dropped to 33 % (light red area) and to 5 % (white area) for angular distances above 40 degrees from the distance of symmetry. In the second case (cells with 4 protrusions) 78 % of the angular distances measured are within 20 degrees from the distance of symmetry (darkest area) and 19 % of the distances measured are located from 20 to 40 degrees away from this distance (light red area). 3 % are above 40 degrees from it.

These results show that the protrusions of the cell tend to develop in order to maximize the distance between them, which leads to the observed symmetrical morphologies.

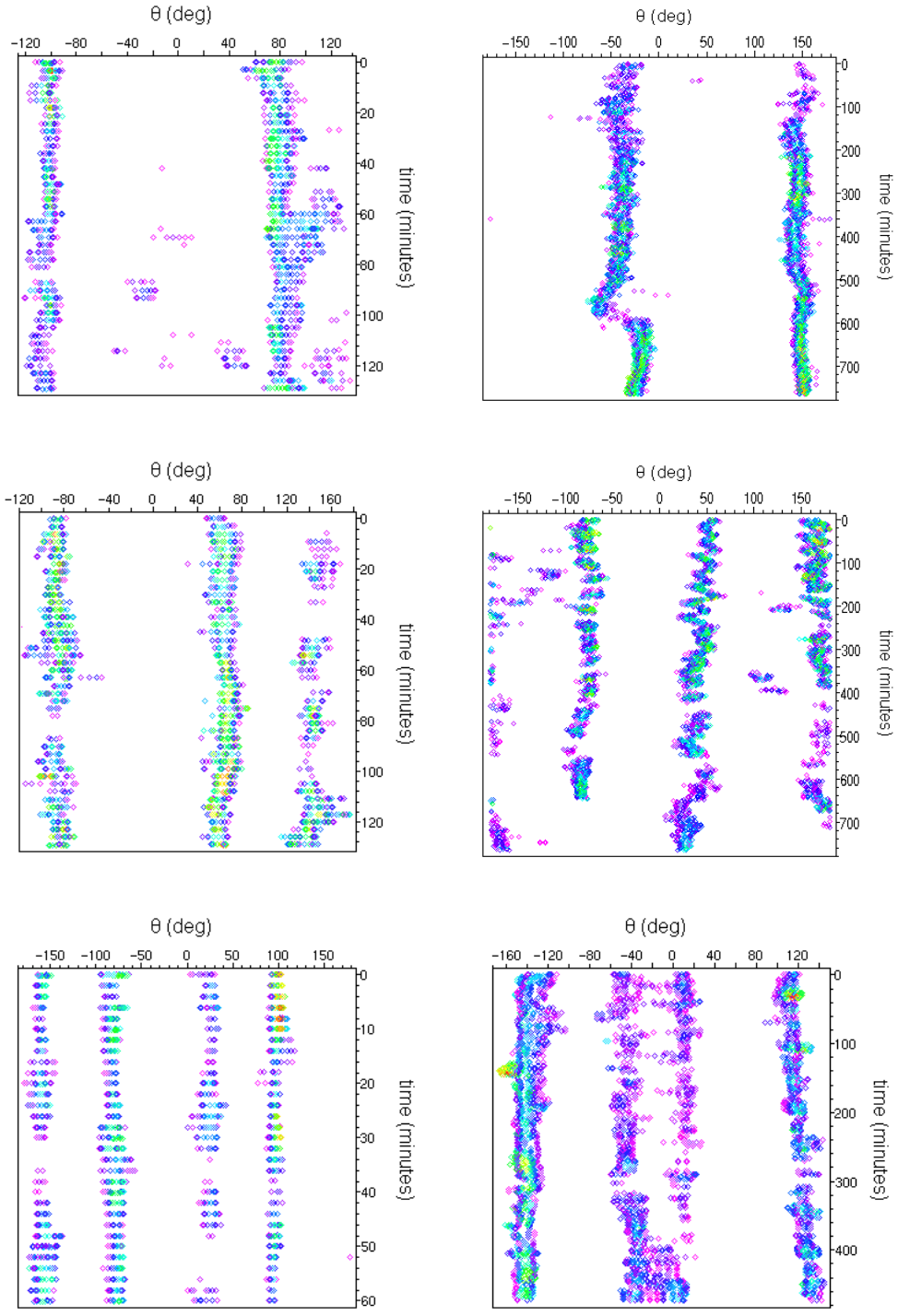

Figure 6.1: Spatio-temporal representation of a variety of cell morphologies; upper graph: cells with 2 protrusions (S_2c_3, S_4c_6); middle graph: cells with 3 protrusions (S_2c_2, S_4c_1); lower graph: cells with 4 protrusions (S_1c_1, S_3c_1). The protrusive directions usually remain located along one axis for significantly long times (up to 12 hours).

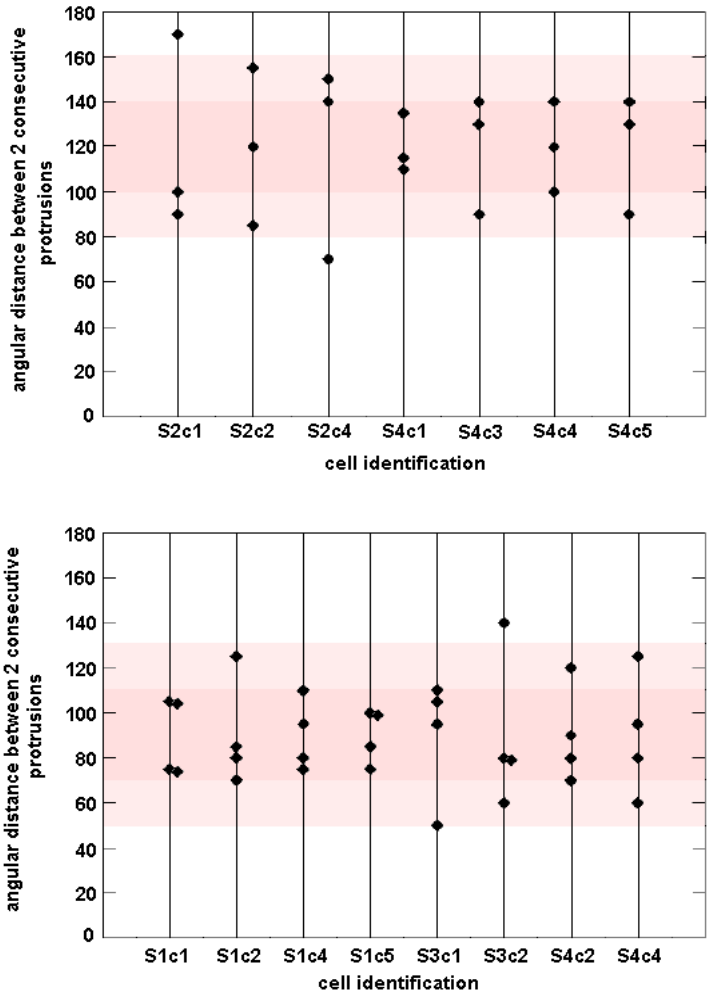

Figure 6.2: Measurements for each cell of the angular width between 2 consecutive protrusive directions. Upper graph: cell presenting 3 protrusions and lower graph: cell presenting 4 protrusions (14 cells are represented). We note that the cell S_4c_4 appears in both graphs as this cell exhibits a transition of morphology.

6.4 The protrusion dynamics

As the protrusions remain located in given directions for significantly long times (up to 12 hours), it gives one the opportunity to isolate and study individually their dynamic of extension/retraction (see chapter 5). From the spatio-temporal maps displayed in Figure 6.1, we see that each protrusion can be isolated on approximately 40-degrees-wide angular windows. As described in the last chapter, the protrusive signals extracted provide the material on which further spatio-temporal analyses can be performed. In Figure 6.3 the results of the calculation from the protrusive signals of the mean membrane extension length for each protrusion of each cell are presented. We observe that for a given cell, the mean protrusion lengths are relatively homogeneous, which means that the cell usually presents equilibrated shapes. We further observe that the mean protrusion lengths calculated are in the range 13 to 36 μm.

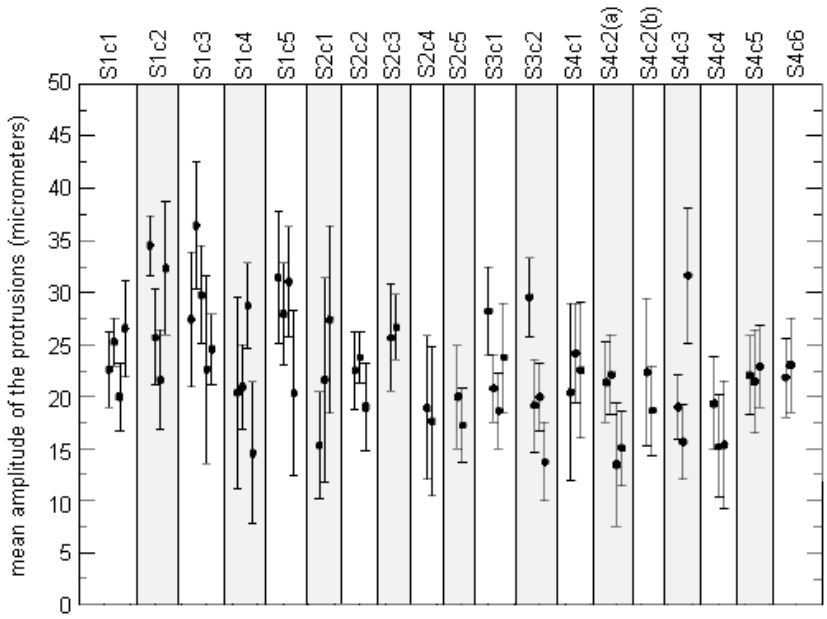

Figure 6.3: Mean amplitude and associated mean variation for each protrusion of each cell studied. Each column is associated with one cell identified by its code $S_i c_j$ (one protrusion of cell $S_2 c_4$ is not shown on the graph with an amplitude of 60 $\mu m \pm$ 9.73)

6.4.1 Temporal analysis of the protrusive signals

Fourier analysis

We propose here to try to detect the existence of any periodic components in the membrane extension/retraction dynamics by means of a Fourier analysis. For each cell the mean periodicity of the membrane extension/retraction dynamics is evaluated from the Fourier transforms of the protrusive signals. Protrusive signals which do not exhibit any periodicity are not considered in the calculation. Therefore, the accuracy of the mean periodicity measured from one cell strongly depends on the number of protrusive signals used relatively to their total number, namely the total number of protrusions of the cell. A reliable periodicity result is thus given for an above defined ratio of 1. If moreover the standard deviation is zero, then it means that all the protrusions of the cell have the same period of membrane extension/retraction. The results obtained are displayed in two tables. Table 6.1 displays the results related to the first three sequences of images and Table 6.2 the results related to the sequence S_4. The results of this last sequence are displayed separately as the duration of this sequence is much longer than the others. The protrusive signals, sometimes, had to be divided in time to separate changes in the protrusive regimes.

For about one third of the measurements we observe that all the protrusions of the cell have the same periodicity (standard deviation ≤ 2) for the dynamic of extension/retraction of the membrane. This applies whatever the number of protrusions exhibited. Two examples of this case are displayed in Figures 6.4 and 6.5. In 24 % of the cases, all the protrusions of the cells have a periodicity but with different periods which is translated by very large standard deviations. For 8 % of the cases (namely 2 cases), no periodicity at all is detected. The 36 % of the remaining cases concern cells where for at least one protrusion, no periodicity is detected.

The measure of the total mean periodicity is about 32.2 minutes. If we calculate separately the mean periodicity between cells which have the same number of protrusions, we observe slight variations from the total mean value. Indeed, the mean value for cells with 4 protrusions is 26 minutes (one cell with 5 protrusions has a periodicity of 26.2 minutes) and increases up to 40.2 and 40.1 minutes for cells with respectively 3 and 2 protrusions. Therefore it seems that the periodicity tends to decrease for an increasing number of protrusions. These observations are consistent with the hypothesis of a travelling wave of deformations around the cell body, assuming that the wave travels at the same speed in each case. It needs more time to travel from one protrusion to another if the protrusions are separated by a wider angular distance which is 90 degrees for 4 protrusions and 120 degrees for 3 protrusions.

Cell identification	time-interval (min) for the measures	mean period (min) and deviation	protrusions with periodicity
S_1c_1	[0,60]	18.3 ± 5.5	3/4
S_1c_2	[0,60]	14.5 ± 20.2	2/4
S_1c_3	[0,60]	26.2 ± 13	5/5
S_1c_4	[0,60]	23 ± 25.0	2/4
S_1c_5	[0,60]	30 ± 0	4/4
S_2c_1	[0,135]	30 ± 8.0	3/3
S_2c_2	[0,135]	32 ± 0	1/3
S_2c_3	[0,135]	37.5 ± 30.25	2/2
S_2c_4	[0,135]	26 ± 0	3/3
S_2c_5	[0,135]	32 ± 0	2/2
S_3c_1	[0,474]	43 ± 0	1/4
S_3c_2	[0,474]	28 ± 0	1/4

Table 6.1: Mean periodicities of the cell membrane extension/retraction dynamics for the cells of the sequences S_1, S_2 and S_3.

Cell identification	time-interval (min) for the measures	mean period (min) and deviation	protrusions with periodicity
S_4c_1	[0,765]	40.5 ± 6.2	2/3
S_4c_1	[0,399]	36 ± 0	3/3
S_4c_1	[402,765]	44 ± 0	3/3
S_4c_2	[0,240]	22.7 ± 0.9	3/4
S_4c_2	[399,765]	28 ± 0	2/2
S_4c_3	[0,432]	33.5 ± 2.2	2/3
S_4c_3	[0,201]	31 ± 18	3/3
S_4c_3	[201,432]	-	0/3
S_4c_4	[0,765]	77 ± 0	3/3
S_4c_4	[0,240]	23 ± 5	4/4
		31.2 ± 28.7	4/4
S_4c_4	[240,600]	47.3 ± 26.9	3/3
		71 ± 0	3/3
S_4c_5	[0,765]	35 ± 0	2/3
S_4c_5	[0,240]	32.7 ± 1.4	3/3
S_4c_5	[240,462]	31 ± 0	2/3
S_4c_5	[462,765]	37 ± 0	1/3
S_4c_6	[0,765]	63 ±	1/2
S_4c_6	[0,600]	-	0/2

Table 6.2: Mean periodicities of the cell membrane extension/retraction dynamics for the cells of the sequences S_4.

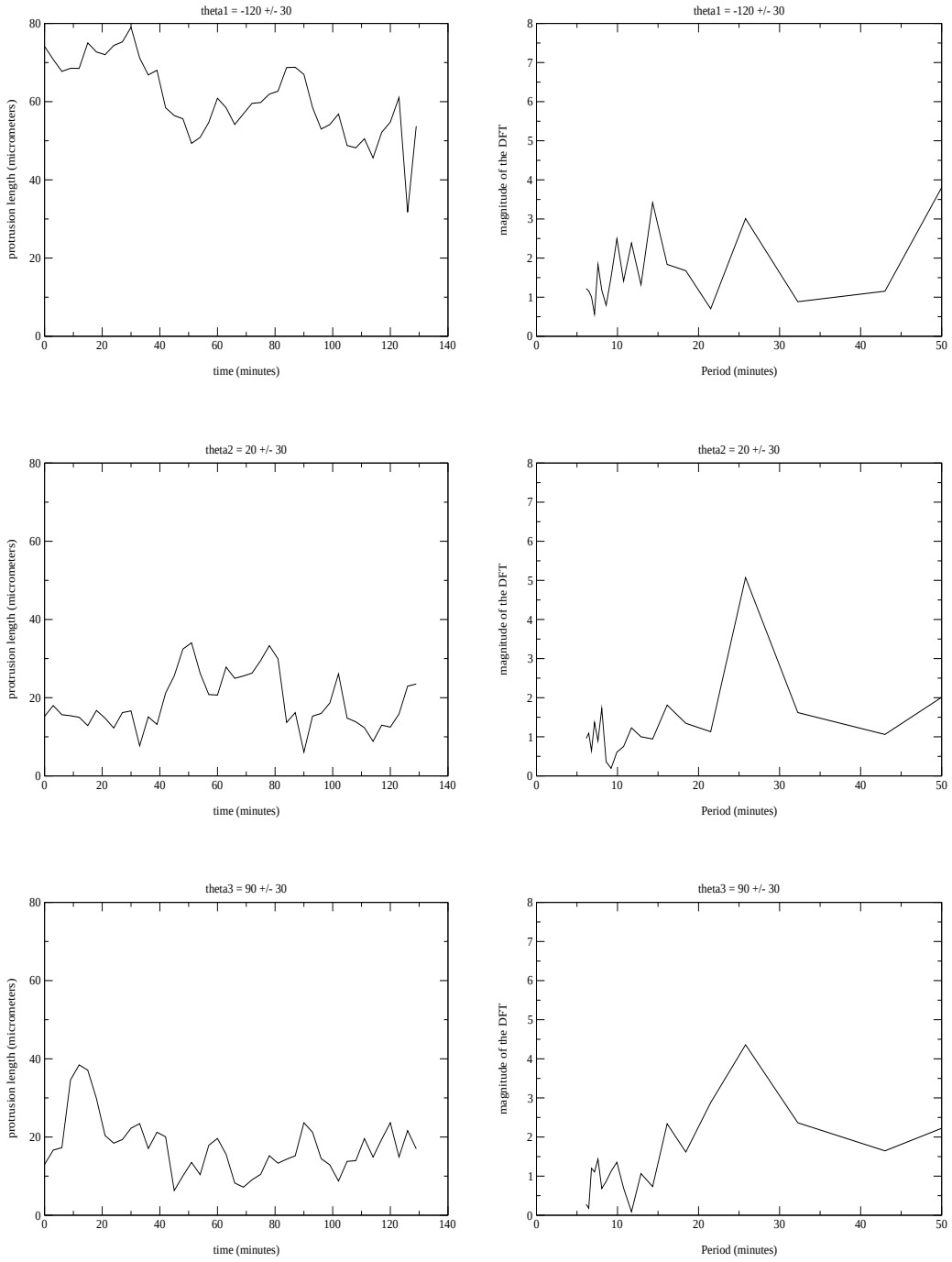

Figure 6.4: Protrusive signals and associated Fourier transforms for each protrusion of the same cell (S_4c_2). A peak of intensity appears in each of the 3 cases for the same period of 26 minutes. A competing peak appears for the first protrusion for a period of 14 minutes, however considering the 2 other non-ambiguous cases we can assume that this period is not relevant for the global dynamic of the cell. From top to bottom: $\theta_1 = -120$ degrees, $\theta_2 = 20$ degrees and $\theta_3 = 90$ degrees.

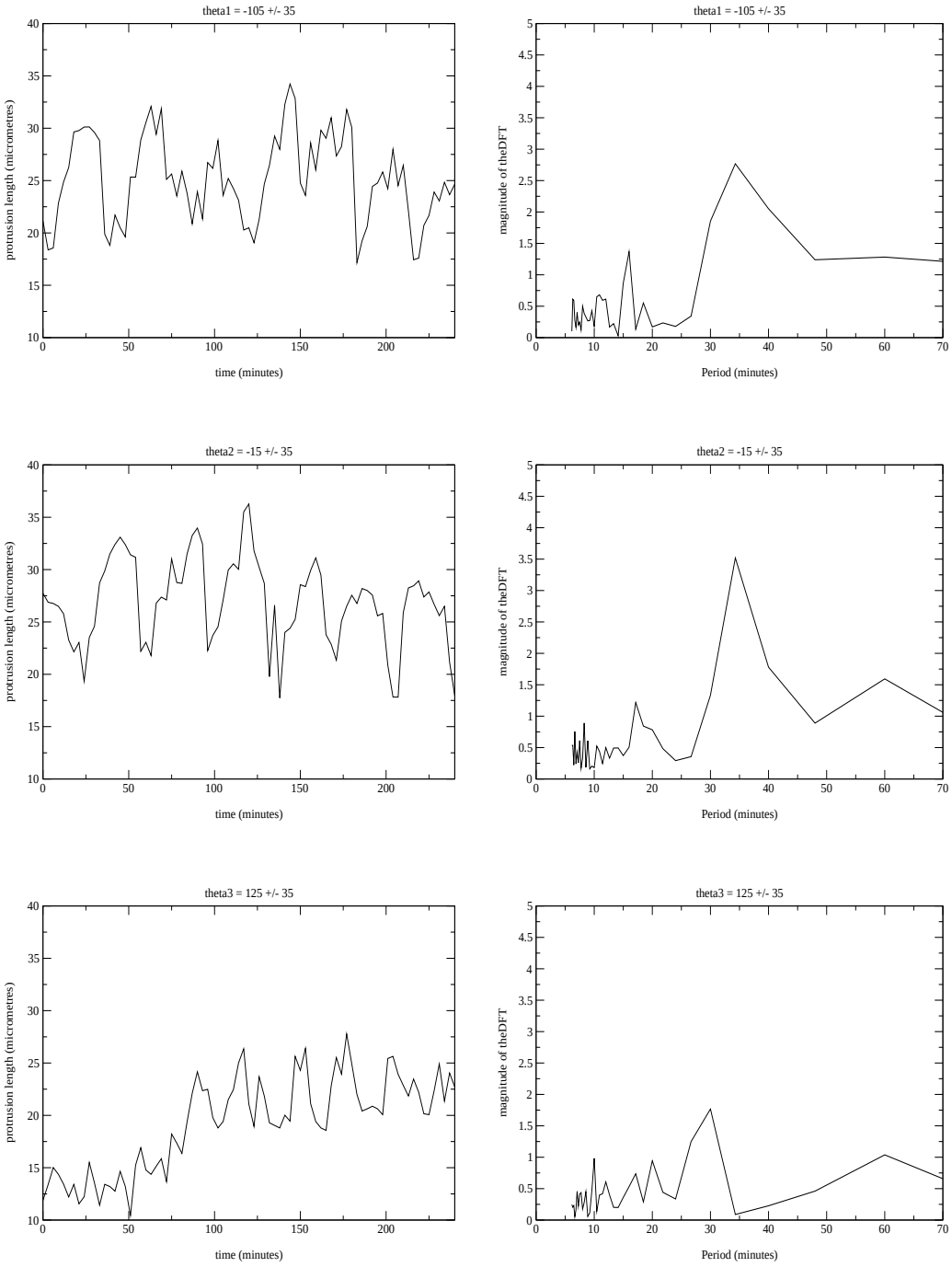

Figure 6.5: Second example of the protrusive signals and their associated Fourier transforms for each protrusion of a particular cell (S_4c_5). In each case a distinctive peak appears. In the first 2 cases for a period of 34 minutes and in the last case for a period of 30 minutes. This gives a mean period of 32.7 $\pm$ 1.4 minutes. From top to bottom: $\theta_1 = -105$ degrees, $\theta_2 = -15$ degrees and $\theta_3 = 125$ degrees.

6.4.2 Coordination of the cell movements

Fourier analysis revealed that for many cells, all the protrusions have close period for the membrane movements. Therefore it is now interesting to determine whether the dynamics of the various protrusions of the cell are correlated to or independent from each other, namely we want to determine if the movements are synchronized.

Figure 6.6 presents simultaneously the 3 protrusive signals associated with the cell S_4c_5 temporally analyzed in Figure 6.5. Typical movements of extension/retraction of the membrane are observed with irregular amplitude variations. Each curve is smoothed by a spline function in order to enhance the main cell membrane displacements. The curves obtained are displayed in Figures 6.7 and 6.8. We clearly see a synchronized pulsation between the protrusive directions 1 and 2 (Figure 6.7) which are displayed perpendicularly from each other. When one protrusion extends the other one simultaneously retracts. However no obvious synchronization appears between the protrusions 1 and 3 ($\Delta\theta_{13} = 130$ deg) and the protrusions 2 and 3 ($\Delta\theta_{23} = 140$ deg) (Figure 6.8).
.

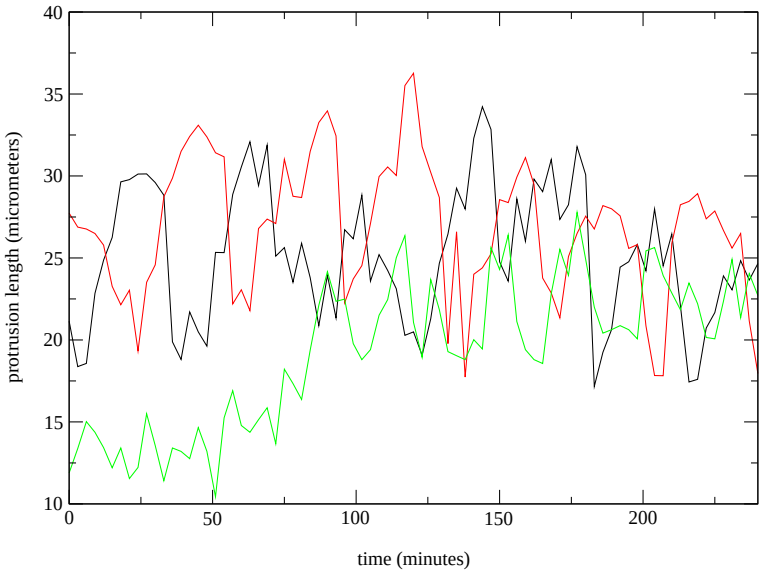

Figure 6.6: Protrusive signals associated with the 3 protrusions of the same cell (S_4c_5). The associated directions are: $\theta_1 = -105$ degrees (black curve), $\theta_2 = -15$ degrees (red curve), $\theta_3 = 125$ degrees (green curve).

Similarly Figure 6.9 presents the 4 simultaneous protrusive signals of a representative cell for this morphology, on a restricted time of one hour. As in the previous example, each curve is smoothed and the resulting curves are displayed in Figure 6.10. Synchronized pulsations between all the protrusive directions are observed, where the extension

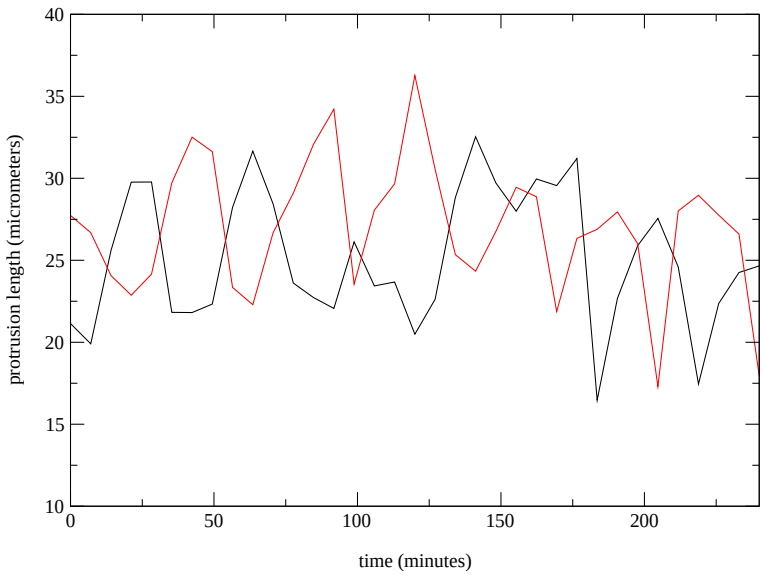

Figure 6.7: The curves of Figure 6.6 associated with $\theta_1 = -105$ degrees (black curve) and $\theta_2 = -15$ degrees (red curve) respectively (i.e. $\Delta_{12} = 90$ degrees), have been smoothed by a spline function and are presented here simultaneously in order to exhibit their strong synchronism. We observed that the amplitudes of pulsation of the two curves are similar

of the protrusions directed along a same axis goes simultaneously with the retraction of the protrusions located in the quasi perpendicular direction.

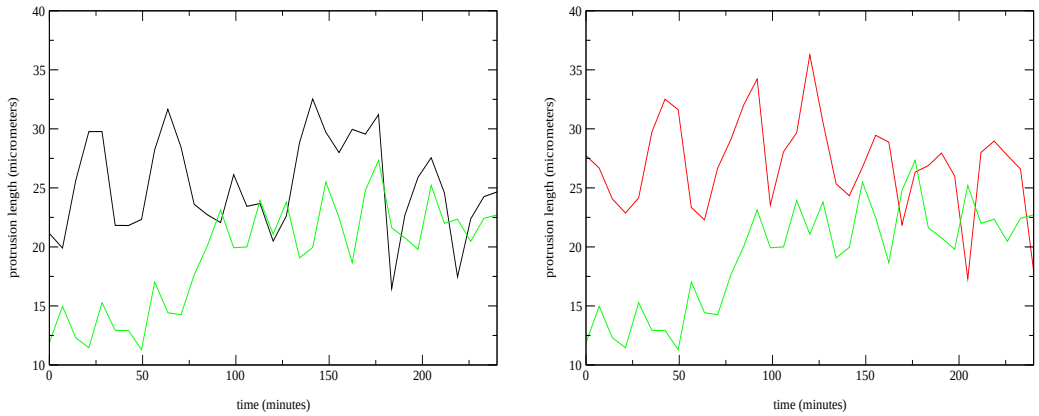

Figure 6.8: Similarly, the smoothed curves associated with $\theta_1 = -105$ degrees (black curve) and $\theta_2 = -15$ degrees (red curve) are plotted simultaneously with the smoothed curve of $\theta_3 = 125$ degrees (green curve). In the first case (on the left), $\Delta\theta_{13} = 130$ degrees and in the second case on the right, $\Delta\theta_{23} = 140$ degrees. This time the directions simultaneously considered are not perpendicular and no obvious synchronism is observed.

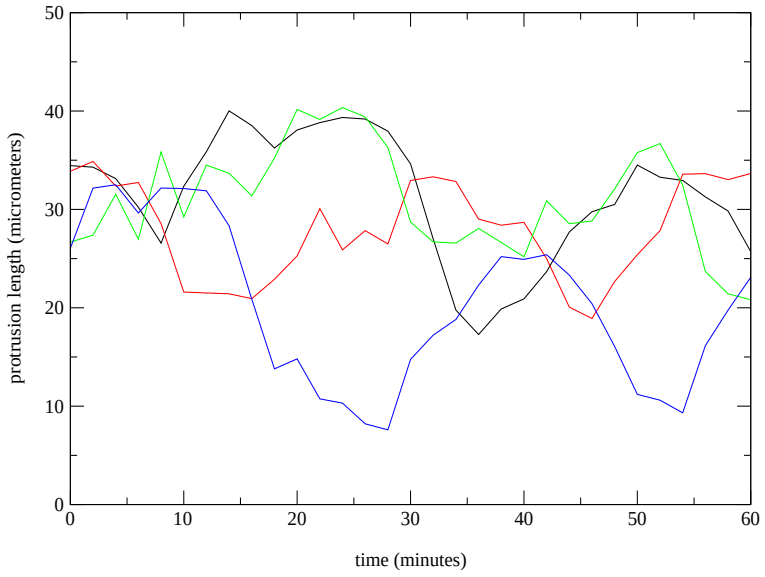

Figure 6.9: Protrusive signals associated with the 4 protrusions of a same cell (S_2c_5). The associated directions are: $\theta_1 = -110$ degrees (black curve), $\theta_2 = -25$ degrees (red curve), $\theta_3 = 75$ degrees (green curve) and $\theta_4 = 150$ degrees (blue curve).

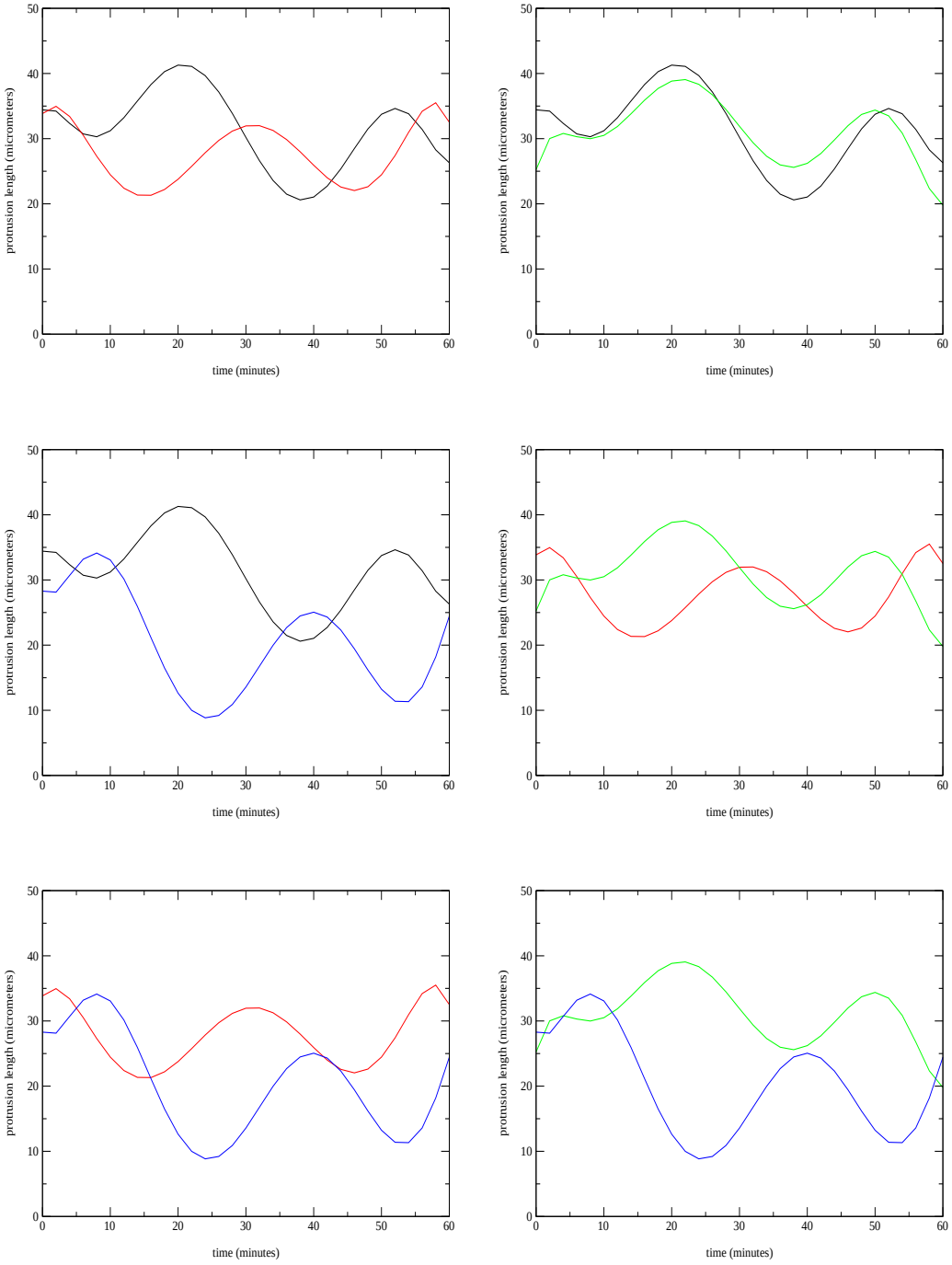

Figure 6.10: In this figure, each curve presented in figure 6.9 has been smoothed with a spline function in order to exhibit the main membrane displacements. The curves are displayed in pairs to exhibit the coordination of the movements between the various protrusive directions. The curves associated with roughly perpendicular directions are in opposition (graphs 1, 3, 4 and 6) whereas curves corresponding to directions globally displayed along a same axis are in phase (graphs 2 and 5).[85] We note that the red curve appears to be slightly ahead of the other curves. $\theta_1 = -110$ degrees (black curve), $\theta_2 = -25$ degrees (red curve), $\theta_3 = 75$ degrees (green curve) and $\theta_4 = 150$ degrees (blue curve).

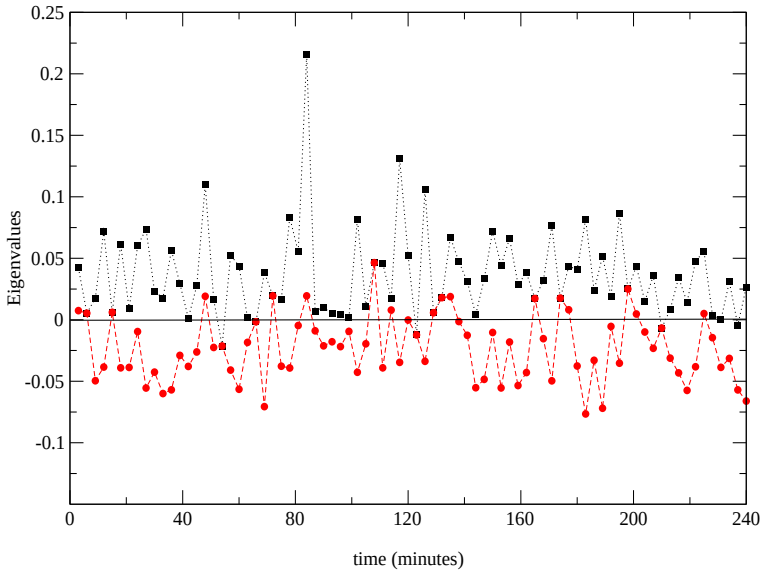

Figure 6.11: Evolution of the real part of the eigenvalues λ_1 (black plot) and λ_2 (red plot) associated with the motion field of cell S_4c_2. The two eigenvalues have mostly opposite signs which is characteristic of a coordinated pulsating movement of extension/retraction of the membrane.

In order to determine if this synchronized behaviour is sustained for longer durations, an optical flow analysis is performed on the cells. As was detailed in chapter 5, this analysis allows us to characterize the nature of the movement from the calculation of the eigenvalues associated with an affine model for cell motion defined *a priori*. It has been demonstrated by the study of Germain *et al.* (1999) that the eigenvalues are reliable descriptors of the cell morphological changes (see Table 5.2).

Figure 6.11 shows the simultaneous evolution of the real part of the eigenvalues estimated from the movements of a cell exhibiting a symmetrical shape with 4 protrusions. We observe that the pairs of eigenvalues have (most of the time) opposite signs which is, according to Table 5.2, the signature of a pulsating movement involving alternative phases of extension/retraction of the cell membrane.

In order to see how the pulsation is spatially organized, the associated evolution of the directions of the eigenvectors are plotted in Figure 6.12. The observation has been restricted in time from t=120 minutes to t=200 minutes for the sake of clarity. We observe that the pulsating movement occurs alternatively between 2 directions, the first direction around 50 $\pm$ 180 degrees and the second direction around 140 $\pm$ 180 degrees. This means a pulsating movement between two perpendicular directions where the extension of the membrane in one direction is associated to the membrane retraction in the other perpendicular direction.

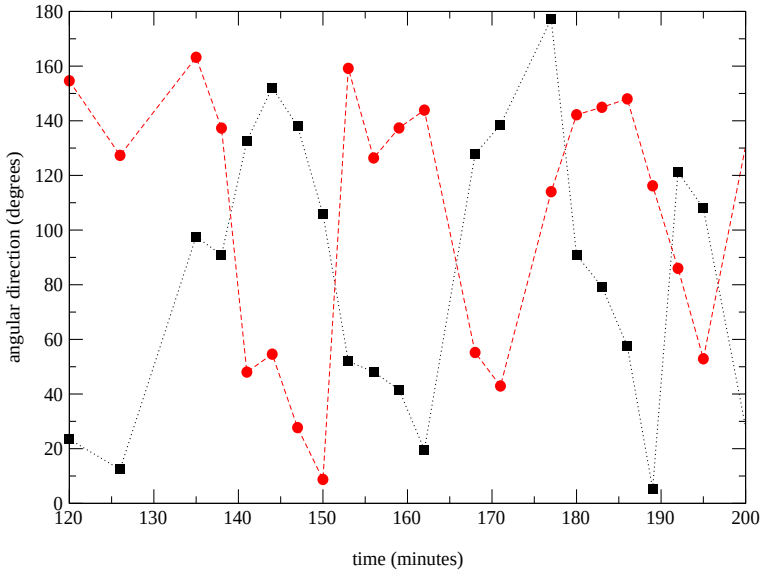

Figure 6.12: Evolution of the eigenvectors' directions related to previous plot (figure 6.11) for the restricted time range from t=120 minutes to t=200 minutes. Two axes for the pulsation can be identified around 50 and 140 degrees (± 180 degrees). Moreover a rough estimation of the period of pulsation can be measured at around 30 minutes

This result is perfectly consistent with the behaviour estimated from the protrusive signals. Hence, optical flow provides a helpful alternative method to the fastidious cell boundary segmentation, where the entire spatio-temporal information is contained in the eigenvalue time-signals. These time signals are moreover amenable to standard Fourier analysis such as those performed previously on the individual protrusive signals.

Figure 6.13 presents the Fourier transform of the first eigenvalues of Figure 6.11 (upper black plot). One relatively isolated peak corresponding to a period of 34 minutes appears. Another related peak corresponding to the half period is also visible.

Fourier analysis from the eigenvalue signals has been performed for all the cells of the sequence S_4 and the results obtained are displayed in Table 6.3. Although the periodicities could not always be detected, they are mostly consistent with the periodicities evaluated from the protrusive signals of each cell.

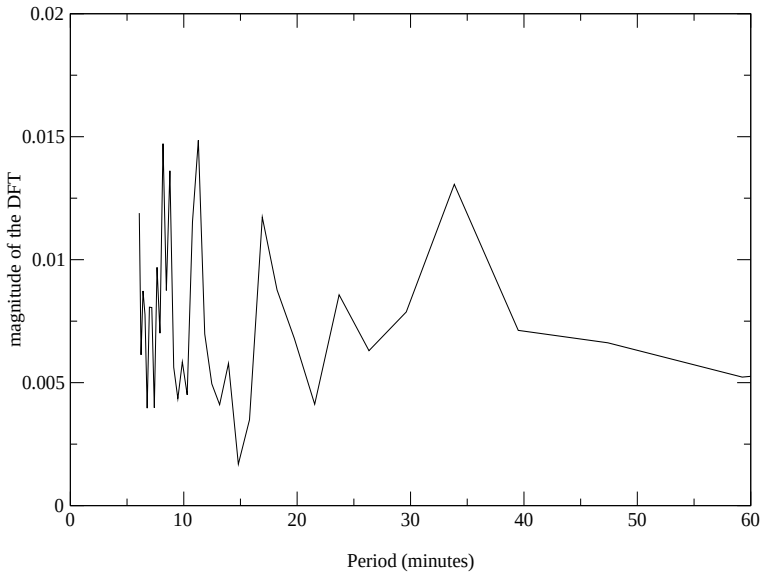

Figure 6.13: Fourier transform of the eigenvalue signal $\lambda_1(t)$. An isolated peak of intensity appears at a period of 34 minutes and a second competing peak associated with a period of 17 minutes.

Cell identification	time-interval (min) for the measures	Period (min) for $\lambda_1(t)$	Period (min) for $\lambda_2(t)$
S_4c_1	[0,765]	17	35
S_4c_1	[0,399]	17	36
S_4c_1	[402,765]	27	32
S_4c_2	[0,240]	34	31
S_4c_2	[399,765]	-	-
S_4c_3	[0,432]	-	-
S_4c_3	[0,201]	-	41
S_4c_3	[201,432]	-	33
S_4c_4	[0,765]	-	-
S_4c_4	[0,240]	35	30
S_4c_4	[240,600]	-	-
S_4c_5	[0,765]	17	34
S_4c_5	[0,240]	35	35
S_4c_5	[240,462]	16 (32)	16 (32)
S_4c_5	[462,765]	12	13
S_4c_6	[0,765]	-	-
S_4c_6	[0,600]	24	-

Table 6.3: Estimations of the periodicities from the Fourier transform of each eigenvalue plot

6.5 Discussion

It is commonly admitted that the cell membrane fluctuates without any specific direction in space and without any particular coherence with time. However, different results support the self-organized character of these cell shape changes. Ehrengruber *et al.* (1995) show that neutrophils undergo periodic cytoskeletal rearrangements that lead to cycles of shape change, ultimately resulting in cell translocation. Rotating waves were also characterized in the case of keratinocytes (Alt *et al.*, 1995).

Our study shows that isolated L929 murine fibroblasts cultured *in vitro* exhibit an auto-organized behaviour. The characterization of the spontaneous deformation of the cells, i.e. without external stimuli except cell adhesion on the glass substratum, is realized on the basis of image analysis of videomicroscopy sequences. A standard method of analysis in order to get a spatio-temporal representation or contour map for the dynamics of cell deformations, is the cell boundary segmentation method. This method allows us to obtain very detailed information on the cell dynamics (amplitudes of extension/retraction of the protrusions, measures of periodicities for the overall dynamics). However, this approach is quite tedious and fastidious as automatic detection of the cell outline remains inefficient in most cases because of the weak video image contrast between the cell membrane and the glass substratum. As an alternative we rather applied a previously developed method based on optical flow analysis. This method indeed allows a rapid and efficient character-

ization of the nature of the cell dynamics (pulsation, oscillation, migration, etc ...) and provides a direct measure of the possible periodicity of the cell deformations. We thus characterized quadrupolar preferential cell morphologies associated with a periodic and synchronized pulsating movement between two perpendicular protrusive directions, where pseudopod retraction along one axis corresponds to the extension in the perpendicular axis.

Comparing these results with those obtained for keratinocytes (Alt *et al.*, 1995), we observed one interesting similarity. In particular, the fact that an extension in one direction is accompanied by the simultaneous retraction in another direction. Beyond the chemical characterization of the recurring pseudopods protrusion and retraction which appear to be driven by actin polymerization/depolymerization cycles (in neutrophils, sinusoidal oscillations of F-actin, with period of 8-10s, were reported (Ehrengruber *et al.*, 1995)), cyclic alteration of the cell body shape can be viewed as the result of an iso-volumetric or iso-mass feedback control. As proposed by Dunn and Zicha (1995), the spread area of a cell could be actively regulated by feedback mechanisms which adjust the rate of protrusion in order to compensate spontaneous fluctuations in retraction. The explanation proposed by Dunn and Zicha (1995) is that retraction involves disassembly of cellular material which is then rapidly transported to other parts of the cell to generate protrusive structures.

The time for recycling of the material which is most probably actin depends on the cell morphologies. In the case of keratinocytes (rounded shapes), circulation of the material through the rotating wave is easy. The periodicity reported by Alt *et al.* (1995) is around 2 minutes, whereas for fibroblasts which exhibit long polarized structures displacement of the material from the tip of one protrusion to another is a much longer process. According to our measurement of the periodicity, this takes around 30 minutes. Despite the strong morphologic differences between the two types of cells, it is possible to suppose a common origin for the underlying processes involved in their respective self-organization. Our aim will be to test this aspect through our theoretical modelling.

Chapter 7

Influence of cell-cell interactions on the spontaneous dynamics

Influence des interactions cellule-cellule sur la dynamique spontanée

L'influence d'interactions entre cellules sur le comportement spontané pulsant caracterisé au chapitre précédent est etudiée à partir de deux situations expérimentales différentes. Dans le premier cas, un groupe de cellule en interaction est considéré. A partir de la définiton de domaines d'influence pour chaque cellule impliquée dans l'interaction, il a été mis en évidence conformément au phenomène d'inhibition de contact que les morphologies cellulaires observées sont fortement conditionnées par les contraintes de voisinage imposées. Ainsi, les cellules adoptent une nouvelle forme leur permettant d'éviter de futurs contact avec leurs voisines. Dans le second cas, un degré de contrainte moins important est considéré afin d'autoriser une plus grande liberté de mouvement aux cellules et d'indentifier d'éventuelles transitions entre états morphologiques déclenchées par un contact. Deux exemples sont présentés où l'on observe une transition accompagnée d'une réduction du nombre de protrusions, de 4 à 2 et de 4 à 3 respectivement. Dans le premier exemple, le nouvel état morphologique est atteint suite à une longue phase transitoire durant laquelle la cellule ne présente plus de dynamique cohérente. Dans le second exemple, la transition s'opère de manière beaucoup plus directe: on observe la disparition d'une protrusion en même temps que la réorganisation symmétrique des protrusions restantes. Pour le premier exemple, le contact s'est effectué au niveau d'une protrusion, alors que dans le second cas, il s'est effectué dans une zone entre les protrusions. Cette observation suggère que la sensibilité de la cellule et plus particulièrement sa réaction est fortement accrue si le contact se produit au niveau des zones protrusives dejà hautement dynamiques. De plus, les mesures des distances angulaires entre les protrusions montrent que les cellules tendent à garder autant que possible des morphologies symétriques qui ne s'expliquent qu'à travers des transitions de régime dynamique de l'actine. Une dernière observation montre qu'une transition de type inverse de celles evoquées c'est à dire vers une morphologie avec plus de protrusions qu'initialement, se produisait également dans le cas par exemple d'une cellule qui retrouve une configuration symétrique après une periode contrainte.

7.1 Introduction

Isolation of the cells is often difficult. In the sequences studied, we have considered as "isolated", cells which do not have permanent contacts with the other cells of the neighbourhood. Consequently, we have called "spontaneous" the behaviour of these cells, although we can never be sure that it is the case. Indeed, each cell (even those perfectly isolated) has an interaction past which can still influence the observed morphology on the available temporal sequence. Therefore, in this chapter, we propose to consider the case of identified direct contact interactions between neighbour cells in order to determine how the contact can shed light on the principles of organization of the cell morphologies and the associated actin dynamics. Cell-cell contact and the related phenomenon of contact inhibition have been extensively studied in the case of migrating cells bumping against each other (Abercrombie and Heaysman, 1953; Harris 1973; Abercrombie 1980; Heaysman and Pegrum, 1982; Middleton and Sharp, 1984). The phenomenon of contact inhibition observed was first described by Abercrombie (1980) as:

" ... the stopping of the continued locomotion of a cell in the direction which has produced a collision with another cell or, alternatively, the prohibition, when contact between cells has occurred, of continued movement such as would carry one cell across the surface of another."

It is strongly suspected that contact inhibition may be due to the loss of local adhesiveness and contraction of the cortex for the cells involved. In our experiment we observed less spectacular contact as our cells are not migrating. Indeed, we consider populations of cells which pulsate without transient displacement of their centre of mass. They occasionally make contacts with their neighbours where inhibition is observed. Two experimental situations are studied. In the first case a group of interacting cells is considered in order to determine how the morphologies of the cells involved adapt to a neighbourhood constraint. In the second case dynamical transitions are considered this time to see how the new constrained morphologies emerge from the contact. We will see in particular that the location of the contact on the cell seems to determine the degree of cell reaction.

7.2 Adapted morphologies of interacting cells

Cells having experienced a contact with a neighbour according to the phenomenon of contact inhibition, tend to reorganize their shape in a suitable way in order to avoid future contact. This leads to a new morphology with usually a reduced number of protrusions. Figure 7.1.a shows a typical case of interaction where each cell has already experienced at least one contact with all its direct neighbours. The 2 cells in the center squeezed between two neighbours at each left and right side present bipolar shapes. The cell on the left of the group, which is only constrained at one side, is free to exhibit one more protrusion in the empty space. The cell on the right of the group seems more seriously inhibited as it exhibits no distinctive membrane protrusions and remains almost motionless during

the complete sequence. We will therefore rather focus on the 3 other cells. Characterization of the protrusive behaviour of interacting cells is performed through the definition of influence domains for each cell within a group of cells. This domain is schematically represented by a circle (see chapter 5 for details) which basically represents the area where the cell can potentially protrude its membrane and consequently interact with other cells which would penetrate the domain. The intersection of two (or more) influence domains (Figure 7.1.b) thus represents the potential interaction zones which can be superimposed on the spatio-temporal map defined for each cell (Figure 7.2). Two levels of interaction are defined depending on the number of influence domains involved: light grey for the superposition of 2 influence domains and dark grey for 3. This code is transferred to the spatio-temporal maps of Figure 7.2. This thus provides a global picture of the contact inhibition phenomenon, where the cell protrusions preferentially appear and remain located outside the darkest interaction zones. The memory of the location of the constraints remains for a relatively long time, here up to 2 hours.

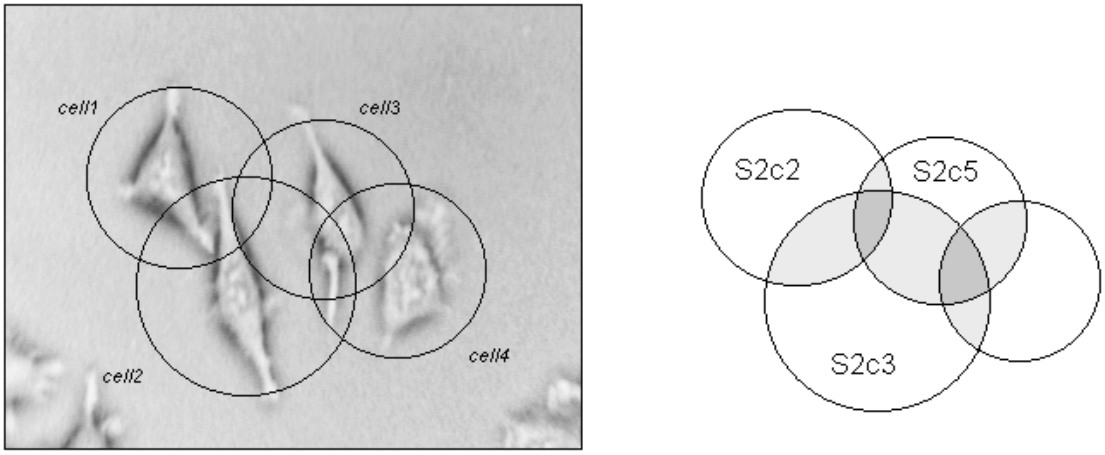

Figure 7.1: A group of 4 interacting cells. For each cell, a domain of influence is defined and represented by a circle centered on the cell nucleus and with a radius corresponding to the maximum amplitude recorded for the protrusions of the cell. The intersection of these domains thus corresponds to interaction zones which are represented in light grey (2 cells involved) and dark grey (3 cells involved) on the right picture. Cell1=S_2c_2, cell2=S_2c_3 and cell3=S_2c_5

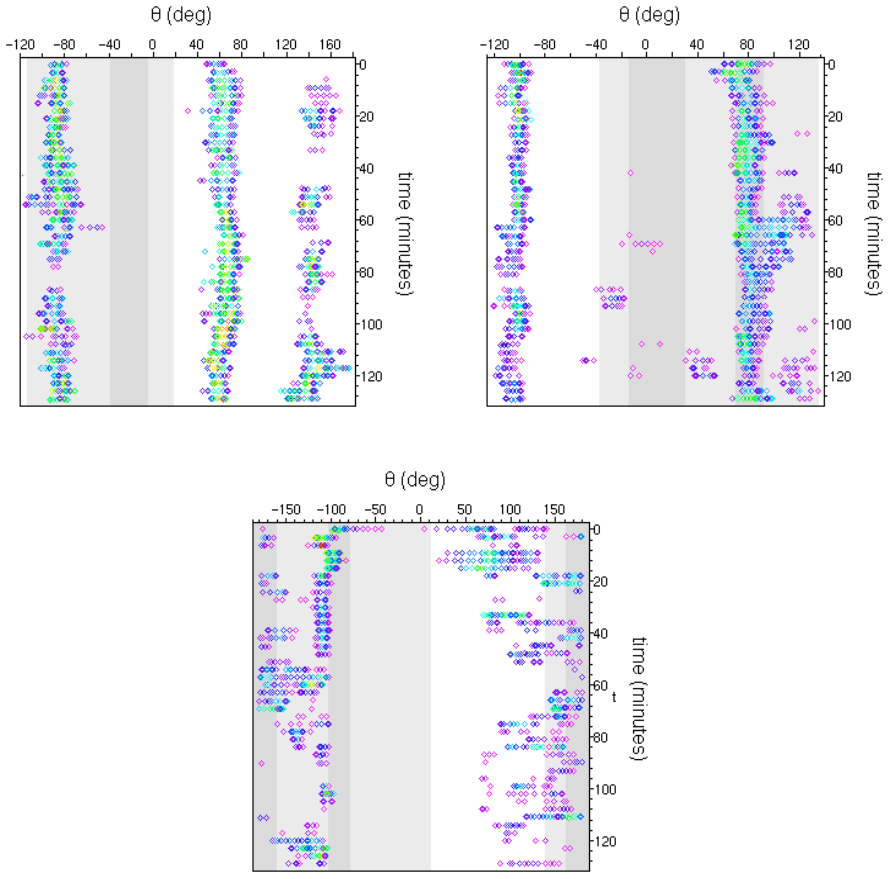

Figure 7.2: Spatio-temporal maps associated with the cell involved in the interaction (except cell 4 which is not considered) i.e. respectively S_2c_2, S_2c_3 and S_2c_5. Interaction zones are represented on each map to provide a comprehensive picture of the interaction-related dynamic of each cell.

7.3 Transitions towards new dynamical states

The other aspect which is of interest is to determine whether the new shapes are organized in accordance with the interaction zones only, or if a symmetrical component exists which needs also to be considered as this is suggested by the results presented in the previous chapter (see Figure 6.2). In other words, does the actin dynamic force the cell to be symmetric ?

In the case of interactions previously studied, a group of cells is considered, consequently the constraint existing on each cell is maintained with time and the resulting morphologies are entirely determined by the constraint state. Here we thus propose to consider cases of contact between isolated cells, namely for cells which are not constrained as much by their environment and are thus free to move and express new dynamical states.

Figure 7.3 presents the spatio-temporal maps of two cells which have each interacted with a separate neighbour (but not with each other). In both cases the cells were initially presenting 4 protrusive directions. A contact triggers for both a bifurcation toward a new morphology.

In the first case (Figure 7.3, left graph), the contact occurs around the instant $t = 180$ minutes which is confirmed by the observation of the associated videomicrograph (Figure 7.5, picture 3). The cell then enters a long perturbed phase which lasts for about 4 hours, where no obvious protrusive direction can be identified and characterized by uncoordinated movements of the membrane (pictures 4, 5 and 6). Finally a new morphology emerges around the instant $t = 420$ (picture 7) where the cell adopts a bipolar stable shape (pictures 8 to 12).

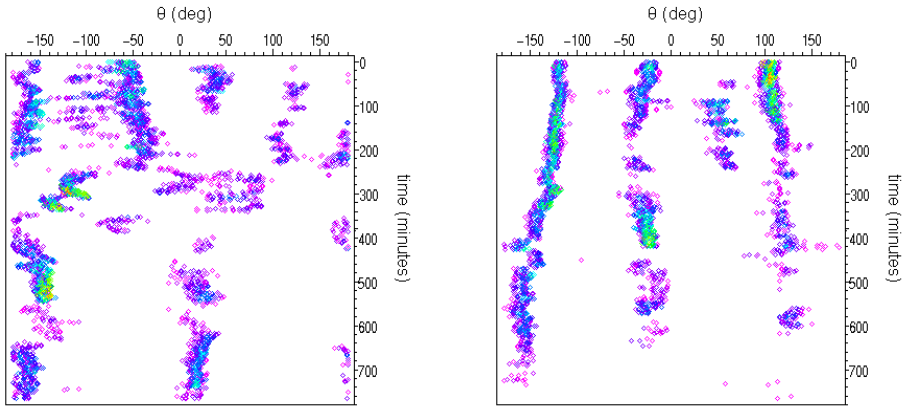

Figure 7.3: Examples of cell morphological transitions triggered by contacts corresponding respectively to cell S_4c_2 and S_4c_4. In the first case, a transition from 4 to 2 protrusions occurs after a long chaotic period from t=200 minutes to t=400 minutes approximatively. In the second case a transition from 4 to 3 protrusions occurs in a continuous way triggered by contact between cells.

In the second case (Figure 7.4, right graph), the bifurcation occurs in a much more direct way, without passing through the long chaotic phase such as previously observed. The contact occurs around the instant $t = 240$ minutes when a cell just appearing from mitosis touches the cell in its spontaneous 4-protrusion pulsating state (Figure 7.6). A transition from 4 to 3 protrusions is observed with the disappearance of the weakest protrusion and the slow spatial redistribution of the 3 remaining protrusions in a symmetrical shape (pictures 5 to 8). Further contacts are later observed from the instant $t = 480$ minutes (pictures 8 to 10) and the cell finally adopts a rounded shape. However it is difficult to determine whether this new shape is the result of the latter contacts or if it is because the cell is entering its mitotic phase (the sequence was interrupted before the probable mitosis could be observed).

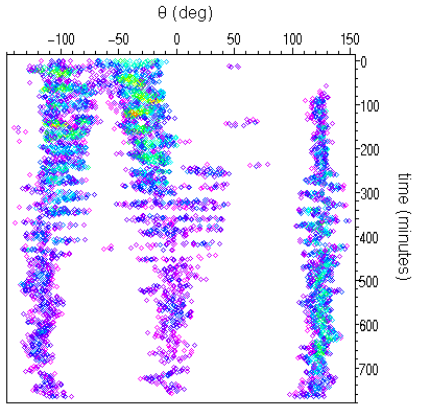

Figure 7.4: Example of the slow emergence of a symmetrical and stable morphology from an initially perturbed state (cell S_4c_5).

Table 7.1 presents for the two cells studied the measures of the angular distance between two consecutive protrusive directions before and after the interaction. The angular width taken to isolate a protrusive direction is quoted once for each first measure. The results show that the protrusions are rather homogeneously displayed around the cell body with an angular distance around 90, 120 and 180 degrees for 4, 3 and 2 protrusions respectively. This thus confirms the idea that the cells tend to keep symmetrical shapes.

The two cases presented above have been concerned with transitions of the initial morphology towards new shapes involving a reduced number of protrusions. We observe a transition from 4 to 2 protrusions in the first case and from 4 to 3 in the second case. However, we can assume that the reverse situation exists. For example when a cell finds itself free of any constraint and then relaxes from a constraint state with a restricted number of protrusions to a state with more protrusions. Such a situation is presented in Figure 7.4. Initially, the cell presents a perturbed shape with no obvious protrusive directions. Two protrusive directions emerge from the same location of the cell periphery and slowly move apart whereas a third protrusion develops in parallel. The resulting shape

Cell identification	$\Delta\theta_i\theta_j$ before the contact	$\Delta\theta'_i\theta'_j$ after the contact
S_4c_2	$\Delta\theta_1\theta_2 = 120 \pm 30$	$\Delta\theta'_1\theta'_2 = 190 \pm 35$
	$\Delta\theta_2\theta_3 = 90$	$\Delta\theta'_2\theta'_1 = 170$
	$\Delta\theta_3\theta_4 = 80$	
	$\Delta\theta_4\theta_1 = 70$	
S_4c_4	$\Delta\theta_1\theta_2 = 95 \pm 25$	$\Delta\theta'_1\theta'_2 = 120 \pm 35$
	$\Delta\theta_2\theta_3 = 80$	$\Delta\theta'_2\theta'_3 = 140$
	$\Delta\theta_3\theta_4 = 60$	$\Delta\theta'_3\theta'_1 = 100$
	$\Delta\theta_4\theta_1 = 125$	

Table 7.1: Angular distance $\Delta\theta_i\theta_j$ between two consecutive protrusive directions θ_i and θ_j before and after the contact.

of the cell is once again symmetrical.

7.4 Discussion

Contact inhibition mechanism affecting protrusion dynamics appears to be a key phenomenon both in the organization of the cell shape and in the organization of cells to form tissues. This organization is driven and regulated by two types of contact interactions namely homotypic and heterotypic contacts. The difference of sensibility between these two types of contact depends on the cell types (Middleton and Sharp, 1984) . For example epithelial cells show an inhibition of motility towards homotypic contact which is much less spectacular than for fibroblasts. This is explained by the fact that *in vivo* epithelial cells are organized in monolayers to form the epithelium, whereas fibroblats are more isolated cells embedded within an extracellular matrix. Comparative studies between normal and cancer cells performed *in vitro* have demonstrated that cancer cells show deficient heterotypic contact inhibition of motility (Heaysman, 1970). This observation gives an explanation for their ability to invade surrounding tissue to form either tumours or metastasis *in vivo*. In our case only homotypic contacts are considered. The aim has been to see how the contact can explain the cell shapes, and how it can provide information on the possible spontaneous pulsating state of the cells and the underlying actin dynamics.

Our observations show that the cells tend to readapt their shapes in order to avoid future contact with their neighbours. Moreover, it appears that the cells try to maintain symmetrical morphologies when submitted to local perturbations as long as there is sufficient space all around to express their new dynamics. These results suggest that there may exist a spontaneous morphology corresponding to the 4-protrusion pulsating state. One example in particular showed that the cell recovers a symmetrical shape with more protrusions when the cell is not constrained any more. The cell seems to relax towards such a spontaneous state.

Another interesting fact in our observations is the influence of the location of the contact on the cell response. We observed that when the contact is made on a protrusion the effect is much more important than when it happens on other parts of the cell. In the first type of contact dramatic disruption of the cell shape was observed followed by a long chaotic phase for the cell membrane movements. In the second type of contact a continuous transition is observed between the two morphologies. In the case of migrating cells, similar effects have been reported (Abercrombie *et al.*, 1970) and these depend on which part of the lamella interacts with the other cell. When the front part of the lamella is contacted, extensive paralysis is observed whereas for adjacent parts only local paralysis occurs.

Since cell protrusive activity is a spatio-temporal coordinated process, it remains to make precise how simultaneous competing lamellipodia can integrate the external signal of contact and trigger morphological cell bifurcation from a free given shape to another constrained one.

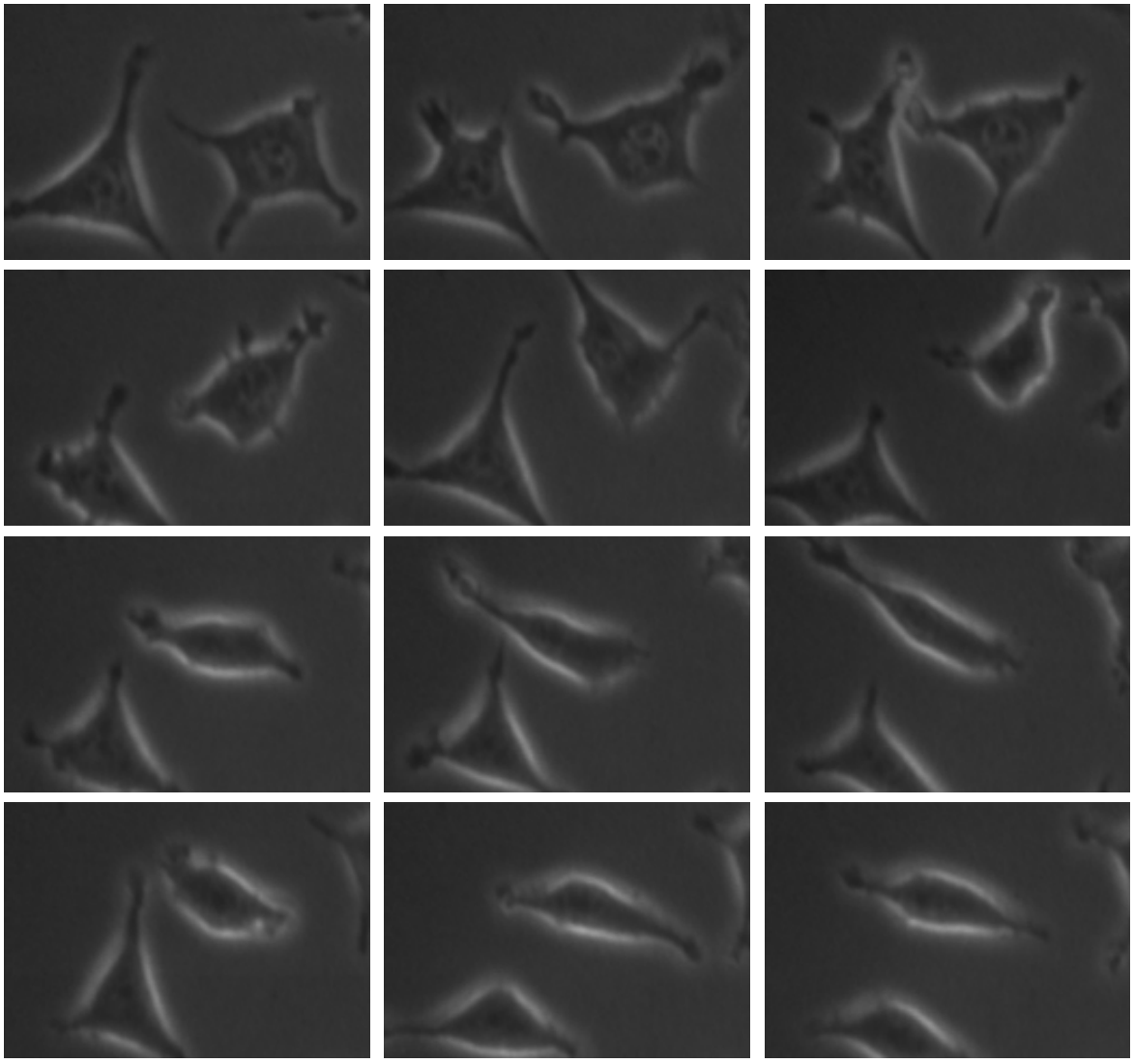

Figure 7.5: Videomicroscopy sequence which shows the interaction leading to the morphological transition of the cell S_4c_2 (cell on the right of the pictures). The first picture correspond to time t=60 minutes and the time interval between two consecutive pictures is one hour. During the three first hours of the sequence, the cell pulsates with a geometry involving 4 protrusions (pictures 1 and 2). Around time $t = 180$ minutes (picture 3), the contact with the neighbouring cell occurs. The cell then enters a chaotic phase with no coherent shape (pictures 4, 5 and 6). Around $t = 420$ minutes (picture 7), the cell seems to be stabilized in a polar shape with two opposite protrusive directions, which lasts during all the remaining time of the sequence (pictures 8 to 12).

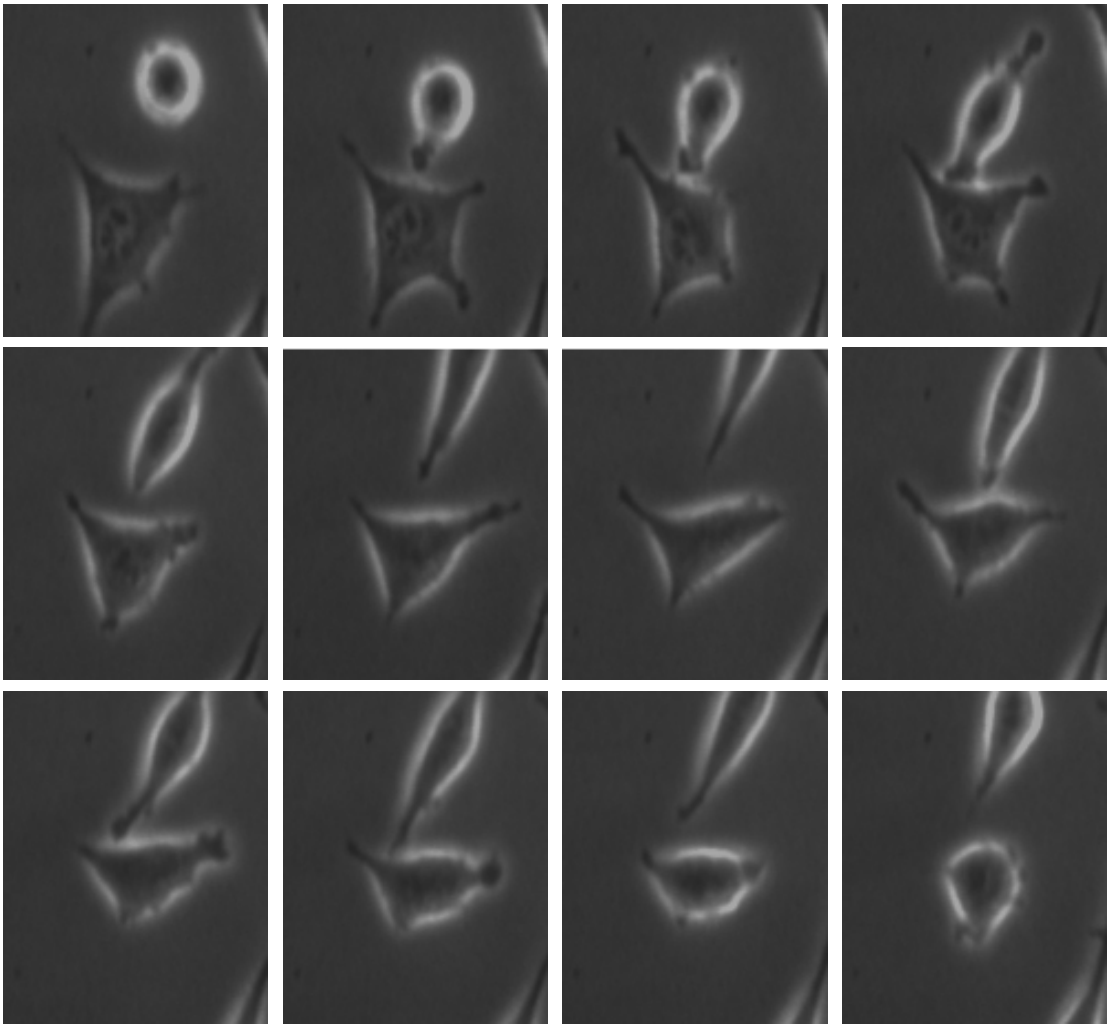

Figure 7.6: Videomicroscopy sequence which shows the interaction leading to the morphological transition of the cell S_4c_4 (cell at the bottom of the pictures). The first picture corresponds to time t=60 minutes and the time interval between two consecutive pictures is one hour. As in the previous case, the cell exhibits an initial pulsating behaviour involving 4 protrusive directions. The contact occurs around $t = 420$ minutes (picture 4). The cell then readapts its shape with the fusion of two of its protrusions. The cell then presents a new symmetrical morphology with 3 protrusions (pictures 5 to 8). Further contacts are made with the neighbouring cells (pictures 9 and 10) which finally lead to a rounded shape which might also be due to the cell entering mitosis (pictures 11 and 12).

Part III

Theoretical Modelling of Cell Membrane Deformations and Cell Migration

Introduction

The self-organized character of cell deformations is due to the dynamics of actin inside the cell cortex. A model already successfully used to describe both qualitatively, in terms of the observed dynamics and quantitatively, in terms of the periodicities of the coordinated movements of extension retraction of the cell membrane, was initially proposed by Alt *et al.* (1995) in a paper which deals with the dynamics of keratinocytes. It is one of those rare models which deals with spontaneous cell deformations as an integrated process at the scale of the whole cell and based on mechano-chemical hypotheses describing the actin dynamics interacting both with the myosin to form a contractile actomyosin cortex and with the membrane.
This model has been chosen because of its relative simplicity as it involves a minimum number of variables, while incorporating salient features of biomechanical cell deformations. It thus provides an ideal basis for further development and refinement that we propose to investigate in the course of the following chapters. The first step has been to investigate the ability of the model to reproduce, at least qualitatively, the standing wave dynamics characterized for the L929 fibroblast line. As the model is only valid in the approximation of small deformations, it is clearly unable to match the starry morphologies of the fibroblasts. However on the basis of the dynamical data taken from the characterization of this cell line, attempts have been made to evaluate the range of the mechanical parameter values in order to discuss their validity. Beyond its ability to deal with spontaneous cell deformations, it is then interesting to determine to which extent this model is a valuable representation for analyzing the various aspects of cell interactions with its environment through a continuous and integrated description of the cell dynamics. The first extension proposed concerns cell-cell interactions and more specifically the phenomenon of contact inhibition resulting in the collision between cells. In the second extension, cell chemotaxis has been investigated through the coupling of a gradient of extracellular factor and the mechanical properties of the cell membrane. In both situations complex pathways of signal transduction are involved from the detection of the signal to the elaboration of the cell response and these processes are clearly out of reach of the present cytomechanical model formulation and are therefore not explicitly described. However, the corresponding effects of this internal signalling can at least be simulated on the basis of experimental observations, and their consequences on the dynamics of the simulated cell examined. Then, the agreement between the model simulations and the observed cell dynamic response will provide an additional step towards the model validation. In the case of contact inhibition for example, the mechanical parameters supposed to be affected by the interaction could

be identified from the scanning acoustic microscopy technique (Bereiter-Hahn and Zoller, 1998) and their relevance in the phenomenon of motility inhibition could be tested through our model (Zoller *et al.*, 1997). In a similar way, concerning cell chemotaxis, it has been suggested by various studies that the observed cell polarization could be the result of a local decrease of the surface membrane tension (Soares and Maghelly, 1999; Raucher and Sheetz, 2000). In our model extension, this effect is modelled by considering a dependence of the tension with regard to the local concentration of extracellular factor on the membrane (Nielsen *et al.*, 1998) and thus allowed to demonstrate the potential importance of this phenomenon in cell migration.

Finally, on returning to the modelling of spontaneous cell deformations, we remained frustrated by the limitation of small membrane deformations imposed by the model. We therefore proposed a new formulation of the model which, while keeping the basic mechanical hypotheses of the initial one, allows us to describe large membrane extensions such as those observed on most fibroblastic cell lines and here more specifically on the L929 line. While the actin dynamics were most of the time restricted to one space dimension further refinements of this new model are proposed in order to tend to an accurate description of the polymer dynamics in a real two-dimensional cell cortex.

Chapter 8

Modelling the spontaneous deformation dynamics of cells

Modélisation de la dynamique spontanée des déformations cellulaires

Parmi les nombreux modèles existants dans la litérature destinés à rendre compte de la dynamique oscillante des déformations membranaires (voir chapitre 2), nous avons choisi comme modèle de base le modèle cytomécanique de Alt et Tranquillo (1995). De même que la plupart des autres modèles, ce modèle est fondé sur la description des interactions de l'actine avec d'une part le cytoplasme, à travers les forces visqueuse et contractile (générée par le complexe actomyosine) et d'autre part la membrane à travers les forces de tensions liées à la courbure locale membranaire. La particularité de ce modèle est de proposer une description de la dynamique de l'actine couplée au mouvement membranaire à l'échelle globale de la cellule et non simplement à un niveau local limité à une région de la membrane. Il permet ainsi de rendre compte de manière coordonnée de l'ensemble des mouvements observés de la cellule.

Le modèle est ainsi décrit par un système de trois équations aux dérivées partielles. Une première équation représente la dynamique de l'actine dans le cortex cellulaire à travers ses déplacements convectifs (dans la direction tangentielle θ) et sa capacité de polymérisation (ou dépolymérisation) dépendante de la densité locale d'actine $a(\theta, t)$ à chaque instant t. Cette densité locale d'actine conditionne la force de rétraction de la part du réseau sur la membrane plasmique qui se trouve contrebalancée par l'existence de la pression hydrostatique interne et modulée par la tension due a la courbure locale de la membrane. Cet équilibre de force est representé par une seconde équation qui permet de suivre la position résultante de la membrane, $L(\theta, t)$, à chaque instant. Les propriétés contractiles et visqueuses du milieu sont considérées par le biais d'une 3 ème équation qui décrit l'équilibre des forces exercées sur le réseau d'actine. Ces forces conditionnent la vitesse de déplacement, $v(\theta, t)$, de l'actine dans le cortex. Les variables décrites par le modèle sont donc la densité d'actine $a(\theta, t)$, sa vitesse de déplacement dans le cortex $v(\theta, t)$ et la largeur local du cortex $L(\theta, t)$. La dérivation du terme de courbure membranaire implique une approximation mono-dimensionnelle de la dynamique

de l'actine qui est alors supposée constante selon l'axe radial de la cellule.

L'analyse de stabilité linéaire du système d'équations aux derivées partielles permet de définir les conditions nécessaires à l'obtention d'une bifurcation vers un état non stationnaire oscillant (bifurcation de Hopf) pour des modes instables donnés. Les simulations effectuées sur la base de cette analyse montrent que le modèle est en effet capable de reproduire des comportements dynamiques pulsants, qualitativement proches de ceux observés expérimentalement sur notre lignée de fibroblastes L929 (voir chapitre 6). Sur la base de ces résultats théoriques, les paramètres du modèle définissant les propriétés intrinsèques mécaniques de la cellule sont evalués à partir d'une calibration effectuée entre les données simulées et les données morphodynamiques issues de la caractérisation expérimentale de la lignée cellulaire L929.

8.1 Introduction

As described in detail in Chapter 2, different hypotheses have been proposed to explain the periodic oscillatory movement of the cell membrane and the role of actin polymerization/depolymerization cycles in the recurring protrusion and retraction dynamic of the lamellipod. Among all the models proposed we have chosen as a basis the model proposed by Alt and Tranquillo (1995). The main reason is that this model considers both the molecular events of the polymerization/depolymerization dynamics and the related mechanical properties of the cell (membrane and cytoskeleton). This model has already been used with success to describe the appearance of rotating waves of deformation around the cell body of keratinocytes (Alt *et al.*, 1995) and leukocytes (Alt 1990). Our aim has then been to investigate further the dynamical states which the model is able to describe. In particular, we have been especially interested to evaluate its ability to generate pulsating dynamical states such as those observed and characterized experimentally on the L929 fibroblast line.

8.2 The Cytomechanical model

The model considers that cell protrusion dynamics is due to the biophysical properties (visco-elasticity, contractility,...) of the cortical polymer layer or network of actin and myosin filaments which underlies the cell membrane and surrounds the cell body (see chapter 1). Moreover, this more or less dense network is able: (i) to disassemble at locations where it becomes condensed, (ii) to reassemble in cell protrusions, like lamellipodia. Cell protrusion then results from a mechanical non-equilibrium state involving both forces acting on the cell periphery and the subsequent polymerization/depolymerization process induced by intra-cellular space variation. The first part of the model depicts the dynamics of the actin in the cell cortex which is mainly responsible for cell shape reorganization through its ability:

- to polymerize into F-actin and depolymerize into G-actin,
- to interact with myosin to generate the contractile activity in the cell,

- to move through the cytoplasm via convection.

The local amount of F-actin also determines the intensity of the resistive stress applied on the membrane as the result of actin cytoskeleton-membrane proteins cross-links (see chapter 1). This resistive stress, together with the cortex-membrane curvature-induced stress, balanced the intra-cellular hydrostatic pressure. This pressure acts as the "driving force" in the model. A schematic representation of the cell such as considered by the model is displayed in Figure 8.1.

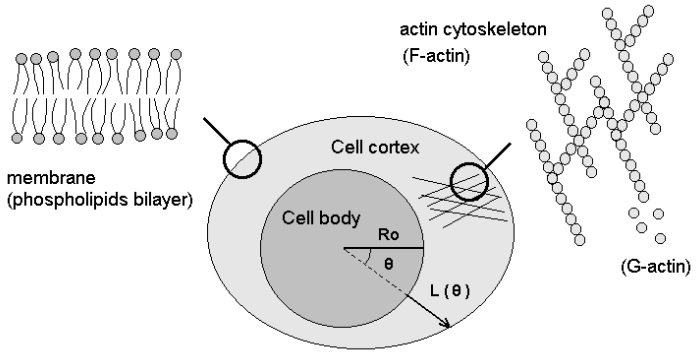

Figure 8.1: Schematic representation of the cell

8.2.1 Membrane curvature tension

The membrane-actin complex is under a tension $\tau(a)$. The origin of this tension is linked to the contractile activity of the actomyosin. The model thus assumes that this tension depends on the local concentration of actin and that a minimum of connections between the cell membrane and the network is necessary for that tension to exist. The tension generated by the membrane-actin complex induces a normal force (pressure) on the F-actin network which depends on the local curvature of the membrane. The curvature tension force is derived in the following way:

$$\mathcal{T}_c = \nabla \cdot [\tau(a)T(x)],$$

where x represents the curvilinear abscissa describing the cell membrane and $T(x)$ the expression of the tangent to the membrane which is given by:

$$T(x) = \frac{1}{R(x)} \frac{\partial R(x)}{\partial x}.$$

In the approximation of small curvature, the curvilinear referential $(\vec{N}, \vec{T})$ and the polar referential $(\overrightarrow{U_r}, \overrightarrow{U_\theta})$ are almost equivalent $(x \equiv \theta)$. We choose the polar notation:.

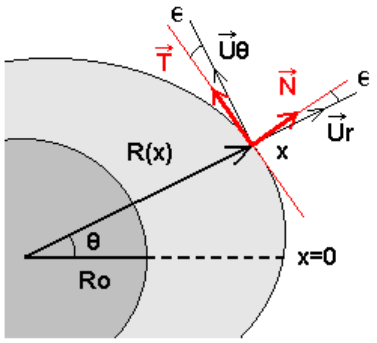

Figure 8.2: Schematic representation of the polar and curvilinear referentials

$$\begin{aligned}
\mathcal{T}_c &= \frac{1}{R(\theta)}\frac{\partial}{\partial\theta}\left(\tau(a)T(\theta)\right) \\
&= \frac{1}{R(\theta)}\frac{\partial}{\partial\theta}\left(\frac{\tau(a)}{R(\theta)}\frac{\partial R(\theta)}{\partial\theta}\right) \\
&= \frac{1}{R(\theta)}\left[\frac{\partial\tau(a)}{\partial\theta}\frac{1}{R(\theta)}\frac{\partial R(\theta)}{\partial\theta} - \frac{\tau(a)}{R(\theta)^2}\left(\frac{\partial R(\theta)}{\partial\theta}\right)^2 + \frac{\tau(a)}{R(\theta)}\frac{\partial^2 R(\theta)}{\partial\theta^2}\right]
\end{aligned}$$

Linearization of this expression with $R(\theta) = R_0 + L(\theta)$ where $L(\theta) \ll R_0$ leads to:

$$\begin{aligned}
\mathcal{T}_c &\approx \frac{1}{R_0}\left(\frac{\partial\tau(a)}{\partial\theta}\frac{1}{R_0}\frac{\partial L(\theta)}{\partial\theta} + \frac{\tau(a)}{R_0}\frac{\partial^2 L(\theta)}{\partial\theta^2}\right) \\
&\approx \frac{1}{{R_0}^2}\frac{\partial}{\partial\theta}\left(\tau(a)\frac{\partial L(\theta)}{\partial\theta}\right)
\end{aligned}$$

If we include the term $1/{R_0}^2$ in the coefficient τ of the function $\tau(a) = \tau a$ we obtain the curvature tension force such as it appears in the model equations i.e.:

$$\mathcal{T}_c = \frac{\partial}{\partial\theta}\left(\tau(a)\frac{\partial L(\theta)}{\partial\theta}\right). \tag{8.1}$$

8.2.2 Equations of the model

For simplicity, we transform the two-dimensional problem into a one-dimensional version. We assume, as in Alt and Tranquillo (1995), that the F-actin density, as well as its convective tangential velocity, is constant in the radial direction. The first assumption is justified when the width of the cell cortex $L(\theta, t)$ remains small in front of the radius of the cell body R_0. The second implies that the cortical network can slip with respect to the membrane, which is also partly justified if considering that membrane proteins involved

in the network-membrane connections are mobile within the membrane.

The three variables considered in the cytomechanical model are thus:

1. the F-actin concentration in the cortex $a(\theta, t)$,
2. the F-actin tangential velocity $v(\theta, t)$,
3. the width of the cell cortex annulus $L(\theta, t)$, given by the membrane position measured from the surface of the cell body (see Figure 8.1).

The spatio-temporal evolution of these three variables is given by the following set of partial differential equations.
The first one represents the conservation of F-actin in the cortex. η characterizes the polymerization rate whose state of polymerization/depolymerization depends on the local value of F-actin concentration relative to the stationary concentration at the chemical equilibrium a_0.

$$\frac{\partial}{\partial t}(La) + \frac{\partial}{\partial \theta}(Lav) = \eta L(a_0 - a). \tag{8.2}$$

The second equation describes the balance of forces applied on the cortex-membrane in the radial direction. The model takes into account:

- a viscous friction which represents the cell adhesion on the substratum, modulated by the coefficient Φ_1,
- the intra-cellular hydrostatic pressure β_1,
- the resistive elastic stress due to the cortical network-membrane attachment with the elasticity coefficient for the actin network γ_1 and
- a curvature-dependent stress due to the surface tension of the actin-membrane complex characterized by the coefficient τ_1.

$$\Phi_1 a \frac{\partial L}{\partial t} = \beta_1 - \gamma_1 La + \frac{\partial}{\partial \theta}\left(\tau_1 a \frac{\partial L}{\partial \theta}\right). \tag{8.3}$$

The third equation concerns the balance of forces in the tangential direction. It includes:

- the frictional force on the network moving in the cytosol, with magnitude controlled by a drag coefficient Φ_0 (related to the attachment of the network with the membrane and the other types of filaments),
- a viscous stress with viscosity coefficient for the cytoplasm μ_0 and
- the membrane curvature induced stress with coefficient τ_0.

$$\Phi_0 av = \frac{\partial}{\partial\theta}\left[\mu_0 a\frac{\partial v}{\partial\theta} + \sigma_0(a) - \frac{\partial}{\partial\theta}\left(\tau_0 a\frac{\partial L}{\partial\theta}\right)\right]. \tag{8.4}$$

The contractile activity of the actomyosin network is modelled by the nonlinear function $\sigma_0(a)$. Two mechanical states have to be distinguished according to the value of the F-actin concentration $a(\theta,t)$ with respect to a saturation concentration a_{sat}. If $a(\theta,t)$ is lower than a_{sat}, the contractile stress increases according to a parabolic law. Above the saturation threshold a_{sat}, the stress decreases exponentially as a consequence of the network swelling. Biological background to such assumptions has been given in Chapter 1. The nonlinear function proposed by Alt and Tranquillo (1995) is the following:

$$\sigma_0(a) = \psi_0 a^2 e^{-a/a_{sat}}, \tag{8.5}$$

where the coefficient ψ_0 controls the magnitude of the contractile stress.

8.2.3 Nondimensionalization of the equations

The partial differential equations system is nondimensionalized by setting the following dimensionless variables:

$$\tilde{t} = t\eta, \qquad \tilde{a} = \frac{a}{a_0}, \qquad \tilde{L} = \frac{L}{R_0}.$$

The normalized parameters are then:

$$\tilde{\beta} = \frac{\beta_1}{\Phi_1 a_0 R_0 \eta}, \quad \tilde{\gamma} = \frac{\gamma_1}{\Phi_1\eta}, \quad \tilde{\mu} = \frac{\mu_0}{\Phi_0}, \quad \tilde{\psi} = \frac{\psi_0 a_0}{\Phi_0 R_0 \eta},$$

$$\tilde{a}_{sat} = \frac{a_{sat}}{a_0}, \quad \tilde{\tau} = \frac{\tau_0}{\Phi_0\eta^2}, \quad \tilde{\delta} = \frac{\tau_1\Phi_0}{\tau_0\Phi_1}.$$

Dropping the tildes for notational simplicity, we obtain the following system of dimensionless partial differential equations:

$$\frac{\partial}{\partial t}(La) = -\frac{\partial}{\partial\theta}(Lav) + L(1-a), \tag{8.6}$$

$$a\frac{\partial L}{\partial t} = \beta - \gamma La + \delta\frac{\partial}{\partial\theta}\left(\tau a\frac{\partial L}{\partial\theta}\right), \tag{8.7}$$

$$av = \frac{\partial}{\partial\theta}\left[\mu a\frac{\partial v}{\partial\theta} + \sigma(a) - \frac{\partial}{\partial\theta}\left(\tau a\frac{\partial L}{\partial\theta}\right)\right]. \tag{8.8}$$

8.3 Linear stability analysis

The linear stability analysis of the dimensionless system (8.6)-(8.8) (for periodic boundary conditions) considers the behaviour of small perturbations of the variables around the homogeneous steady state which is given by:

$$L_s = \frac{\beta}{\gamma}, \qquad a_s = 1, \qquad v_s = 0. \tag{8.9}$$

The linearized form of the dimensionless system is:

$$\begin{pmatrix} \frac{\partial}{\partial t} - \delta\tau\frac{\partial^2}{\partial\theta^2} + \gamma & \beta & 0 \\ \frac{\partial}{\partial t} & \frac{\beta}{\gamma}(\frac{\partial}{\partial t} + 1) & \frac{\beta}{\gamma}\frac{\partial}{\partial\theta} \\ \tau\frac{\partial^3}{\partial\theta^3} & -\rho\frac{\partial}{\partial\theta} & 1 - \mu\frac{\partial^2}{\partial\theta^2} \end{pmatrix} \begin{pmatrix} L - L_s \\ a - a_s \\ v - v_s \end{pmatrix} = 0, \tag{8.10}$$

where $\rho = \frac{d\sigma}{da}|_{a=a_s}$.
We look for solutions of the form:

$$L - L_s \propto e^{\lambda t + im\theta}, \quad a - a_s \propto e^{\lambda t + im\theta}, \quad v - v_s \propto e^{\lambda t + im\theta},$$

where m represents the spatial mode of deformation. By substitution in the linearized system of equations one obtains:

$$\begin{pmatrix} \lambda + \gamma + m^2\delta\tau & \beta & 0 \\ \lambda & \frac{\beta}{\gamma}(1+\lambda) & im\frac{\beta}{\gamma} \\ -im^3\tau & -im\rho & 1 + \mu m^2 \end{pmatrix} \begin{pmatrix} L - L_s \\ a - a_s \\ v - v_s \end{pmatrix} = 0.$$

If M denotes the matrix above, the dispersion relation between λ and m which has to be satisfied for the system to have a non-trivial solution is given by:

$$det(M) = (\lambda + \gamma + m^2\delta\tau)\left[\frac{\beta}{\gamma}(1+\lambda)(1+\mu m^2) - m^2\rho\frac{\beta}{\gamma}\right] - \beta\left[\lambda(1+\mu m^2) - m^4\tau\frac{\beta}{\gamma}\right] = 0$$

$$\text{i.e.} \quad \lambda^2 + \lambda\left(m^2\delta\tau + 1 - \frac{m^2\rho}{1+\mu m^2}\right) + \underbrace{\frac{m^4\tau\beta}{1+\mu m^2}}_{C} + \underbrace{(\gamma + m^2\delta\tau)}_{A}\underbrace{\left(1 - \frac{m^2\rho}{1+\mu m^2}\right)}_{B} = 0$$

or in a simplified form we can write:

$$\lambda^2 + \lambda(-\gamma + A + B) + AB + C = 0.$$

The discriminant of this equation is:

$$\begin{aligned} \Delta &= (-\gamma + A + B)^2 - 4AB - 4C \\ &= (\gamma - B + A)^2 - 4C - 4\gamma A \\ &= \left(\gamma - 1 + \frac{m^2\rho}{1+\mu m^2} + \gamma + m^2\delta\tau\right)^2 - 4\frac{m^4\tau\beta}{1+\mu m^2} - 4\gamma(\gamma + m^2\delta\tau). \end{aligned}$$

Thus the roots of the dispersion relation, which give the temporal evolution of perturbations with spatial mode m, are given by the following pair of eigenvalues of the matrix M:

$$\lambda(m) = \frac{1}{2}\left[-1 + \frac{m^2\rho}{1+\mu m^2} - m^2\delta\tau\right] \pm \frac{1}{2}\sqrt{\left(2\gamma - 1 + \frac{m^2\rho}{1+\mu m^2} + m^2\delta\tau\right)^2 - 4\gamma(\gamma + m^2\delta\tau) - 4\frac{m^4\beta\tau}{1+\mu m^2}} \tag{8.11}$$

8.3.1 Conditions for the existence of an oscillating state

A simple way to look for self-sustained oscillations of the plasma membrane is to find model parameters which correspond to a destabilization of the uniform steady state of the variable L. If this destabilization occurs through a Hopf bifurcation, standard theory predicts the existence of limit cycle type solutions. According to the experimental results, we are looking for spatially non-uniform solutions in order to represent the appearance of extending/retracting protrusions along different axes. These axes will be determined by the existence of unstable spatial modes for the cytomechanical model solutions. A Hopf bifurcation then occurs for complex eigenvalues i.e. when $Re[\lambda(m)] = 0$. We thus have:

$$Max\left[Re[\lambda(m)]\right] = 0. \tag{8.12}$$

We first look for the value of m which maximizes the function $Re[\lambda(m)]$. This value is given by:

$$m_0 = \sqrt{\frac{1}{\mu}\left(\sqrt{\frac{\rho}{\delta\tau}} - 1\right)}. \tag{8.13}$$

We note that the coefficients β and γ, which represent the protrusive hydrostatic pressure and the elasticity coefficient of the network controlling the retraction of the lamellipod respectively, have no influence on the determination of the deformation modes. The key parameters are the cytoplasm viscosity μ and the actin-membrane complex elasticity τ. As intuitively expected, large values of τ and μ correspond to small value of m_0, i.e. to a small number of potential membrane protrusions. Conversely, large values of the parameter ρ, which monitors the contractility of the F-actin network, can lead to large values of m_0 and thus of the number of protrusions.

By evaluating $Re[\lambda(m_0)]$, one obtains:

$$\rho = \delta\tau + 2\sqrt{\mu\delta\tau} + \mu. \tag{8.14}$$

Further substitution in the expression of m_0 gives:

$$\mu\delta\tau = \frac{1}{{m_0}^4}. \tag{8.15}$$

The key parameters for determining the unstable modes are thus the viscosity coefficient μ, the actin-membrane complex elasticity coefficient τ (controlling the surface tension) and the drag coefficient δ. As can be intuitively understood, high values of μ and τ

tend to strengthen the cell actin-membrane complex. This tends to reduce the number of unstable modes. On the other hand, high values of ψ, which characterizes the intensity of the actomyosin network contractility, can favour the destabilization of a larger number of spatial modes.

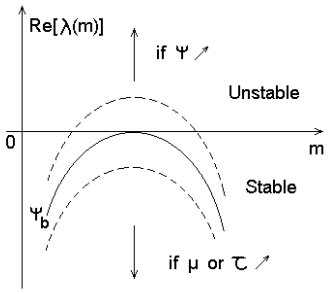

Figure 8.3: Stability diagram

8.4 Numerical methods

The equations of the model are numerically solved by finite difference methods based on the Crank-Nicholson scheme (Strikverda 1989). Solving hyperbolic and parabolic equations, associated respectively with the conservation of actin $a(\theta, t)$ and the cell membrane position $L(\theta, t)$, furthermore implies the matrix inversion method known as the Thomas Algorithm (Strikverda 1989), adapted to periodic boundary conditions. The equation for the mechanical equilibrium of the network is solved using a successive over-relaxation (SOR) method.

8.5 Simulation results of the deformation dynamics of cells

Whereas rotating waves of deformations were generated to simulate the behaviour observed on leukocytes (Alt 1990) and keratinocytes (Alt *et al.*, 1995), the aim of the simulations presented here were rather to focus on the simulations of standing wave protrusions for various modes of deformation defined in agreement with the stability analysis. Two typical behaviours corresponding to some experimentally observed situations (see Chapter 6), have been simulated and are described here in detail.

For each case presented, the initial conditions are taken as small random perturbations ϵ of the homogeneous steady state (L_s, a_s, v_s), with:

$$L(\theta, 0) = 1.0, \qquad a(\theta, 0) = 1.0 \pm \epsilon, \qquad v(\theta, 0) = 0.0,$$

where $|\epsilon| \leq 0.05$.
The system of equations is solved with periodic boundary conditions given by:

m_0	$\beta = \gamma$	μ	τ	δ	ρ	ψ_b	ψ
2	0.5	2	1.5	0.02	2.5	5.3	6.0
4	0.5	2	1.5	0.001	2.1	4.9	5.5
6	0.5	1	1	0.001	1	2.13	3.0

Table 8.1: Parameters used in the simulations

$$L(0,t) = L(2\pi,t), \qquad a(0,t) = a(2\pi,t), \qquad v(0,t) = v(2\pi,t).$$

Using the stability analysis, the model parameters have been chosen in order to select a given mode of deformation in the following way; imposed values for the cytoplasm viscosity μ and the membrane elasticity τ allow the calculation of the parameter δ and then ρ with the respective expressions (8.15) and (8.14). This choice of parameters thus corresponds to a Hopf bifurcation point. The parameter ψ representing the contractile activity of the actin network, which is directly deduced from $\rho = \frac{d\sigma}{da}(a_0)$, is chosen as the bifurcation parameter. In order to destabilize the bifurcation state, we increase the value of ψ, which corresponds to an intensification of the actomyosin complex. The parameters β and γ, which represent the protrusive hydrostatic pressure and the elasticity coefficient of the actin network respectively, are not concerned with the mode selection and are chosen independently. They are both fixed for the simulations to the value of 0.5.

For the first simulation, the mode $m_0 = 2$ is selected, which means two extrema i.e. namely one protrusion. With the imposed values $\mu = 2$ and $\tau = 1.5$ for the cytoplasm viscosity and the actin-membrane complex elasticity respectively, these lead to $\delta = 0.02$ and $\rho = 2.5$. At the Hopf bifurcation, we thus have $\psi_b = 5.3$. A slight increase of this parameter up to a value of 5.5 generates a pulsating movement of the membrane between two opposite sides in the cell. However, just a few pulsations are observed before a rotating wave around the cell body appears as the asymptotic state (Figures 8.4, (a)-(b)). This behaviour is typically the case reported by Alt in the simulations of the keratinocytes movements (Alt *et al.*, 1995).

In the next two simulations, higher modes of deformation are selected i.e. namely $m_0 = 4$ and $m_0 = 6$, which correspond to 2 and 3 simultaneous protrusions respectively. The parameters used for the simulations in both cases appear in Table 8.1. The results of the simulations for the variable $L(\theta,t)$ are displayed in Figure 8.4 (c)-(f).

The results where the mode 4 is isolated (Figures 8.4 (c)-(d)) is of particular interest. Indeed, the pulsation which involves two perpendicular protrusive directions is qualitatively similar to the spontaneous behaviour that we characterize on isolated L929 fibroblasts. The simulation result for mode $m_0 = 6$ exhibits a more complex behaviour involving up to 3 simultaneous protrusives zones (Figure 8.4 (e)-(f)). Figure 8.5 presents for each simulation the associated evolution profiles of each variables $L(t)$, $a(t)$ and $v(t)$ in the protrusive directions.

For the last two simulations corresponding to the modes of deformation 4 and 6 respectively, sequences of the movement are displayed (Figures 8.6 and 8.8) together with the associated distribution of actin in the cell cortex (Figures 8.7 and 8.9). In agreement with the model hypotheses, we observe that the protrusions of the membrane occur in a zone of low actin concentration, where the retraction force from the actin filaments is weaker than the protrusive force due to the internal hydrostatic pressure. Alternatively, a local increase of actin allows the retraction force to overtake the pressure. Actin then flows in two opposite directions in the cell cortex. The concentration thus remains symmetrical with 2 axes of symmetry corresponding to the 2 protrusive axes for the simulation related to the mode 4 and a unique axis of symmetry for the simulation related to the mode 6 which exhibits more complex patterns of actin distribution but is still controlled by two opposite flows of actin.

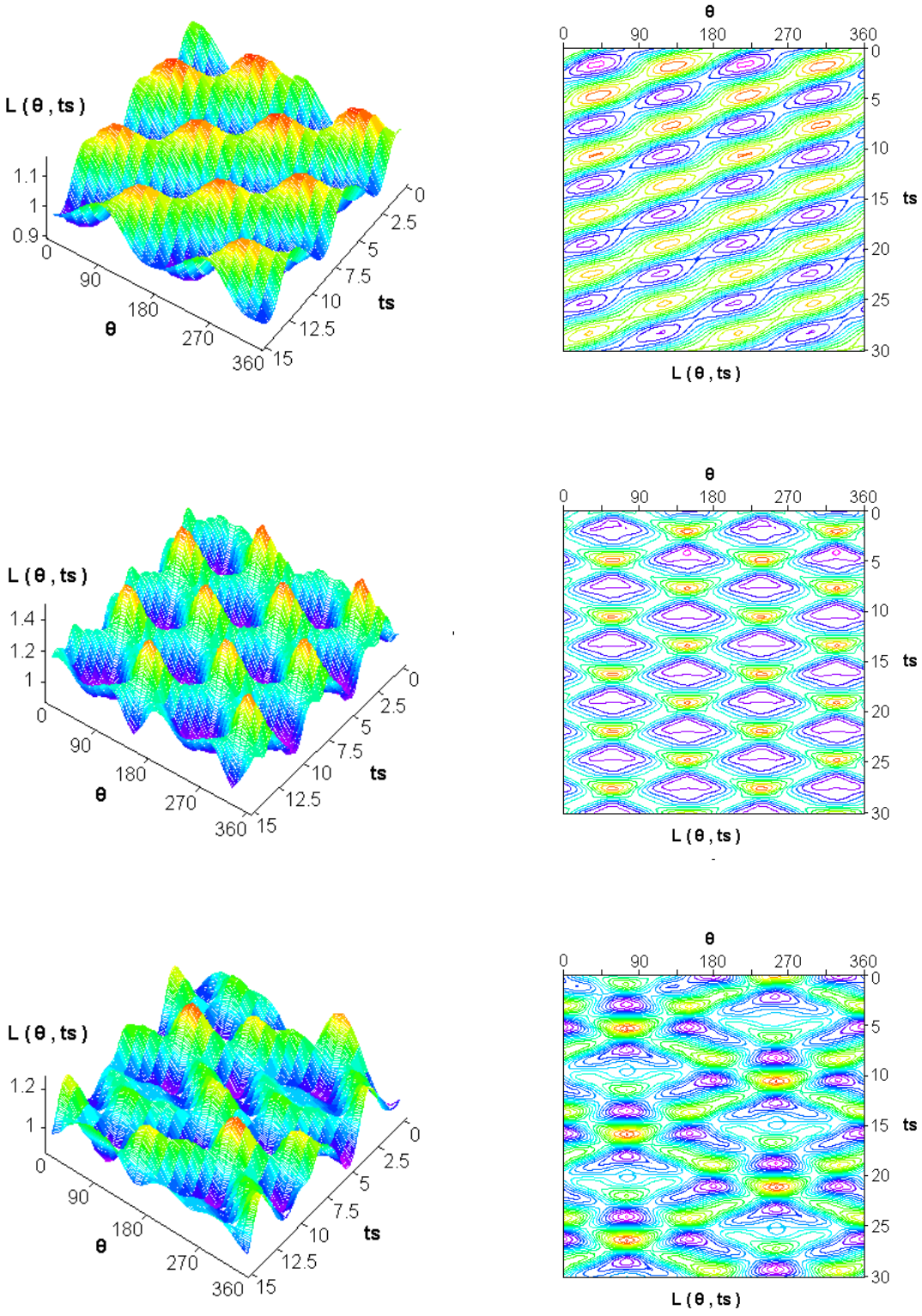

Figure 8.4: Spatio-temporal 3D maps and contour maps of cell membrane deformations. Mode 2 (a),(b), mode 4 (c),(d) and mode 6 (e),(f)

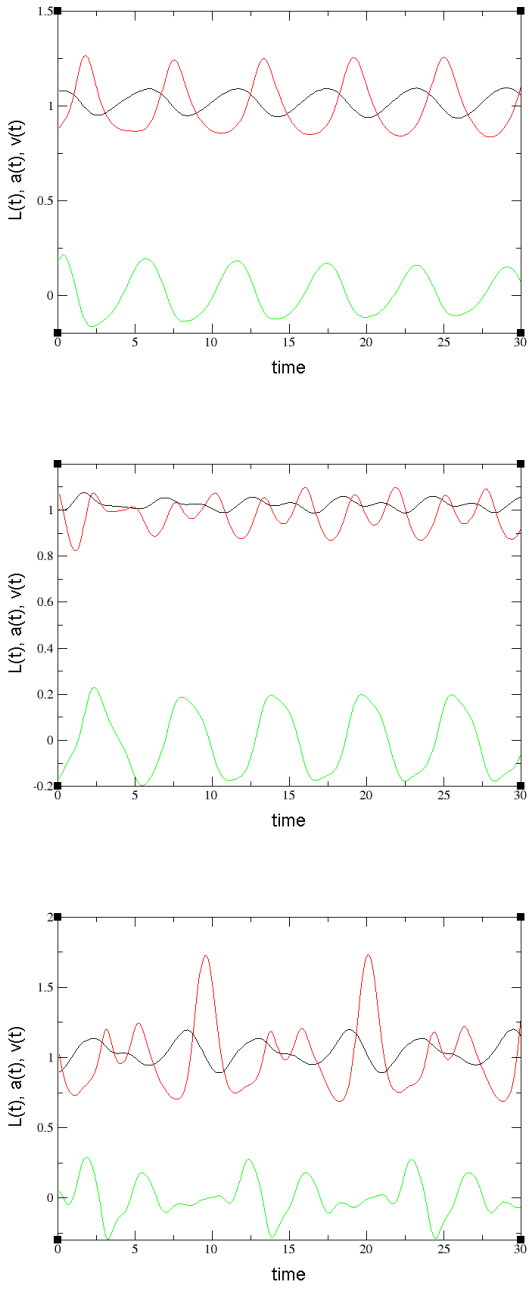

Figure 8.5: Evolution of $L(t)$ (black), $a(t)$ (red) and $v(t)$ (green) for a given direction of space corresponding to a protrusive zone. (a) mode 2; (b) mode 4 for $\theta = 317$ degrees and (c) mode 6 for $\theta = 259$ degrees.

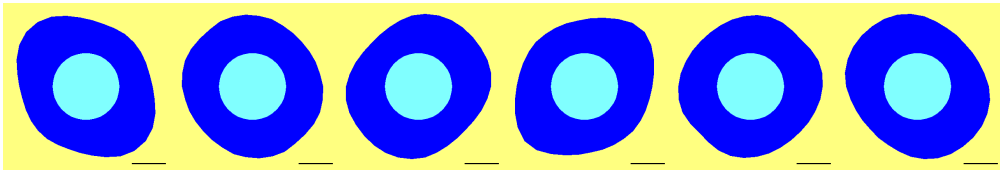

Figure 8.6: Sequence covering about a period of cell deformations associated with the mode $m = 4$. Snapshots are taken from $t_s = 0$ to $t_s = 5$ (normalized time unit) with a step of 1 normalised time unit between each frame. The simulated cell exhibits a pulsating movement of extension/retraction between 2 perpendicular directions.

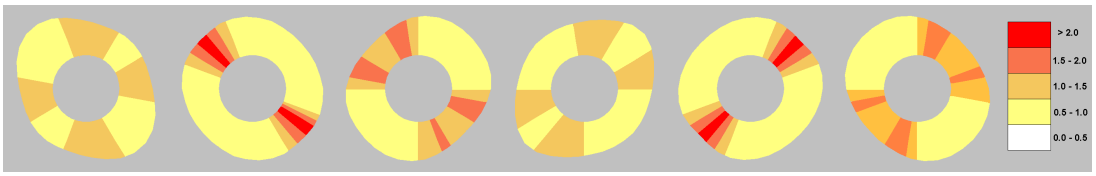

Figure 8.7: Actin distribution in the cell cortex associated with the mode-4 sequence of deformation. Two counter-flows of actin are observed and lead to a symmetrical distribution in the cortex. Minimum concentrations of actin are associated to membrane extensions, whereas maximum concentrations lead to retractions.

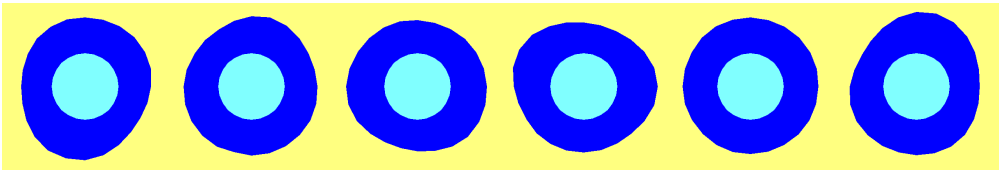

Figure 8.8: Sequence covering about half a period of cell deformations associated with the mode $m = 6$. Snapshots are taken from $t_s = 0$ to $t_s = 5$ (normalized time unit) with a step of 1 normalised time unit between each frame.

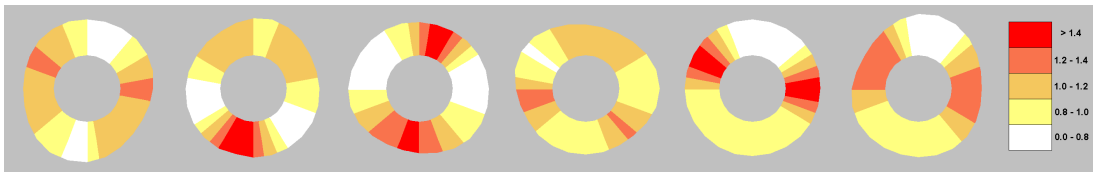

Figure 8.9: Actin distribution in the cell cortex associated with the mode-6 sequence of deformation. As previously, 2 counter-flows of actin are observed and lead to a symmetrical distribution in the cortex with this time one axis of symmetry instead of 2 in the previous case.

8.6 Model validation from experimental data

Experimental characterization of the L929 fibroblast line revealed the existence of a pulsating behaviour in the form of standing waves of deformations whose spatio-temporal dynamics could be quantified in terms of the membrane extension length and of the movement periodicity. In this chapter we have been able to simulate qualitatively the spontaneous standing wave behaviour which involves the coordinated movements of protrusion and retraction of the membrane between 2 perpendicular protrusive directions. The second step towards the model validation is now to evaluate the set of mechano-chemical parameters required for the simulated results to match the experimental ones.

The mechano-chemical parameters used in the model and assumed here to define the properties of the whole L929 cell line are:

- the coefficient controlling the polymerization/depolymerization process of actin η;
- the actin concentration at the chemical equilibrium a_0;
- the internal hydrostatic pressure β_1;
- the elasticity of the actin network γ_1;
- the coefficients controlling the curvature tension in the actin-membrane complex τ_1 and in the actin network τ_0;
- the friction coefficients Φ_1 for cell substrate adhesion and Φ_0 for friction within the network;
- the cytoplasm viscosity μ_0;
- the coefficient defining the contractile activity of the actomyosin complex ψ_0.

The normalized coefficients used to simulate the spontaneous pulsating behaviour (mode 4) from which the model validation is based are:

$$\beta = \gamma = 0.5, \qquad \mu = 2, \qquad \tau = 1.5, \qquad \psi = 5.5, \qquad \delta = 0.001.$$

8.6.1 Estimation of the polymerization rate from the periodicity

According to our time-scaling, the real time is given by:

$$t_{real} = \frac{t_{simul}}{\eta}.$$

Experimentally, the estimated periodicity of the cell movements is about 30 minutes (T_{exp}). Theoretically, the period of the pulsating movement determined from the simulated spatio-temporal contour map (Figure 8.4) corresponds to 6 normalized time units (T_{simul}). The polymerization rate is thus estimated as follows:

$$\eta = \frac{T_{simul}}{T_{exp}} = 0.2 \quad min^{-1}.$$

8.6.2 Estimation of the mechanical parameters

The mechanical parameters essentially available in the literature concern the cytoplasmic medium viscosity, the network elasticity and the traction forces exerted by the cell on its substrate (See Chapter 3). Few data are available concerning the measures of internal pressure in the cell, and friction forces of the cell on its substrate. Therefore, the missing parameters are inferred from the available measurements.

The parameters η (controlling the polymerization rate) and R_0 (radius of the cell body) were used to normalize the system of equations in time and space respectively. These are given by:

$$\eta = 0.2\ min^{-1} \quad \text{and} \quad R_0 = 10\ \mu m.$$

The average F-actin density at the chemical equilibrium is evaluated from the measures of F-actin at the lamellipodial margin presented in Table 1.2 (chapter 1). This value is thus set to:

$$a_0 = 10\ \mu m^{-1}.$$

Different studies using different techniques of measurement (Thoumine and Ott, 1997; Bausch *et al.*, 1998; Zaner and Valberg, 1989; Valberg and Albertini, 1985), agree on the following value for the cytoplasm viscosity:

$$\mu_0 = 2000\ Ns/m^2.$$

The determination of the parameter for the actin network elasticity is complicated by an enormous range of values, depending both on the techniques and on the experimental conditions used. Intracellular measurements performed on neutrophils with optical tweezers (Yanai *et al.*, 1999) report for the elasticity of the cell body a value of about,

$$\gamma_0 = 1\ N/m^2.$$

The other parameters of the cytomechanical model inferred from these values are given in Table 8.2.

The value calculated for the contractile force of the actomyosin complex $\psi_0 = 2\ nN$, is in the range of values reported by Guilford *et al.* (1995) for their measurements with magnetic tweezers of the traction force exerted by macrophage cells.

Parameter	Estimated Value	References
β_1	$0.41\ N/m^2$	calculated
γ_1	$1\ N/m^2$	[1]
μ_0	$2000\ Ns/m^2$	[2],[3],[4],[5]
τ_0	$0.02\ N/m^2$	calculated
τ_1	$1.2 \times 10^{-5}\ N/m^2$	calculated
Φ_0	$1000\ Ns/m^2$	calculated
Φ_1	$600\ Ns/m^2$	calculated
ψ_0	$2.10^{-9}\ N$	calculated, [6]

Table 8.2: Estimations of the values of the mechanical parameters for the simulation of the pulsating behaviour such as observed on L929 fibrobalsts. [1] Yanai *et al.* (1999), [2] Thoumine and Ott (1997), [3] Bausch *et al.* (1998), [4] Zaner and Valberg (1989), [5] Valberg and Albertini (1985), [6] Guilford *et al.* (1995)

8.7 Discussion

Following the model of Alt and Tranquillo (1995), we have investigated the ability of this model to generate standing wave oscillations of the membrane such as those we have characterized for the L929 fibroblast line. This was performed from a linear stability analysis where parameters were defined in order to select a Hopf bifurcation i.e. namely a transition of the stable state towards oscillating states and more particularly standing wave states. Killich *et al.* (1993, 1994) observed such a variety of behaviours from rotating waves of deformations to pulsating waves, all in a single type of cell, the amoebae *Dictyostelium*. They proposed a purely descriptive model based on the interaction of superimposed waves. They have shown that the interference patterns of two interacting waves were sufficient to describe the overall diversity of oscillating states observed in the amoebae. They proposed that actin dynamics might account for these oscillations. This is confirmed by the cytomechanical model we analyzed. Its biomechanical hypotheses allow us to account for the wide variety of patterns of cell membrane deformations. This also confirms the idea that the same basic mechanisms might apply in all types of cells from rounded leukocytes to the large pseudopods of fibroblasts.

Moreover, quantitatively, we have seen that the model parameters can globally be connected to realistic experimental data thus reinforcing the relevance of the model hypothesis formulated to describe cell movements dynamic.

On the basis of this model, we then propose to investigate in the next chapters the influence on the spontaneous pulsating behaviour of the cell of external interactions such as cell-cell contact (Chapter 9) and cell chemotaxis (migration induced by an extracellular factor, in Chapter 10). Our aim is to provide a continuous description from the spontaneous state to a perturbed one which leads to new cell behaviours such as cell paralysis and cell migration respectively.

Chapter 9

Modelling cell-cell interactions

Modélisation des interactions cellule-cellule

Nous nous sommes intéressés dans ce chapitre à la modélisation du phénomène d'inhibition de contact déclenché par le contact entre cellules. Ce phénomène où les cellules montrent une réduction sensible de leur activité protrusive dans la zone de contact a été abordé dans notre partie expérimentale (chapitre 7). Nos observations ont permis de proposer une interprétation des morphologies résultantes de contact comme des états contraints d'un état spontané, plutôt que comme de nouveaux états dynamiques indépendants. La modélisation de ce phéenomène consiste donc à créer une modification locale des propriétés mécaniques de la cellule dans la zone de contact. L'approche par microscopie acoustique à balayage suggère que les paramètres mécaniques affectés lors du contact sont les coefficients d'élasticité du cytosquelette γ et du complexe membrane-cortex τ. Afin de tester leurs influences respectives, 3 simulations sont d'abord proposées. La première, où seul le coefficient d'élasticité du complexe membrane-cortex est affecté, montre une décroissance significative de l'amplitude de la dynamique protrusive dans la zone d'interaction. Dans la seconde simulation, on considère en plus l'influence d'une augmentation de la rigidité du cortex. La simulation montre un comportement qualitativement similaire au précédent. La troisième simulation a eu pour but d'évaluer l'influence du terme de rigidité membranaire en l'absence d'autre contrainte. Cette fois, aucune décroissance locale de l'amplitude de la dynamique des déformations n'est observée, mais l'ensemble de la dynamique cellulaire apparait légèrement perturbée. Ces résultats suggèrent que l'altération des propriétés mécaniques du complexe membrane-cortex est bien un facteur déterminant pour l'altération de la dynamique protrusive de la cellule après un contact. Une dernière simulation est alors proposée afin d'évaluer l'influence de la position relative de la zone d'interaction par rapport à la morphologie initiale de la cellule. On simule la situation où seul le coefficient d'élasticité du complexe membrane-cortex est affecté, mais cette fois la zone d'interaction est deplacée de 30 degrés par rapport à une zone protrusive de la cellule. La simulation montre l'apparition progressive d'une onde en rotation autour du corps cellulaire, et donc une modification de la dynamique globale de déformation de la cellule. On note qu'une décroissance de l'amplitude des déformations apparaît de plus nettement dans la zone d'interaction.

9.1 Introduction

There exist many ways in which cells can communicate and therefore interact with each other. One way is the release of a chemical substance which diffuses in the environment and that the cells are able to detect and integrate in order to react in the most appropriate way. A typical example is the amoebae *Dictyostelium discoideum* which releases cAMP when deprived of nutrients. Deprivation of the medium thus triggers an aggregation phase during which the cells respond to the cAMP chemical signal by migrating towards the source. This chemoattractant-induced reaction is a property of many cells and will be studied in detail in the next chapter. Another way for the cells to communicate at a distance is to exert mechanical tensions on the extracellular matrix. Cellular traction forces have been indeed largely documented since the well-known experiments of Harris (1984) in which traction forces exerted by fibroblasts cultured on silicon substrate creates wrinkles on this substrate. Such tensions and associated deformations of the extracellular matrix can thus be detected by neighbouring cells. In return, deformations of the substrate are known to influence the behaviour of the cells. For example, Curtis and Wilkinson (1997, 1998) have clearly demonstrated that the cells tend to adapt their morphologies to the changing topography of the surrounding medium. However, the most direct way for the cells to interact is of course by direct cell-cell contact. Whereas epithelial cells tend to maintain contact with their neighbours, fibroblasts rather tend to move apart as a result of the phenomenon of contact inhibition that we have already tackled in our previous experimental part in chapter 7. Our experimental observations show that after an initial contact L929 fibroblasts tend to adopt new morphologies in order to avoid further contacts. As a conclusion to our observations, we propose to consider the new morphologies observed as constraint states of a spontaneous pulsating one rather than as new independent dynamical states.

From the mathematical point of view, this suggests that the effect of the contact phenomenon should be obtained by acting locally on the relevant parameters of the model rather than from a global change in the parameters such as in Figure 9.1. In that simulation we present the transition from the mode 6 to the mode 4 pulsating state, both considered in the previous chapter (Figure 8.4). The continuous transition is performed by a global change in the set of parameters required to generate the new state and not through a local perturbation as it is the case experimentally.

Theoretically, bifurcation between pulsating modes induced by a perturbation can occur if the modes considered are intricated (or competing modes).

The basic assumption is that a contact signal can be transduced through different signalling pathways into structural modifications of the local cell mechanical properties. This then leads to the re-adapted coordination of the cell protrusions. Whereas it is commonly admitted that signal transduction is a molecular process, we propose the involvement of a mechanical component suggested by our simulation results. This hypothesis is discussed on the basis of the tensegrity (Ingber 1993, 1997) and percolation (Forgacs 1995) theories both founded on the properties of the cell architecture as a carrier of the information.

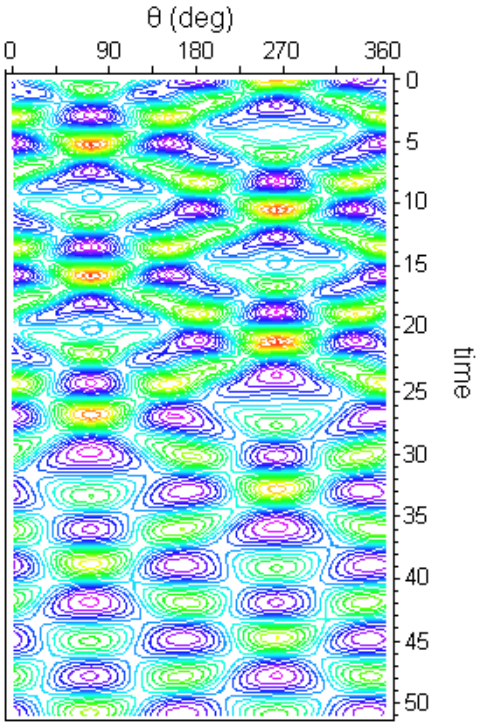

Figure 9.1: Theoretical transition from one pulsating state (mode 6) to another (mode 4). Parameters are given in Table 8.1

9.2 Development of the cytomechanical model

Up to now the most adapted method to investigate the mechanical effects due to cell-cell contact in living cells is the scanning acoustic microscopy (Zoller *et al.*, 1997). This technique allows one to map the motility domains in the cells i.e. domains associated with variations in the mechanical parameters of elasticity or stiffness of the sub-membrane cortex. The method applied to fibroblast cells has shown that minor movements of the membrane stops after contact. This translates into a decrease of cell motility, which can be related to the local increase of the stiffness (Bereiter-Hahn and Luers, 1998). In the paper by Zoller *et al.*, (1997) motility domains (i.e. protrusive zones) are supposed to be created by contraction and relaxation of the actomyosin cortex underneath the plasma membrane. In their study, inhibition of motility is assumed to be described by changes in the cell surface mechanical properties. On the basis of these hypotheses, we propose to investigate the effects of local changes in the related mechanical parameters of our model. We have thus simulated the local increase of the network elasticity γ and analyzed the influence of the membrane-cortex surface tension characterized by the coefficient τ.

In the model, local mechanical changes of these two relevant parameters are represented by step-functions which describe the angular parameter variations in any given interaction window $[\theta_1, \theta_2]$ (defined in the same way as the interaction zones considered in the experimental part of chapter 7):

$$\gamma(\theta) = \begin{cases} \gamma & \text{if} \quad \theta < \theta_1 \text{ and } \theta > \theta_2, \\ \gamma_{int} & \text{if} \quad \theta_1 \leq \theta \leq \theta_2, \end{cases}$$

$$\tau(\theta) = \begin{cases} \tau & \text{if} \quad \theta < \theta_1 \text{ and } \theta > \theta_2, \\ \tau_{int} & \text{if} \quad \theta_1 \leq \theta \leq \theta_2, \end{cases}$$

where γ_{int} and τ_{int} are the modified values of the parameters in the interaction zone.
The cytomechanical model described in Chapter 8 (equations 8.6, 8.7, 8.8) thus becomes:

$$\frac{\partial}{\partial t}(La) = -\frac{\partial}{\partial \theta}(Lav) + L(1-a), \tag{9.1}$$

$$a\frac{\partial L}{\partial t} = \beta - \gamma(\theta)La + d\frac{\partial}{\partial \theta}\left(\tau(\theta)a\frac{\partial L}{\partial \theta}\right), \tag{9.2}$$

$$av = \frac{\partial}{\partial \theta}\left[\mu a\frac{\partial v}{\partial \theta} + \sigma(a) - \frac{\partial}{\partial \theta}\left(\tau(\theta)a\frac{\partial L}{\partial \theta}\right)\right]. \tag{9.3}$$

The derivative of $\tau(\theta)$ taken in the sense of distributions is given by:

$$\frac{\partial \tau(\theta)}{\partial \theta} = \tau'(\theta) + \sum_k [\tau]_k \delta(\theta - \theta_k)$$

where $\delta(\theta)$ is the Dirac delta function:

$$\delta(\theta) = \begin{cases} 1 & \text{if} \quad \theta = 0, \\ 0 & \text{if} \quad \theta \neq 0. \end{cases}$$

and $\tau'(\theta)$ represents the piecewise derivative of the function $\tau(\theta)$ taken on each interval. As $\tau(\theta)$ is constant on each interval, $\tau'(\theta) = 0$. τ_k corresponds to the amplitude of the step-function at the point θ_k. Thus the expression of the derivative is:

$$\frac{\partial \tau(\theta)}{\partial \theta} = (\tau - \tau_{int})[\delta(\theta - \theta_2) - \delta(\theta - \theta_1)].$$

9.3 Simulation of mechanically perturbed cell oscillatory morphologies

As an initial cell morphology and dynamical state, we consider the spontaneous pulsating movements of extension/retraction of the cell membrane between two perpendicular directions (mode 4). This behaviour is simulated with the following set of model parameters:

$$\beta = \gamma = 0.5, \qquad \mu = 2, \qquad \tau = 1.5, \qquad \delta = 0.001, \qquad a_{sat} = 2, \qquad \text{and} \quad \psi = 5.5.$$

The corresponding spatio-temporal map $L(\theta, t)$ of the dynamics of the simulated membrane deformations is plotted in Figure 9.2.a and will be used as a reference for the interaction simulations. Modifications of the model parameters are applied to this asymptotic periodic steady state in order to simulate the cell response to neighbourgh cell contact. The progressively emerging dynamical state is then recorded. The interaction window $[\theta_1, \theta_2]$ (75 degrees for all the simulations) is indicated at the bottom of each simulated maps. In the first simulation (Figure 9.2.b), the local decrease of the membrane-cortex elasticity is simulated with the following step-function:

$$\tau(\theta) = \begin{cases} 1.5 & \text{if } \theta < 135 \text{ and } \theta > 210, \\ 0.75 & \text{if } 135 \leq \theta \leq 210. \end{cases}$$

A modification of the protrusive dynamic rapidly occurs (from $t = 4$) in the zone of interaction, with a decrease in the amplitude of membrane deformations. This is in agreement with the scanning acoustic microscopy observations of reduced motility (Zoller *et al.*, 1997).

In another simulation, we have simulated the effect of an associated increase in the cytoskeleton elasticity. In this case, both the membrane-cortex related surface tension and the cytoskeleton elasticity are supposed to be affected by the contact with:

$$\tau(\theta) = \begin{cases} 1.5 & \text{if } \theta < 135 \text{ and } \theta > 210, \\ 0.75 & \text{if } 135 \leq \theta \leq 210, \end{cases}$$

$$\gamma(\theta) = \begin{cases} 0.5 & \text{if } \theta < 135 \text{ and } \theta > 210, \\ 0.6 & \text{if } 135 \leq \theta \leq 210. \end{cases}$$

The result of this simulation presented in Figure 9.2.c is qualitatively similar to the previous one. In order to estimate the influence of an increased elasticity of the network γ, we propose a simulation where this parameter alone is assumed to be affected by the contact. The simulation result displayed in Figure 9.2.d shows no local alterations of the protrusive dynamics, but rather a slight global perturbation of the dynamic all over the cell, without any decrease in the deformation amplitude. This result tends to prove that an increase of the cytoskeleton elasticity is not the major event of the cell response to contact. Conversely, tension of the cell membrane-cortex is more likely to play the leading role.

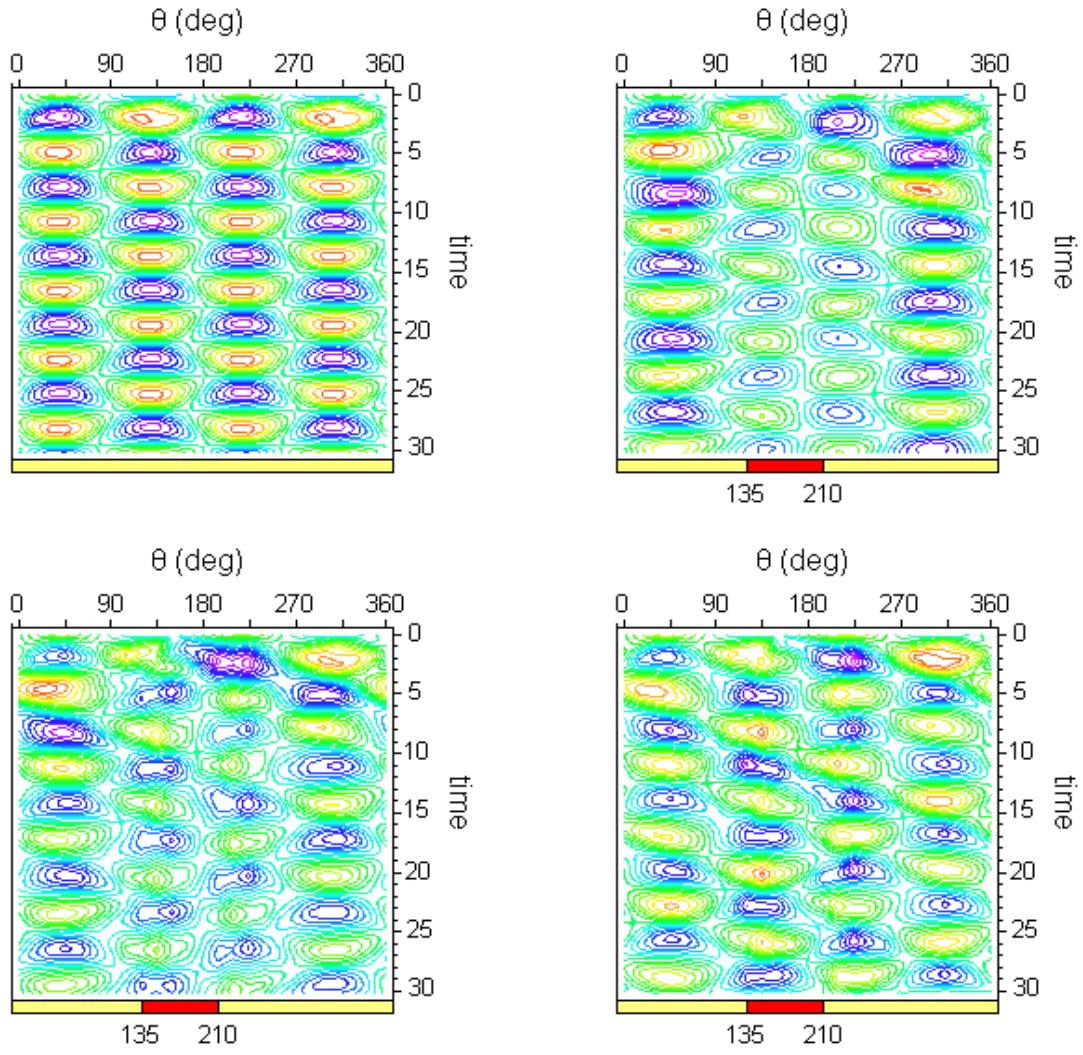

Figure 9.2: Spatio-temporal maps of cell membrane deformations: (a) map of reference corresponding to the unaltered state associated with the mode of deformation $m = 4$ (see previous chapter). The membrane-cortex coefficient in this case is $\tau = 1.5$ and the network stiffness is $\gamma = 0.5$; (b) decrease of the membrane-cortex coefficient in the interaction zone where $\tau_{int} = 0.75$; (c) decrease of the membrane-cortex coefficient together with the increase of the network stiffness in the interaction zone with $\tau_{int} = 0.75$ and $\gamma_{int} = 0.6$ respectively; (d) increase of the network stiffness coefficient in the interaction zone where $\gamma_{int} = 0.6$. The interaction zone is represented by a red rectangle at the bottom of the maps.

We then have investigated the influence of the stimulus location relative to the initial cell morphology. We consider the simulation with the decrease of the membrane-cortex tension coefficient as a reference (Figure 9.3.a) and reproduce the same simulation but this time with a slight displacement of 30 degrees to the right of the interaction zone:

$$\tau(\theta) = \begin{cases} 1.5 & \text{if } \theta < 165 \text{ and } \theta > 240, \\ 0.75 & \text{if } 165 \leq \theta \leq 240. \end{cases}$$

The simulation displayed in Figure 9.3.b shows that the entire cell dynamics tends to be affected with the progressive appearance of a rotating wave of deformations which slowly replaces the pulsating behaviour. We note however that the amplitudes of the deformations remain mainly affected in the zone of interaction.

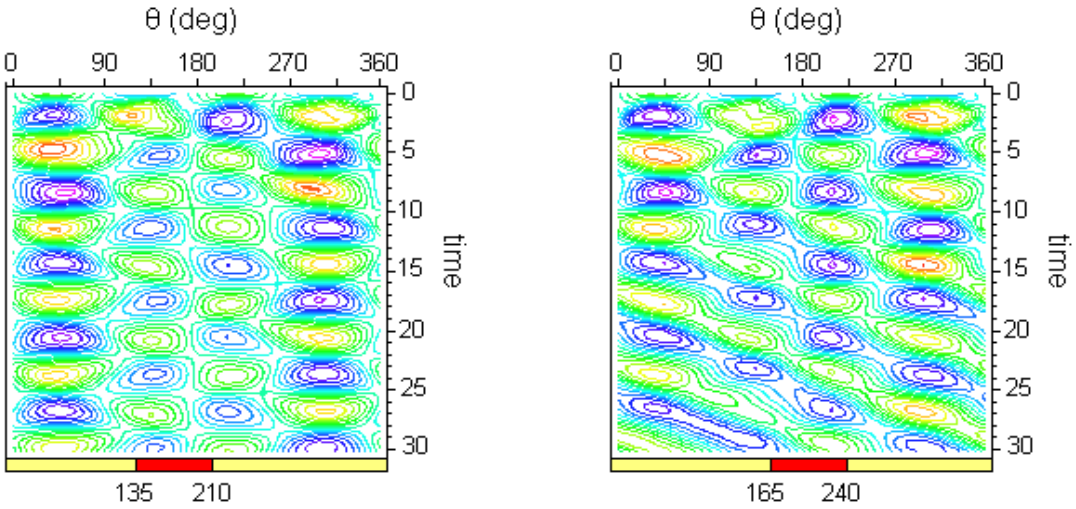

Figure 9.3: Spatio-temporal maps of cell membrane deformations: (a) is the same map as in Figure 9.2.b, which is used as a reference in order to test the influence of the position of the interaction zone relative to the cell protrusive directions; (b) the interaction zone is shifted 30 degrees to the right. In both cases the membrane-cortex coefficient in the interaction zone is $\tau_{int} = 0.75$.

9.4 Discussion

In the proceedings of a symposium on cell behaviour, Harris (1999), considered a series of long standing questions about "how tissue cells crawl", in the light of the molecular information accumulated over the recent years. One of these questions relates to the molecular basis of contact inhibition. Although the phenomenon of contact inhibition is well described (Abercrombie *et al.*, 1970) (see definition given in chapter 7), there are

still no definite explanations and the origin of the membrane retraction process is not understood.

Opposing theories about these questions are considered. In the first theory defended by Harris himself, it is assumed that cell-cell contact inhibits the adhesiveness of the cell (i.e. the ability of the cell to form further contacts with its substrate). Therefore the contractile tension existing in the network is not counterbalanced any more by the adhesion force and the membrane is pulled backwards. In the opposing view proposed by Abercrombie (1980), it was suggested that it is rather the increase of the network contractility which is responsible for the breaking of the attachment of the cell to its substrate. Such increased contractility is exactly what has been observed by the scanning acoustic microscopy (SAM) approach (Zoller *et al.*, 1997; Bereiter-Hahn and Luers 1998). However, it is not excluded that the increased contractility may be due to the loss of adhesiveness. Thus SAM does not allow one to discriminate between these two theories.

At this period it was strongly suspected that cell-cell contact inhibits actin assembly. Evidence of this statement came a year later with a paper of Waterman-Storer *et al.* (2000). They demonstrated for the first time that actin polymerization as well as the retrograde flow observed at the leading edge of migrating cells, is inhibited by contact between cells. It was then concluded that cell-cell contact regulates actin dynamics. Both the points of view of Harris on adhesiveness inhibition and the demonstration of actin polymerization inhibition tend to call for a molecular mechanism at the origin of membrane retraction. However our simulation results tend to show that it is a mechanical process, namely the decrease of the cell membrane-cortex tension which is responsible for the appearance of a new dynamical state for actin and not the opposite. The influence of this membrane-cortex tension was already suspected by Abercrombie (1980) and by Zoller *et al.* (1997) from the results of SAM measurements.

As an alternative to purely molecular signal transduction, we thus put forward the involvement of a mechanical component in the transduction pathway. This idea gained some interest with the theory of cell tensegrity (Ingber 1993). In this theory, the cell is considered as a pre-stressed structure which is able to sense a constraint through the slight modifications induced on the tensional integrity (tensegrity) of the structure. Therefore, modifications in the structure can be transmitted to the nucleus which will then elaborate the appropriate answer to the signal. An alternative hypothesis, which describes the network of interconnected filaments of the cytoskeleton as a percolation structure (Forgacs 1995), proposes that the transmission of the signal to the nucleus is not necessarily required for the cell to react to specific external stimuli. In this theory, the signal is assumed to be detected and transmitted through the binding of ligands to transmembrane receptors such as cadherins (cell-cell contact) or integrins (cell-matrix contact) which have a transmembrane domain directly connected to the actin network. The ligation of a membrane receptor then triggers a modification in the mechanical state of the cytoskeletal network such as a local increase or decrease of the stress. Signaling molecules can thus be activated (or deactivated) by the new state of stress and can either diffuse in the cortex to trigger further modifications in the structure or can induce directly local reorganization in the cytoskeletal architecture leading to shape changes. This scenario provides a good interpretation of our simulation results and explains both local changes and global reorganization

of the cell shape. In our case, membrane-cortex tension is equivalent to a conformational change in the membrane curvature which leads to the reorganization of actin in the cell cortex.

The possibility of the involvement of a mechanical component in signal transduction is often underestimated. However, it appears that molecular and mechanical mechanisms can hardly be dissociated. We hope our results will contribute to a better consideration of such mechanical effects generated by cell-cell contact.

Chapter 10

A mathematical model for cell chemotaxis

Un modèle mathématique pour la chimiotaxie cellulaire

Le modèle cytomécanique a été développé de façon à prendre en compte la migration cellulaire par chimiotaxie. Le couplage avec un gradient de facteur extracellulaire est realisé au niveau du terme de tension de courbure membranaire qui est supposé dépendre de la concentration du facteur. Ainsi, plus la concentration de facteur extracellulaire est importante et plus la tension de membrane décroît créant une instabilité morphologique qui se traduit par la polarisation de la cellule selon l'axe du gradient. Lorsque la polarisation, c'est à dire le déplacement du centre de gravité de la cellule par rapport au centre du corps cellulaire, atteint un certain seuil que l'on admet correspondre au seuil au delà duquel la force d'adhésion l'emporte sur la force de tension dans le cortex, alors le corps cellulaire se déplace afin de reéquilibrer les forces dans la cellule et restabiliser la structure. On génère ainsi un mouvement migratoire en deux temps, polarisation puis translocation du corps cellulaire conforme à l'observation expérimentale. Deux situations expérimentales sont simulées en considérant une cellule dans un état initial non polarisé (circulaire avec une distribution homogène d'actine) soumise à un gradient stationnaire de facteur extracellulaire. Dans le premier cas, la source de chimioattractant est retirée avant que la cellule ne l'atteigne. Conformément à ce qui était attendu, la cellule cesse de migrer et retrouve sa configuration initiale stationnaire et non polarisée. Dans le second cas, au même temps que précédement, la source est deplacée à la position d'origine de la cellule. Celle-ci opère alors un demi-tour pour ensuite aller se fixer sur la source. Une troisième simulation est proposée, avec cette fois un gradient de facteur extracellulaire non stationnaire. On observe une migration lente de la cellule qui s'arrête de migrer lorsque la pente du gradient devient trop faible. De nouvelles simulations sont ensuite proposées de façon à prendre en compte le cas d'une cellule dans un état initial pulsant. La cellule, soumise à des conditions identiques aux précédentes, réagit de manière similaire. En particulier, la cellule reste capable de détecter et de suivre des déplacements de la source. Les simulations effectuées montrent l'apparition de pics d'intensité d'actine orientés dans la direc-

tion de la source juste après le déplacement de celle-ci. Ce résultat se rapproche d'observations expérimentales où la concentration d'actine domine sur le front de migration de la cellule.

Deux moyens sont alors proposés dans le but de contrôler la vitesse de migration. Tout d'abord, l'influence de la pente du gradient est analysée afin d'évaluer s'il existe un gradient optimum, permettant de générer la plus grande vitesse de migration. Un autre moyen d'agir sur la vitesse de migration est de modifier l'adhésivité de la cellule que l'on suppose liée à son degré de polarisation et contrôlé par la définition d'une valeur seuil de polarisation (i.e. d'adhésion) au delà de laquelle la cellule migre. Conformément à ce qui est attendu, plus le seuil est faible (c'est à dire plus l'adhésion est faible) et plus la vitesse de migration est importante.

Dans l'ensemble des simulations effectuées, on observe que les morphologies cellulaires simulées restent faiblement deformées en raison de la limitation du modèle, qui reste valide pour de faibles déformations. Cependant, il est possible de générer de plus fortes déformations de façon à observer les deux phases de la migration qui sont l'extension membranaire suivi de la translocation du corps cellulaire en considérant un front de gradient linéaire (plutôt qu'une source ponctuelle) de chimioattractant.

10.1 Introduction

There are many different types of cell migration related to the many different causes. In ***random migration*** for example (Dunn, 1990), there is no external signal or un-oriented external signals detected by the cell which moves with no particular purpose and in no particular direction as if exploring its environment. In this specific case the forces acting inside the cell have not reached any equilibrium, as the adhesion force is never strong enough to prevent the cell from moving according to the external fluctuations perceived on the substrate or more generally in the surrounding medium. In the case of *in vitro* wound healing where an artificial wound is created by scratching with a razor blade a layer of confluent cells, a form of ***pseudo-directed migration*** is observed for the cells at the edge of the wound. In this case, contact inhibition (such as defined in chapter 7) is the phenomenon mainly responsible for the orientation and displacement of cells of the edge which are forced to move and colonize the empty space until they meet the cells of the other edge and become contact inhibited at both sides and therefore stop moving (Middleton and Sharp, 1984). There exist many forms of ***directed migration***, such as *topology guidance* where the cells tend to direct their migration along certain directions imposed by the topology of the medium (Curtis and Wilkinson 1997, 1998), *haptotaxis* where the cells follow gradients of substrate adhesiveness, or *chemotaxis* where the cells migrate up chemical gradients. It is this latter case which is the most widely studied. Indeed, this form of migration involves the coordination of many complex processes from the detection of the gradient signal, its integration by the cell and the elaboration of an adapted response which can lead either to the migration up or down the gradient depending on the situation. Moreover, it is relatively easy to set up experiments to test the ability of the cells to move towards a source of chemical at the tip of a pipette which is moved from place to place. It is this form of migration that we chose to investigate.

A wide variety of locomotory behaviour is observed depending on the cell type (Cramer *et al.*, 1997). Whereas fibroblasts exhibit a two-step behaviour with lamellipodial extension at the front followed by cell body translocation, in fast moving cells more specialized for migration such as keratocytes or neutrophils, these two phases are almost simultaneous so that the cells seem to glide on the substrate. Despite these variations in behaviour, it is assumed that the same basic mechanisms operate for all migrating cells.

Enormous progress has been made in the understanding of the molecular mechanisms involved in chemotaxis. In particular the role of Rho-like GTP-ases which are regulator proteins for the type of actin organization (network in lamellipods or bundles in filopods) have been identified to be essential in the cytoskeleton reorganization in response to receptor stimulation (Hall 1998). The involvement of the Arp2/3 complex which catalyzes the actin assembly has proved to be essential in the force generation required in cell translocation (see chapter 2).

As mentioned in the introduction of this theoretical part of the thesis, molecular pathways of signal transduction cannot be explicitly considered by the cytomechanical model and it is not our aim to do so. Here, however, our interest is to investigate the role of the mechanical processes involved in migration. In particular the role of the mechanical properties of the cell membrane in cell shape stabilization. These properties have already been stressed by various studies (Nielsen *et al.*, 1998; Fournier 1996). We therefore propose to test their relevance in migration by considering a coupling between the mechanical properties of the membrane and the local concentration of extracellular factor which is supposed to influence the local membrane tension (Soares and Maghelly, 1999; Raucher and Sheetz, 2000).

10.2 The model

10.2.1 Influence of the extracellular factor (EF) on the cell membrane mechanical properties

The presence of an EF is perceived by the cell when the molecules of the factor bind with the receptors of the membrane. This event is presumed to trigger a chain of molecular events responsible for cell migration. From a purely mechanical point of view, recent studies have shown that the intercalation in the phospholipid bilayer of particles which can either be membrane proteins or latex beads are responsible for alteration of the curvature and therefore energy of the membrane (Nielsen *et al.*, 1998). Such alterations can lead to morphological instabilities which have been shown to be related to a decrease in surface tension (Soares and Maghelly, 1999). On the basis of these results we propose considering a coupling of the form membrane-EF where the concentration of EF directly influences the tension of the membrane through the cortex-membrane elasticity coefficient $\tau(a)$. In this new model, this coefficient is not a constant any more but we assume it to depend on the local concentration of the extracellular factor (EF) near the membrane in the following way:

$$\tau(Cs) = \tau - \Lambda Cs \tag{10.1}$$

where Cs represents the concentration of EF in the membrane and Λ is a coefficient which characterizes the sensitivity of the molecules of EF with the receptors of the cell membrane.

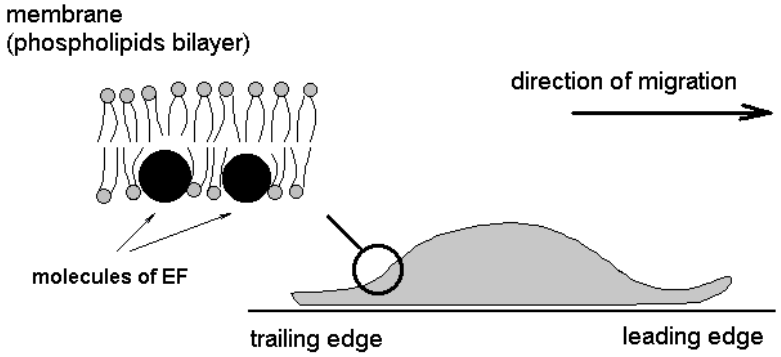

Figure 10.1: Schematic representation of a migrating cell exhibiting a characteristic dome-like shape where the thickest part represents the cell body. From the mechanical point of view, intercalation of molecules in the membrane are responsible for cell morphological instabilities

10.2.2 Equations of the model

The system of equations (8.6), (8.7), (8.8) is modified in order to integrate the coupling with the concentration of EF. The new is system is then given by:

$$\frac{\partial(La)}{\partial t} = -\frac{\partial(Lav)}{\partial\theta} + L(1-a), \tag{10.2}$$

$$a\frac{\partial L}{\partial t} = \beta - \gamma La + \delta\frac{\partial}{\partial\theta}\left(a\tau(Cs)\frac{\partial L}{\partial\theta}\right), \tag{10.3}$$

$$av = \frac{\partial}{\partial\theta}\left[\mu a\frac{\partial v}{\partial\theta} + \sigma(a) - \frac{\partial}{\partial\theta}\left(a\tau(Cs)\frac{\partial L}{\partial\theta}\right)\right]. \tag{10.4}$$

When the concentration of EF increases, the membrane stress decreases, destabilizing morphologically the membrane which tends to polarize in the direction up the gradient. It is obvious that the adhesion of the cell on the substrate is a necessary condition for the cell to create the force required to move forward, but this phenomenon is not described explicitly by the model. We assume that the recycling of the receptors is a secondary event which results from the polarization of the cell. The polarization leads to an asymmetry of the cell shape relative to the perpendicular axis of the direction of migration. This asymmetry is measured by the displacement of the cell geometrical barycentre from its initial position. When this displacement exceeds a given threshold, which corresponds to the limit above which the adhesion force at the leading edge of the cell overcomes the tension force within the cortex, the cell is allowed to move forward. The cell moves in

order to make its mass centre coincide with the position of the geometrical barycentre. Then the cell can re-stabilize its shape. Therefore, as long as a gradient can be detected by the cell, the cell moves toward the source according to a two-phase mechanism i.e. polarization of the cell membrane and then cell body translocation which corresponds to the displacement of the centre of mass (see Figure 10.2). These two-phase movements agree with experimental observations of many migrating cells.

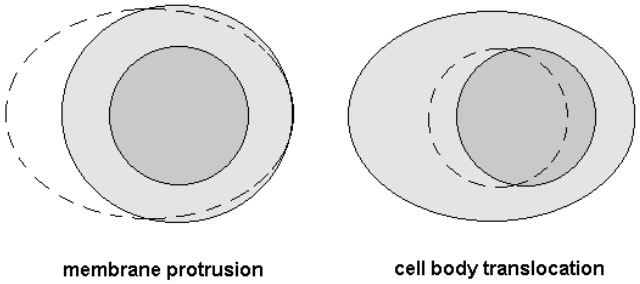

Figure 10.2: Schematic diagram of how a cell migrates according to a two-step process. First there is the membrane protrusion towards the direction of migration and secondly there is the cell body translocation where the adhesion force overcomes the tension force in the cell cortex

10.2.3 Distribution of the chemoattractant

The extracellular factor (or chemoattractant) of concentration C is assumed to be released homogeneously in the medium by a punctual source which diffuses according to the equation:

$$\frac{\partial C}{\partial t} = D\frac{\partial^2 C}{\partial r^2}, \tag{10.5}$$

where D is the diffusion coefficient of the chemoattractant.

The solution to this equation for an infinite medium with initial condition $C(r, t = 0) = Q_0\delta(r)$ is given by:

$$C(r,t) = \frac{Q_0}{2\sqrt{\pi D t}} \exp\left(-\frac{r^2}{4Dt}\right), \tag{10.6}$$

where Q_0 represents the released amount of chemoattractant.

From a numerical point of view, the generation of the cell migration from a chemoattractant source is a very delicate task as it requires one to find the right balance between the parameters controlling the cell dynamics and those controlling the distribution of chemoattractant. Therefore, in the whole of the simulations presented, except one (Figure 10.7), we have assumed for simplicity that the time scale of the diffusion process is

large enough compared to the cell migration velocity such that a stationary distribution $C(r, t_0) = C(r)$ of the chemoattractant can be considered.

10.3 Simulation results

10.3.1 Chemotaxis of non-polarized cells

For the two first simulations (Figures 10.4 and 10.5), the parameters of the cell correspond to the homogeneous steady state, namely a circular and non polar cell with a uniform cortical distribution of F-actin given by $L = \beta/\gamma$, $a = 1$ and $v = 0$. The parameters used for each simulation presented are displayed in Table 10.1. The associated chemoattactant profile is plotted in Figure 10.3.

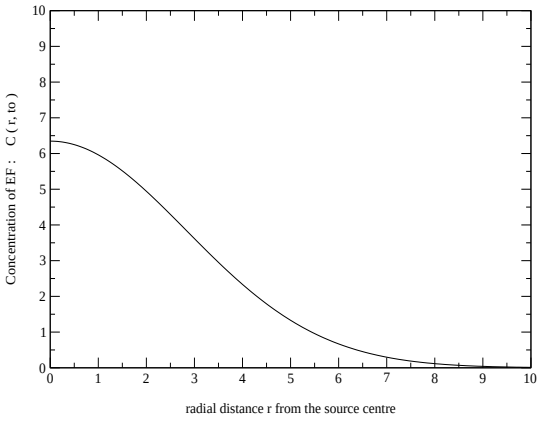

Figure 10.3: Chemoattractant distribution along any radial direction r used for the first 2 sets of simulation (Figures 10.4 and 10.5). Parameters used in the EF profile calculation (equation 10.6): $Q_0 = 45$, $D = 4$, $t_0 = 1$.

The cell is initially located at a normalized distance $d_0 = 4.5$ from the point source of chemoattractant and the threshold for the displacement of the geometric barycentre controlling the adhesion strength is set to 0.1.

The simulations presented Figure 10.4 and 10.5 are identical. That is we observe the progressive destabilization of the cell membrane at the leading front of the cell, with concomitant appearance of leading protrusions and cell polarization in pace with a slow translocation in the direction of the source.

In the first case of Figure 10.4, the source is removed when the cell is about to reach it. As expected, after a slight drift, the cell recovers its original homogeneous shape before it stops moving.

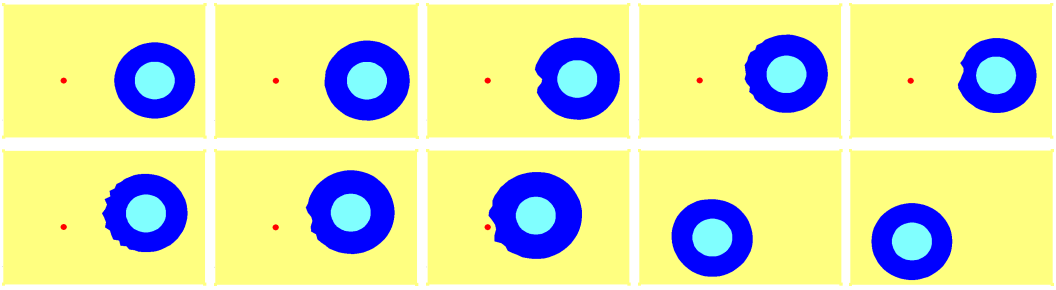

Figure 10.4: Migration of the cell towards the source of chemoattractant. Snapshots taken every 10 normalized time unit *(n.t.u.)* from $t = 0$ to $t = 90$ *n.t.u.* The source is removed at time $t = 74$.

In the second case (Figure 10.5), the position of the source is instantaneously moved to the original position of the cell when the cell is getting closer to it. The cell then re-organizes its shape rapidly and polarizes in the opposite direction toward the new source location.

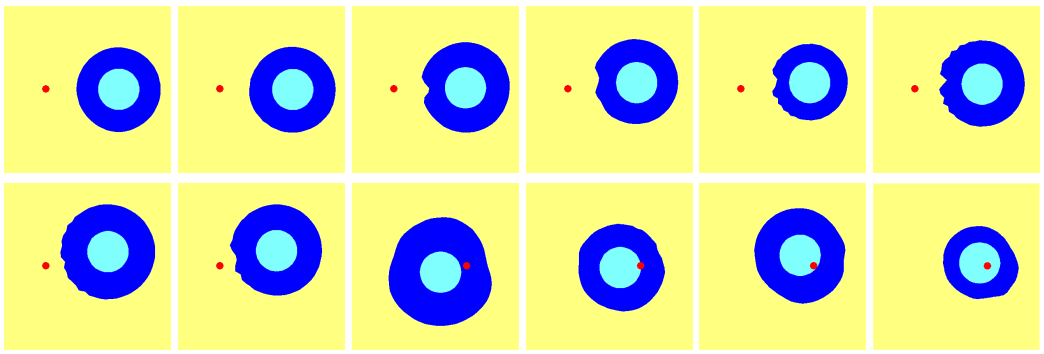

Figure 10.5: Migration of the cell towards the source of chemoattractant. Snapshots taken every 8 *n.t.u.* from $t = 4$ to $t = 92$. The source is moved at time $t = 65$ to the position initially occupied by the cell centre.

The third simulation is also identical to the two previous ones, but this time a non-stationary gradient of chemoattractant is considered, whose profile evolution is displayed in Figure 10.6.

The same migrating process as before is observed but this time the cell slows down as the slope of the gradient decreases. The cell is even unable to reach its goal, namely the source, as the gradient becomes too weak to maintain any cell polarization. The cell then

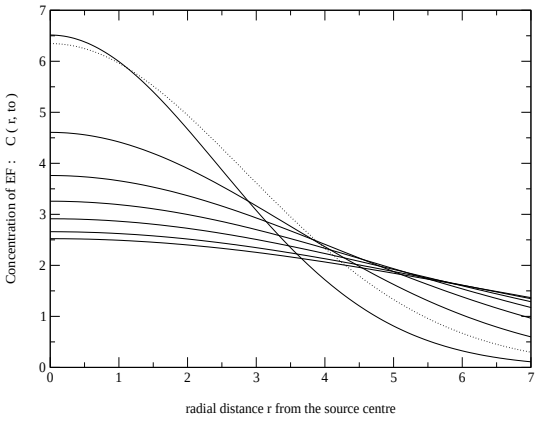

Figure 10.6: Evolution of the chemoattractant distribution from $t = 0$ to $t = 200$ normalized time unit *(n.t.u.)* Each curve corresponds to a snapshot of the simulation displayed Figure 10.7. The dotted-line corresponds to the EF profile used in the two previous simulations. Parameters used in the EF profile calculation (equation 10.6): $Q_0 = 40$, $D = 0.1$

recovers its homogeneous state and stops migrating.

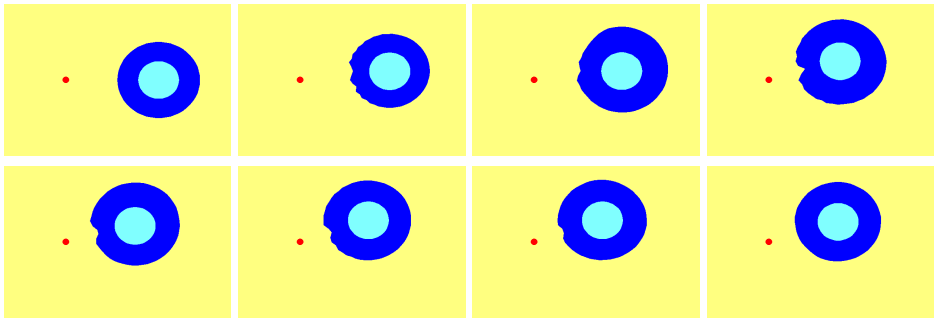

Figure 10.7: Migration of the cell towards a non-stationary source of chemoattractant Snapshots taken every 30 normalized time unit *(n.t.u.)* from $t = 0$ to $t = 200$ *n.t.u.*

For each of the three simulations performed, the trajectories of the cell nucleus centre are plotted in Figure 10.8. The speed of migration is evaluated in each case by measuring the total distance followed by the cell divided by the time.

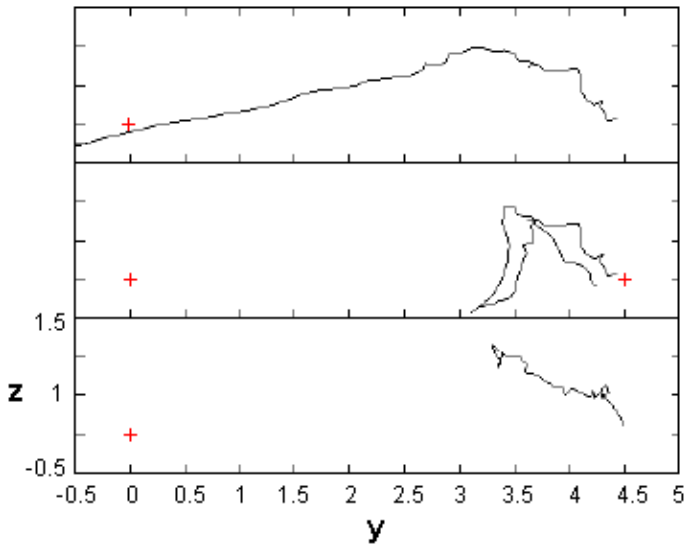

Figure 10.8: Trajectories followed by the centre of the cell body corresponding to the first three simulations presented. The cell speed is estimated from the direct measurements of the time and distance covered until the cell stops moving: $v = 0.68$ (upper graph), $v = 0.47$ (middle graph) and $v = 0.13$ (lower graph) $\mu m/n.t.u.$

10.3.2 Chemotaxis of pulsating cells

Whereas in the previous section only cells in their non-polar homogeneous stationary state were considered, we have been interested in this section in the migration of pulsating cells. The situation is thus more complicated. In the preceding case, the morphological instability occurring at the leading front of the cell was always stabilized as the cell tends to recover its homogeneous stationary state. Whereas in this new situation, the cell's endogeneous dynamics can either amplify as well as stabilize the primary deformations of the front.

Two simulations have been performed. In both cases the considered pulsating state corresponds to the mode-4-pulsating-state simulated in chapter 8. In the first case, a circular cell with a homogeneous distribution of actin in the cortex was taken as an initial condition. In the second case, a deformed cell associated with a non-homogeneous F-actin distribution in the cortex, corresponding to a snapshot of the asymptotic state was taken as the new initial condition. In both cases cell migration towards the source of chemoattractant was observed (the simulations are not displayed as they are similar to

the previous examples).

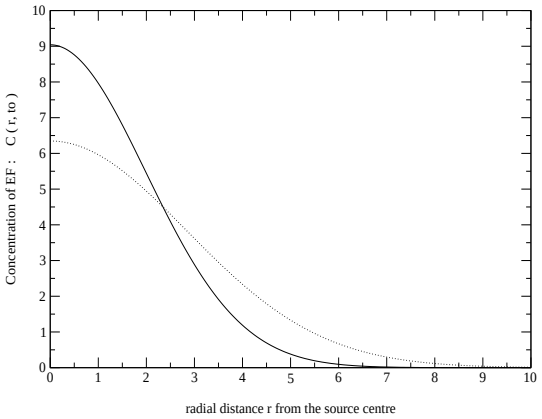

Figure 10.9: Chemoattractant distribution along any radial direction r used for the simulation displayed figure 10.10. Parameters used in the EF profile calculation (equation 10.6): $Q_0 = 45$, $D = 2.7$, $t_0 = 0.73$ (The dotted line represents the distribution used in the previous simulations)

For the last case presented (Figure 10.10), the previous simulation is repeated with the non-homogeneous asymptotic state as the cell initial condition, but this time the displacement of the source is tested. The source is moved twice in order to see the ability of the pulsating cell to respond to a new source location. The source is first moved in a perpendicular direction relative to the initial trajectory of the cell. We observe that even if the cell tends to polarize in the correct direction, it has some difficulty to get closer to this new source location. The cell is still competing with its spontaneous dynamics which impose specific protrusive directions which are not necessarily oriented in the direction of migration. The source is then shifted to the right and the cell exhibits a pseudopod in the correct direction. The associated distribution of actin in the cell cortex is displayed in Figure 10.11. We do not observe anymore symmetric distribution of the actin concentration as was the case for standing pulsating cells. A rotating movement of actin is observed while the cell is moving forward. However, it is important to note that when the source is moved, the front of the cell facing the new position of the source presents a maximum concentration of actin. Experimentally it is indeed reported that the leading front of migrating cells remains predominantly rich in actin (Theriot and Mitchison, 1991; Condeelis, 1993a).

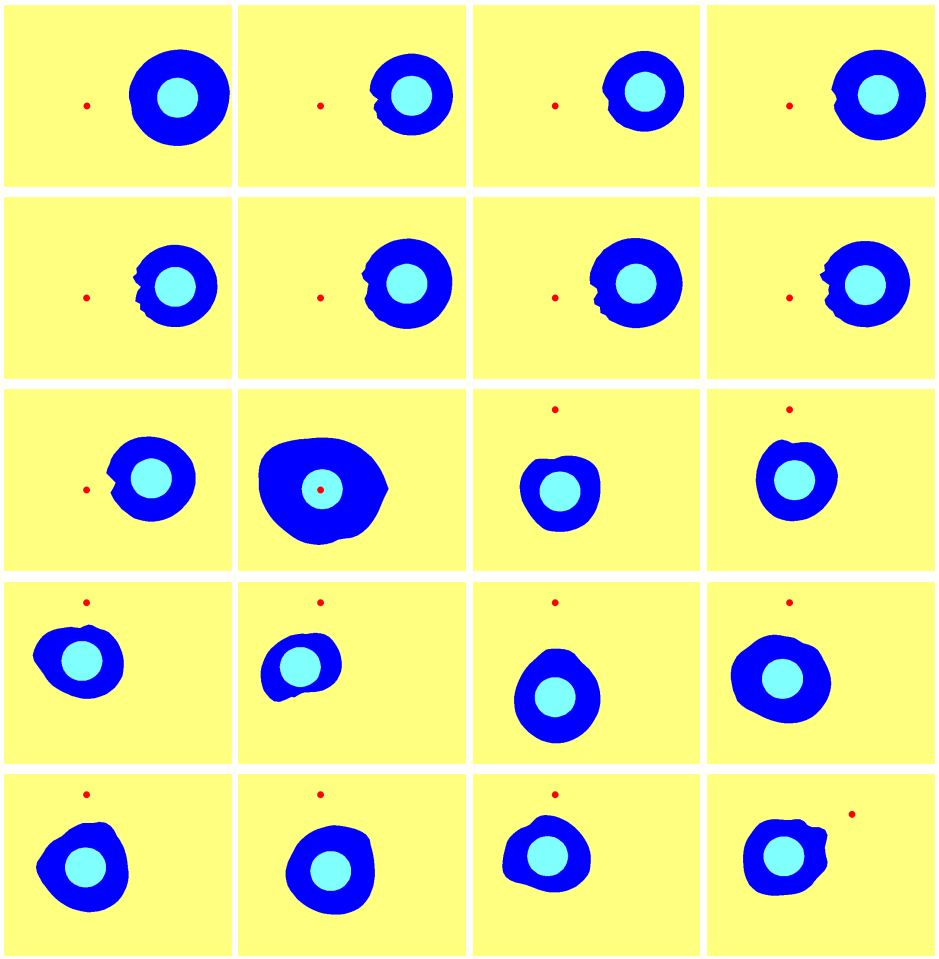

Figure 10.10: Migration of the cell towards a moving source of chemoattractant. Snapshots taken every 3 *n.t.u.* from $t = 0$ to $t = 57$. The source is moved twice at time $t = 29.37$ and $t = 55$. (To be read horizontally).

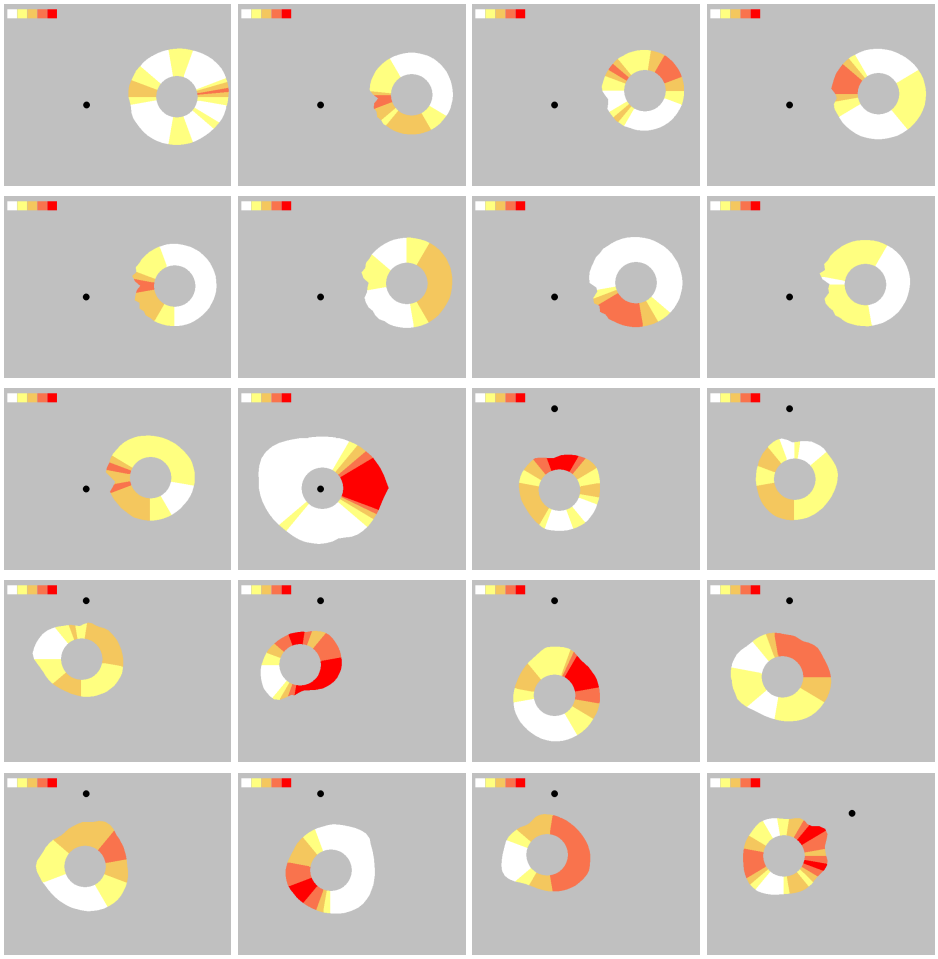

Figure 10.11: Corresponding actin distribution in the cell cortex for each of the snapshots presented in Figure 10.10. Each time the source is moved (snapshots 11 and 20), a maximum of the actin concentration appears at the leading edge of the cell.

10.3.3 Control of the cell migration speed

In order to simulate possible experimental control of cell migration through variations of the extracellular gradients, cell chemotaxis has been simulated using different concentration profiles $C(r)$ of the chemoattractant. Modulation of the chemoattractant gradient can be obtained by varying the diffusion parameter D. An equivalent effect can also be obtained by considering a different instant t_0 in the diffusion process.

.

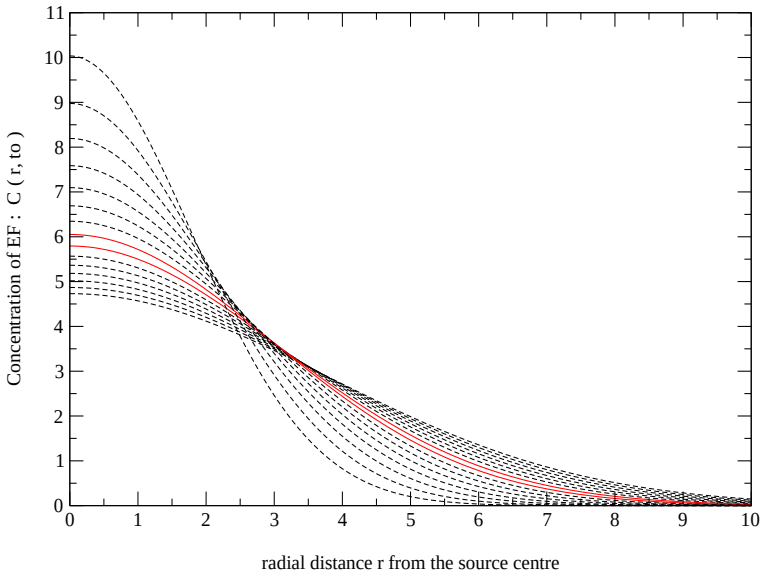

Figure 10.12: Distribution of the EF concentration for values of t_0 ranging from 0.4 to 1.8. The straight curves show the optimum gradients for fast cell migration

Cell speeds are then estimated from the measurements of the distance covered by the cell and the time required to reach a target which is defined by a circle centered on the source with radius r_{target}. The targets are used in order to suppress the spiral movement of the cell when approaching the source (see Figure 10.13) which tends to slow down the cell speed if included.
The speeds obtained for t_0 ranging from 0.4 to 1.7 are plotted in Figure 10.14 for two different choices of the target radius $r_{target} = 2.55\ \mu m$ (black curve) and $r_{target} = 0.75\ \mu m$ (red curve).

For increasing values of the parameter t_0, corresponding to a more advanced stage in the diffusion process where the chemoattractant gradient is smaller, a nonlinear variation of the migration velocity is observed, initially increasing from 0.37 to 0.74 μm per normalized-time unit, then decreasing down to 0.39 μm per time unit. These results show that an optimum gradient can be found in order to obtain the highest (or lowest) speed of migration. Here the optimum gradient is obtained for values of t_0 ranging from 1.1 to 1.2

(see Figure 10.12).

Another way of controlling the cell migration is to change the admissible threshold of cell deformation. This concerns the stress threshold above which the link between the membrane receptors, like integrin and the substrate, are broken. The results are presented in Figure 10.15 where the cell migration velocity has been computed for thresholds ranging from 0.06 to 0.12. As expected, stronger cell-substratum attachment is correlated with slower cell translocations. Globally, the cell velocity decreases in a non-linear way from 0.67 to 0.56 μm per normalized time-unit with increasing values of the threshold.

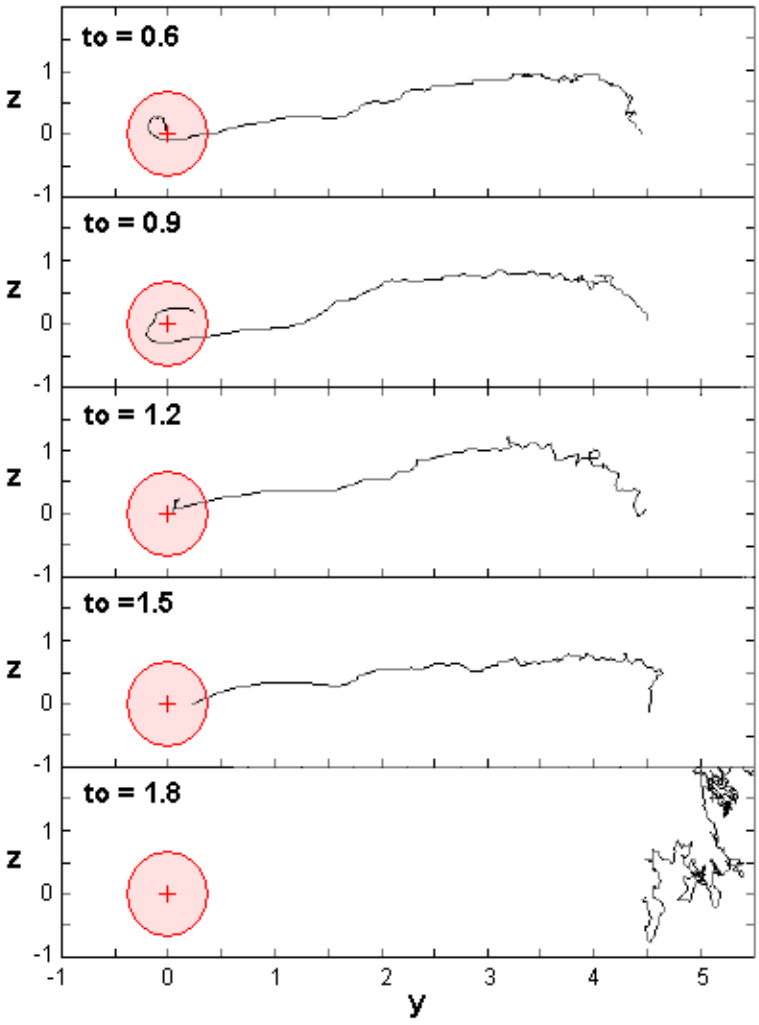

Figure 10.13: Trajectories followed by the centre of the cell body for increasing values of t_0 associated with the decrease of the gradient slope. The circle represents the target from the surface of which is measured the distance covered by the cell for the calculation of the cell speed.

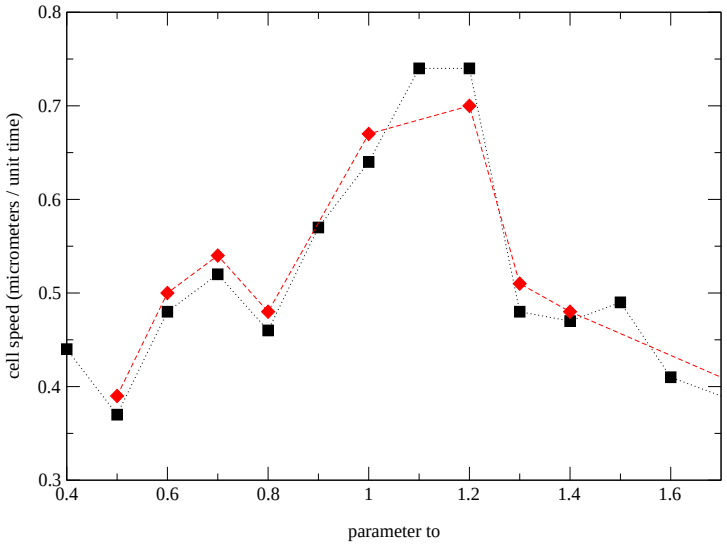

Figure 10.14: Evolution of the cell speed with increasing value of the parameter t_0 controlling the slope of the EF gradient. The black curve corresponds to the speed measured with a target of radius $r_{target} = 2.55\ \mu m$, and the red curve for a target with radius $r_{target} = 0.75\ \mu m$.

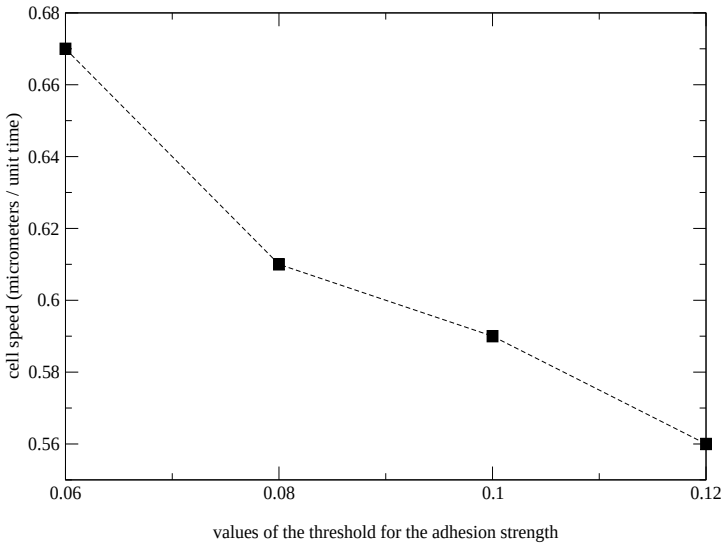

Figure 10.15: Plot of the cell speed against values of the threshold representing the adhesion strength.

10.3.4 Lamellipodial extension and cell body translocation

In all of the simulations presented, it remains difficult to identify the two-phases of the migration process which are the lamellipodial extension followed by the cell body translocation. The reason is that the model is based on an approximation of small deformations in order to avoid sharp variations in the membrane curvature. We propose here to show that it is possible to obtain important local membrane extension. However in this situation, the simulation of the cell migration remains limited due to numerical difficulties in solving the equations.
In this case a front of chemoattractant is considered. The stationary distribution of chemoattractant is given by:

$$\begin{cases} C(y) = C_0 & \text{if } y \leq 0 \\ C(y) = C_0 \left(1 - \frac{y}{y_0}\right) & \text{if } 0 < y < y_0 \\ C(y) = 0 & \text{if } y \geq y_0 \end{cases} \tag{10.7}$$

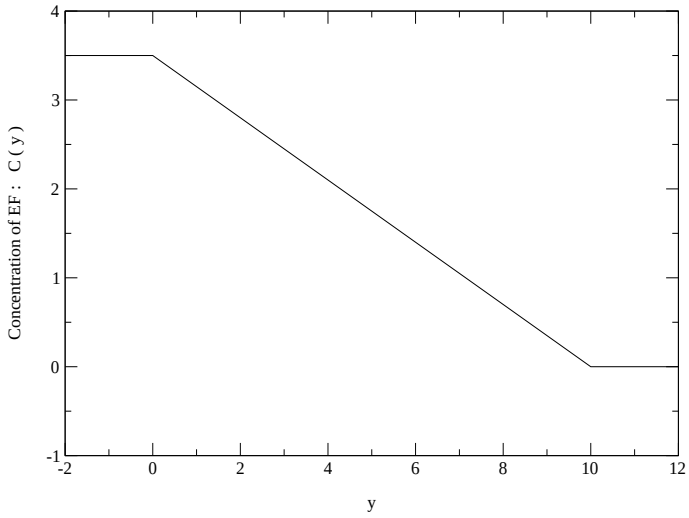

Figure 10.16: Linear gradient of chemoattractant profile defined from the values $C(y = 0) = C_0 = 3.5$ and $C(y_0 = 10) = 0$ in equation (10.7).

We observe this time (Figure 10.17) the slow appearance of a membrane extension oriented in the direction of the chemoattractant front. The deformations generated are too important to allow any re-stabilization of the cell morphology which is supposed to occur when the cell centre is moved at the location of the new cell barycentre. Therefore the deformations are amplified at each new iteration of the simulation until numerical instabilities interrupt the simulation before the cell was able to reach the source.

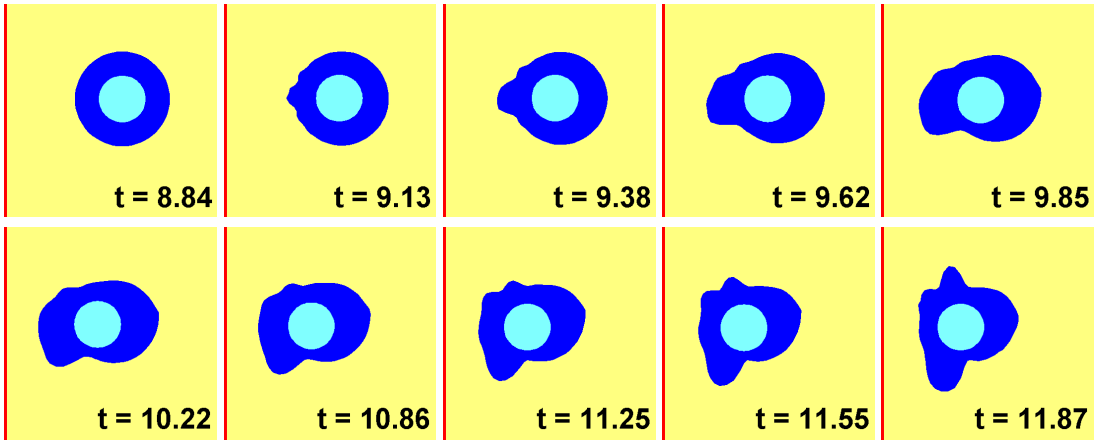

Figure 10.17: Migration of the cell towards a stationary linear front of chemoattractant (see Figure 10.16) whose origin is represented by the red line

10.4 Discussion

The original cytomechanical model presented in chapter 8 has been extended to take into account cell chemotaxis. Spatial inhomogeneous variations of the surface tension of the cortical actin/cell membrane complex have thus been considered. Our hypothesis is that cell membrane protrusions are associated with a decrease in cell surface tension. This is in agreement with recent experimental data of Raucher and Sheetz (2000) and with scanning acoustic microscopy measurements (Zoller *et al.*, 1997; Bereiter-Hahn and Luers, 1998), which reveal that lamellipodia extensions take place in cellular regions of relatively low stiffness. Experimentally, it has also been reported in the case of phospholipid bilayers (Nielsen *et al.*, 1998) that the incorporation of molecules in the membrane decreases the membrane stiffness.

Our model thus provides a continuous description of the successive stages of the cell morphological changes, from spontaneous oscillatory deformations, to polarization and then actual migration. Furthermore, it provides realistic simulations of cell migration, which keeps some random (stochastic) aspects of the cell trajectory and in which the direction of locomotion is determined by the result of competing lamellipodia occurring simultaneously around the cell and cell progressive polarization. We specifically focus on chemotaxis which is simulated by considering that the binding of chemoattractant molecules to membrane receptors triggers a transduction pathway which finally results in a decrease in the cortical surface tension. On the other hand, cell adhesion is necessary to ensure further development of the cellular traction forces pulling the cell body; this is one of the five-step scenario described by Sheetz *et al.*, (1999) for cell migration: membrane extension, attachment to the substratum, cell contraction, release of the attachment at the trailing edge and recycling of the receptors. We do not explicitly consider all these steps but rather propose a simplified view of this mechanism as an all or none process. If the

polarization of the cell exceeds some threshold corresponding to some value of intra cellular stress, then local breakdown of cell-substrate will occur. However simple this approach seems, it still can take into account data on cell adhesion forces as well as observations of integrin tracks left behind a moving cell as a testimony of the focal adhesions breakdown.

Another extension of this theoretical approach is the ability of the model to define optimum conditions for cell migration. Controlling cell migration is indeed crucial in many events such as wound healing, where fibroblast or myofibroblast migration is critical, or tumour invasion, where a decrease of the migration speed would help to reduce cancer cell infiltration of normal tissue.

Here we have illustrated the influence of: (i) the slope of the chemoattractant gradient and, (ii) the strength of the cell-substratum attachment. Another way to control cell migration is through direct modification of the cell characteristic parameters, including the cytomechanical parameters. One can thus define a "model driven acquisition" approach, where biological hypotheses will be translated into modifications of the cytomechanical model parameter values. Associated model simulations will identify the corresponding cell responses (membrane extension rate, number and frequency of membrane extensions, cell velocity , ...) and thus the range of experimental conditions within which such theoretical cell responses could be potentially observed. For example, the cell response and adaptation to extracellular factors can be investigated in connection with the results of Raucher and Sheetz (2000), which reported a greater than expected increase of lamellipodial extension rate in PDGF-activated cells. This was interpreted as a result of a localized decrease in the apparent membrane tension, compared to the more global effects of detergent addition, like desoxycholate, which still decrease in a similar way the membrane tension but also initiate cell membrane extensions at many new sites. The cytomechanical model presented here can take into account such global shape changes, while distinguishing between different parameters which determine the apparent membrane tension, including the bilayer tension and the membrane-cytoskeleton adhesion modulated by the F-actin concentrations.

simulation	μ	Q_0	D	t_0	d_0	thr.
fig.10.4	4	45	4	1	4.5	0.1
fig.10.5	4	45	4	1	4.5	0.1
fig.10.7	4	40	0.1	t	4.5	0.1
/	2	45	2.7	0.73	4.5	0.1
/*	2	45	2.7	0.73	4.5	0.1
fig.10.10*	2	45	2.7	0.73	4.5	0.1
fig.10.17	4	/	/	/	4.0	0.05
fig.10.14	4	45	4	0.4-1.8	4.5	0.06
fig.10.15	4	45	4	1.5	4.5	0.06-1.2

Table 10.1: Cell and gradient parameters used in the simulations. d_0 is the initial position of the cell from the source of chemoattractant (in unit of the cell radius); thr. is the threshold controlling the adhesion strength. * designates the simulation where the pulsating state of the cell is taken as initial condition. The other cell parameters are set to the following values: $\beta = \gamma = 0.5$, $\delta = 0.001$, $\tau = 1.5$, $a_{sat} = 2$, $a_{max} = 10$, $\psi = 5.5$, the number of points taken to define the cell boundary is $m = 54$ except the simulation of Figure 10.17 where $m = 64$.

t_0	r_{min} (μm)	$t_{r<2.55}$ time unit	d_c (μm)	speed (μm/t.u.)	$t_{r<0.75}$ time unit	d_c (μm)	speed (μm/t.u.)
0.4	1.50	127.03	56.40	0.44	/	/	/
0.5	0.39	119.60	43.80	0.37	120.41	46.65	0.39
0.6	0.43	101.65	49.27	0.48	116.62	58.42	0.50
0.7	0.28	90.62	46.87	0.52	90.93	48.82	0.54
0.8	0.49	110.79	51.60	0.46	111.21	53.47	0.48
0.9	1.05	82.76	46.95	0.57	/	/	/
1.0	0.55	71.72	46.05	0.64	72.01	48.00	0.67
1.1	2.02	68.70	51.15	0.74	/	/	/
1.2	0.23	71.88	53.25	0.74	82.28	57.90	0.70
1.3	0.29	127.55	60.82	0.48	129.02	65.55	0.51
1.4	0.26	146.21	69.15	0.47	146.33	70.72	0.48
1.5	1.65	103.68	51.00	0.49	/	/	/
1.6	2.55	156.06	64.05	0.41	/	/	/
1.7	0.41	208.22	81.00	0.39	209.56	85.65	0.41

Table 10.2: Cell speed calculated from the distance covered (d_c) and the time (t) required by the cell to reach the targets of diameter $r_{target} = 2.55$ and $r_{target} = 0.75$ μm. r_{min} represents the minimum distance measured between the source of chemoattractant and the cell centre.

Chapter 11

A model for large membrane deformations

Un modèle pour les grandes déformations membranaires

Nous proposons dans ce chapitre une nouvelle formulation des hypothèses biomécaniques utilisées dans le modèle de Alt et Tranquillo (1995) dans le but de prendre en compte les longues déformations membranaires observées sur les fibroblastes. Cette composante est hors de portée de ce dernier modèle en raison de l'hypothèse nécessaire de faibles déformations imposées dans la dérivation du terme de courbure membranaire. Pour résoudre ce problème, nous avons tout d'abord considéré un modèle très simple pour décrire les morphologies possibles que pouvaient adopter la membrane. La forme membranaire résulte de l'équilibre des contraintes appliquées, c'est à dire une contrainte de pression hydrostatique pour la protrusion et une contrainte de rétraction représentée par une fonction statique modulée de façon sinusoidale le long du pourtour cellulaire. Cette force pouvant être interprétée comme résultante d'un état stationnaire de la distribution de l'actine dans le cortex qui comme nous l'avons vu dans le modèle précédent détermine l'intensité de la rétraction. Ces deux contraintes sont modulées par la force de tension de courbure dont une nouvelle dérivation est proposée de façon cette fois à considérer les longues extensions membranaires. Plusieurs morphologies possibles obtenues en fonction du choix du mode de déformation sont proposées. L'influence du terme de courbure est evaluée dans chaque cas pour différentes valeurs du paramètres d'élasticité de la membrane.

Dans un second temps, ce modèle de membrane a été couplé à un modèle décrivant la dynamique de l'actine dont la formulation est inspirée du modèle de Lewis et Murray (1991) pour décrire un cytogel d'actomyosine, mais tout en gardant les hypothèses du modèle de Alt. Sur la base d'une approximation monodimensionnelle de la dynamique de l'actine, nous avons pu reproduire l'ensemble des comportements observés dans le cadre du modèle précédent, mais cette fois sans la limitation de faible extension de la membrane. Une simulation proposée montre de plus la génération d'un état morphologique et dynamique très proche d'un état observé expérimentalement sur les fibroblastes. Ce résultat conforte les hypothèses mécanochimiques formulées.

Nous considérons enfin en discussion les évolutions futures que suggèrent le modèle, en particulier la possibilité d'une description bidimensionnelle de la dynamique de l'actine qui permettrait d'aborder toute la complexité architecturale du cytosquelette.

11.1 Introduction

In the previous chapters, the mathematical model used is based on the hypothesis of small membrane deformations. This condition is imposed by the approximation made in the derivation of the curvature term (see section 8.2.1). Therefore we have been restricted to a qualitative description of the cell behaviour observed with fibroblasts which exhibit long membrane extensions. In this chapter we thus propose a new formulation of the model in order to provide a more realistic description of the morphologies observed.

In the initial model of Alt and Tranquillo (1995), the movements of the membrane essentially result from the interaction between a constant protrusive hydrostatic pressure (P) and a retraction component which was assumed to depend linearly on the local amount of actin (γLa), both being modulated by an additional curvature-dependent term. The influence of actin density thus occurs through the retraction term.

As a starting point, we consider here a very simple description of the forces acting on the cell membrane by replacing the actin-dependent retraction term by a sinusoidal function which can be assumed to represent a non-homogeneous static actin distribution in the cell cortex. The aim is thus to generate the potential cell shapes that can be generated and to evaluate the importance of the curvature-dependent stress whose new derivation, this time, allows us to take into account large membrane extensions and curvatures.

The second step is then to restore the coupling between the membrane and the actin distribution. This is performed on the same principle as in the model previously used, namely that the actin concentration influences the strength of the retraction stress which leads the membrane extension length to be the mirror image of the actin distribution at the periphery of the cell body (as high actin density corresponds to a strong retraction, therefore to a small extension of the membrane). Actin dynamics in that case is described through a one-dimensional (1D) approximation of the mechanochemical model for an actin cytogel proposed by Lewis and Murray (1991).

The last step towards a precise description of both the actin dynamics and the related cell morphologies is to consider the two-dimensional (2D) formulation of the model. In the 1D approximation, the actin density is supposed to be constant in the radial direction. We can justify this assumption by the fact that filaments tend to be organized radially in the protrusions (especially in filopod-like protrusions). However, experimentally radial heterogeneities are reported for the actin density and especially a gradient of actin due to the treadmilling process is observed with usually an increased density at the cortex periphery (see Figure 1.8). Various extensions of the model in this sense are suggested in the discussion.

11.2 Static membrane deformations

In this section we first of all present a simple model to describe the membrane deformations independent of the actin dynamics. The aim of this exercise is to evaluate the potential final "steady-state" deformations which can be obtained from the mechanical forces assumed to act on the membrane, namely:

- a protrusive force P (due to the hydrostatic pressure inside the cell),
- a retraction force $\gamma(\theta)$ which is modulated along the angular position θ, and which could reflect a static state of the actin distribution,
- a curvature-dependent force τK_L,
- a friction force between the membrane and the substrate, $\Phi \partial L/\partial t$.

The deformations of the membrane, in a similar way as in the model previously studied, are thus given by the equation:

$$\Phi \frac{\partial L}{\partial t} = P - \gamma(\theta) L - \tau K_L \tag{11.1}$$

where $\gamma(\theta) = \gamma_0[\alpha + \sin(m\theta)]$, α and m represent the coefficients which control the amplitude of the deformation and the mode of deformation respectively.

The membrane curvature K_L in polar coordinates is given by the following expression (the derivation is detailed in the appendix):

$$K_L = \frac{2(\frac{\partial L}{\partial \theta})^2 - [L(\theta) + R_0]\frac{\partial^2 L}{\partial \theta^2} + [L(\theta) + R_0]^2}{\left[(\frac{\partial L}{\partial \theta})^2 + [L(\theta) + R_0]^2\right]^{\frac{3}{2}}}, \tag{11.2}$$

where R_0 represents the radius of the cell body.

11.2.1 Influence of the curvature term

Whereas in the model of Alt and Tranquillo (1995), the curvature-dependent stress depends on the amount of actin in order to represent the membrane-cortex stress, we consider here a pure curvature stress independent of the actin density since the membrane and actin network are un-coupled for simplicity in this first stage.

To evaluate the influence of this curvature stress, we compare numerical solutions of the equation (11.1) for various values of the parameter τ (representing the membrane stiffness) with the analytical solution of this equation for $\tau = 0$ (i.e. no curvature stress). The analytical solution with the initial condition $L(t = 0) = L_0$ is given by:

$$L(\theta, t) = \frac{P}{\gamma(\theta)} + \left(L_0 - \frac{P}{\gamma(\theta)}\right) e^{-\gamma(\theta) t}. \tag{11.3}$$

The asymptotic steady-state solution is given by:

$$\lim_{t \to +\infty} L(\theta, t) = \frac{P}{\gamma(\theta)} = \frac{P}{\gamma_0[\alpha + \sin(m\theta)]}, \tag{11.4}$$

and hence

$$\frac{P}{\gamma_0(\alpha+1)} \leq L(\theta) \leq \frac{P}{\gamma_0(\alpha-1)} \tag{11.5}$$

The maximum amplitude of deformation ΔL_{max} is thus:

$$\Delta L_{max} = \frac{2P}{\gamma_0(\alpha+1)(\alpha-1)}. \tag{11.6}$$

The solutions of the equation (11.1) including the curvature term are non-trivial. Therefore they are calculated numerically using a central finite difference scheme which leads to a tridiagonal matrix system which is solved by the Thomas Algorithm (see Strikverda 1989).

Figure 11.1 shows the comparison between the analytical solution (external blue curves) and the numerical solution (internal red curves) for asymptotic states of various modes of deformation. We observe that the more the curvature is important the more the curvature stress becomes significant in smoothing the membrane shape.

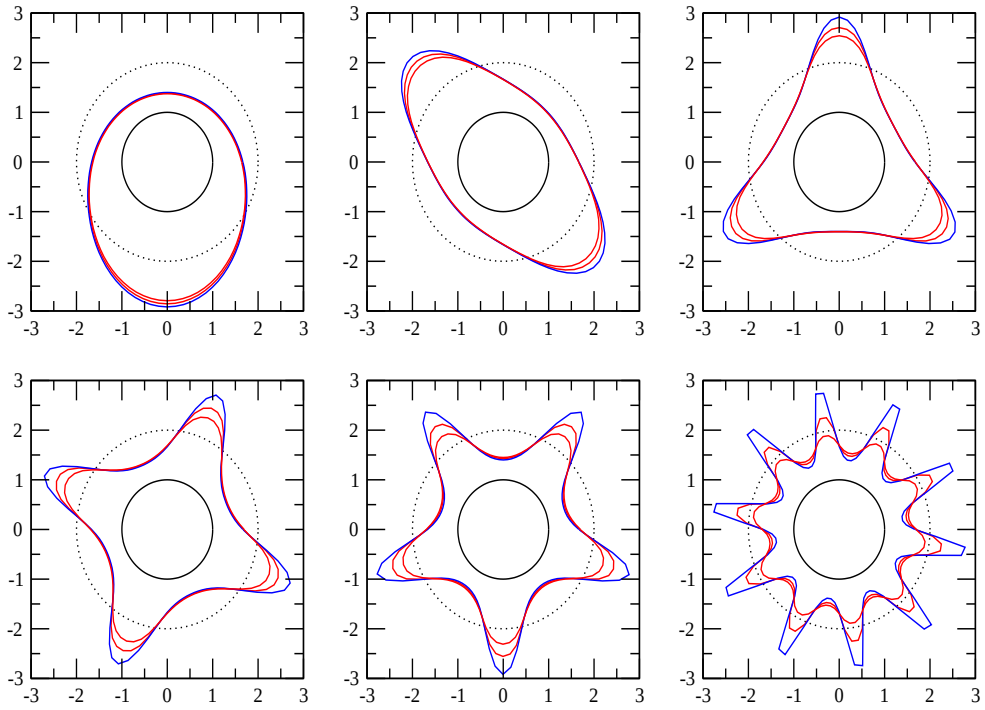

Figure 11.1: Potential cell morphologies for various modes of deformation of $\gamma(\theta)$ ($m = 1, 2, 3, 4, 5$ and 10). In each graph, the dotted curve represents the initial position of the membrane ($L(\theta, t = 0) = L_0$). The blue curve (external curve) represents the analytical solution of the equation for the membrane deformations (equation 11.1) for $\tau = 0$. The red curves (internal curves) are the numerical solutions of this equation for $\tau = 0.05$ and $\tau = 0.1$.

11.3 The dynamical model

The aim of this section is to restore the coupling between the movements of the membrane and the actin dynamics via the retraction force.

The model considered to describe the actin dynamics extends and develops the mechanochemical model proposed by Lewis and Murray (1991, 1992) to deal with an actomyosin cytogel (see section 2.3.2). The model couples 2 equations, one describing the chemical dynamics of the material and the second describing its mechanical properties. We assume that the actomyosin network of our model retains the same mechanical properties of the actomyosin cytogel considered by Lewis and Murray (1991). The stress tensor thus consists of viscous σ_v, elastic σ_e, contractile σ_c and osmotic stress σ_p components. In Lewis's model, sol/gel transition kinetics were considered whereas in our case we focus on the polymerization kinetics of actin as in the model of Alt and Tranquillo (1995). The system of equations to describe the actin dynamics is thus written as:

$$\nabla \cdot (\sigma_v + \sigma_e + \sigma_c + \sigma_p) = 0, \tag{11.7}$$

$$\frac{\partial a}{\partial t} + \nabla \cdot \left(a \frac{\partial \mathbf{u}}{\partial t} \right) - D\Delta a = k_a(a_c - a), \tag{11.8}$$

a represents the F-actin concentration, a_c the F-actin concentration at the chemical equilibrium which differentiate the states of polymerization and depolymerization whose rate of polymerization is controlled by k_a; D is the diffusion coefficient for F-actin; $\mathbf{u}$ is a vector denoting the displacement of the elements of the actomyosin network from their original unstrained position; σ_v, σ_e, σ_c, σ_p are respectively given by:

$$\sigma_v = \mu_1 \dot{\epsilon} + \mu_2 \dot{\phi} I, \tag{11.9}$$

$$\sigma_e = E'[\epsilon + \nu' \phi I], \tag{11.10}$$

$$\sigma_c = \sigma(a) I = \psi a^2 e^{-a/a_{sat}} I, \tag{11.11}$$

$$\sigma_p = -p(\phi) I = \frac{p}{1+\phi} I, \tag{11.12}$$

where $\epsilon = \frac{1}{2}(\nabla u + u \nabla)$ is the strain tensor, I is the identity tensor, $\phi = \nabla \cdot \mathbf{u}$ the dilation, μ_1 and μ_2 are shear and bulk viscosities of the F-actin network; finally $E' = E/(1+\nu)$, $\nu' = \nu/(1-2\nu)$ where E is Young's modulus and ν the Poisson ratio. The function $\sigma(a)$ represents the contractile activity of the actomyosin network and is taken as in the previous model of Alt and Tranquillo (1995). This function models the fact that the contractility increases according to a parabolic law with the actin concentration until a saturation concentration $2a_{sat}$ from which an effect of compaction of the network occurs and leads the contractility to decrease exponentially. $p(\phi)$ represents the osmotic stress which depends on the dilation ϕ.

For simplification, and especially to avoid the problem of a free, moving boundary, we consider a one-dimensional approximation for actin on a circle of radius r_*. With such an approximation, the two components of the mechanical equilibrium equation can

be reduced to a unique equation whose derivation in polar coordinates (developed in the appendix) leads to the following expression:

$$\frac{\partial}{\partial\theta}\left[\mu\dot{\phi} + \hat{E}\phi + \sigma(a) - p(\phi)\right] = \frac{\alpha}{2}\frac{v}{r_*}, \tag{11.13}$$

where $\mu = \mu_1 + \mu_2$, $\hat{E} = E'(1+\nu')$ and $\alpha = E' - \mu_1 E'(\nu' + \frac{3}{2})/(\frac{3}{2}\mu_1 + \mu_2)$.

Membrane and actin network dynamics are coupled by means of the following equation which describes the conservation of the amount of actin, $Q = La$, inside the cell:

$$\frac{\partial Q}{\partial t} - \frac{D}{r_*^2}\frac{\partial^2 Q}{\partial\theta^2} + \frac{1}{r_*}\frac{\partial}{\partial\theta}(Q\dot{v}) = k_a(Q_c - Q). \tag{11.14}$$

Whereas in the model of Alt and Tranquillo (1995), a linear relation ($\gamma_1 La$) for the retraction force exerted by the network on the membrane was considered, we replace here that linear dependency by the non-linear function $\sigma(a)$. This function is related to the active contraction of the network rather than a passive restoring force. The deformation of the membrane is thus given by:

$$\frac{\partial L}{\partial t} = P - \sigma(a)L - \tau K_L$$

11.4 Nondimensionalization and linear stability analysis

11.4.1 Nondimensionalization

We nondimensionalize the equations by making the following substitutions:

$$\tilde{t} = \frac{t}{T} = tk_a, \qquad \tilde{a} = \frac{a}{a_c}, \qquad \tilde{v} = \frac{v}{X}, \qquad \tilde{L} = \frac{L}{L_0}, \qquad \tilde{D} = \frac{D}{k_a X^2}, \qquad \tilde{E} = \frac{\hat{E}}{k_a\mu},$$

$$\tilde{P} = \frac{P}{k_a L_0 \Phi}, \qquad \tilde{\tau} = \frac{\tau}{k_a L_0 \Phi}, \qquad \tilde{\alpha} = \frac{\alpha}{k_a\mu}, \qquad \tilde{p} = \frac{p}{k_a\mu}, \qquad \tilde{\psi} = \frac{\psi {a_c}^2}{k_a\mu}, \qquad \tilde{a}_{sat} = \frac{a_{sat}}{a_c}.$$

Dropping the tildes for notational convenience, the equations are written as:

$$\frac{\partial}{\partial\theta}\left[\frac{1}{r_*}\frac{\partial\dot{v}}{\partial\theta} + \frac{E}{r_*}\frac{\partial v}{\partial\theta} + \sigma(a) - p(\phi)\right] = \frac{\alpha}{2}\frac{v}{r_*}, \tag{11.15}$$

$$\frac{\partial}{\partial t}(La) - \frac{D}{r_*^2}\frac{\partial^2}{\partial\theta^2}(La) + \frac{1}{r_*}\frac{\partial}{\partial\theta}(La\dot{v}) = L(1-a), \tag{11.16}$$

$$\frac{\partial L}{\partial t} = P - \sigma(a)L - \tau K_L. \tag{11.17}$$

11.4.2 Linear Stability Analysis

The linear stability analysis is performed around the following steady state:

$$a_0 = 1, \qquad L_0 = \frac{P}{\sigma(1)}, \qquad v_0 = 0, \tag{11.18}$$

and all the equations are linearized about this steady state. The solutions of the linearized system are proportional to $e^{\lambda t + ik\theta}$. By substitution of this expression in the linearized equations we obtain the system:

$$\begin{pmatrix} \lambda + \sigma(1) & L_0\sigma'(1) & 0 \\ \lambda + \frac{D}{r_*^2}k^2 & L_0(\lambda + \frac{D}{r_*^2}k^2 + 1) & ik\frac{L_0}{r_*}\lambda \\ 0 & ikr_*\sigma'(1) & -(\lambda+\Omega)k^2 - \frac{\alpha}{2} \end{pmatrix} \begin{pmatrix} L - L_0 \\ a - a_0 \\ v - v_0 \end{pmatrix} = \vec{0}, \tag{11.19}$$

with $\Omega = E - p$. The dispersion equation associated with this system is given by $det(M) = 0$ (where M is the matrix above), i.e:

$$k^2\lambda^3 + a(k^2)\lambda^2 + b(k^2)\lambda + c(k^2) = 0, \tag{11.20}$$

where

$$\begin{aligned} a(k^2) &= \frac{D}{r_*^2}k^4 + [\Omega + 1 + \sigma(1) - 2\sigma'(1)]k^2 + \frac{\alpha}{2}, \\ b(k^2) &= \frac{D}{r_*^2}[\Omega + \sigma(1) - \sigma'(1)]k^4 + \left[\frac{\alpha}{2}\frac{D}{r_*^2} + \Omega\left(1 + \sigma(1) - \sigma'(1)\right) + \sigma(1)\left(1 - \sigma'(1)\right)\right]k^2 \\ &\quad + \frac{\alpha}{2}\left[1 + \sigma(1) - \sigma'(1)\right], \\ c(k^2) &= \frac{D}{r_*^2}\Omega\left[\sigma(1) - \sigma'(1)\right]k^4 + \left[\frac{\alpha}{2}\frac{D}{r_*^2}\left(\sigma(1) - \sigma'(1)\right) + \sigma(1)\Omega\right]k^2 + \frac{\alpha}{2}\sigma(1). \end{aligned}$$

According to the Routh-Hurwitz criteria the condition for the roots of the dispersion equation to have a negative real part ($Re\lambda < 0$) is:

$$a(k^2) > 0\ , \quad c(k^2) > 0 \quad \text{and} \quad a(k^2)b(k^2) - c(k^2) > 0 \tag{11.21}$$

For simplicity, we represent the functions $a(k^2)$, $b(k^2)$ and $c(k^2)$ by:

$$\begin{aligned} a(k^2) &= a_1k^4 + a_2k^2 + a_3 \\ b(k^2) &= b_1k^4 + b_2k^2 + b_3 \\ c(k^2) &= c_1k^4 + c_2k^2 + c_3 \end{aligned}$$

and we have $a_1 > 0$, $a_3 > 0$, $c_3 > 0$ and $c_1 < 0$. a_2, b_1, b_2, b_3 and c_2 are not well-defined. As c_1 is negative, it means that the number of wave numbers k for which $c(k^2)$ is positive, is limited, i.e. $c(k^2) > 0$ only for $k^2 \in [0, k^2_{max}]$. As $a(k^2)$ is required to be positive at least for $k^2 < k^2_{max}$, it means that $b(k^2)$ must also be positive to fulfill the condition $a(k^2)b(k^2) - c(k^2) > 0$.

Conditions for a bifurcation

The stability analysis is thus performed as follow: first we determined the value of k^2_{max} for the condition $c(k^2) > 0$, then as a_1 and a_3 are positive but a_2 can be negative, it means that a bifurcation occurs when $a(k_c^2) = 0$. The wave number k_c^2 is the point for which the function $a(k^2)$ has its minimum at 0. We then have to make sure that the function $b(k^2)$ remains positive for $k^2 < k^2_{max}$ according to the conditions obtained for the choice of the parameters.

determination of k^2_{max}
As c_1 is negative, $c(k^2)$ can be positive only for a finite number of wave numbers k^2. $c(0) = c_3$ being positive, the range of k^2 for which the function $c(k^2)$ is positive is thus given by $k \in [0, k^2_{max}]$, where k^2_{max} is solution of $c(k^2) = 0$, i.e.

$$c_1 k^4 + c_2 k^2 + c_3 = 0, \qquad \text{with the solution:} \qquad k^2_{max} = \frac{2\sigma(1)}{\frac{D}{r_*^2}[\sigma'(1) - \sigma(1)]}.$$

determination of the conditions for a bifurcation
As a_1 and a_3 are positive, a bifurcation occurs for the wave number k_c^2 where $a(k_c^2) = 0$, k_c^2 being the wave number for which the function $a(k^2)$ is minimum, i.e,

$$\frac{da(k_c^2)}{dk^2} = 2a_1 k_c^2 + a_2 = 0 \quad \Rightarrow \quad \begin{aligned} k_c^2 &= -\frac{a_2}{2a_1} > 0, \\ k_c^2 &= \frac{2\sigma'(1) - \sigma(1) - \Omega - 1}{2\frac{D}{r_*^2}} > 0. \end{aligned}$$

The condition for k_c^2 to exist is that: $2\sigma'(1) > \sigma(1) + \Omega + 1$. The bifurcation occurs for $a(k_c^2) = 0$, thus if we replace the expression found for k_c^2 in this equation we obtain the condition that the parameters must obey at the bifurcation point, i.e.:

$$2\sigma'(1) - \sigma(1) - \Omega - 1 = \frac{\sqrt{2\alpha D}}{r_*}. \tag{11.22}$$

Moreover, we must have $k_c^2 < k^2_{max}$
verification that $b(k^2)$ is positive
The most favourable situation would be to have $b(k^2) > 0$ for any $k^2 \in [0, k^2_{max}]$. For such a situation, b_1 and b_3 must be positive i.e:

$$\begin{aligned} b_1 > 0 \quad &\Rightarrow \quad \Omega + \sigma(1) - \sigma'(1) > 0, \\ b_3 > 0 \quad &\Rightarrow \quad 1 + \sigma(1) - \sigma'(1) > 0, \\ &\text{if} \quad \Omega > 1 \quad \text{then} \quad b_3 > 0 \quad \Rightarrow \quad b_1 > 0. \end{aligned}$$

Thus $b(k^2) > 0$ for any k if the minimun of the function $b(k^2)$ is positive, i.e.

$$\frac{db(k_0^2)}{dk^2} = 0 \quad \text{and} \quad b(k_0^2) > 0 \quad \Rightarrow \quad k_0^2 = -\frac{b_2}{2b_1} \quad \Rightarrow \quad b_2 < 0.$$

Figures	D	τ	α	ψ	a_{sat}	p	P	Ω
11.2.a-b	0.134	0	21.798	9	1.1	1	4	2
11.2.c-d	0.075	0	38.946	8	1.1	1	4	2
11.2.e-f	0.00962	0.1	303.5752	10	1.1	1	4	2

Table 11.1: Parameters of the simulations

So we have the condition:

$$\frac{\alpha}{2}\frac{D}{r_*^2} + \Omega[1 + \sigma(1) - \sigma'(1)] < \sigma(1)[1 - \sigma'(1)]. \tag{11.23}$$

The condition $b(k^2) > 0$ is true if $b(k_0^2) > 0$ i.e:

$$b(k_0^2) = b_1 k_0^4 + b_2 k_0^2 + b_3 \quad > 0 \qquad \Rightarrow \qquad 2\sqrt{b_1 b_3} > b_2 \quad \text{always true as } b_2 < 0.$$

11.5 Simulation results

The numerical method used to solve the system of equations is based on the finite difference scheme of Crank-Nicholson. The associated matrix inversion was solved using the Thomas algorithm (Strikverda, 1989) adapted to periodic boundary conditions. The initial conditions are random perturbations of the F-actin concentration around the homogeneous steady-state where the cell is perfectly circular.

The results of the simulations carried out are presented in Figure 11.2. In each case, the spatio-temporal maps for the membrane extension $L(\theta, t)$ are displayed together with the associated actin distributions $a(\theta, t)$. The parameters used for the simulations are given in Table 11.1.

The two first simulations (Figure 11.2.a-b and 11.2.c-d) reproduce the behaviours simulated with the previous model, namely a rotating wave of deformation around the cell body in the first case and the pulsating state of mode 4 in the second case.

For the third simulation (Figure 11.2.e-f) parameters were defined according to the stability analysis in order to select higher modes of deformations. The sequence exhibiting the associated cell movements is displayed in Figure 11.3. Snapshots of the simulated cell are taken to cover a full period of deformations. The simulated cell exhibits coordinated movements of extension/retraction of the membrane involving up to 4 protrusions simultaneously which occur in perpendicular directions from each other. This simulated dynamics of cell deformations is consistent with the movements observed on a fibroblast whose videomicroscopy sequence is presented in Figure 11.4. This time, the model is able to represent quantitatively the large membrane extensions such as observed on the fibroblasts. On the simulated sequence we observe that a developing protrusion presents a wide front (under the effect of the pressure) whereas during the retraction process the pseudopods become thinner (the actomyosin network pulls on the membrane). Experimentally the difference is not as obvious, however developing protrusions exhibit at their tips some

kind of blobs which disappear as soon as the pseudopods start to retract (see pseudopod on the top of the cell during the first half of the experimental sequence and the pseudopod on the right of the cell during the second half).

Figure 11.5 proposes to follow simultaneously the evolution of the actin distribution as well as its tangential displacement. The 4 graphs presented correspond respectively to the snapshots 1, 3, 4 and 5 of Figure 11.3 (associated simulation times are t=5; 5.4; 5.6 and 5.8 normalized units). In the protrusive areas (or pseudopods) the actin density is low and starts to polymerize (and reversely depolymerize in the areas where the critical density is reached, $a_c = 1$). Simultaneously, radial displacements of actin are observed from zones of low density to zones of higher density which tends to the homogenization of the actin distribution in the cell (graph 1). Actin progressively increases at the neighbourhood of the pseudopods. The intensification of the retraction force thus leads to the narrowing of the protrusions (graph 2). The actin then enters almost instantaneously in the remaining pseudopods (graph 3) and the distributions of actin in the cell are reversed. The retraction at the tips of the pseudopods is thus suddenly increased and leads to their total retraction (graph 4). New pseudopods then appear in zones of low actin density and a new cycle can start.

Figure 11.6 gives a more detailed representation of the oscillating dynamics on a longer time scale (up to $t = 20$ normalized time units). The upper graph shows the simultaneous evolution of the amplitude of the cell membrane deformation associated with the actin concentration for a given direction corresponding to a pseudopod, and the lower graph shows the simultaneous evolution of the amplitude of two protrusive directions distant from each other with a 45-degree angle. Oscillations of the cell shape are exhibited with alternated directions of deformation from one cycle to the next one.

11.6 Discussion

This new formulation of the mechanochemical hypotheses for the actin dynamics is globally satisfying on several aspects.

Firstly we have been able on the basis of the stability analysis to re-simulate the behaviours obtained with the previous model of Alt and Tranquillo (1995).

Secondly we are now able to describe long membrane deformations such as observed on fibroblasts. In particular we have provided a very realistic sequence of deformations which catch the main features of a real fibroblast. This is achieved through a fine tuning between the two key concentrations for actin; - the concentration at the chemical equilibrium a_c which determines the polymerization and depolymerization state of actin and - the saturation concentration $2a_{sat}$ which regulates the intensity of the retraction force. Considering the relatively good qualitative agreement with experimental observations, the assumption of radially constant actin density appears justified to deal with fibroblasts deformations. It seems from experimental observations that this preferential radial orientation of the actin filaments in the cell tends to stabilize the shape (Cramer, 1995). This stabilizing effect probably linked to the development of new adhesion site in coordination with the formation of bundles of filaments is not taken into account by the model and leads to a

very motile cell with protrusions occurring in many different directions of space. Future work should focus on a way to take into account this higher level of organization of the actin into bundles of filaments as well as the resulting dynamics of attachment/detachment to the substrate.

Thirdly, in order to consider higher organization of actin in the cortex, a 2D description of the actin dynamics in the cortex will be required and the model in its new formulation provides a very good basis to investigate further this 2D dynamics.

Other improvements should also be made to refine the molecular aspect of the model in particular to take explicitly into account interacting species with F-actin such as myosin or G-actin and other proteins evoked in the review of chapter 1, whose involvement in the regulation of the mechanical properties of the cytoskeleton is essential.

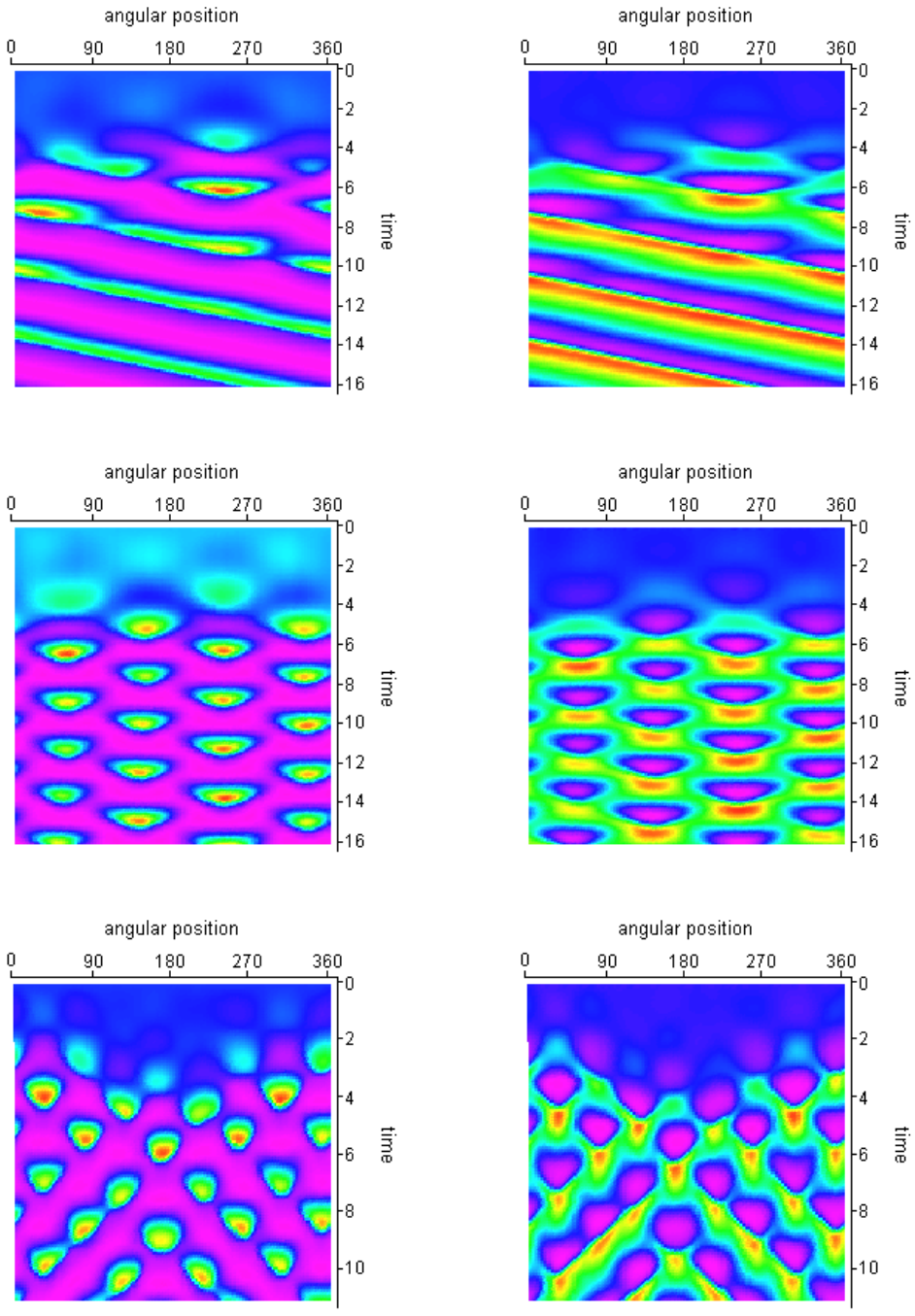

Figure 11.2: Spatio-temporal evolution of cell membrane deformations (a)-(c)-(e) and associated actin distribution (b)-(d)-(f).

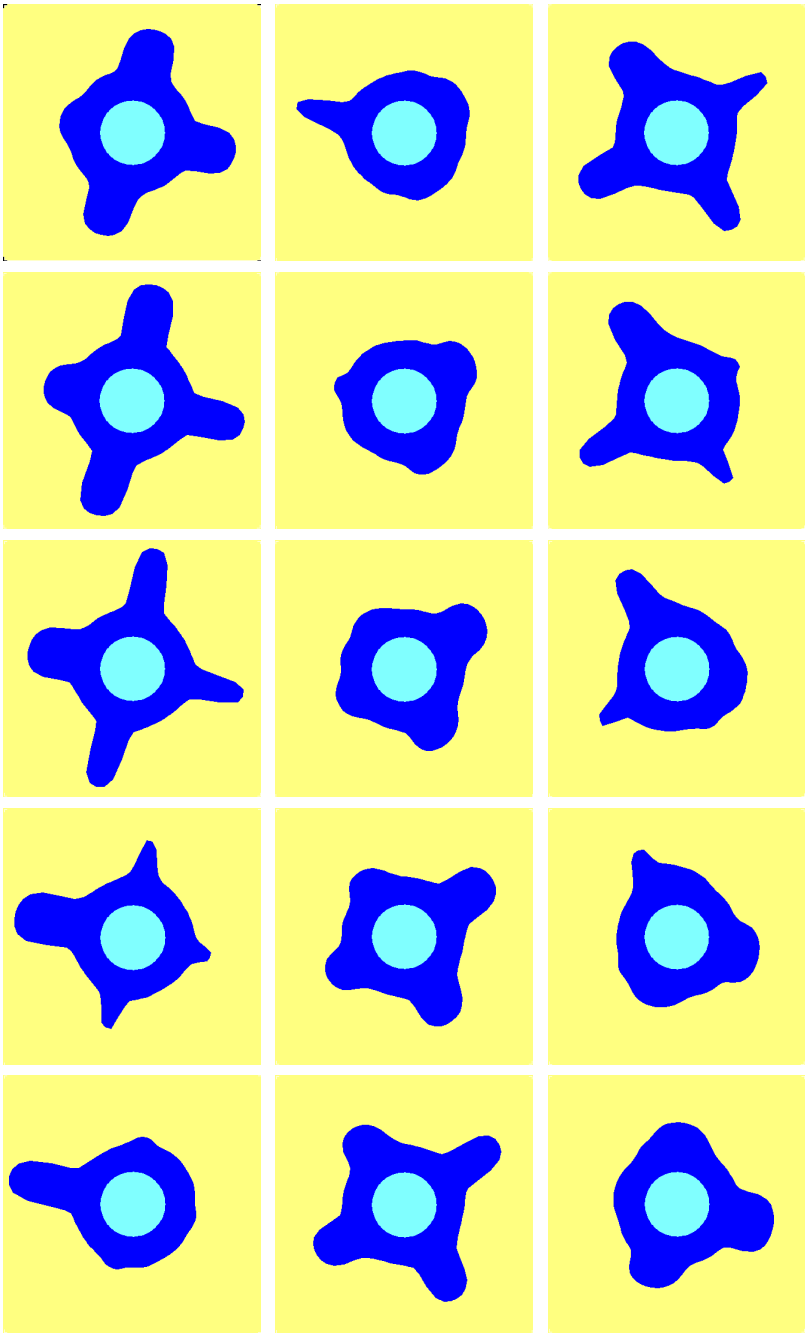

Figure 11.3: Simulated cell membrane deformations. Snapshots are taken every 200 iterations ($\Delta t = 0.2$). Associated simulation times from $t = 5$ to $t = 6.8$ normalized units (sequence to be read from top to bottom)

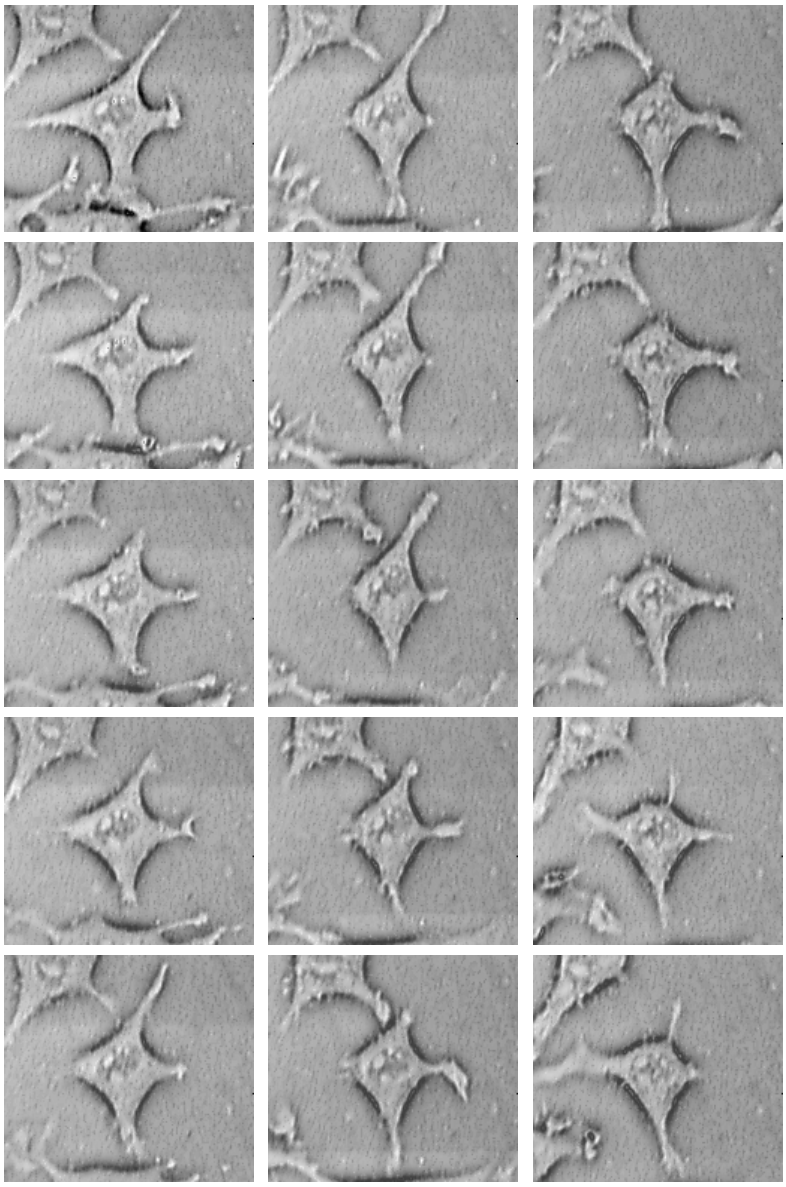

Figure 11.4: Videomicroscopy sequence of a L929 fibroblast. The time interval is of about 2 minutes between 2 consecutive images (sequence to be read from top to bottom)

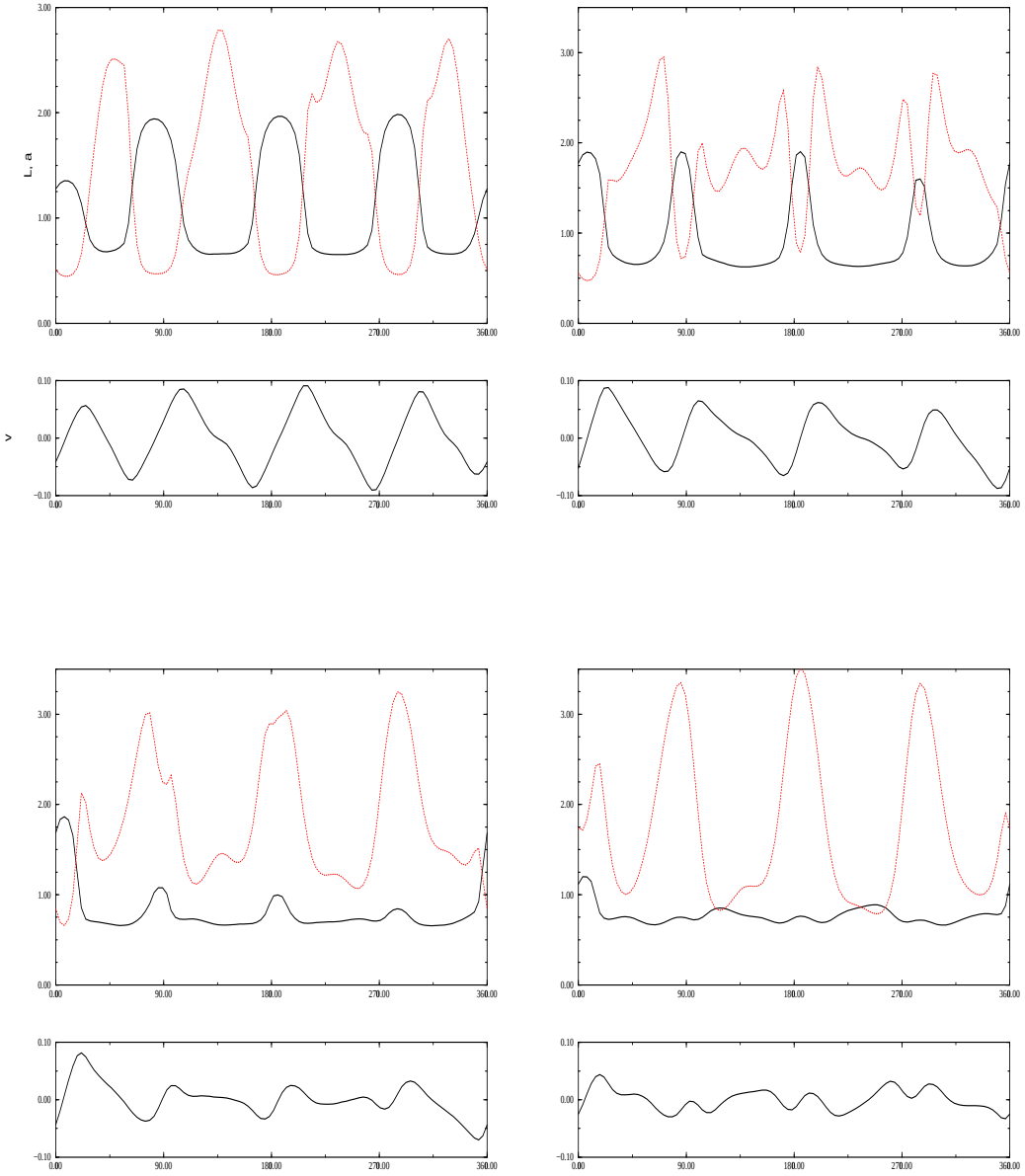

Figure 11.5: Simultaneous plots of actin distribution (dotted red curves) and corresponding membrane deformations (black curves) in upper graphs. In the lower rectangular graphs, the associated tangential displacements of actin are displayed. These 4 graphs correspond to the snapshots 1, 3, 4 and 5 of the sequence of Figure 11.3 associated with the normalized times 5, 5.4, 5.6 and 5.8 respectively.

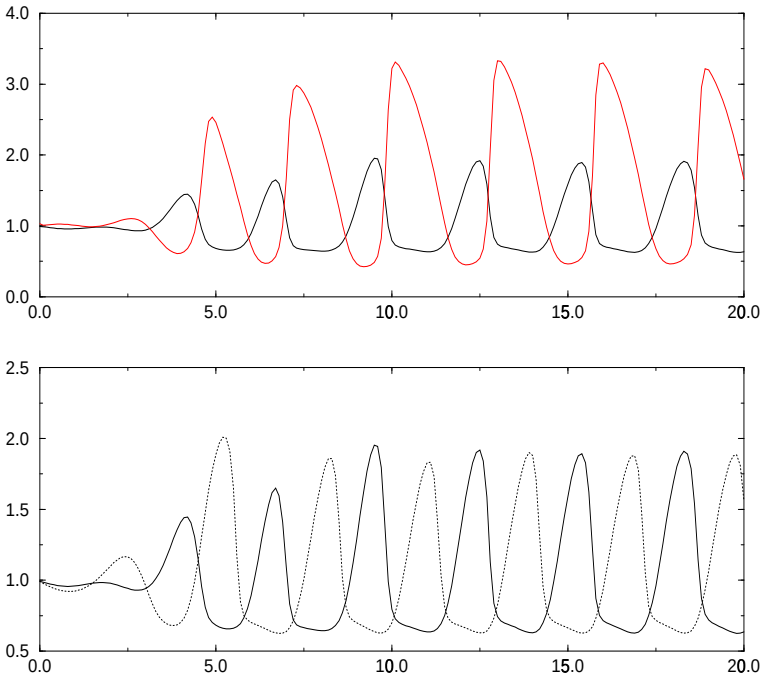

Figure 11.6: Upper graph: evolutions with time of the cell membrane deformations (black curve) and of the associated actin distribution (dotted red curve) in normalized units, for a given protrusive direction. Lower graph: simultaneous evolution of the membrane deformations for two protrusive directions at 45 degrees from each other

General Conclusion

Conclusion Générale

La caractérisation expérimentale réalisée sur la lignée de fibroblastes murins L929 a permis de mettre en évidence l'existence d'un comportement auto-organisé des déformations de ces cellules. Un telle auto-organisation avait été jusque là reportée uniquement pour des cellules présentant des morphologies arrondies, c'est à dire des structures cytosqueletiques peu complexes (Alt, 1990; Alt *et al.*, 1995; Killich *et al.*, 1993, 1994). Dans notre cas, les fibroblastes présentent une organisation du cytosquelette d'actine qui comporte differents types de structures, où les filaments d'actine s'organisent en paquets dont le rôle a pour but de stabiliser la structure sans pour autant priver la cellule de ses capacitées motiles. Nous avons demontré à travers deux méthodes d'analyse d'image complémentaires (la segmentation et le flot optique) que les fibroblastes de la lignée L929 présentaient préférentiellement des morphologies symétriques impliquant de 2 à 4 protrusions simultanées. En l'absence de voisinage proche, la cellule adopte une morphologie à 4 protrusions et développe un mouvement pulsant synchronisé où l'extension des pseudopodes alignés sur le même axe s'accompagne de la rétraction des pseudopodes dans la direction perpendiculaire, puis réciproquement. Nous avons de plus montré que les pulsations observées sont globalement périodiques avec une période d'environ 30 minutes. Sur la base d'hypothèses biomécaniques (Alt and Tranquillo, 1995; Lewis and Murray, 1991, 1992) qui considèrent la dynamique de polymérisation d'actine et les interactions mécaniques entre la membrane et le réseau contractile d'actomyosine nous avons pu simuler ce comportement qualifié de spontané. Une tentative de rapprochement des approches expérimentales et théoriques a en particulier été proposée par l'identification des valeurs de paramètres biomécaniques à partir des données de la litérature.

Deux situations typiques d'interaction de la cellule avec son environnement ont été abordées à travers deux extensions du modèle théorique. La première extension a concerné la prise en compte de l'interaction cellule-cellule caracterisée par un phénomène d'inhibition de contact de l'activité protrusive. Cet effet a été simulé en considérant une altération locale des propriétés élastiques de la membrane et du cytosquelette. Une réorganisation réaliste de la dynamique de l'actine permet de renforcer l'hypothèse d'une composante mécanique dans le processus de transduction du signal comme cela est proposé par les théories de tensegrité (Ingber, 1997) et de percolation (Forgacs, 1995). Sur le même principe le modèle a été étendu de façon à prendre en compte le phénomène de chimiotaxie où la cellule migre en remontant un gradient de chimioattractant. Ce phénomène a été simulé en considérant une dépendance des propriétés mécaniques membranaires avec la concentration locale du facteur extracellulaire (chimioattrac-

tant). Sur la base de cette hypothèse, confirmée par diverses études expérimentales (Bereiter-Hahn and Luers, 1998; Raucher and Sheetz, 2000), nous avons pu simuler un comportement là aussi réaliste de migration de la cellule vers la source de chimioattractant. L'ensemble des résultats obtenus par la modélisation tendent à renforcer l'importance de l'aspect mécanique de la cellule souvent négligé par les approches moléculaires. Il est évident qu'une meilleure compréhension de ces aspects mécaniques permettrait d'orienter efficacement la détection des mécanismes et acteurs moléculaires impliqués.

Deux perspectives principales se dégagent de ce travail. Tout d'abord, la mise en évidence de l'existence d'un état spontané de la cellule caracterisé morpho-dynamiquement propose la possibilité d'utiliser les critères morpho-dynamiques (nombre de protrusions, disposition relative des protrusions, nature des déformations: ondes pulsantes stationnaires ou en rotation, amplitude moyenne des extensions, périodicité du mouvement, et autres critères plus spécifiques aux différents types de cellules rencontrés) à des fins d'identification des cellules. L'identification de différents phénotypes cellulaires, en particulier la différenciation des phénotypes normaux et tumoraux, pourrait être envisagée dans la mesure où les critères morpho-dynamiques des état spontanés de chacun soient suffisament discriminés. Cette nouvelle méthode d'identifiaction apparaitrait comme une excellente alternative aux méthodes classiquement utilisées qui requièrent pour l'instant des techniques de réactivités moléculaires complexes.

La seconde perspective est de proposer une réelle orientation de l'expérience par le modèle. Nous avons vu dans le modèle de migration présenté au chapitre 10, que la vitesse de migration pouvait être controlée en agissant soit sur l'intensité de la pente du gradient soit en agissant sur l'affinité de la cellule avec son substrat (paramètre du seuil d'adhésion). Nous avons vu qu'il existait en particulier un gradient optimal pour la vitesse de migration. Il est envisageable sur la base d'un modèle correctement calibré par des données expérimentales, de définir théoriquement les conditions optimales de la migration. En particulier le modèle rend possible l'identification et l'évaluation de l'importance des différents paramètres mécaniques impliqués dans la réponse cellulaire.

En conclusion, beaucoup de travail reste à faire à la fois sur les plans expérimental et théorique. Expérimentalement, une étude comparative des paramètres morpho-dynamiques entre cellules normales et cellules transformées s'impose pour permettre de confirmer ou d'infirmer l'hypothèse de l'utilisation de ces critères comme signature spécifique de la cellule. Théoriquement, une évolution du modèle pour une prise en compte plus précise de la nature hétérogène de l'organisation de l'actine serait nécessaire en particulier dans le but d'un rapprochement attendu des approches moléculaires et mécaniques.

The experimental work in this thesis concerning cell shape characterization performed on the L929 fibroblast line, has shown the existence of the self-organizing behaviour of these cells. Such a self-organization was reported only for cells presenting rounded morphologies, namely those involving simple cytoskeletal structures (Alt, 1990; Alt *et al.*, 1995; Killich *et al.*, 1993, 1994). In our case, the fibroblasts present an actin cytoskeletal

organization which consists of different structures, where actin filaments are organized into bundles. The role of the bundles is to stabilize the structure without however depriving the cell from its motile ability. We have shown, using two complementary methods for image analysis (segmentation and optical flow), that L929 fibroblasts were preferentially exhibiting symmetrical morphologies involving 2 to 4 simultaneous stable protrusions. In the absence of a nearby neighbourhood, the cell adopts a 4 protrusions morphology and develops a synchronized pulsating movement where the extension of the pseudopods oriented along one axis goes with the retraction of the pseudopods oriented in the perpendicular direction and so on. Moreover we have shown that the observed pulsations are globally periodical with a period of about 30 minutes. On the basis of biomechanical hypotheses (Alt and Tranquillo, 1995; Lewis and Murray, 1991, 1992) which consider the polymerization dynamics of actin and the mechanical interactions between the membrane and the contractile actomyosin network, we have been able to simulate this experimental behaviour considered as spontaneous. One attempt to link the experimental and theoretical approaches has been proposed with the identification of the biomechanical parameter values from data found in the current literature.

Two typical situations of interaction of the cell with its environment have been tackled through two theoretical model extensions. The first extension has concerned the cell-cell interactions characterized by the phenomenon of contact inhibition of the protrusive activity. This effect has been simulated by considering the local alteration of the elastic properties of the membrane and of the cytoskeleton. A realistic reorganization of the actin dynamics allows us to reinforce the hypothesis that a mechanical component might exist in the process of signal transduction, as was suggested by tensegrity (Ingber, 1997) and percolation theories (Forgacs, 1995). The model has been extended in order to take into account chemotaxis where the cell migrates up a gradient of chemoattractant. This phenomenon has been simulated by considering a dependence between the mechanical properties of the membrane with the local concentration of the extracellular factor (chemoattractant). On the basis of this hypothesis confirmed by various experimental studies (Bereiter-Hahn and Luers, 1998; Raucher and Sheetz, 2000), , we have been able to simulate once again a realistic behaviour of the cell migration towards the source of chemoattractant. All of these results obtained through modelling tend to reinforce the importance of the mechanical aspect of the cell often neglected by the molecular approaches. It is obvious that a better understanding of these mechanical aspects would allow us to orientate efficiently the detection of the mechanisms and the molecular players involved.

Two main perspectives emerge from this work. First, the exhibition of the potential existence of a spontaneous cell state, morpho-dynamically characterized, proposes the possibility to use these morpho-dynamical criteria (number of protrusions, relative disposition of the protrusions, mean extension amplitude, movement periodicity, and other criteria specific to the cell types encountered) to identify the cells. The identification of the various cell phenotypes and in particular the differentiation between normal and tumoral phenotypes could be considered assuming that the morpho-dynamical criteria are sufficiently discriminated. This new method of identification would appear as an excellent alternative to the classical methods used which require complex techniques of cell molecular reactivity.

The second perspective is to propose a real “model-driven experimentation”. As it was

seen in the model for chemotaxis presented in chapter 10, the cell speed can be controlled either by varying the intensity of the slope of the gradient or by varying the affinity of the cell with its substrate (threshold parameter for cell adhesion). We have seen that there exists an optimal gradient for the cell speed. It is thus possible, on the basis of a well experimentally-calibrated model, to define theoretically the optimum conditions for migration. In particular, the model allows us to identify and evaluate the relative importance of the different mechanical parameters involved in the cell response.

In conclusion, a lot of work remains to be done both experimentally and theoretically. Experimentally, a comparative study of the morpho-dynamical parameters between normal and transformed cells is necessary to confirm or overturn the hypothesis of the use of these criteria as a specific cell signature. Theoretically, a more refined and detailed model which takes into account the heterogeneous nature of the actin organization would be required in order to provide the long expected link between the molecular and mechanical approaches.

Bibliography

[1] M. Abercrombie. The crawling movement of metazoan cells. *Proc. R. Soc. Lond.*, 207(B):129–147, 1980.

[2] M. Abercrombie and J.E.M. Heaysman. Observations on the social behaviour of cells in tissue culture. I. Speed of movement of chick heart fibroblasts in relation to their mutual contacts. *Experimental Cell Research*, 5:111–131, 1953.

[3] M. Abercrombie, J.E.M. Heaysman, and S.M. Pegrum. The locomotion of fibroblasts in culture. *Experimental Cell Research*, 59:393–398, 1970.

[4] M. Abercrombie, J.E.M. Heaysman, and S.M. Pegrum. The locomotion of fibroblasts in culture. *Experimental Cell Research*, 60:437–444, 1970.

[5] V.C. Abraham, V. Krishnamurthi, D. Lansing Taylor, and F. Lanni. The actin based nanomachine at the leading edge of migrating cells. *Biophysical journal*, 77:1721–1732, 1999.

[6] D.S. Adams. Mechanisms of cell shape change: the cytomechanics of cellular response to chemical environment and mechanical loading. *Journal of Cell Biology*, 117:83–93, 1992.

[7] F.J. Alenghat, B. Fabry, K.Y. Tsai, W.H. Goldmann, and D.E. Ingber. Analysis of cell mechanics in single vinculin-deficient cells using a magnetic tweezer. *Biochemical and Biophysical Research Communications*, 277:93–99, 2000.

[8] W. Alt. Mathematical models and analysing methods for the lamellipodial activity of leukocytes. *NATO ASI (Adv.Sci.Inst.) Ser.H, Cell Biology*, 42:407–422, 1990.

[9] W. Alt, O. Brosteanu, B. Hinz, and W.H. Kaiser. Patterns of spontaneous motility in videomicrographs of human epidermal keratinocytes. *Biochemical Cell Biology*, 73:441–459, 1995.

[10] W. Alt and M. Dembo. Cytoplasm dynamics and cell motion: two phase flow models. *Mathematical Biosciences*, 156:207–228, 1999.

[11] W. Alt and R.T. Tranquillo. Basic morphogenetic system modeling shape changes of migrating cells: how to explain fluctuating lamellipodial dynamics. *J. Biol. Syst.*, 3:905–916, 1995.

[12] R. Bar-Ziv, E. Moses, and P. Nelson. Dynamic excitations in membranes induced by optical tweezers. *Biophysical Journal*, 75:294–320, 1998.

[13] A.R. Bausch, W. Moller, and E. Sackmann. Measurement of local viscoelasticity and forces in living cells by magnetic tweezers. *Biophysical Journal*, 76:573–579, 1999.

[14] A.R. Bausch, F. Ziemann, A.A. Boulbitch, K. Jacobson, and E. Sackmann. Local measurements of viscoelastic parameters of adherent cell surfaces by magnetic bead microrheometry. *Biophysical Journal*, 75:2038–2049, 1998.

[15] J. Bereiter-Hahn and H. Luers. Subcellular tension fields and mechanical resistance of the lamella front related to the direction of locomotion. *Cell Biochemistry and Biophysics*, 29:243–262, 1998.

[16] G.G. Borisy and T.M. Svitkina. Actin machinery: pushing the envelope. *Current Opinion in Cell Biology*, 12:104–112, 2000.

[17] M. Bornens, M. Paintraud, and C. Celati. The cortical microfilament system of lymphoblasts displays a periodic oscillatory activity in the absence of microtubules: implications for cell polarity. *Journal of Cell Biology*, 109:1071–1083, 1989.

[18] K. Burton, J.H. Park, and D. Lansing Taylor. Keratocytes generate traction forces in two phases. *Molecular biology of the cell*, 10:3745–3769, 1999.

[19] M.F. Carlier and D. Pantaloni. Control of actin dynamics in cell motility. *J.Mol.Biol.*, 269:459–467, 1997.

[20] G. Cevc and D. Marsh. Phospholipid bilayers. Wiley New-York. 1987.

[21] C.Y. Chung, S. Lee, C. Briscoe, C. Ellsworth, and R.A. Firtel. Role of Rac in controlling the actin cytoskeleton and chemotaxis in motile cells. *PNAS*, 97(10):5225–5230, 2000.

[22] E.A. Clark, W.G. King, J.S. Brugge, M. Symmons, and R.O. Hynes. Integrin-mediated signals regulated by members of the Rho family of GTPases. *The Journal of Cell Biology*, 142:573–586, 1998.

[23] J. Condeelis. Life at the leading edge: the formation of cell protrusions. *Annu. Rev. Cell Biol.*, 9:411–444, 1993.

[24] J. Condeelis. Understanding the cortex of crawling cells: insight from dictyostelium. *Trends in cell biology*, 3:371–376, 1993.

[25] E.A. Cox, S.K. Sastry, and A. Huttenlocher. Integrin-mediated adhesion regulates cell polarity and membrane protrusion through the Rho family of GTPases. *Molecular Biology of the Cell*, 12:265–277, 2001.

[26] L.P. Cramer, M. Siebert, and T.J. Mitchison. Identification of novel graded polarity actin filaments bundles in locomoting heart fibroblasts: implications for the generation of motile force. *The Journal of Cell Biology*, 136(6):1287–1305, 1997.

[27] A. Curtis and C. Wilkinson. Topographical control of cells. *Biomaterials*, 18(24):1573–1583, 1997.

[28] A. Curtis and C.D. Wilkinson. Reactions of cells to topography. *J. Biomater. Sci. Polym. Ed.*, 9(12):1313–1329, 1998.

[29] M. Dembo, T. Oliver, A. Ishihara, and K. Jacobson. Imaging the traction forces exerted by by locomoting cells with the elastic substratum method. *Biophysical Journal*, 70:2008–2022, 1996.

[30] M. Dembo and Y.L. Wang. Stresses at the cell-to-substrate interface during locomotion of fibroblasts. *Biophysical journal*, 76:2307–2316, 1999.

[31] A.G. Dunn. Conceptual problems with kinesis and taxis. *Biology of the chemotactic response, Edited by J.P. Armitage and J.M. Lackie, Cambridge University Press*, pages 1–13, 1990.

[32] G. Dunn and D. Zicha. Dynamics of fibroblasts spreading. *Journal of Cell Science*, 108:1239–1249, 1995.

[33] E.H. Egelman. The structure of actin. *J. Muscle Res. Cell Motil.*, 6:129–151, 1985.

[34] M.U. Ehrengruber, T.D. Coates, and D.A. Deranleau. Shape oscillations: a fundamental response of human neutrophils stimulated by chemotactic peptides. *FEBS Letter*, 259:229–232, 1995.

[35] L. Eichinger, B. Koppel, A.A. Noegel, M. Schleicher, M. Schliwa, K. Weijer, W. Witke, and P.A. Janmey. Mechanical perturbation elicits a phenotypic difference between Dictyostelium wild-type cells and cytoskeletal mutants. *Biophysical Journal*, 70:1054–1060, 1996.

[36] G.W. Fisher, P.A. Conrad, R.L. DeBiasio, and D.L. Taylor. Centripetal transport of cytoplasm, actin, and the cell surface in lamellipodia of fibroblasts. *Cell Motil. Cytoskeleton*, 11:235–247, 1988.

[37] G. Forgacs. On the possible role of cytoskeletal filamentous networks in intracellular signaling: an approach based on percolation. *Journal of cell Science*, 108:2131–2143, 1995.

[38] J.B. Fournier. Nontopological saddle-splay and curvature instabilities from anisotropic membrane inclusions. *Physical Review Letters*, 76:4436–4439, 2001.

[39] C.G. Galbraith and M.P. Sheetz. A micromachined device provides a new bend on fibroblast traction forces. *Proc.Natl.Acad.Sci.*, 94:9114–9118, 1997.

[40] C.G. Galbraith and M.P. Sheetz. Keratocytes pull with similar forces on their dorsal and ventral surfaces. *Journal of cell biology*, 147:1313–1323, 1999.

[41] F. Germain, A. Doisy, X. Ronot, and P. Tracqui. Characterisation of cell defromation and migration using a parametric estimation of image motion. *IEEE Trans. Biom. Eng.*, 46:584–600, 1999.

[42] R.J. Goldacre. The role of the cell membrane in the locomotion of amoebae and the source of the motive force and its control by feedback. *Experimental Cell Research Suppl.*, 8:11–16, 1961.

[43] W.H. Goldmann. Binding of tropomyosin-troponin to actin increases filament beding stiffness. *Biochemical and Biophysical Research Communications*, 276:1225–1228, 2000.

[44] W.H. Guilford, R.C. Lantz, and R.W. Gore. Locomotive forces produced by single leukocytes in vivo and in vitro. *Am. J. Physiol.*, 268:C1308–C1312, 1995.

[45] H. Le Guyader and C. Hyver. Periodic activity of the cortical cytoskeleton of the lymphoblast: modelling by a reaction-diffusion system. *C.R. Acad. Sci. Paris*, 320:59–65, 1997.

[46] A. Hall. Rho GTPases and the actin cytoskeleton. *Science*, 279:509–514, 1998.

[47] A. Harris. Location of cellular adhesion to solid substrata. *Developmental Biology*, 35:97–115, 1973.

[48] A. Harris. Tissue culture cells on deformable substrata: biomechanical implications. *Journal of Biomechanical Engineering*, 106:19–24, 1984.

[49] A. Harris, D. Stopak, and P. Wild. Silicon rubber substrata: a new wrinkle in the study of cell locomotion. *Science*, 208:177–179, 1980.

[50] A.K. Harris. A dozen questions about how tissue cells crawl. *Biochem. Soc. Symp.*, 65:315–341, 1999.

[51] J.E.M. Heaysman. Non-reciprocal contact inhibition. *Experientia*, 26:1344, 1970.

[52] J.E.M. Heaysman and S.M. Pegrum. Early cell contact in culture. *in R. Bellairs, A. Curtis and G. Dunn (eds); Cell Behaviour (Cambridge University Press)*, pages 49–76, 1982.

[53] T.L. Hill. Microfilament or microtubule assembly or disassembly against a force. *Proc. Natl. Acad. Sci.*, 78:5613–5617, 1981.

[54] S. Hvidt and K. Heller. Viscoelastic properties of biological networks and gels. *In* Physical Networks: Polymers and Gels. W. Burchard and S. Ross-Murphy editors, Elsiever, London. pages 195–208, 1990.

[55] D.E. Ingber. Cellular tensegrity: defining new rules of biological design that govern the cytoskeleton. *Journal of Cell Science*, 104:613–627, 1993.

[56] D.E. Ingber. Tensegrity: the architectural basis of cellular mechanotransduction. *Annu.Rev.Physiol.*, 59:575–599, 1997.

[57] L. Jaffe. Calcium explosions as triggers for development. *Ann. N.Y. Acad. Sci.*, 339:86–101, 1980.

[58] P.A. Janmey, S. Hvidt, A. Kas, D. Lerche, A.C. Maggs, E. Sackmann, M. Schliwa, and T.P. Stossel. The mechanical properties of actin gels. *J. Biol. Chem.*, 269:32503–32513, 1994.

[59] T. Killich, P.J. Plath, H. Bultmann, L. Rensing, and M.G. Vicker. The locomotion shape and pseudopodial dynamics of unstimulated dictyostelium cells are not random. *Journal of Cell Science*, 106:1005–1013, 1993.

[60] T. Killich, P.J. Plath, H. Bultmann, L. Rensing, and M.G. Vicker. Cell movement and shape are non-random and determined by intracellular, oscillatory rotating waves in dictyostelium amoebae. *Biosystems*, 33:75–87, 1994.

[61] J. Lee, A. Ishihara, and K. Jacobson. How do cells move along surfaces ? *Trends in Cell Biology*, 3:366–370, 1993.

[62] M.A. Lewis and J.D. Murray. Analysis of stable two-dimensional patterns in contractile cytogel. *J. Nonlinear Sci.*, 1:289–311, 1991.

[63] M.A. Lewis and J.D. Murray. Analysis of dynamic and stationary pattern formation in the cell cortex. *J. Math. Biol.*, 31:25–71, 1992.

[64] L.M. Machesky, S.J. Atkinson, C. Ampe, J. Vandekerckhove, and T.D. Pollard. Purification of a cortical complex containing two unconventional actins from Acanthamoebae by affinity chromatography on profilin-agarose. *Journal of Cell Biology*, 127:107–115, 1994.

[65] L.M. Machesky and R.H. Insall. Signaling to actin dynamics. *The Journal of Cell Biology*, 146:267–272, 1999.

[66] L.M. Machesky, E. Reeves, F. Wientjes, F.J. Mattheyse, A. Grogan, N.F. Totty, A.L. Burlingame, J.J. Hsuan, and A.W. Segal. Mammalian actin-related protein 2/3 complex localizes to regions of lamellipodial protrusion and is composed of evolutionarily conserved proteins. *Biochem. J.*, 328:105–112, 1997.

[67] R. Merkel, R. Simson, D.A. Simson, M. Hohenadl, A. Boulbitch, E. Wallraff, and E. Sackmann. A micromechanic study of cell polarity and plasma membrane cell body coupling in Dictyostelium. *Biophysical Journal*, 79:707–719, 2000.

[68] C.A. Middleton and J.A. Sharp. The social behaviour of cells in culture. *from: Cell locomotion in vitro; Croom Helm Applied Biology Series, Ed Peter J. Baron*, pages 137–160, 1984.

[69] A. Mogilner and G. Oster. The physics of lamellipodial protrusion. *Eur. Biophys. J.*, 25:47–53, 1996.

[70] R.D. Mullins, W.F. Stafford, and T.D. Pollard. Structure, subunits topology, and actin-binding activity of the Arp2/3 complex from Acanthamoebae. *Journal of Cell Biology*, 136:331–343, 1997.

[71] C. Nielsen, M. Goulian, and O.S. Andersen. Energetics of inclusion-induced bilayer deformations. *Biophysical Journal*, 74:1966–1983, 1998.

[72] C.D. Nobes and A. Hall. Rho GTPases control polarity, protrusion, and adhesion during cell movement. *The Journal of Cell Biology*, 144(6):1235–1244, 1999.

[73] T. Oliver, M. Dembo, and K. Jacobson. Traction forces in locomoting cells. *Cell Motility and the Cytoskeleton*, 31:225–240, 1995.

[74] T. Oliver, M. Dembo, and K. Jacobson. Separation of propulsive and adhesive traction stresses in locomoting keratocytes. *The Journal of Cell Biology*, 145:589–604, 1999.

[75] G.F. Oster. On the crawling of cells. *J. Embryol. exp. Morph., Supplement*, 83:329–364, 1984.

[76] A. Palmer, T.G. Mason, J. Xu, S.C. Kuo, and D. Wirtz. Diffusing wave spectroscopy mocrorheology of actin filament networks. *Biophysical Journal*, 79:1063–1071, 1999.

[77] P.P Parnigotto, M.T. Conconi, V. Bassani, S. Pastore, E. Contiero, and R. Cortivo. Interaction between keratynocytes and fibroblasts cultured in vitro: morphology, morphometry and growth. *Italian Journal of Anatomy and Embryology*, 98:31–39, 1993.

[78] M. Peckham, C. Wells, P. Taylor-Harris, D. Coles, D. Zicha, and G.A. Dunn. Using molecular genetics as a tool in understanding crawling cell locomotion in myoblasts. *Biochem. Soc. Symp.*, 65:281–299, 1999.

[79] R.J. Pelham and Y.L. Wang. High resolution detection of mechanical forces exerted by locomoting fibroblasts on the substrate. *Molecular Biology of the Cell*, 10:935–945, 1999.

[80] C.S. Peskin, G.M. Odell, and G.F. Oster. Cellular motions and thermal fluctuations: the brownian ratchet. *Biophys. J.*, 65:316–324, 1993.

[81] T. Pollard. Rate constants for the reactions of ATP- and ADP-actin with the end of actin filaments. *Journal of Cell Biology*, 103:2747–2754, 1986.

[82] T.D. Pollard, L. Blanchoin, and R.D. Mullins. Molecular mechanisms controlling actin filament dynamics in nonmuscle cells. *Annu. Rev. Biophys. Biomol. Sruct.*, 29:545–576, 2000.

[83] J. Pourati, A. Maniotis, D. Spiegel, J.L. Schaffer, J.P. Butler, J.J. Fredberg, D.E. Ingber, D. Stamenovic, and N. Wang. Is cytoskeletal tension a major determinant of cell deformability in adherent endothelial cells ? *Am.J.Physiol. (Cell physiol.)*, 274(43):C1283–C1289, 1998.

[84] M. Radmacher, M. Fritz, C.M. Kacher, J.P. Cleveland, and P.K. Hansma. Measuring the viscoelastic properties of human platelets with the atomic force microscope. *Biophysical Journal*, 70:556–567, 1996.

[85] G. Ragsdale, K.J. Phelps, and K. Luby-Phelps. Viscoelastic response of fibroblasts to tension transmitted through adherents junctions. *Biophysical Journal*, 73:2798–2808, 1997.

[86] D. Raucher and M.P. Sheetz. Cell spreading and lamellipodial extension is regulated by membrane tension. *Journal of cell biology*, 148:127–136, 2000.

[87] C. Rotsch, K. Jacobson, and M. Radmacher. Dimensional and mechanical dynamics of active and stable edges in motile fibroblasts investigated by using atomic force microscopy. *Proc.Natl.Acad.Sci*, 96:921–926, 1999.

[88] C. Rotsch and M. Radmacher. Drug-induced changes of cytoskeletal structure and mechanics in fibroblasts: an atomic force microscopy study. *Biophysical journal*, 78:520–535, 2000.

[89] D.A. Schafer and T.A. Schroer. Actin-related proteins. *Annu. Rev. Cell Dev. Biol.*, 15:341–363, 1999.

[90] D.A. Schafer, M.D. Welch, L.M. Machesky, P.C. Brigdman, S.M. Meyer, and J.A. Cooper. Visualization and molecular analysis of actin assembly in living cells. *Journal of Cell Biology*, 143:1919–1930, 1998.

[91] M.P. Sheetz, D. Felsenfeld, C.G. Galbraith, and D. Choquet. Cell migration as a five-step cycle. *Biochem. Soc. Symp.*, 65:233–243, 1999.

[92] R. Simson, E. Wallraff, J. Faix, J. Niewohner, G. Gerisch, and E. Sackmann. Membrane bending modulus and adhesion energy of wild-type and mutant cells in Dictyostelium lacking talin or cortexillins. *Biophysical Journal*, 74:514–522, 1998.

[93] J.V. Small. Getting the actin filaments straight: nucleation-release or treadmilling. *Trends in Cell Biology*, 5:52–54, 1995.

[94] J.V. Small, I. Kaverina, O. Krylyshkina, and K. Rottner. Cytoskeleton cross-talk during motility. *FEBS Letter*, 452:96–99, 1999.

[95] J.V. Small, A. Rohlfs, and M. Herzog. Actin and cell movement. *Cell Behaviour: Adhesion and Motility. Ed G. Jones, C. Wigley and R. Warn. The Society of Experimental Biology*, pages 57–71, 1993.

[96] K.M. Soares and C.C. Maghelly. Linear instability analysis and mechanical interfacial tension. *J. theor. Biol.*, 196:169–179, 1999.

[97] J.C. Strikverda. Finite difference schemes and partial differential equations. *Wadsworth and Brooks/Cole, Mathematics Series*, 1989.

[98] K.L. Sung, P.C. Dong, G.W. Scmidt-Schonbein, S. Chien, and R. Skalak. Leukocyte relaxation properties. *Biophysical Journal*, 54:331–336, 1988.

[99] T.M. Svitkina and G.G. Borisy. Arp2/3 complex and ADF/cofilin in dendritic organization and treadmilling of actin filament array in lamellipodia. *J. Cell Biol.*, 145:1009–1026, 1999.

[100] T.M. Svitkina and G.G. Borisy. Progress in protrusion: the tell-tale Scar. *Trends Biochem. Sci.*, 24:432–436, 1999.

[101] T.M. Svitkina, A.B. Verkhovsky, and G.G. Borisy. Improved procedures for electron microscopy visualization of the cytoskeleton of cultured cells. *J. Struct. Biol.*, 115:290–303, 1995.

[102] J.A. Theriot and T.J. Mitchison. Actin microfilament dynamics in locomoting cells. *Nature*, 352:126–131, 1991.

[103] J.P. Thiery and M. Grassi. Dynamique de la cellule vivante: enjeux et perspectives aux niveaux cellulaire et moléculaire. *Dynamique de la cellule vivante, éd X. Ronot et D. Schoevaert-Brossault - Paris: INSERM (Méthodologie)*, pages 37–50, 1999.

[104] O. Thoumine and A. Ott. Time scale dependent viscoelastic and contractile regimes in fibroblasts probed by microplate manipulation. *Journal of Cell Science*, 110:2109–2116, 1997.

[105] P.A. Valberg and D.F. Albertini. Cytoplasmic motions, rheology and structure probed by a novel magnetic particle method. *Journal of Cell Biology*, 101:130–140, 1985.

[106] D. Wachstock, W.H. Schwarz, and T.D. Pollard. Affinity of α-actinin for actin determines the structure and mechanical properties of actin filament gels. *Biophysical Journal*, 65:205–214, 1993.

[107] O. Wagner, J. Zinke, P. Dancker, W. Grill, and J. Bereiter-Hahn. Visvoelastic properties of f-actin, microtubules, f-actin/α-actinin, and f-actin/α-hexokinase determined in microliter volumes with a novel nondestructive method. *Biophysical Journal*, 76:2784–2796, 1999.

[108] N. Wang, J.P. Butler, and D.E. Ingber. Mechanotransduction across the cell surface and through the cytoskeleton. *Science*, 260:1124–1127, 1993.

[109] C.M. Waterman-Storer and E.D. Salmon. Positive feedback interaction between microtubule and actin dynamics during cell motility. *Current Opinion in Cell Biology*, 11:61–67, 1999.

[110] C.M. Waterman-Storer, W.C. Salmon, and E.D. Salmon. Feedback interactions between cell-cell adherens junctions and cytoskeletal dynamics in newt lung epithelial cells. *Molecula biology of the cell*, 11:2471–2483, 2000.

[111] P. Weiss. Guiding principles in cell locomotion and cell aggregation. *Experimental Cell Research Suppl.*, 8:260–281, 61.

[112] M.D. Welch, A. Iwamatsu, and T.J. Mitchison. Actin polymerization is induced by Arp2/3 protein complex at the surface of Listeria momocytogenes. *NATURE*, 385:265–269, 1997.

[113] J. Xu, A. Palmer, and D. Wirtz. Rheology and microrheology of semiflexible polymer solutions: actin filament networks. *Macromolecules*, 31:6486–6492, 1998a.

[114] S. Yamada, D. Wirtz, and S.C. Kuo. Mechanics of living cells measured by laser tracking microrheology. *Biophysical journal*, 78:1736–1747, 2000.

[115] M. Yanai, J.P. Butler, T. Suzuki, A. Kanda, M. Kurachi, H. Tashiro, and H. Sasaki. Intracellular elasticity and viscosity in the body, leading and trailing regions of lomoting neutrophils. *Am.J.Physiol. (Cell physiol.)*, 277(46):C432–C440, 1999.

[116] G.I. Zahalak, W.B. McConnaughey, and E.L. Elson. Determination of cellular mechanical properties by cell poking, with an application to leukocytes. *J. Biomech. Eng.*, 112:283–294, 1990.

[117] K.S. Zaner and P.A. Valberg. Viscoelasticity of F-actin measured with magnetic microparticles. *Journal of Cell Biology*, 109:2233–2243, 1989.

[118] C. Zhu, G. Bao, and N. Wang. Cell Mechanics: Mechanical response, cell adhesion and molecular deformation. *Annu. Rev. Biomed. Eng.*, 2:189–226, 2000.

[119] J. Zoller, K. Brandle, and J. Bereiter-Hahn. Cellular motility in vitro as revealed by scanning acoustic microscopy depends on cell-cell contacts. *Cell Tissue Res.*, 290:43–50, 1997.

Publications

Analysis of cell motility combining cytomechanical model simulations and an optical flow method

Angélique Stéphanou[1], Xavier Ronot[2], Philippe Tracqui[1]
[1] *Laboratoire TIMC-IMAG, UMR CNRS 5525, Faculté de Médecine de Grenoble, 38706 La Tronche Cedex, France*
[2] *E.P.H.E., Institut Albert Bonniot, 38706 La Tronche Cedex, France*

Abstract

We developed a combined analysis of isolated cell dynamics based on both the extraction of relevant data obtained from time-lapse video-sequences analysis, such as velocities, periodic components, preferential morphologies, and the simulation of cells dynamical behaviour from theoretical models. Two methods have been alternatively used for analyzing the videomicroscopy sequences. The first one is based on an optical flow approach and relies on the conservation of light intensity in order to estimate the parameters of an affine model of cell deformations. A refined analysis of localized cell movements such as lamellipodial extension or retraction has been undertaken using a more classical segmentation of cell outlines. Various tools have been subsequently used to analyze the corresponding data time-amplitude and contours mapping, time variation of the motion model eigenvalues, including Fourier analyses. In association with this quantification of cell shape dynamics, we consider a continuous cytomechanical model of cell deformations. The model relies on the description of mechanical and chemical interactions between the cytoplasm, the actin cytoskeleton and the cell membrane. Different patterns of cell morphological changes have been simulated, considering different values of the model parameters. Specific illustration of these combined approaches is proposed for the study of fibroblasts deformations (L929 cell lines).

To appear in "Polymer and Cell Dynamics - Multiscale Modeling and Numerical Simulations" Eds W.Alt, Birkhauser-Verlag, Basel.

Cytomechanics of cell deformations and migration: from models to experiments

A. Stéphanou and P. Tracqui
Laboratoire TIMC-IMAG, UMR CNRS 5525, Faculté de Médecine de Grenoble, 38706 La Tronche Cedex, France

Abstract

A cytomechanical model has been proposed to analyse cell-cell interactions and cell migration through chemotaxis. We consider as the leading assumption that the cell cortical tension is locally modified by the protrusive activity of neighbour cells and binding of chemoattractant molecules to membrane receptors respectively. The model derives from the one initially proposed by Alt and Tranquillo (1995) which successfully describes experimentally observed cyclic autonomous cell shape changes. It is based on force balance equations coupling intracellular hydrostatic pressure and cell cortex contraction. Considering the protrusive dynamics of L929 fibroblats observed by videomicroscopy, we simulated the influence of neighbouring protrusions on a cell spontaneous pulsating behaviour. We further investigated the role of an extracellular gradient as another kind of external stimulus. The model illustrates how binding of chemoattractant molecules can induce a cell morphological instability which, above an intracellular stress threshold, will break the cell-substratum attachment. As a result, realistic cell chemotaxis can be simulated.

Résumé

En nous appuyant sur un modèle cytomécanique, nous proposons dans cet article une analyse des interactions cellule-cellule et de la migration cellulaire par chimiotaxie. Nous considérons comme hypothèse principale qu'une modification de la tension corticale cellulaire est induite, dans un cas par l'activité protrusive des cellules voisines, dans l'autre cas par la fixation de molécules de chimioattractant sur les récepteurs membranaires. Ce modèle, initialement proposé par Alt et Tranquillo (1995), permet de décrire de façon satisfaisante les changements cycliques et spontanés des morphologies cellulaires observées expérimentalement. Il est basé sur l'écriture d'équations d'équilibre mécanique, couplant la pression hydrostatique intracellulaire à la contraction du cortex de la cellule. A partir d'une étude expérimentale de la dynamique protrusive de fibroblastes L929 observée en vidéomicroscopie, nous avons simulé l'influence de protrusions voisines sur le comportement pulsant spontané d'une cellule. Nous avons étudié ensuite l'effet d'un autre stimulus extracellulaire tel qu'un gradient de chimioattractant. Le modèle montre comment la fixation des molécules de chimioattractant induit une instabilité morphologique suivie, au delà d'un certain niveau de contraintes intracellulaires, par la rupture des adhésions cellule-substrat, l'ensemble conduisant une simulation réaliste de la migration cellulaire par chimiotaxie.

To appear in the "Compte Rendu de l'Académie des Sciences".

Appendix A

Derivation of the curvature term

A.1 The curvature of plane curves

From "The elementary differential geometry of plane curves" (chap III)
R.H. Fowler (Cambridge University Press, London 1929)

The definition of the curvature K of a plane curve is given by:

$$K = \frac{1}{\rho} = \lim_{Q \to P} \frac{\psi_Q - \psi_P}{s_Q - s_P} = \lim_{Q \to P} \frac{\delta\psi}{\delta s},$$

where s_Q and s_P represents the curvilinear coordinates of the points P and Q respectively and ψ_Q and ψ_P the angle between the tangent of the curve at these points, with the horizontal axis. Thus:

$$K = \lim_{Q \to P} \frac{\delta\psi}{\delta s}.$$

We take this definition as a starting point to construct the general expression of any curve given by a function $y = f(x)$ in the cartesian referential (Oxy).

$$\frac{\delta\psi}{\delta s} = \frac{\delta\psi}{\delta x}\frac{\delta x}{\delta s},$$

so we have to determine the expressions of $\delta\psi/\delta x$ and $\delta x/\delta s$ for the cartesian coordinates x and y.

Determination of $\delta\psi/\delta x$:

$$\begin{aligned}(\tan\psi)' &= \frac{\delta}{\delta x}(\tan\psi) \\ &= (1+\tan^2\psi)\frac{\delta\psi}{\delta x},\end{aligned}$$

then,

$$\frac{\delta\psi}{\delta x} = \frac{(\tan\psi)'}{1+\tan^2\psi} = \frac{f''(x)}{1+f'(x)^2}.$$

Determination of $\delta x/\delta s$
If the curve is expressed by the function $y = f(x)$ then the tangent is:

$$\tan\psi = \frac{\delta y}{\delta x} = f'(x).$$

An elementary displacement along the curve can be approximated by:

$$\delta s = \sqrt{\delta x^2 + \delta y^2} = \delta x\sqrt{1 + \left(\frac{\delta y}{\delta x}\right)^2} = \delta x\sqrt{1 + f'(x)^2}.$$

By integrating δs we obtain the desire expression,

$$s = \int_P^Q \delta s = \int_x^{x+\delta x} \left(1 + f'(x)\right)^{\frac{1}{2}} dx \qquad \Rightarrow \qquad \lim_{\delta x\to 0} \frac{\delta x}{\delta s} = \frac{1}{[1 + f'(x)^2]^{\frac{1}{2}}}.$$

The expression of the curvature for the function $y = f(x)$ is:

$$K = \frac{1}{\rho} = \frac{f''(x)}{[1 + f'(x)^2]^{\frac{3}{2}}} = \frac{\frac{\partial^2 y}{\partial x^2}}{\left[1 + \left(\frac{\partial y}{\partial x}\right)^2\right]^{\frac{3}{2}}}.$$

A.2 A formula for the mean curvature K

From "Differential geometry"
J.J.Stoker (Wiley - Intersciences 1969)

If we denote by $\theta(s)$ the angle between the horizontal (Ox) axis and the tangent of the curve, we can write the curvature $K(s)$ as:

$$K(s) = \lim_{\Delta s\to 0} \frac{\theta(s + \Delta s) - \theta(s)}{\Delta s} = \frac{\partial\theta}{\partial s}.$$

The tangent $\vec{T}$ of the curve is:

$$\vec{T} = \frac{\partial\vec{X}}{\partial s} = \cos\theta\vec{U}_x + \sin\theta\vec{U}_y.$$

The expression of the successive derivatives of $X(s)$ are then:

$$\begin{aligned}
\dot{X}(s) = \frac{\partial X}{\partial s} &= \cos\theta(s)\vec{U}_x + \sin\theta(s)\vec{U}_y, \qquad \text{unit vector,} \\
\ddot{X}(s) = \frac{\partial\dot{X}}{\partial s} &= \frac{\partial}{\partial\theta}\left(\cos\theta(s)\vec{U}_x + \sin\theta(s)\vec{U}_y\right)\cdot\frac{\partial\theta}{\partial s}, \\
&= \left(-\sin\theta(s)\vec{U}_x + \cos\theta(s)\vec{U}_y\right)\cdot K(s),
\end{aligned}$$

which gives:

$$|K| = |\ddot{X}|.$$

We here note that:

$$\dot{X}\Lambda\ddot{X} = \begin{pmatrix} \cos\theta \\ \sin\theta \end{pmatrix} \Lambda \begin{pmatrix} -K\sin\theta \\ K\cos\theta \end{pmatrix} = K(\vec{U}_x \Lambda \vec{U}_y).$$

If we denote $\dot{x}$ and $\dot{y}$ the coordinates of $\dot{X}$ and $\ddot{x}$, $\ddot{y}$ the coordinates of $\ddot{X}$ then:

$$\dot{X}\Lambda\ddot{X} = (\dot{x}\ddot{y} - \ddot{x}\dot{y})(\vec{U}_x \Lambda \vec{U}_y).$$

Finally by identification of the two last expressions we obtain:

$$K = \dot{x}\ddot{y} - \ddot{x}\dot{y}.$$

Parametric case $X(t)$:
We will now look for the expression of the curvature K for the parametric case $X(t)$:

$$\begin{aligned}
\dot{X} &= \frac{dX}{ds} = \frac{dX}{dt}\frac{dt}{ds} = X'\frac{dt}{ds}, \\
\ddot{X} &= \frac{d\dot{X}}{ds} = \frac{d}{dt}\left(X'\frac{dt}{ds}\right)\frac{dt}{ds} = \frac{d}{dt}\left(\frac{dX}{dt}\frac{dt}{ds}\right)\frac{dt}{ds}, \\
&= \left(\frac{d^2X}{dt^2}\frac{dt}{ds} + \frac{dX}{dt}\frac{d}{ds}\right)\frac{dt}{ds} = \left(\frac{d^2X}{dt^2}(\frac{dt}{ds})^2 + \frac{dX}{dt}\frac{d^2t}{ds^2}\right), \\
&= X''\left(\frac{dt}{ds}\right)^2 + X'\left(\frac{d^2t}{ds^2}\right).
\end{aligned}$$

Thus,

$$\begin{aligned}
\dot{X}\Lambda\ddot{X} &= \left(X'\frac{dt}{ds}\right)\Lambda\left[X''\left(\frac{dt}{ds}\right)^2 + X'\left(\frac{d^2t}{ds^2}\right)\right], \\
&= (X'\Lambda X'')\left(\frac{dt}{ds}\right)^3.
\end{aligned}$$

The expression of dt/ds is obtained from the length of a distance on the curve:

$$s(t) = L = \int \sqrt{X'(\tau)X'(\tau)}d\tau \quad \Rightarrow \quad \frac{dt}{ds}\sqrt{X'X'(t)}.$$

In the equation A.2 we had:

$$K(\vec{U}_x \Lambda \vec{U}_y) = \dot{X}\Lambda\ddot{X}.$$

Thus,

$$K = (\vec{U}_x \Lambda \vec{U}_y) = \frac{X'\Lambda X'}{(X'X')^{\frac{3}{2}}}.$$

Finally the expression for the curvature is given by:

$$K = \frac{x'y'' - x''y'}{(x'^2 + y'^2)^{\frac{3}{2}}}.$$

A.3 The curvature in polar coordinates

We apply the formula we have just obtained to determine the curvature in polar coordinates, using it under the more adapted form:

$$K = \frac{\delta x \delta^2 y - \delta y \delta^2 x}{(\delta x^2 + \delta y^2)^{\frac{3}{2}}}.$$

In polar coordinates we have:

$$\left\{ \begin{array}{l} x = r\cos\theta, \\ y = r\sin\theta. \end{array} \right.$$

We then have to determine the expressions of δx, δy, $\delta^2 x$, $\delta^2 y$, δx^2 and δy^2.

$$\begin{aligned} \delta x &= \cos\theta\delta r - r\sin\theta\delta\theta, \\ \delta^2 x &= \cos\theta\delta^2 r - 2\sin\theta\delta r\delta\theta - r\cos\theta(\delta\theta)^2 - r\sin\theta\delta^2\theta, \end{aligned}$$

$$\begin{aligned} \delta y &= \sin\theta\delta r + r\cos\theta\delta\theta, \\ \delta^2 y &= \sin\theta\delta^2 r + 2\cos\theta\delta r\delta\theta - r\sin\theta(\delta\theta)^2 + r\cos\theta\delta^2\theta, \end{aligned}$$

$$\begin{aligned} \delta x^2 + \delta y^2 &= (\cos\theta\delta r - r\sin\theta\delta\theta)^2 + (\sin\theta\delta r + r\cos\theta\delta\theta)^2 \\ &= (\delta r)^2 + r^2(\delta\theta)^2 \\ &= (\delta\theta)^2\left[r^2 + \left(\frac{\delta r}{\delta\theta}\right)^2\right] \\ &= (\delta\theta)^2[r^2 + r'^2]. \end{aligned}$$

$$\begin{aligned} \delta x\delta^2 y &= (\cos\theta\delta r - r\sin\theta\delta\theta)(\sin\theta\delta^2 r + 2\cos\theta\delta r\delta\theta - r\sin\theta(\delta\theta)^2 + r\cos\theta\delta^2\theta) \\ &= \sin\theta\cos\theta\delta r\delta^2 r + 2\cos^2\theta(\delta r)^2\delta\theta - 3r\sin\theta\cos\theta\delta r(\delta\theta)^2 \\ &+ r\cos^2\theta\delta r\delta^2\theta - r\sin^2\theta\delta\theta\delta^2 r + r^2\sin^2\theta(\delta\theta)^3 - r^2\sin\theta\cos\theta\delta\theta\delta^2\theta. \end{aligned}$$

$$\begin{aligned} \delta y\delta^2 x &= (\sin\theta\delta r + r\cos\theta\delta\theta)(\cos\theta\delta^2 r - 2\sin\theta\delta r\delta\theta - r\cos\theta(\delta\theta)^2 - r\sin\theta\delta^2\theta) \\ &= \sin\theta\cos\theta\delta r\delta^2 r - 2\sin^2\theta(\delta r)^2\delta\theta - -3r\sin\theta\cos\theta\delta r(\delta\theta)^2 \\ &- r\sin^2\delta r\delta^2\theta + r\cos^2\theta\delta^2 r\delta\theta - r^2\cos^2\theta(\delta\theta)^3 - r^2\sin\theta\cos\theta\delta\theta\delta^2\theta. \end{aligned}$$

$$\begin{aligned}
\delta x\delta^2 y - \delta y\delta^2 x &= 2(\delta r)^2\delta\theta + r\delta r\delta^2\theta + r^2(\delta\theta)^3 - r\delta^2 r\delta\theta \\
&= (\delta\theta)^3\left[2\left(\frac{\delta r}{\delta\theta}\right)^2 + r\frac{\delta r\delta^2\theta}{(\delta\theta)^3} + r^2 - r\frac{\delta^2 r}{\delta\theta^2}\right] \\
&= (\delta\theta)^3\left[2r'^2 + r^2 - rr'' + \underbrace{rr'\frac{\delta^2\theta}{(\delta\theta)^2}}_{=0}\right].
\end{aligned}$$

note:

$$rr'\frac{\delta^2\theta}{(\delta\theta)^2} = 0 \quad \text{as} \quad \frac{\delta^2\theta}{(\delta\theta)^2} = \frac{\delta}{\delta\theta}\left(\frac{\delta}{\delta\theta}\theta\right) = \frac{\delta}{\delta\theta}1 = 0.$$

Thus the expression of the curvature for polar coordinates where $r = r(\theta)$, $r' = \partial r/\partial\theta$, and $r'' = \partial^2 r/\partial\theta^2$ is:

$$K = \frac{2r'^2 - rr'' + r^2}{(r'^2 + r^2)^{\frac{3}{2}}}.$$

We can thus deduce from this expression the curvature of the cell membrane in the geometry of our model where R_0 is the internal radius of the cell delimitating the cell body and $L(\theta)$ being the extension of the membrane taken from the surface of the cell body. The curvature is:

$$K = \frac{2\left(\frac{\partial L}{\partial\theta}\right)^2 - (L(\theta) + R_0)\frac{\partial^2 L}{\partial\theta^2} + (L(\theta) + R_0)^2}{\left[\left(\frac{\partial L}{\partial\theta}\right)^2 + (L(\theta) + R_0)^2\right]^{\frac{3}{2}}}.$$

Appendix B

Derivation of the mechanical equilibrium equation in polar coordinates

The mechanical equilibrium equation given by:

$$\nabla \cdot [\mu_1 \dot{\epsilon} + \mu_2 \dot{\phi} I + E'(\epsilon + \nu' \phi I) + \sigma(a) I - p(\phi) I] = 0. \tag{B.1}$$

This equation is derived in a 1D approximation where ($u = 0$ and $\frac{\partial}{\partial r} = 0$)
The strain tensor in polar coordinates is given by:

$$\epsilon = \begin{pmatrix} \frac{\partial u}{\partial r} & \frac{1}{2}\left(\frac{1}{r}\frac{\partial u}{\partial \theta} + \frac{\partial v}{\partial r} - \frac{v}{r}\right) \\ \frac{1}{2}\left(\frac{1}{r}\frac{\partial u}{\partial \theta} + \frac{\partial v}{\partial r} - \frac{v}{r}\right) & \frac{1}{r}\frac{\partial v}{\partial \theta} + \frac{u}{r} \end{pmatrix} = \begin{pmatrix} 0 & -\frac{v}{2} \\ -\frac{v}{2} & \theta \end{pmatrix},$$

thus the dilation is $\phi = \nabla \cdot u = tr(\epsilon) = \frac{\partial u}{\partial r} + \frac{1}{r}\frac{\partial v}{\partial \theta} + \frac{u}{r} = \frac{1}{r}\frac{\partial v}{\partial \theta} + \frac{u}{r}$.
The divergence of a tensor in polar coordinates is:

$$\nabla \cdot \sigma = \begin{cases} \frac{\partial}{\partial r}\sigma_{rr} + \frac{1}{r}\frac{\partial}{\partial \theta}\sigma_{r\theta} + \frac{\sigma_{rr} - \sigma_{\theta\theta}}{r} = 0 \\ \left(\frac{\partial}{\partial r} + \frac{2}{r}\right)\sigma_{r\theta} + \frac{1}{r}\frac{\partial}{\partial \theta}\sigma_{\theta\theta} = 0 \end{cases}$$

Components of the stress tensor:

$$\begin{cases} \sigma_{rr} = \mu_2 \dot{\phi} + E'\nu'\phi + \sigma(a) - p(\phi) \\ \sigma_{r\theta} = -\frac{1}{2r}(\mu_1 \dot{v} + E'v) \\ \sigma_{\theta\theta} = (\mu_1 + \mu_2)\dot{\phi} + E'(1+\nu')\phi + \sigma(a) - p(\phi) \\ \sigma_{rr} - \sigma_{\theta\theta} = -(\mu_1 \dot{\phi} + E'\phi) \end{cases}$$

We look for simplicity solutions (u,v) of the system where u=0. The equations for the mechanical equilibrium in polar coordinates for $u = 0$ and $\frac{\partial}{\partial r} = 0$ are thus:

$$\begin{aligned} (\frac{3}{2}\mu_1 + \mu_2)\dot{\phi} + E'(\nu' + \frac{3}{2})\phi &= 0, \\ \frac{\partial}{\partial \theta}\left[(\mu_1 + \mu_2)\dot{\phi} + E'(1+\nu')\phi + \sigma(a) - p(\phi)\right] &= \frac{1}{2r}(\mu_1 \dot{v} + E'v). \end{aligned}$$

Integration of the first equation gives the following expression for $\dot{v}$:

$$\dot{v} = -sv + C_0 \quad \text{with} \quad s = \frac{E'(\nu' + \frac{3}{2})}{\frac{3}{2}\mu_1 + \mu_2} \quad \text{and} \quad C_0 \text{ is a constant}$$

Replacement of this expression in the second equation gives:

$$\frac{\partial}{\partial\theta}\left[(\mu_1 + \mu_2)\dot{\phi} + E'(1+\nu')\phi + \sigma(a) - p(\phi)\right] = \frac{1}{2r}[(E' - \mu_1 s)v + \mu_1 C_0].$$

The equation can be re-written as follows:

$$\frac{\partial}{\partial\theta}\left[\mu\dot{\phi} + \hat{E}\phi + \sigma(a) - p(\phi)\right] = \frac{1}{2r}(\alpha v + \gamma),$$

with:

$$\mu = \mu_1 + \mu_2, \qquad \hat{E} = E'(1+\nu'), \qquad \alpha = E' - \mu_1 s, \qquad \gamma = \mu_1 C_0.$$

The resulting equation is thus given by:

$$\frac{\partial}{\partial\theta}\left[\mu\dot{\phi} + \hat{E}\phi + \sigma(a) - p(\phi)\right] = \frac{1}{2r}(\alpha v + \gamma). \tag{B.2}$$